



The Journal of
Gemmology

Volume 29 No. 7/8
July/October 2005



Gemmological Association and Gem Testing Laboratory of Great Britain

Registered Charity No. 1109555

27 Greville Street, London EC1N 8TN

Tel: +44 (0)20 7404 3334 | Fax: +44 (0)20 7404 8843

e-mail: information@gem-a.info | Website: www.gem-a.info

President: E A Jobbins

Vice-Presidents: N W Deeks, R A Howie, D G Kent, R K Mitchell

Honorary Fellows: Chen Zhonghui, R A Howie, K Nassau

Honorary Life Members: H Bank, D J Callaghan, E A Jobbins, J I Koivula, I Thomson, H Tillander

Chief Executive Officer: J M Ogden

Council: A T Collins – Chairman, S Burgoyne, T M J Davidson, S A Everitt, E A Jobbins, M McCallum, M J O'Donoghue, E Stern, P J Wates

Members' Audit Committee: A J Allnutt, J W Collingridge, P Dwyer-Hickey, J Greatwood, G M Green, B Jackson, D J Lancaster, C H Winter

Branch Chairmen: Midlands – G M Green, North East – S North and M Houghton, North West – D M Brady, Scottish – B Jackson, South East – C H Winter, South West – R M Slater

Examiners: C Abbott, A J Allnutt MSc PhD FGA, L Bartlett BSc, MPhil FGA DGA, He Ok Chang FGA DGA, Chen Meihua BSc PhD FGA DGA, Prof A T Collins BSc PhD, A G Good FGA DGA, D Gravier FGA, J Greatwood FGA, S Greatwood FGA DGA, G M Green FGA DGA, G M Howe FGA DGA, B Jackson FGA DGA, B Jensen BSc (Geol), T A Johne FGA, L Joyner PhD FGA, H Kitawaki FGA CGJ, Li Li Ping FGA DGA, M A Medniuk FGA DGA, T Miyata MSc PhD FGA, C J E Oldershaw BSc (Hons) FGA DGA, H L Plumb BSc FGA DGA, N R Rose FGA DGA, R D Ross BSc FGA DGA, J-C Ruffi FGA, E Stern FGA DGA, S M Stocklmayer BSc (Hons) FGA, Prof I Sunagawa DSc, M Tilley GG FGA, R K Vartiainen FGA, P Vuillet à Ciles FGA, C M Woodward BSc FGA DGA

The Journal of Gemmology

Editor: Dr R R Harding

Assistant Editors: M J O'Donoghue, P G Read

Associate Editors: Dr C E S Arps (Leiden), G Bosshart (Zurich), Prof A T Collins (London), Dr J W Harris (Glasgow), Prof R A Howie (Derbyshire), E A Jobbins (Caterham), Dr J M Ogden (Hildesheim), Prof A H Rankin (Kingston upon Thames), Dr J E Shigley (Carlsbad), Prof D C Smith (Paris), E Stern (London), Prof I Sunagawa (Tokyo), Dr M Superchi (Milan)

Production Editor: M A Burland

A venture into the interior of natural diamond: genetic information and implications for the gem industry

Part I: The main types of internal growth structures

G.P. Bulanova¹, A.V. Varshavsky² and V.A. Kotegov³

1. Earth Sciences, University of Bristol, Wills Memorial Building, Queens Rd., Bristol BS8 1RG, UK
2. Teaneck, New Jersey 07666, U.S.A.
3. The Institute of Geology of Diamonds and Precious Metals, 39 Lenin Av., Yakutsk 677891, Russia

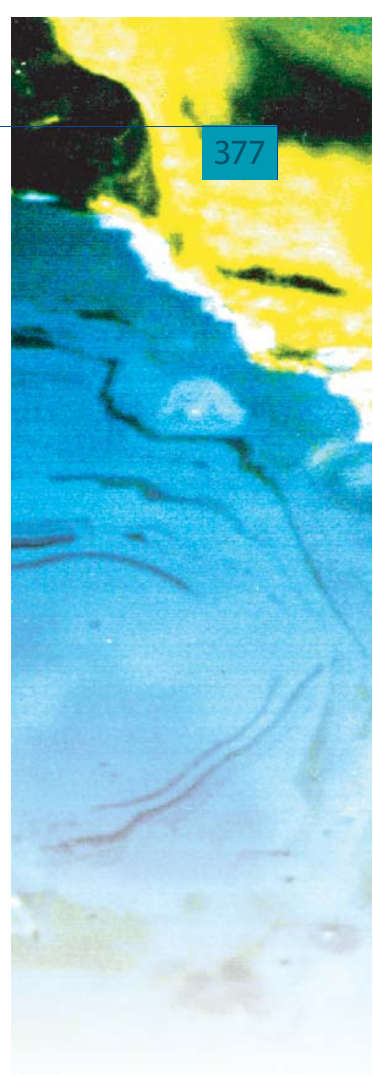
Abstract: Natural diamonds are rarely homogeneous. Crystals contain evidence of complicated histories of growth, changes of habit, chemistry, stages of growth and resorption. To extract genetic information recorded during diamond formation they should be studied by modern methods of microanalysis in polished plates. The best way to polish diamond to reveal internal zonation is described and the interpretation of different types of internal morphology of diamonds from cathodoluminescence imagery is given. Knowledge of the internal structures of diamonds is not only useful for scientific observations, but also allows a better determination of their likely behaviour during the cutting and polishing processes. This gives an opportunity for more economic use of individual stones during gem production.

Keywords: cathodoluminescence, diamond, gem industry, internal structure, polished plates

Introduction

The internal inhomogeneity of diamond monocrystals revealed first by Raman and Rendal (1944), has continued to be the subject of intensive study (Seal, 1962; Tolansky, 1966; Varshavsky, 1968; Moore and Lang, 1972; Lang, 1979, and many others). The early workers studied whole stones in their research using such optical properties of diamond as anomalous

birefringence (ABR), photoluminescence (PL) and X-ray topography, or more rarely studied diamond sections and plates by etching. Genshaft *et al.* (1977) and Beskrovanov (1992) for example investigated the growth history of Yakutian diamonds by photoluminescence microtopography of polished plates. Although destructive to diamond, the method of using polished



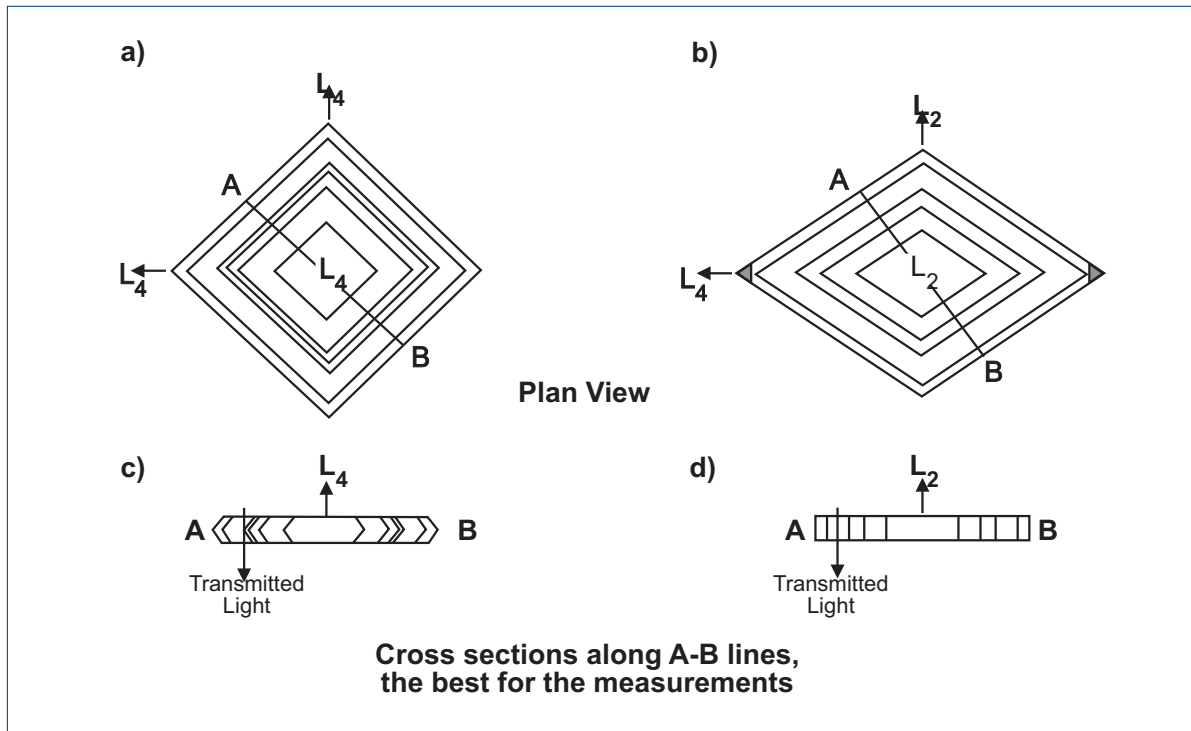


Figure 1: Central plates of diamond polished along the cubic (a) and dodecahedral (b) planes. Configuration of octahedral zones are revealed inside cross sections of both types of plates (c and d). The octahedral zones in the cubic plate are inclined for transmitted light (a, c), but are parallel inside the dodecahedral plate (b, d).

plates provides the opportunity to study a whole population, including opaque stones, coated, frosted, resorbed and sculptured crystals. Cathodoluminescence (CL) imaging of diamond plates and sections coupled with quantitative measurements of homogeneous growth zones by infrared spectra (FTIR) are powerful methods to constrain the history of diamond growth and to relate it to nitrogen content and aggregation state (Milledge *et al.*, 1995 and many others). Also, in the context of diamond internal structure, isotope composition related to *in situ* syngenetic inclusions is being used more widely (Bulanova *et al.*, 1993, 2002; Harte *et al.*, 1999).

In spite of the increasing number of such studies around the world (e.g. Zedgenizov *et al.*, 1999; Kaminsky and Khachatryan, 2004; Appleyard *et al.*, 2004; Schulze *et al.*, 2004; Taylor and Anand, 2004), there is a lack of published information about the best crystallographic directions for diamond cutting, the methodologies for preparation of diamond plates and interpretation of CL-images of different types of internal structures. The aim of this paper is to

share our knowledge and experience of (a) diamond sawing and polishing, (b) the study of the internal morphology of diamonds and (c) establishing constraints in diamond growth history. In pursuing the first objective some practical observations of diamond behaviour have been noted, which could be of benefit to the gem cutting industry.

Diamonds used in these studies are from the Yakutian Kimberlite pipes at Mir, 23rd Party Congress, Udachnaya and Aikhal. They are of commercial size (2-5 mm), of gem quality and mainly of octahedral morphology. Octahedral diamonds are the most important for study because dodecahedral stones, also widely used by the gem industry, are almost always formed by resorption of octahedra, so their internal structure also shows octahedral zoning. Stones with cubic habit and fibrous structure are not used in the gem industry, but coated diamonds can be used if the fibrous coat is thin enough and the internal octahedral part of the stone is of sufficient size for cutting as a gem.

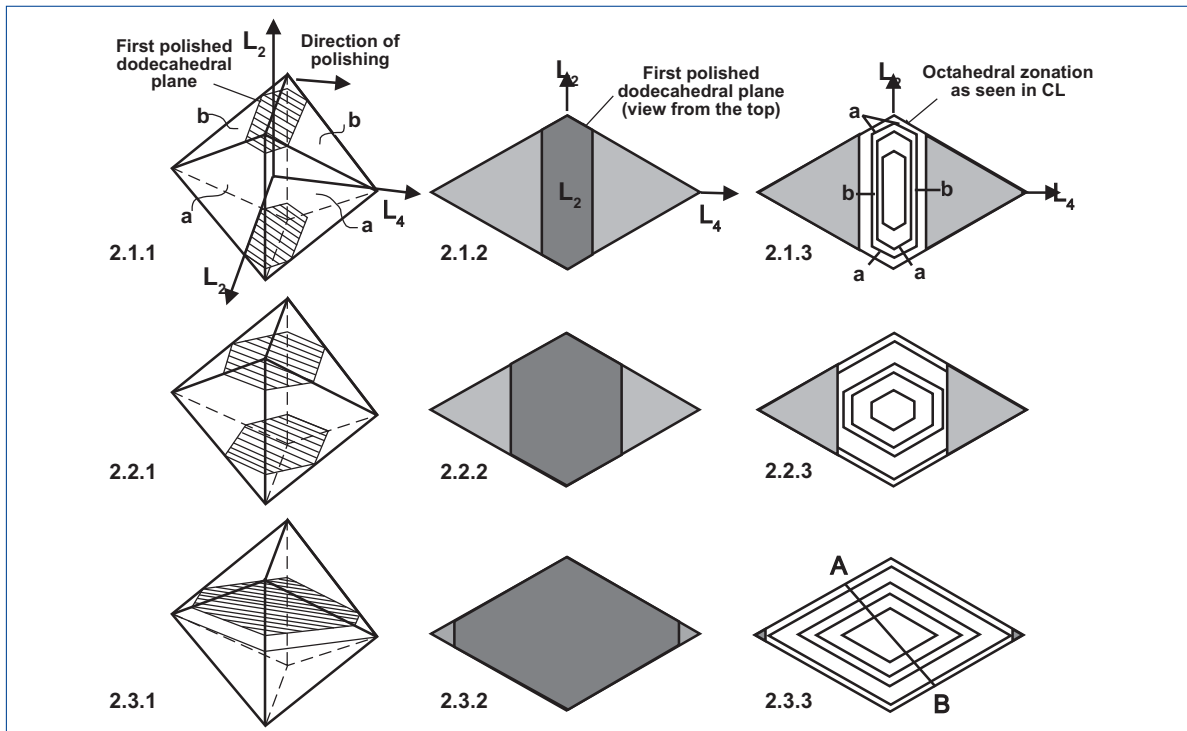


Figure 2: Models of an octahedral diamond and the resulting octahedral zonation revealed during gradual progressive polishing along the dodecahedral plane. For the practical convenience of understanding the process of polishing using a horizontally positioned polishing wheel, a non-standard crystallographic orientation of diamond crystal is shown where the L_2 axis is vertical. (The standard orientation would be L_4 vertical).

Figure 2.1.1: The first stage of polishing showing the configuration of vertical octahedral zones (belt 'a' faces and zones) and those inclined at 35° (the interfacial angle between octahedron and dodecahedron) to the surface of polishing (belt 'b');

Figure 2.1.2: The first polished plane;

Figure 2.1.3: Configuration of octahedral zones on the CL image.

Figures 2.2.1 - 2.2.3: The same after the intermediate stage of polishing.

Figures 2.3.1 - 2.3.3: The same after a final polishing producing the diamond central plate. The best line of profile for the measurement is shown by the line AB on 2.3.3.

Diamond sawing and polishing

The crystalline structure of diamond possesses two 'soft' directions, the cubic and dodecahedral, for relatively easy cutting and polishing. In the gem industry, the cubic direction is the most economical, so the first plates made from diamonds for scientific studies were sawn and polished along (100) planes (Lang, 1979). Cut and polished dodecahedral surfaces for scientific research were first used in Russia by Bulanova *et al.* (1979) and Beskrovanov (1986, 1992). *Figures 1a* and *b* exhibit a sketch of these two types of central diamond plates. The cross sections through the plates (*Figures 1c* and *d*) illustrate that for any plate polished along the cubic plane transmitted light would cross complex and inhomogeneous zones.

In contrast, a plate polished along the dodecahedral plane, allows transmission of light along homogeneous zones. From the geometry of zones inside the plates it follows that the dodecahedral plane is preferable for the study of diamond's internal structure and the measurement of IR and other optical properties.

Most single natural diamonds grow as polyhedral crystals by octahedral growth layers (Sunagawa, 1984), and an example is shown in *Figure 2*. Let us consider a first configuration of octahedral zones on the plate surface if an octahedral diamond is polished along the dodecahedral plane. In this situation, the set of four octahedral faces (marked as 'a' on *Figure 2.1*) are vertically

parallel to the L_2 axis of the diamond, and are normal (perpendicular) to the dodecahedral plane of polishing. The other four octahedral faces (two of which are shown as 'b' on *Figure 2.1*) are inclined to the plane of polishing and need to be completely removed by polishing to expose the set 'a' of octahedral zones shown in *Figures 2.3.1* and *2.3.3*. If such polishing is made from both sides of the crystal (*Figure 2.2*), even a relatively thick plate could be used for studying the rim and intermediate parts of a diamond using the exposed set of 'a' zones. In a central plate <1 mm thick (*Figure 2.3*), the dynamics of diamond development, comprising the history of growth, evolution of habit, change of PL and CL-colours and distribution of optical defects (by FTIR and PL microspectroscopy), can all be studied.

The term 'central' used here does not refer to the geometric centre, but describes the real diamond growth nucleus. These two positions very seldom coincide. The position of nucleation (the genetic centre) can be identified by ABR-imaging of the crystal before and during polishing. In many cases a single inclusion or group of microinclusions are located in it, being seeds or catalysts for diamond nucleation and subsequent growth (Varshavsky, 1968; Bulanova *et al.*, 1979). Dislocation bundles commonly start from these central inclusions and radiate perpendicular to the growing octahedral zones. These may be observed by ABR-imaging, and further assist in the identification of the diamond genetic centre. Additionally, PL-imaging reveals the differences of colours between growth zones in the diamond and therefore also provides useful information. Thus, both PL- and ABR-images should be used as an aid in exposing the central growth zone.

Small octahedral diamonds (1-2 mm) can be directly polished from both sides until the central plate is complete. Ideally the two planes of the diamond plate should be parallel for FTIR measurements, but a small angle between them does not prevent one obtaining satisfactory results. Sections markedly inclined to the dodecahedral

planes are not good for FTIR and can also give false information on CL images, so the correct orientation for polishing is very important. For other well-shaped crystals such as dodecahedra and cubes, polishing is also relatively easy. For complex morphologies and resorbed stones, the crystallographic orientation of etching pits and sculptures of growth and resorption on diamond surfaces are useful for finding the correct orientation for polishing.

Large diamonds (>2.5 mm) should be sawn into two parts, either mechanically or by laser. The cut should be made at just a small distance from the growth centre so that the diamond central zones can be easily exposed by subsequent polishing.

Many diamonds have complicated types of internal morphology, where a change of habit took place or mixed mechanism of growth has occurred (*Figure 3*). It is understood that for such crystals, only the central section will display the correct sequences of growth events. For more complex internal structures such as multicentred crystals, it is important to have a series of sawn and polished diamond sections and plates for scientific study.

CL-imagery of different types of structures of diamonds

General information about the physical mechanisms of CL emission, principles of CL-SEM technique and their application are well described by Sapharin and Obyden (1988). One of the limitations of CL imagery is that it forms only a detailed image of an object's surface to a depth of 1-5 microns. Therefore when using CL for study of diamond growth structures it is important to have a central section of the crystal because CL provides only a virtual two-dimensional image. PL- and ABR-imaging should be used simultaneously with CL studies as they will show a three dimensional image of the internal structure of a diamond and enable a more accurate interpretation of growth zones.

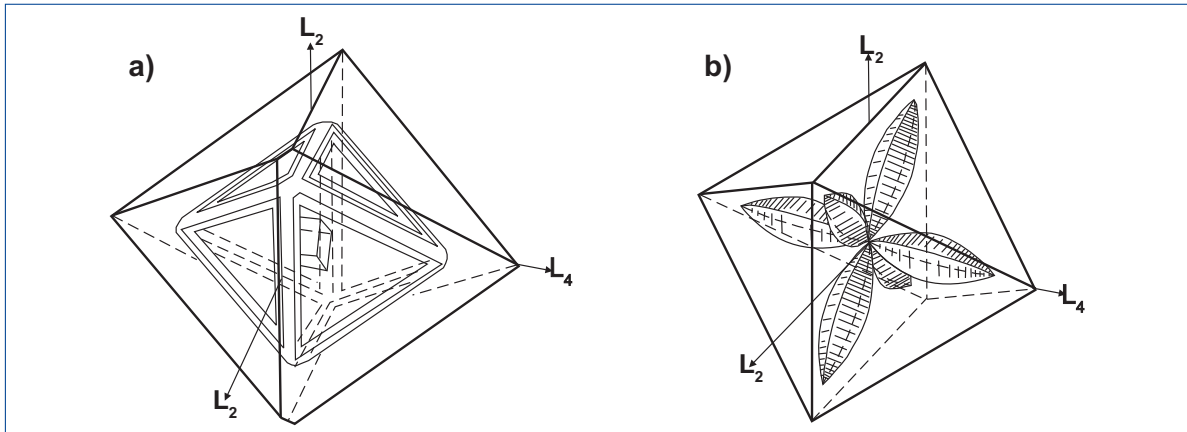


Figure 3: Models of complex diamond internal morphology:

a. Cube \rightarrow rough layered octahedron \rightarrow flat octahedron.

b. Cubo-octahedron \rightarrow octahedron (the earliest cubo-octahedron is formed by a combination of six cubic growth lobes and octahedral zones between them. Selective absorption of nitrogen impurities by octahedral zones slows down their growth rate, thus resulting in the final shape of a pure octahedron.).

Let us consider how CL images of the main internal structures appear in octahedral diamonds polished along a dodecahedral plane.

1. Simple octahedral zonation

After polishing diamond to a small depth, the octahedral zonation will appear as a hexagonal shape (Figure 2.1.3). The belt 'a' of octahedral faces with related zones is orthogonal to the dodecahedral plane of polishing and the four 'b' faces and zones are inclined to it. Correspondingly, the four 'a' zones are the only ones in a position to display the true growth boundaries and any peculiarities in growth micro-structures. The 'b' set of growth boundaries are inclined octahedral zones projected onto the polished surface as lines parallel to the cubic planes (Figure 2.1.3), and these may be mistaken for cubic zones. CL imaging of the deeper sections of the crystal will show increases in the lengths of the 'a' sets of octahedral zones (Figure 2.2.3) which are the most important for study. After reaching the growth centre of the crystal, the overlying 'b' octahedral zones will have been removed, the 'a' set of octahedral zones will be completely exposed and CL and ABR images of simple octahedral zoning in central diamond plates will display a parallelogram shape (Figure 2.3.3). The best direction for measurements of optical properties is also shown on Figure 2.3.3.

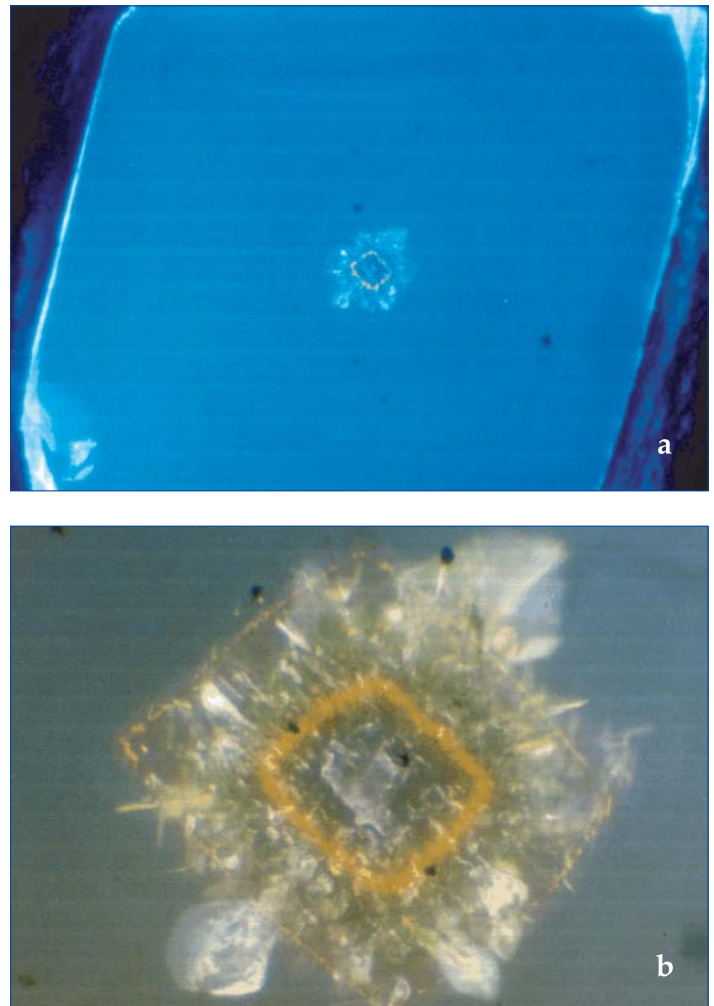


Figure 4: Evolution of diamond habit: cube \rightarrow octahedron. CL image of plate sawn on (110) plane of diamond 670 from the Mir pipe; width of crystal 3.5 mm.

a. View of the whole plate.

b. Central cubic zone.

2. Complex zonation.

Bulanova (1995) described the five main types of core → rim changes in the internal morphology of diamond and these are:

Cube → octahedron;

Cubo-octahedron → octahedron;

Cube → rough layered octahedron or rounded → flat octahedron;

Uncertain (Rounded) → rough layered octahedron → flat octahedron;

Multicentred → rounded or agate-like → octahedron.

An example of a CL image of cube → octahedron type diamond zonation is shown

in *Figure 4*. The size of the core cubic zone is always so small that only in the central section is it possible to have a true image of the change of diamond growth habit. The CL image of the other side of the diamond plate should show whether all central zones are exposed on this surface and whether they are of sufficient size for FTIR measurements (Mendelsohn and Milledge, 1995). If the zones on the two sides do not match then FTIR would give spectra for mixed zones which are difficult to interpret.

The ideal model of a cubo-octahedron → octahedron internal diamond zonation (which gives rise to the so-called central cross structure) is shown in *Figure 3b*. *Figure 5a* shows that the off-central section along (110) of such a mixed structure will display cubic sectors only along the short diagonal of the plate (shown by the faint yellow CL colour), surrounded by larger areas of octahedral growth zones (shown by light blue CL). In the central section (*Figure 5b*), the two other cubic lobes of the cubo-octahedron appear and are in the best position for FTIR measurements. The earliest stage of growth for such sectorial diamonds takes place by mixed mechanisms of tangential and unfaceted, hummocky growth followed by a faceted tangential one. When any changes of habit and mechanism of growth have taken place in the cubic growth sectors, unusual microstructures may be observed. Usually, these are located in the areas at the tops of the 'b'- sets of octahedral zones (see *Figure 5* and Bulanova *et al.*, 2002).

The evolution of diamond internal morphology for the cube → rough layered octahedron or rounded → flat octahedron development is illustrated well in Bulanova (1995). The second stage of rough layered octahedral or even rounded zonation is most unusual and can be difficult to interpret. Such rounded almost undefined shape can also occur in initial growth zones.

In the case of such roughly layered octahedral, almost rounded shapes, unusual structures appear on CL images of the off-centre sections. For example, the CL images shown in *Figure 6a, b* display an off-centre zonal structure very difficult to explain,

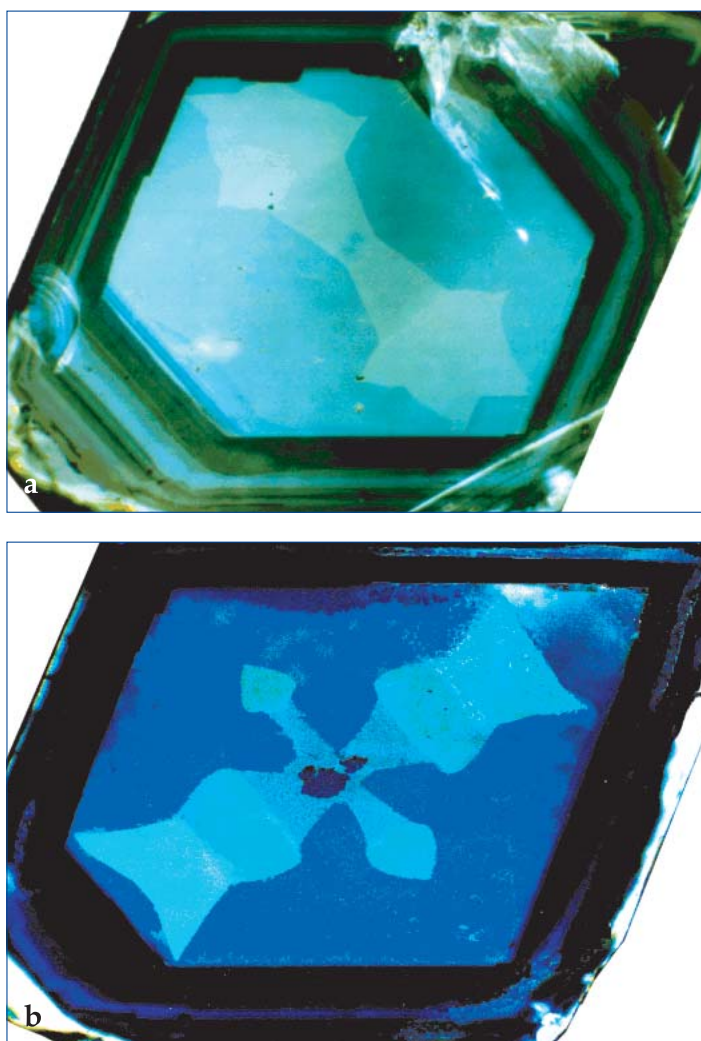


Figure 5: Change of diamond morphology: cubo-octahedron (mixed growth) → octahedron (tangential growth). CL image of plate sawn on (110) plane of diamond 1137 from Mir pipe, width 2.5 mm.

a. Off-centre side of the plate.

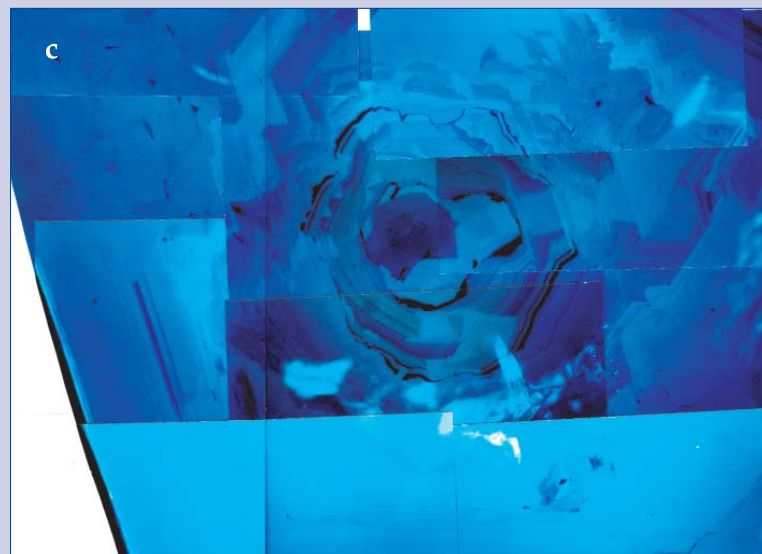
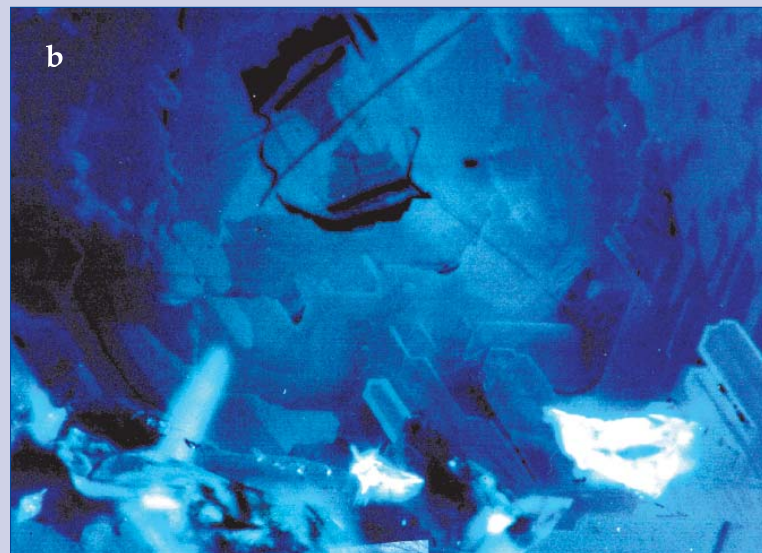
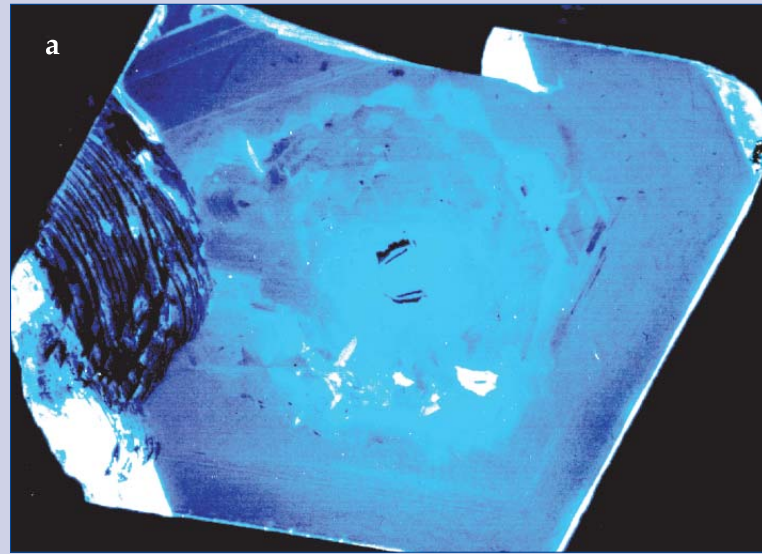
b. Central plane of the plate.

but if polished to the diamond centre (see *Figure 6c*), the pattern becomes much clearer. The real internal growth structure is one which evolves thus: rounded → intergrowths-1 → intergrowths-2 → rounded → cubo-octahedron → rough layered octahedron → flat octahedron. In the first off-centre diamond CL image made on the level of the intermediate, rough-layered octahedral zones (*Figure 6a, b*), the tops of the octahedrons are not single, but appear to consist of many points. Also, the edges are not single, but are composed of many narrow vicinal faces, which are close to the position of a dodecahedron or trigonal-tris-octahedron. The off-centre section also gives a visual impression that in the areas where octahedral points and edges exist, the latest zones are intruded into the earliest zones, as found in rim to core 'druse' formation (*Figure 6b*). This artefact disappears in the central section of the crystal (*Figure 6c*). Thus we believe that the mechanism of diamond growth from the periphery to the centre of a crystal proposed by Zezin *et al.* (1992) is not real and can be explained by the reasons and mechanisms outlined above.

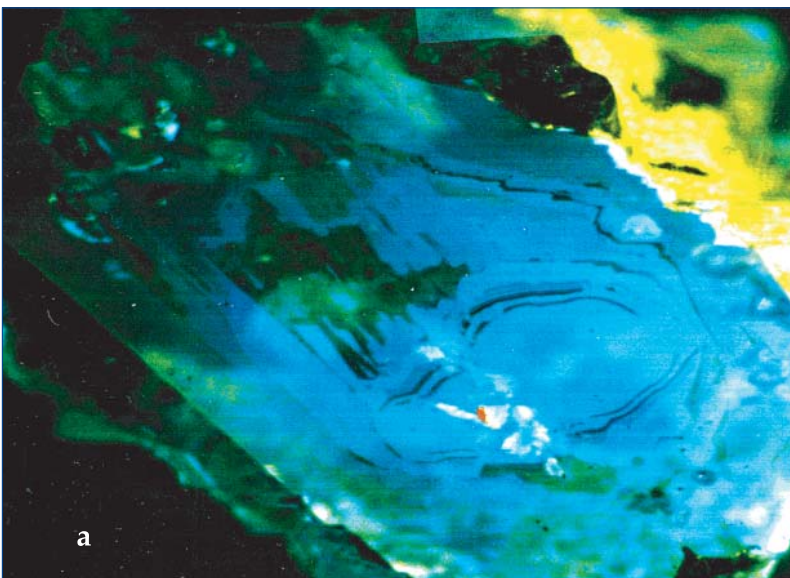
A multicentred type of diamond zoning is shown in *Figure 7*. In an early stage of the diamond polishing a rounded zonal structure was observed in the centre of which an inclusion of calcite was located (*Figure 7a*). In spite of the visual impression that it might be a centre of nucleation, the real centres of growth are still deeper within the diamond. CL images of the three plates made from this diamond provide a three dimensional tomographic picture of its internal morphology. The reconstructed history

Figure 6: Complex type of diamond internal morphology: rounded → intergrowths-1 → intergrowths-2 → rounded → cubo-octahedron → rough layered octahedron → flat octahedron. CL image of plate sawn on (110) plane of eclogitic diamond 4173 from the 23rd Party Congress pipe; width 4.5 mm.

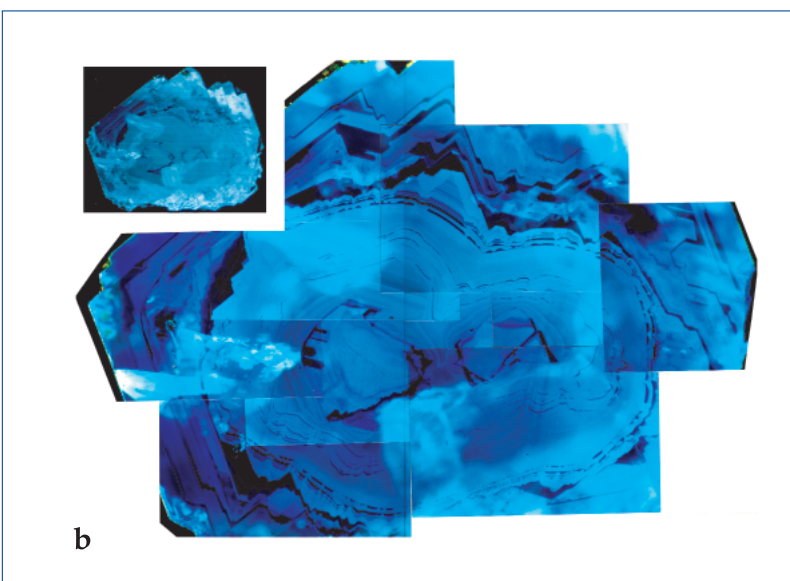
- The off-centre section shows rough layered octahedral zonation in this intermediate part of the diamond giving a false visual impression that in the areas of octahedron points and edges the latest zones are intruded into earlier zones.
- Detailed view of the middle of the off-centre plate.
- True zonation revealed in the central plate.



of the diamond therefore is: two regrown broken diamonds → rounded oscillatory zones → rough layered octahedral. The revealed internal morphology provides an explanation



a



b

Figure 7: The internal structure of a multicentred type of diamond. The CL image is of a plate sawn on the (110) plane of eclogitic diamond 1584 from the Mir pipe; width 5 mm.

- a. An off-centre diamond section showing rounded internal zoning and an inclusion of calcite, showing red CL, is located in what, falsely, has the appearance of a growth 'centre'.
- b. A plate across the central part of the diamond displaying zonation: two regrown broken crystals/aggregate → rounded oscillatory zones → rough layered octahedron. Both seeds of broken crystals/aggregate are surrounded by a narrow type II diamond zone (dark in CL), filling in also the four deep channels of etching in the left side of the largest one.

for the external shape of this diamond, which was elongated along one of the L_2 axes. The diamond external morphology was inherited from and controlled by the elongated oscillatory intermediate zones which overgrew the two diamond seeds, located at some distance from each other (Figure 7b) Some specific microstructures again developed in the areas of the octahedral points (Figure 7b) during a period of habit change from rounded to octahedral, the growth mechanism going from hummocky to tangential.

From the above description it follows that only central plates polished along the dodecahedral planes of diamonds indicate true sequences of growth events and allow constraints to be placed on the evolution of diamond crystal shapes. CL images of such central plates can be used as the maps for further *in situ* studies such as FTIR, isotope measurements, stratigraphic location of inclusions, the study of their chemical composition, their age and their isotope composition. Additional important genetic information from CL images includes areas of plastic and brittle deformations, radiation damage, fractures and the presence of fresh or re-healed cracks.

Implications for the gem industry

Ideal, isometric, sharp-edged, regular crystals of natural diamonds, called 'glassies' in the trade, are rare. Most rough diamonds contain different defects, irregularities and stresses, such as internal twinning, aggregates, plastic and brittle deformation. These cause local hard directions inside stones which give problems for cutters and polishers who therefore need to study the diamond in preparation for their work. The use of optical polarizing microscopes and ultraviolet (PL) microscopes in these preliminary studies would enhance recognition of such defects. Even if a diamond looks perfect in ordinary light, investigation with ABR and PL will highlight the type of internal structure and location

of growth centre or centres, thus allowing a better understanding of how to cut the stones in a more economic way.

For example, our results show that it is important that two- or multi-centred crystals should be recognized prior to deciding the best diamond cut and polishing. The external shape of such stones may be distorted in the sense of being elongated along one crystallographic axis. The best cuts for such diamonds would be either between the different growth centres, or with both seeds left in the largest part of the stone. Cutting directly through one of the growth centres would not be recommended because multiple cracks would be generated from the seed area into the diamond-host.

Black micro-inclusion seeds in the central diamond growth zones very often contain gas or fluid phases. When the 'hidden' pressure associated with such phases is released by exposure of these inclusions on the surface during polishing, mini-explosions take place followed by a dramatic increase of cracks in the diamond-host. To escape this negative effect, the groups of central micro-inclusions should either be left inside the stone or completely polished away.

Conclusions

1. The (110) plane of central plates of diamonds is the best for the study of their internal structures and history of growth using CL images and FTIR measurements.
2. Because CL imagery provides almost a two-dimensional picture of an object's surface, all three methods (ABR, PL, and CL) should be combined for study of the internal structure of diamonds, complementing one another to locate the true central section of a diamond.
3. During the interpretation of microstructures in inclined sections or thick plates of diamonds care should be exercised to ensure that the real sequence of growth events and conditions are determined.
4. In diamond plates polished parallel to (110) planes, zones near the points of

octahedra (cubic directions), may exhibit unusual textures and prompt misleading interpretations of growth histories.

5. The rough layered octahedral and rounded shapes of internal zones can produce other peculiar artefacts on CL images, but these will disappear after polishing down to the growth centre of the crystals.
6. When interpreting CL images of diamond plates and sections, the third dimension and the possibility of non-isometrically shaped internal zones should always be kept in mind.
7. Study of internal structure of natural diamonds using ABR and PL is useful for the gem industry. It will highlight potential difficulties for cutting and polishing of individual stones and will allow it to be done in the most economic way.

Acknowledgements

Professor J. Harris is thanked for his most helpful review. The authors are grateful to Professor G. Davies and D. Wiggers de Vries for their improving of the manuscript. Many thanks to Chris B. Smith for his constant support and help throughout writing the paper.

Most of the CL images involved in this work were obtained in the Department of Earth Sciences at University College London in collaboration with Dr J. Milledge and her colleagues over the years, with the technical assistance of P.A. Woods. The CL data were combined with mid-infrared microspectroscopy, usually by making measurements at intervals along traverses of the plates, and these results will be discussed in the second part of this paper.

References

- Appleyard, C.M., Viljoen, K.S., and Dobbe R., 2004. A study of eclogitic diamonds and their inclusions from the Finsch kimberlite pipe, South Africa. *Lithos*, 77(1-4), 317-32
- Besrovanov, V.V., 1986. The principles for classification of diamond. In: *Physical properties and mineralogy of natural diamond*. Yakutian Branch of Russian Academy of Sciences, 11-21 (in Russian)
- Beskrovanov, V.V., 1992. *Ontogeny of diamond*. Novosibirsk, Nauka, p.165 (in Russian)

- Bulanova, G.P., Varshavsky, A.V., Leskova, N.V., and Nikishova, L.V., 1979. About 'central' inclusions in natural diamonds. *Doklady Akademii Nauk USSR*, 244(3), 704-6 (in Russian)
- Bulanova, G.P., Barashkov, Yu.P., Talnikova, S.B., and Smelova, G.B., 1993. *Natural diamond – genetic aspects*. Nauka, Novosibirsk, 176 pp (in Russian)
- Bulanova, G.P., 1995. The formation of diamond. *Journal of Geochemical Exploration*, 53, 1-53
- Bulanova, G.P., Pearson, D.G., Hauri, E.H., and Griffin, B.J., 2002. Carbon and nitrogen isotope systematics within a sector-growth diamond from the Mir kimberlite, Yakutia. *Chemical Geology*, 188, 105-23
- Genshaft, Y.S., Yakubova, S.A., and Volkova, L.M., 1977. *Internal morphology of natural diamonds*. In: Genshaft, Y.S., *Investigation of high pressure minerals*. Publishing house of the Institute of Physics of the Earth, Moscow, 5-131
- Harte, B., Fitzsimons, C.W., Harris, J.W., and Otter, M.L., 1999. Carbon isotope ratios and nitrogen abundances in relation to cathodoluminescence characteristics for some diamonds from Kaapvaal Province, S. Africa. *Min. Mag.*, 63 (6), 829-56
- Kaminsky, F.V., and Khachatryan, G.K., 2004. The relationship between the distribution of nitrogen impurity centres in diamond crystals and their internal structure and mechanism of growth. *Lithos*, 77, 8th IKC selected papers, 2, 255-71
- Lang, A.R., 1967. Causes of birefringence in diamond. *Nature*, 213, 5073
- Lang, A.R., 1979. *Internal structure*. In: J. E. Field (Ed.), *The Properties of Diamond*, Academic Press, London, 425-69
- Mendelsohn, M.J., and Milledge, H.J., 1995. Geologically significant information from routine analysis of the mid-infrared spectra of diamonds. *Inter. Geol. Review*, 37, 95-110
- Milledge, H.J., Bulanova, G.P., Taylor, W.R., Woods, P.A., and Turner, P.H., 1995. Internal morphology of Yakutian diamonds – a cathodoluminescence and infrared mapping study. *Extended Abstracts, Sixth International Kimberlite Conference*, Novosibirsk, August, 384-386
- Moore, M., and Lang, A.R., 1972. On the internal structure of natural diamonds of cubic habit. *Phil. Mag.*, 26(6), 1313-26
- Raman, C.V., and Rendal, G.R., 1944. Birefringence patterns in diamond. *Proc. Indian Acad. Science*, 19, A, N5
- Schulze, D.J., Harte B., Valley, J.W., and Channer, D.M.DeR., 2004. Evidence of subduction and crust-mantle mixing from a single diamond. *Lithos*, 77(1-4), 349-58
- Seal, M., 1962. The growth history of natural diamond as revealed by etching experiments. *Proc. of the 1st. Intern. Congress on Diamond in Industry*, Paris, London, 361-75
- Sapharin, G.V. and Obyden, S.K., 1988. Colour cathodoluminescence display of video information in scanning electron microscopy: principles and applications to physics, geology, soil science, biology and medicine. *Scanning*, 10, 87-106
- Sunagawa, I., 1984. Morphology of natural and synthetic diamond crystals. In: I. Sunagawa (Ed.) *Materials science of the earth's interior*. Terra Scientific Publishing Co., Tokyo, 303-31
- Taylor, A., and Anand, M., 2004. Diamonds: time capsules from Siberian Mantle. In: *Chemie der Erde Geochemistry* (in press)
- Tolansky, S., 1966. Birefringence of diamond. *Nature*, 211, 158-160
- Varshavsky, A.V., 1968. *Anomalous birefringence and internal morphology of diamonds*. Nauka, Moscow, 89 pp (in Russian)
- Zedgenizov, D.A., Rylov, G.M., and Shatsky, V.S., 1999. Internal structure of microdiamonds from Udachnaya kimberlite pipe. *Geologiya and Geofysika*, 40(1), 113-20
- Zezin, R.B., Smirnova, E.P., Sapharin, G.V., and Obyden, S.K., 1992. New growth features of natural diamonds revealed by colour cathodoluminescence scanning electron microscope (CCL SEM) technique. *Scanning*, 14, 3-10

As-grown, green synthetic diamonds

Christopher M. Breeding, James E. Shigley and Andy H. Shen

Gemological Institute of America, Carlsbad, CA 92008, U.S.A.

Abstract: *Green synthetic diamonds showing no evidence of irradiation or other laboratory treatment were examined to determine the nature of the coloration. The occurrence of distinct yellow and blue internal growth zones as well as absorption spectra indicating the presence of both isolated nitrogen and boron strongly suggest that the green colour is a result of the intergrowth of boron- and nitrogen-rich sectors. Variations in the boron/nitrogen concentration ratio during synthesis can produce as-grown diamond colours ranging from dark blue to green to yellow.*

Keywords: *boron, Chatham, colour origin, mixed growth, nitrogen, synthetic diamond*

Introduction

Natural gem diamonds displaying a green bodycolour are rare, and hence are highly valued in the marketplace (Genis, 2003). Artificial irradiation treatments are commonly applied to many types of natural and synthetic diamonds to induce green coloration (e.g., Collins, 1982; Vins, 2002). High-pressure, high-temperature (HPHT) treatment of type Ia diamonds has also produced attractive yellowish-green colours (Reinitz *et al.*, 2000). Although some visible clues may be present, separation of natural from treated-colour green diamonds is often difficult for gemmological laboratories because the effects of laboratory irradiation and heating are very similar to processes in the Earth that generate green coloration. Consequently, green diamonds that can be proven to be of natural colour are quite rare.

As an alternative to treated colour natural diamonds, producers of gem-quality synthetic diamonds offer as-grown (i.e. untreated) yellow and blue laboratory-created diamonds (pink synthetic diamonds have periodically been presented as untreated, but

at this time, all known synthetic pinks are treated colours) (Moses *et al.*, 1993; Shigley *et al.*, 2004). Green coloration is not common in synthetic diamonds and, when present, has usually been the result of post-growth irradiation. Rarely, elevated concentrations of Ni impurities have also been thought to be a cause of green coloration (Kanda, 1999). However, Chatham Created Gems of San Francisco, California, has recently made available a new kind of as-grown, green synthetic diamond that shows neither abnormal Ni content, nor any indication of irradiation or other post-growth treatment. We present gemmological and spectroscopic data from these synthetic diamonds illustrating the cause of this green coloration.

Materials and methods

A recent examination of 129 synthetic diamonds (Shigley *et al.*, 2004) loaned to the Gemological Institute of America (GIA) by Chatham Created Gems included 16 samples that show a face-up green colour





Figure 1: The green synthetic diamonds provided by Chatham Created Gems range from green to bluish-, greyish- and yellowish-green hues. These two representative round brilliants weigh 0.19 – 0.34 ct. Photo by Maha Tannous Calderon, copyright GIA.

(Figure 1). These synthetic diamonds are the focus of this study. The colours consisted of pure green, as well as bluish-, greyish- and yellowish-green hues. Note, however, that GIA does not issue colour reports for synthetic diamonds. Thirteen of the samples had been faceted into round brilliants weighing 0.16 – 0.41 ct. The other three were 0.79 – 1.06 ct uncut crystals.

Details of the gemmological features, reactions to ultraviolet radiation, chemical analysis, and photoluminescence spectra for all colours of the Chatham synthetic diamonds examined (including green) are presented in Shigley *et al.*, 2004. The absorption spectra presented herein were collected in the mid-infrared range (6000–400 cm^{-1} ; 1 cm^{-1} resolution) at room temperature using a Thermo-Nicolet Nexus 670 Fourier-transform infrared spectrometer and in the ultraviolet-visible-near infrared range (250–850 nm; 0.1 nm sampling interval) at liquid nitrogen temperature (~77 K) using a Thermo-Spectronic Unicam UV500 spectrophotometer at GIA in Carlsbad, CA.

Results and discussion

The 16 green synthetic diamonds fall into two distinct groups. Eight (including all three crystals) are type IIa and clearly show absorption features indicative of radiation damage (Figure 2, A and B) (see Collins, 1982) whereas the other eight lack these distinct spectroscopic features (Figures 2C and D). Exposure of diamond to radiation produces general radiation (GR) absorption features at the red and blue ends of the electromagnetic spectrum. The combination of the GR features and typical diamond absorption produces a green bodycolour. Irradiation treatment of natural and synthetic diamonds to artificially induce a green coloration is not unusual; therefore, this study will focus on the eight green diamonds showing no indication of treatment.

The untreated samples exhibit mid-infrared absorption spectra with detectable concentrations of both boron (2803 and 2457 cm^{-1} peaks) and isolated nitrogen (indicated by 1344 cm^{-1} peak) impurities (Figure 2C) (Zaitsev, 2001). In natural diamonds, B and N rarely occur together in a single crystal

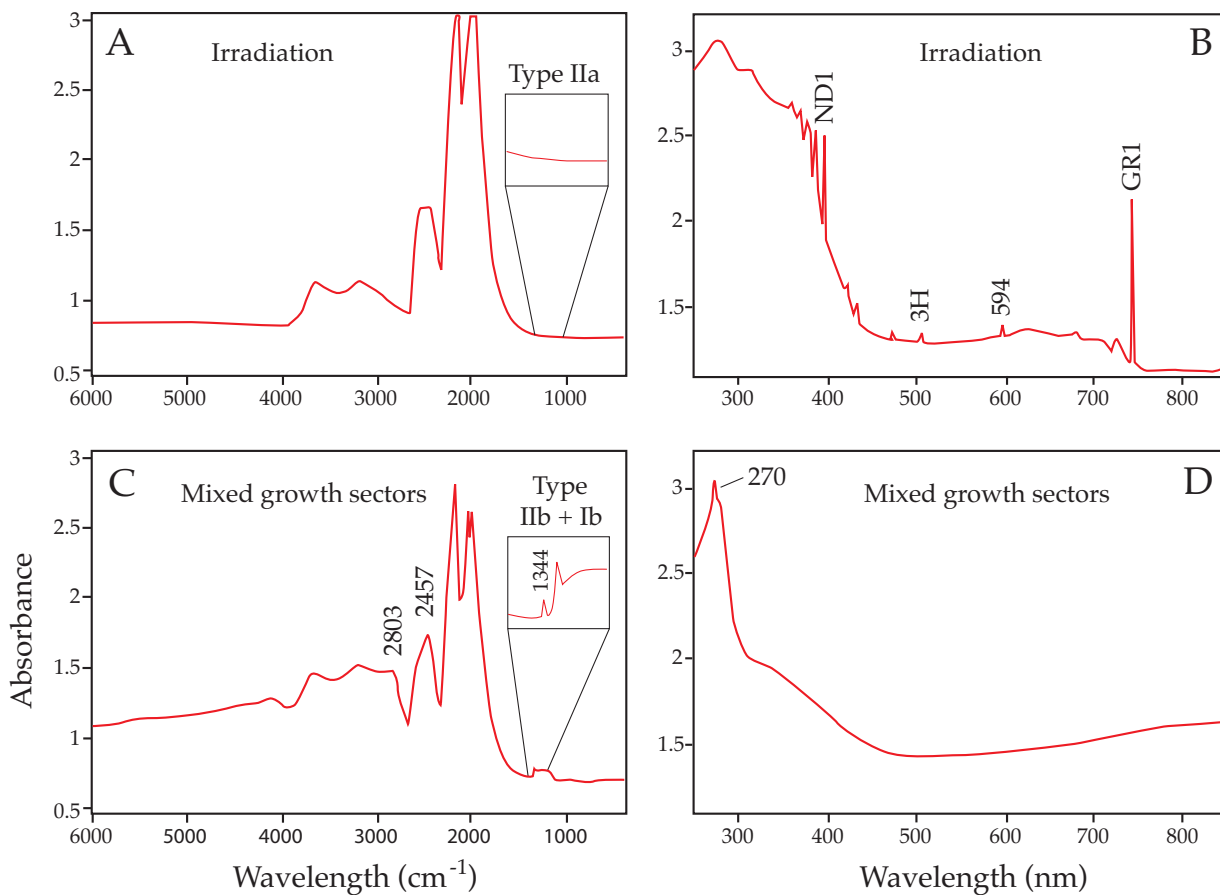


Figure 2: Mid-infrared (A,C) and UV-visible-NIR (B,D) absorption spectra for two types of green synthetic diamonds. A-B. Type IIa synthetic diamonds that exhibit features clearly due to irradiation (GR1 at 741 nm, ND1 at 393 nm, 3H at 503 nm, and 594 nm line; Zaitsev, 2001). C-D. Synthetic diamonds with mixed IIb and Ib growth zones show evidence for both boron (see 2457 and 2803 cm^{-1} peaks in C, and increase in absorption toward 850 nm in D) and isolated nitrogen (see 1344 cm^{-1} peak in C and 270 nm peak in D). The peaks indicating irradiation are not present in these mixed type synthetic diamonds. Spectra redrawn from original data.

in measurable quantities (Rooney *et al.*, 1993; Hainschwang and Katruscha, 2003).

The presence of both impurities implies a mixed type of IIb + Ib for these green synthetic diamonds.

Absorption in the ultraviolet-visible-near infrared range reveals three distinct features: a broad absorption band decreasing from 850 nm to ~600 nm, a smaller increase in absorption from ~400 nm to ~300 nm, and a distinct, rounded peak centred at ~270 nm (Figure 2D). The broad band at 850-600 nm is due to boron and produces the blue colour that is typical of IIb diamonds. The peak at ~270 nm indicates the presence of isolated nitrogen. In the absence of other colour centres, strong absorption due to isolated

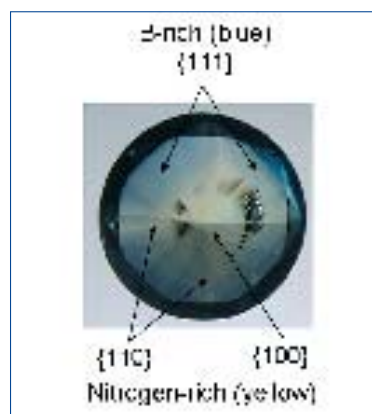


Figure 3: Colour zoning in untreated 0.16 ct green synthetic diamond immersed in water. Distinct yellow and blue zones correspond to particular cuboctahedral growth sectors and indicate nitrogen- and boron-rich regions (Welbourn *et al.*, 1996). Combination of these coloured sectors makes the diamond appear green. Photo by J.E. Shigley, copyright GIA.

nitrogen at wavelengths less than ~500 nm produces the deep yellow seen in 'canary' diamonds (Collins, 1982; Zaitsev, 2001). The band at 400-300 nm is probably related to nitrogen as well. The combination of these absorption features results in a transmission 'window' from ~600 nm to 450 nm that produces the face-up green coloration.

Colour zoning, visible when the synthetic diamonds are immersed in water to reduce surface reflections, supports the spectroscopic evidence (Figure 3). Distinct yellow and blue zones were observed to correspond with particular internal growth sectors in the green synthetic diamonds.

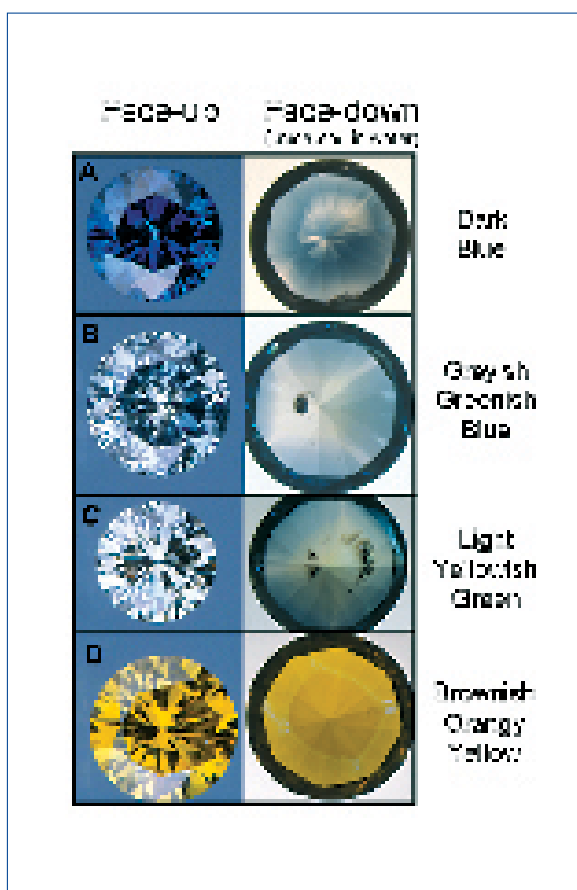


Figure 4: Face-up and face-down views of dark blue, lighter blue, green and yellow as-grown synthetic diamonds. Colour zoning in the face-down view is easier to see by immersion in water. A. (0.27 ct). A fully saturated overall blue colour consists of dark blue and colourless zones. B. (0.31 ct) Less saturated blues exhibit blue and very pale yellow zones. C. (0.16 ct). Light green diamonds show distinct blue and yellow regions. D. (0.60 ct). Deep yellow samples consist of yellow and colourless growth sectors. Dark spots are metallic flux inclusions. Photos by Maha Tannous Calderon and J.E. Shigley, copyright GIA.

The yellow zones, which are presumably rich in isolated nitrogen, correspond to {110} dodecahedral and {100} cubic growth sectors, whereas the blue zones, which are enriched in boron, comprise the {111} octahedral growth zones (Welbourn *et al.*, 1996). Synthetic diamonds grown by the HPHT temperature gradient technique commonly exhibit mixed cuboctahedral crystal forms with enrichments of either nitrogen or boron along specific growth planes (Strong and Wentorf, 1991; Scarratt *et al.*, 1996; Welbourn *et al.*, 1996). In general, both impurities are preferentially incorporated into octahedral growth sectors followed by cubic and/or dodecahedral sectors in synthetic diamond. In the case of these green samples, elevated concentrations of boron (relative to nitrogen) resulted in boron-dominated, blue octahedral growth sectors. Smaller concentrations of isolated nitrogen were taken up by the cubic and dodecahedral sectors. Although, the occurrence of both nitrogen and boron at concentrations necessary to generate yellow and blue growth sectors has been reported in synthetic diamonds (Shigley *et al.*, 1992; Rooney *et al.*, 1993; Hainschwang and Katrusha, 2003), mixed colour zones of strong enough intensity to give the faceted sample a face-up green coloration are unique. This mechanism of causing green by mixing yellow and blue growth sectors indicates that the samples represent as-grown, untreated synthetic diamonds.

In order to fully understand the nature of the mixed colour zoning and resultant green, we examined blue and yellow synthetic diamonds with face-up hues similar to those observed in the individual growth sectors. Just like the green synthetic diamonds, the yellows and blues appear to represent as-grown colours with no evidence for post-growth treatment. The blue diamonds range from dark blue to lighter hues including greyish or greenish blue. The darker blue hues represent IIb diamonds with relatively high boron content and mixed blue (IIb) and colourless (IIa) zones (Figures 4A, 5A, 6A). Lighter blue samples contain elevated boron concentrations, but, like the green synthetic

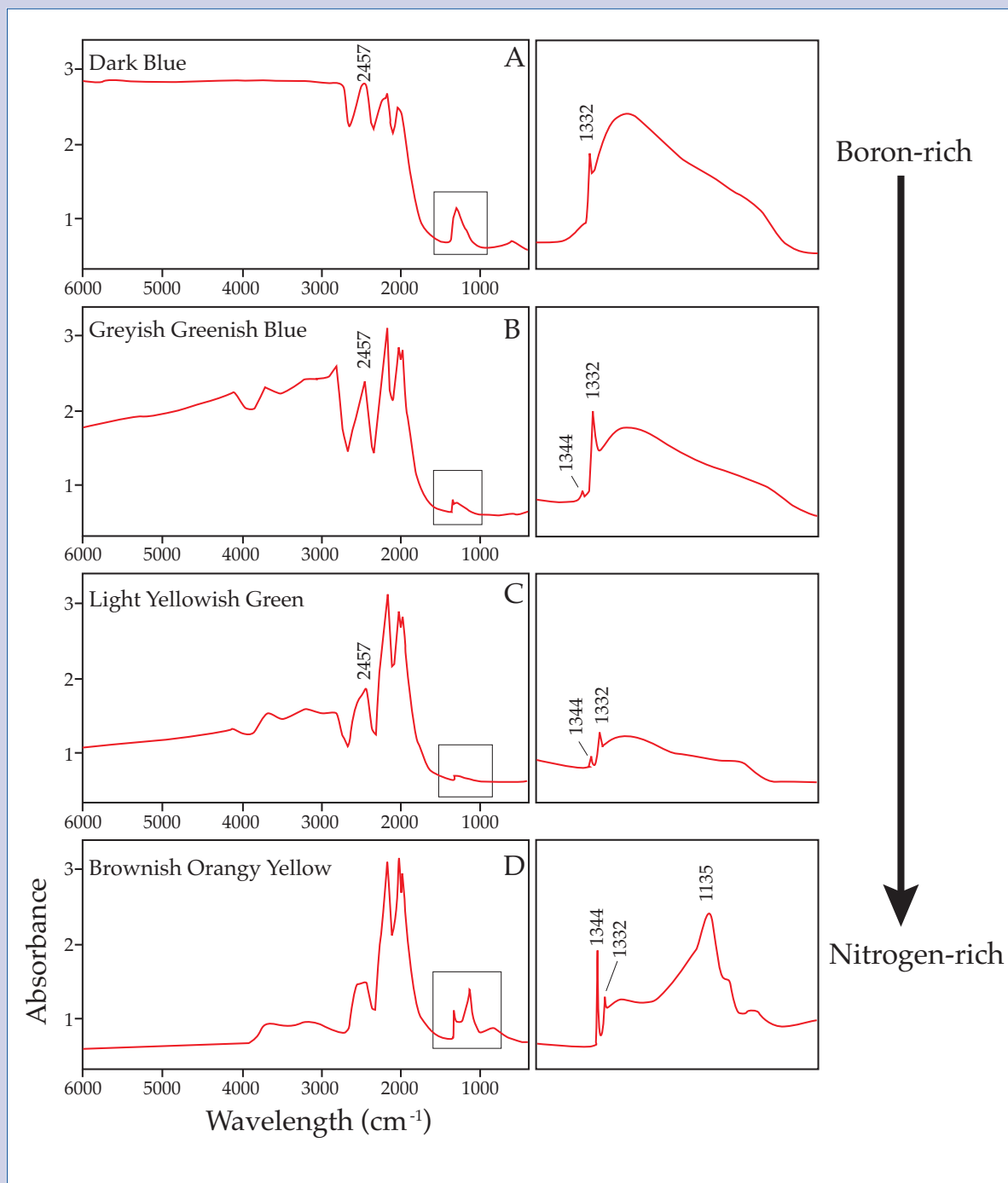


Figure 5: Mid-infrared absorption spectra for the blue, light blue, green and yellow synthetic diamonds shown in Figure 4. The one phonon diamond region has been expanded in the column on the right to better show features due to nitrogen impurities. A. Dark blue diamonds contain high boron (2457 and 2803 cm^{-1} peaks) and little to no evidence for nitrogen. B. Greyish-greenish blue colour is associated with lower boron concentrations and small amounts of isolated nitrogen (1344 cm^{-1} peak). C. The yellowish-green diamond contains even less boron and more isolated nitrogen. D. The deep yellow colour is produced by significant isolated nitrogen and the absence of boron. Sample sizes were similar and are given in Figure 4. Spectra redrawn from original data.

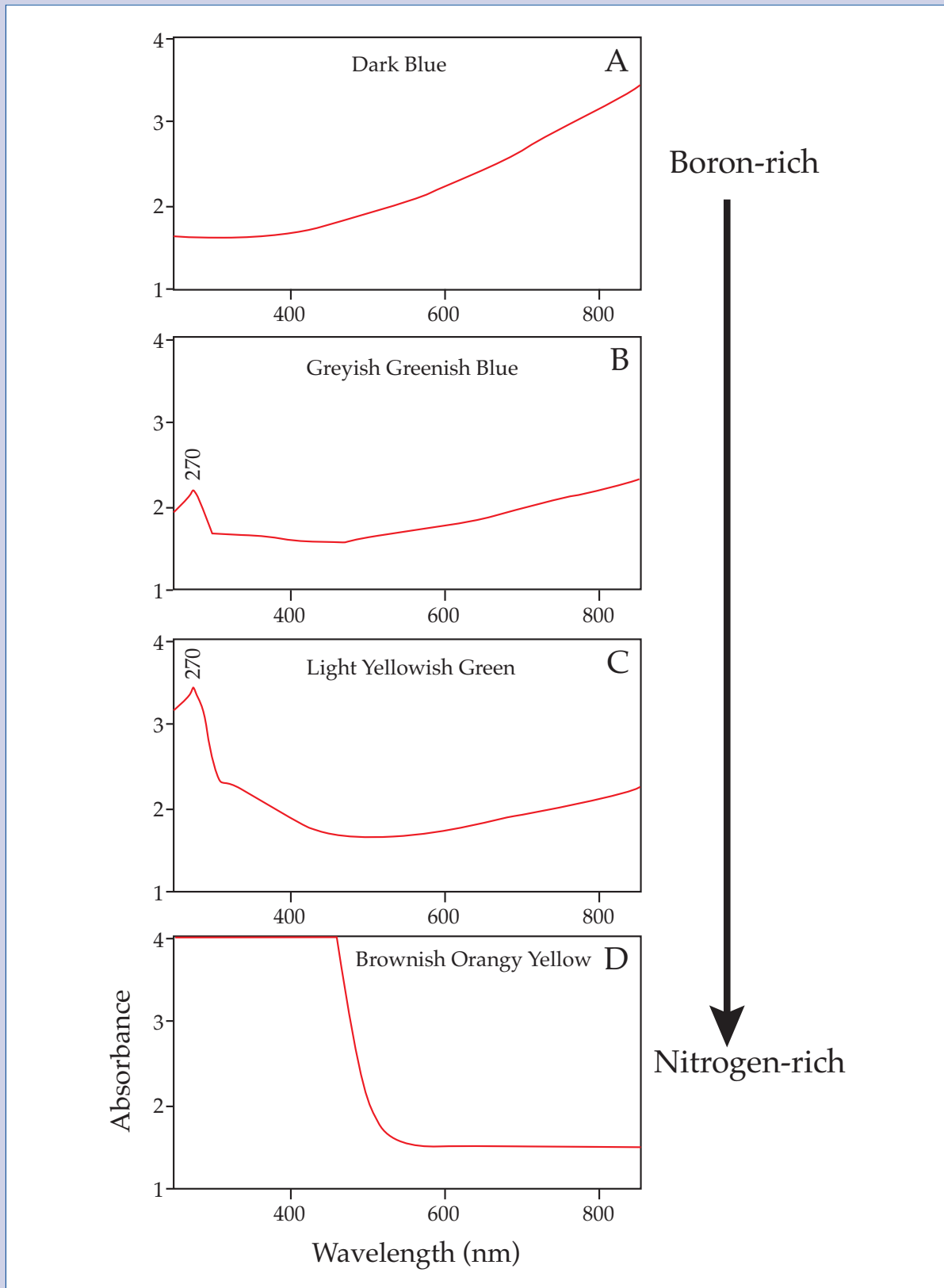


Figure 6: Ultraviolet-visible-NIR absorption features for the synthetic diamonds in Figures 4 and 5. A. The dark blue diamond exhibits broadly increasing absorption toward 850 nm that produces a blue transmission window typical of IIb diamonds. B. A less saturated blue diamond shows less intense IIb absorption and a small broad peak due to isolated nitrogen at 270 nm, resulting in a greenish-blue colour. C. Increases in isolated nitrogen and decreases in boron shift the transmission window toward longer wavelengths and a yellowish green colour. D. Intense absorption due to isolated nitrogen and the absence of IIb absorption produces a deep yellow synthetic type Ib diamond. Sample sizes were similar and are given in Figure 4. Spectra redrawn from original data.

diamonds, also show the 1344 cm^{-1} and 270 nm peaks indicating isolated nitrogen (Figures 5B, 6B). Growth sectors alternate between blue and very pale yellow, combining to give the faceted samples a light blue or greenish-blue face-up colour (Figure 4B). The yellow synthetic diamonds range from greenish-yellow to brownish orangy yellow and are type Ib with relatively high concentrations of isolated nitrogen (Figures 4D, 5D, 6D). The yellows exhibit mixed colour zoning with distinct deep yellow (Ib) and colourless (IIa) sectors.

The sequence of Chatham synthetic diamonds shown in Figure 4, A-D, illustrates the variation in colour from dark blue, to greyish greenish blue, to yellowish green, to deep yellow. Correspondingly, changes in colour zone combinations from blue-colourless to blue-very pale yellow to blue-yellow to yellow-colourless accompany the changes in face-up hue. Mid-infrared absorption spectra indicate that decreasing blue coloration is accompanied by decreases in B concentration (as noted from the intensity of the 2457 cm^{-1} peak) and increases in the amount of isolated N present (1344 cm^{-1} peak) (Figure 5, A-D). In response to changing B and N contents, absorption in the visible spectral range produces transmission windows that shift from $\sim 400 - 500\text{ nm}$ (producing dark blue) to $\sim 450 - 550\text{ nm}$ (greyish-greenish-blue) to $\sim 500 - 600\text{ nm}$ (light yellowish-green) to $\sim 550 - 700\text{ nm}$ (deep brownish-orangy yellow) (Figure 6, A-D).

The wide range of blue to green to yellow synthetic diamonds that are available for study exhibit a smooth gradation in boron/nitrogen ratios, suggesting that the intermixing of blue and yellow growth sectors is not caused by simple temperature fluctuations, but instead is a controlled process involving variations in the addition of impurities to the growth chambers. Although the conditions employed during synthesis of these diamonds have not been revealed, it is evident from the spectroscopic characteristics that changes in the relative concentration ratio of boron to 'nitrogen getters' (elements that remove ambient nitrogen from the growth environment to control the concentration of available

nitrogen; Rooney *et al.*, 1993; Zaitsev, 2001) can have profound effects on the colour of newly-grown synthetic diamonds. A precise control of the mixtures of these impurities during growth can result in green colours without the use of irradiation or post-growth heating.

Conclusions

Of the synthetic green diamonds made available to us for study by Chatham Created Gems, half of them represent a new kind of green coloration that has not been previously described in detail. The colour is caused by a mixture of boron-rich, blue growth sectors and nitrogen-rich yellow sectors. Absorptions due to boron and isolated nitrogen produce a transmission window in the yellow-green region of the visible spectrum resulting in a face-up green appearance. No evidence of irradiation or post-growth heating was detected and the derivation of green solely from mixed growth zones of blue and yellow indicates that the colours are as-grown. Simple variations in the boron/nitrogen ratios in the growth chamber can produce gem-quality synthetic diamonds ranging from dark blue to green to deep yellow.

Acknowledgements

We thank Tom Chatham of Chatham Created Gems for the generous loan of synthetic diamonds for our study. Discussions and comments from Shane McClure, Dr Wuyi Wang, Tom Moses and Dino DeGhionno were very helpful in revising the manuscript. Colour grading by Scott Guhin, photography by Maha Tannous, and spectroscopic support from Shane Elen and Sam Muhlmeister are greatly appreciated.

References

- Collins, A.T., 1982. Colour centres in diamond. *Journal of Gemmology*, 18(1), 37-75
- Genis, R., 2003. Green diamonds. *Rapaport Diamond Report*, Oct 2003, 166-7
- Hainschwang, T., and Katrusha, A., 2003. Gem News International: A bicolored synthetic

- diamond. *Gems & Gemology*, 39(2), 163-4
- Kanda, H., 1999. International Gemological Symposium Abstract: Colors of high-pressure synthetic diamonds. *Gems & Gemology*, 35(3), 174-5
- Moses, T., Reinitz, I., Fritsch, E., and Shigley, J.E., 1993. Two treated-color synthetic red diamonds seen in the trade. *Gems & Gemology*, 29(3), 182-90
- Reinitz, I., Buerki, P.R., Shigley, J.E., McClure, S.F., and Moses, T., 2000. Identification of HPHT-treated yellow to green diamonds. *Gems & Gemology*, 36(2), 128-37
- Rooney, M-L.T., Welbourn, C.M., Shigley, J.E., Fritsch, E., and Reinitz, I., 1993. De Beers near colorless-to-blue experimental gem-quality synthetic diamonds. *Gems & Gemology*, 29 (1), 38-45
- Scarratt, K., Dunaigre, C.M., and Du Toit, G., 1996. Chatham synthetic diamonds. *Journal of the Gemmological Association of Hong Kong*, 19, 6-12
- Shigley, J.E., Fritsch, E., Reinitz, I., and Moon, M., 1992. An update on Sumitomo gem-quality synthetic diamonds. *Gems & Gemology*, 28(2), 116-22
- Shigley, J.E., McClure, S.F., Breeding, C.M., Shen, A.H., and Muhlmeister, S., 2004. Chatham synthetic diamonds. *Gems & Gemology*, 40(2), 128-45
- Strong, H.M., and Wentorf, R.H., 1991. Growth of large, high-quality diamond crystals at General Electric. *American Journal of Physics*, 59(11), 1005-8
- Vins, V., 2002. Change of colour produced in synthetic diamonds by β HT-processing. *Gemmological Bulletin*, 1(5), 26-32
- Welbourn, C.M., Cooper, M., and Spear, P.M., 1996. De Beers natural versus synthetic diamond verification instruments. *Gems & Gemology*, 32(3), 159-69
- Zaitsev, A.M., 2001. *Optical Properties of Diamond: A Data Handbook*. Springer Verlag, Berlin, Germany

Iridescent colours of the abalone shell (*Haliotis glabra*)

T.L. Tan, D. Wong and P. Lee

Natural Sciences and Science Education, National Institute of Education, Nanyang Technological University, 1 Nanyang Walk, Singapore 637616

Abstract: Shells and pearls of some molluscs are popular ornaments primarily due to the beauty of their natural iridescent colours. Strong iridescent colours are very evident on the polished shell of the mollusc *Haliotis glabra*, commonly known as abalone. A scanning electron microscope (SEM) was used to determine the origin of these colours, and the surface of the abalone was found to have a fine-scale diffraction grating structure of 2 μm groove width. From the diffraction patterns that were obtained using He-Ne and Nd: YAG lasers illuminating the shell, the groove density of the grating structure was derived. Good agreement was found between the groove density derived by diffraction experiments and that measured directly using the SEM. The strong iridescent colours of the shell are caused by diffraction which is the result of high groove density on the surface. The crystalline structure of the nacreous layers of the shell was studied using Fourier transform infrared spectroscopy (FTIR), and peaks at 700 cm^{-1} , 713 cm^{-1} , 862 cm^{-1} and 1083 cm^{-1} confirmed that the crystalline structure of the nacre of the shell is basically aragonite.

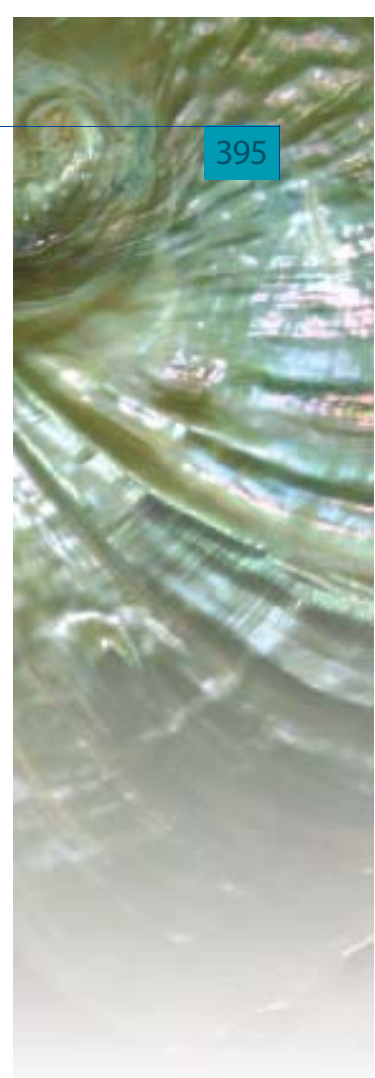
Keywords: aragonite, FTIR, *Haliotis glabra*, iridescence, SEM, shell structure

Introduction

The iridescent effect of colours or 'orient' caused by interference or diffraction from surface microstructures is a well-known phenomenon in plants, insects, the feathers of birds and seashells (Lee, 1997; Brink and Lee, 1998; Brink *et al.*, 1995; Tada *et al.*, 1998; Brink and Lee, 1999; Parker, 2000; Weiner *et al.*, 2000). Iridescent colours in seashells and pearls are usually attributed to a diffraction effect caused by an evenly grooved surface structure similar to that of a diffraction grating (Liu *et al.*, 1999; Nassau, 2001). Moreover interference of light in multiple-layered microstructure just below the surface can also result in iridescent colours (Nassau, 2001; Brink *et al.*, 2002) and studies on pearls have shown that iridescence is

caused by both diffraction and interference (Nassau, 2001). Nevertheless, diffraction and interference studies on the iridescent colours of abalone shell are still limited, although recently, X-ray diffraction studies were carried out on the microstructure of the shell of the red abalone (*Haliotis rufescens*) by DiMasi and Sarikaya (2004).

In this work, we studied a polished shell of the mollusc *Haliotis glabra*, commonly known as abalone, which showed very strong iridescent colours (Figure 1). This iridescent effect is even stronger than that observed for pearls and mother-of-pearl materials. The colours of the abalone shell under white light vary with changes in the angle of observation.



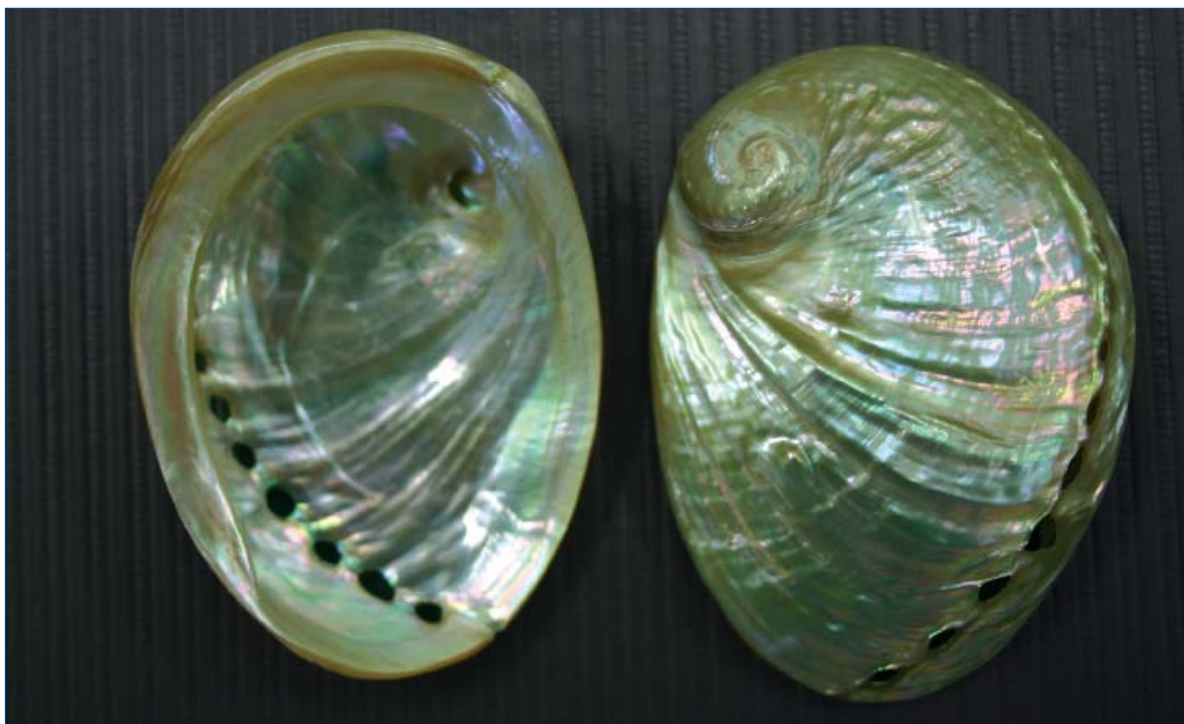


Figure 1: The iridescent colours of a polished shell of the mollusc *Haliotis glabra* (abalone).

Materials and experimental methods

The polished shell of a mollusc *Haliotis glabra*, indigenous to the seas around the Philippine islands was used in this investigation and is shown in Figure 1. Patches of colours of pink and blue-green are seen throughout the smooth polished surface. The surface of the whole abalone shell is polished with a diamond polishing compound to a final grade of 0.25 μm and then washed in ethanol to remove any traces of polishing residue. This method is similar to that of Brink *et al.*, 2002.

A He-Ne laser ($\lambda = 632.8 \text{ nm}$) and a Nd:YAG laser ($\lambda = 532 \text{ nm}$) were used to investigate the diffraction effect of the shell. A schematic diagram of the principal features of the laser diffraction experiment is shown in Figure 2. The laser beam was incident directly on the shell and the reflected beam (which is also diffracted) was captured on a screen. Measurements of the fringe separation x in the diffraction pattern were carried out on a white screen to an accuracy of $\pm 1 \text{ mm}$.

Scanning electron microscope (SEM) observations were carried out to study the microstructure of the shell sample. Before every experiment, the surface of the shell was cleaned using ethanol in order to remove any contaminant derived from handling. Samples of about 5 mm x 5 mm area were cut from the shell and examined up to magnifications of 7000x. Before the SEM experiments the samples were coated with a thin layer of gold to disperse the electrons and prevent charge build-up which would adversely affect the resolution of the micrograph. SEM work was carried out using a JEOL JSM – 5600LV SEM/EDX microscope with a working voltage of 20 kV.

To investigate the crystalline structure of the nacreous layers of the shell, a Perkin Elmer (Model Spectrum One) Fourier transform infrared (FTIR) spectrometer was used to record the spectra of the shell in the wavenumber range 450 to 4000 cm^{-1} . The accuracy of the absorption peaks was $\pm 1 \text{ cm}^{-1}$. Since pure shell material is opaque to most infrared radiation, a diluted sample in an infrared-transparent matrix of potassium bromide (KBr) is needed for FTIR work. The

shell material was ground to a fine powder, mixed with KBr, and compacted in a 10-tonne press to make flat circular pellets. These pellets are translucent and allow infrared light to pass through and be absorbed. The infrared transmission spectra were recorded to give absorption peaks for identification.

Results and discussion

In the diffraction experiments using the lasers, the incident laser beam is oriented at right angles to the shell surface giving a spot size of about 3 mm on the shell. The reflected beam shows a diffraction pattern on a screen with several orders of bright fringes or spots (*Figure 2*). The typical diffraction patterns of three bright spots are shown in *Figure 3(a)* and *(b)* for He-Ne and Nd:YAG lasers respectively. Higher orders of the diffraction fringes or spots are too weak to be observed. The phenomenon of diffraction patterns formed by the interference of reflected light rays at different angles from the fine grating structure of a surface is well established and described by Wilson and Buffa (1997). The bright fringes are not sharp since the groove microstructures are somewhat uneven across the surface, in contrast to the regularity of a compact disc.

In *Figure 3(a)* and *(b)* the 3 bright spots in the diffraction patterns of both lasers show that the fringe separation x for each pattern is quite uniform. The groove width

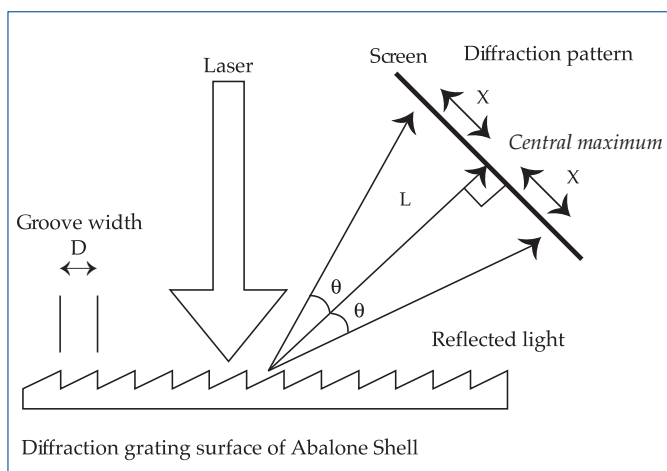


Figure 2: A schematic diagram of the laser diffraction experimental set-up.

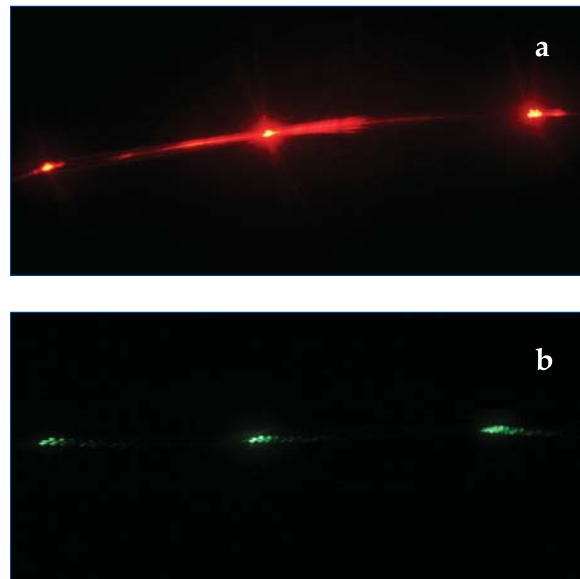


Figure 3: A typical laser diffraction pattern produced by the shell observed up to the first order ($n = 1$).
(a) He-Ne laser diffraction pattern ($\lambda = 632.8 \mu\text{m}$),
(b) Nd:YAG laser diffraction pattern ($\lambda = 532 \mu\text{m}$).

d of the grating can be calculated using the diffraction formula: $d = n\lambda/\sin\theta$ (Wilson and Buffa, 1997) where n is the order of the bright fringe, λ is the wavelength of light and θ is the angle of deviation as shown in *Figure 2*. Only the first order ($n = 1$) bright fringe at either side of the central maximum can be observed and used for calculations (*Figure 3*). The angle θ can be derived from the calculation of $\tan\theta = x/L$ where L is the distance from the point of incidence of laser light at the shell to the screen at the central maximum, as shown in *Figure 2*. In the diffraction experiments the measurements of groove width d were repeated at 5 different areas of the shell. For the He-Ne laser ($\lambda = 632.8 \text{ nm}$) diffraction experiment, L is 14.3 cm, the bright fringe separation x ranges from 4.7 to 5.0 cm, and the mean value of groove width d is found to be $1.97 \pm 0.05 \mu\text{m}$. Similar experiments using Nd:YAG laser ($\lambda = 532 \text{ nm}$) of $L = 13.7 \text{ cm}$ and x ranging from 3.6 to 4.6 cm give the mean value of groove width d to be $1.88 \pm 0.05 \mu\text{m}$. Using an overall average of $1.93 \pm 0.05 \mu\text{m}$ for the groove width, a groove density of 518 ± 13 grooves/mm for the grating structure of the shell surface has been derived. These results show that the strong iridescent colours of

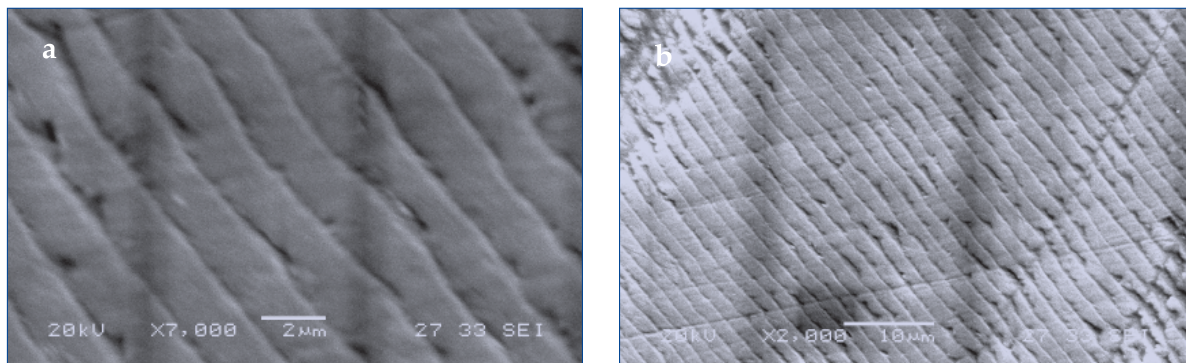


Figure 4: SEM micrographs showing typical groove structures on the shell surface. (a) Fine closely-spaced grooves of about 2 μm width, at magnification of 7000x (b) Fine closely-spaced grooves of about 2 μm width at magnification of 2000x.

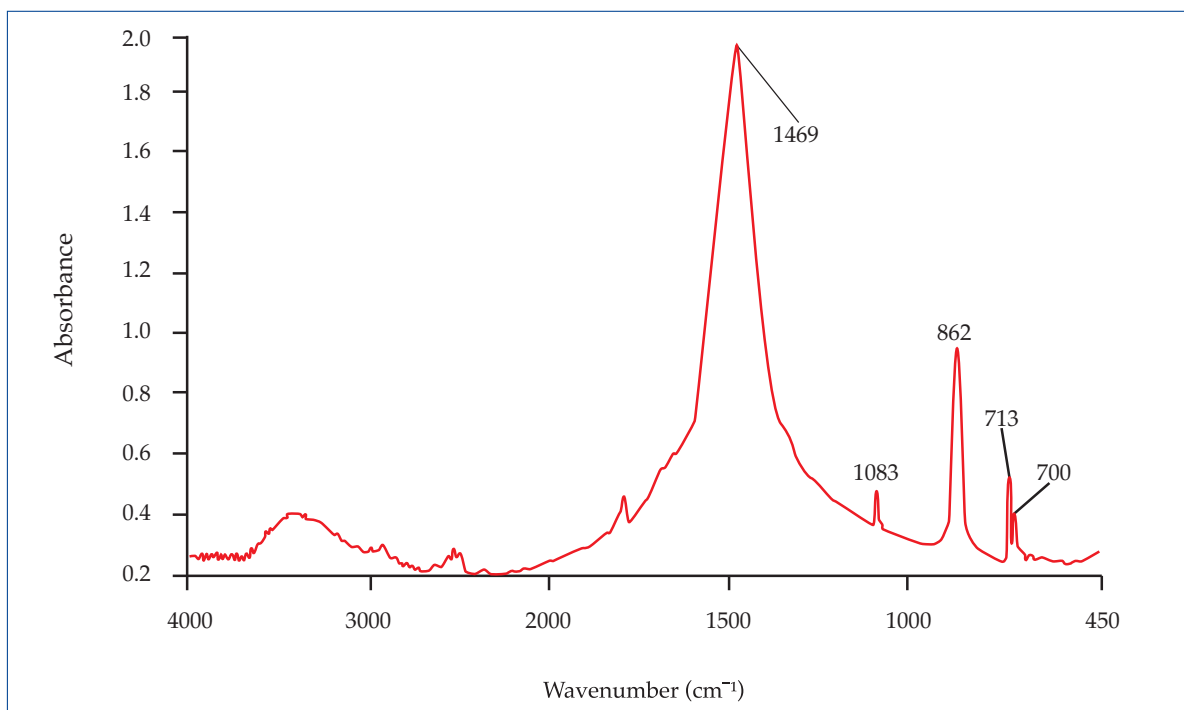


Figure 5: The FTIR spectrum of the nacreous layer of shell. Peaks at 700 and 713 cm^{-1} (from carbon-oxygen bond in-plane bending) and 862 cm^{-1} (out-of-plane bending) are characteristic of aragonite.

abalone can be correlated with this high groove density. A high groove density or low groove width which results in large deviation angle θ usually causes the iridescent colours to be strong. This is because a large θ allows the colours to be well separated, resulting in better observation of several distinct colours. In a previous investigation, iridescent colours of lower strength on the shell of *Pinctada margaritifera* were observed with a groove width of 3.38 μm and groove density of 296 grooves/mm (Liu *et al.*, 1999).

The microstructure of the various parts of the surface of the shell was also investigated

using the SEM. Figure 4(a) shows the typical groove structure of about 2 μm width at 7000x magnification. The pattern is found to be uniform over a larger area as shown in Figure 4(b) (magnification 2000x). Closer examination gives a value of $2.0 \pm 0.2 \mu\text{m}$ for the groove width with an estimated uncertainty of 10%. This results in a groove density of 500 ± 50 grooves/mm which is in good agreement with the value of 518 ± 13 derived from the laser diffraction experiments. The results indicate that the laser diffraction method can be used to derive the groove density of the fine grating

structure of a shell with a conservative estimate of uncertainty of about 10%. Furthermore, both investigations strengthen the concept that the iridescent colours are caused by the fine reflection grating structure of the abalone shell. This is very similar to the strong iridescent colours seen on the surface of a compact disc (Wilson and Buffa, 1997).

A Fourier transform infrared (FTIR) spectrum typical of the nacreous layers of the shell is shown in *Figure 5*. The absorption peaks at 700 cm^{-1} , 713 cm^{-1} , 862 cm^{-1} , 1083 cm^{-1} show that CaCO_3 in the nacreous layers of the shell has a structure that is basically aragonite (see Smith, 1999; and Baird and Soloman, 1979). Specifically, aragonite contains carbon-oxygen bonds which bend in-plane giving absorption peaks at 700 and 713 cm^{-1} , and bend out-of-plane giving a peak at 862 cm^{-1} . The largest absorption peak at 1469 cm^{-1} is typically observed for all crystalline forms of CaCO_3 . The peak is attributed to the carbon-oxygen stretching vibration in the molecule.

The infrared spectroscopy results are consistent with the SEM observations that the calcium carbonate layers are composed of aragonite, and are similar to the layers found in pearl (Landman *et al.*, 2001; Wada, 1999). A grating structure of pearl similar to that of the abalone in this investigation has also been observed by Landman *et al.* (2001).

Conclusion

The polished shell of the abalone *Haliotis glabra* shows very strong iridescent colours, mostly pink and blue-green. The cause of the strong iridescent colours was studied by examining the microstructure of the surface of the shell using SEM and diffraction laser energy. Regular $2\text{-}\mu\text{m}$ grooves were observed over a large area of the shell, and the laser diffraction experiments indicate that this grooved density (about 518 grooves/mm) can generate strong iridescent colours. The infrared absorption peaks using FTIR spectroscopy confirm the aragonite structure of the nacreous layers of the shell.

Acknowledgement

The authors are grateful for the financial support of National Institute of Education through the research grant RP7/02 TTL.

References

- Baird, T., and Soloman S.E., 1979. Calcite and aragonite in the eggshell of *Chelonia mydas* L. *J. exp. mar. biol. eco.*, 36, 295-303
- Brink D. J., Van der Berg, N. G., and Botha, A. J., 2002. Iridescent colours on seashell; and optical and structural investigation of *Helcion pruinosus*. *Appl. Opt.* 41, 717-22
- Brink, D. J., and Lee, M. E., 1998. Thin-film biological reflectors: optical characterization of the *Chrysidia croesus* moth. *Appl. Opt.* 37, 4213-7
- Brink, D. J., and Lee, M. E., 1999. Confined blue iridescence by a diffracting microstructure: an optical investigation of the *Cyandra opis* butterfly. *Appl. Opt.* 38, 5282-9
- Brink, D. J., Smit, J. E., Lee, M. E., and Moller, A., 1995. Optical diffraction by the microstructure of the wing of a moth. *Appl. Opt.* 34, 6049-57
- DiMasi, E., and Sarikaya, M., 2004. Synchrotron x-ray microbeam diffraction from abalone shell. *J. of Materials Research* 19, 1471-6
- Landman, N. H., Mikkelsen, P.M., Bieler, R., and Bronson, B., 2001. *Pearls, A Natural History*. Harry N. Abrams, New York, USA, 23-61
- Lee, D. W., 1997. Iridescent blue plants. *Am. Sci.* 85, 56-63
- Liu, Y., Shigley, J. E., and Hurwit, K. N., 1999. Iridescence color of a shell of the mollusc *Pinctada margaritifera* caused by diffraction. *Optics Express* 4, 177-82
- Nassau, K., 2001. *The physics and chemistry of color – the fifteen causes of color*. John Wiley & Sons, New York, USA, 247-77
- Parker, A. R., 2000. 515 million years of structural color. *J. Opt. A: Pure Appl. Opt.* 2, 15-28
- Smith, B., 1999. *Infrared Spectral Interpretation – A systematic approach*. CRC press, London, UK, 31-112, 171
- Tada, H., Mann, S. E., Miaoulis, I. N., and Wong, P. Y., 1998. Effects of a butterfly scale microstructure on the iridescent color observed at different angles. *Appl. Opt.* 37, 1579-84
- Wada, K., 1999. Formation and Quality of Pearls. *The Journal of the Gemmological Society of Japan* 20(1-4), 47-56
- Weiner, S., Addadi, L., and Wagner, H. D., 2000. Materials design in biology. *Materials Science and Engineering: C*, 11, 1-8
- Wilson, J. D., and Buffa, A. J., 1997. *College Physics*, Prentice Hall, New Jersey, USA, 747-50

WORKSHOPS

The autumn calendar of one-day workshops held at the Gem-A London headquarters

VALUING MODERN GEM-SET JEWELLERY

14 November

Guest lecturer Brian Dunn will start the day with a practical session on the identification of styles and method of manufacture of modern jewellery. A discussion will follow on the effects on value of gemstone treatments and synthesis.

Gem-A members £140.00 (non members £155.00)

VALUING ANTIQUE JEWELLERY

15 November

Guest lecturer Brian Dunn will start the day with a practical session on the identification of styles, method of manufacture and dating of antique jewellery. A discussion will follow on the effects on value the alteration or repair of a piece of jewellery.

Gem-A members £140.00 (non members £155.00)

GEMSTONES FOR CURATORS AND CONSERVATORS

21 November

Find out more about gems of the past and their use in jewellery with Dr Jack Ogden. The course will cover the history and characterisation of gems and their simulants, and how gem identification can help in assessments relating to dating, authentication and conservation practice.

Gem-A members £138.65 (non members £150.40)

GEM TRAITS

22 November

An opportunity to handle a wide selection of gemstones whilst learning about their beauty, rarity, durability, lore and history. Whether you work in the trade, are an interested hobbyist or you simply enjoy wearing gems in jewellery, this day is for you.

Gem-A members £122.20 (non members £135.13)

For further details on short courses and workshops and a booking form visit www.gem-a.info/education/londonWrkshops.cfm or call Claire on 020 7404 3334

New titles from Gem-A Instruments

ARTIFICIAL GEMSTONES

by MICHAEL O'DONOGHUE £30.00

GEMMOLOGY (3RD EDN)

by PETER READ £24.99

TIFFANY DIAMONDS

by JOHN LORING £25.95



PROFESSIONAL JEWELLERY

APPRAISING: JEWELLERY VALUATION

THEORY AND PRACTICE

by RICHARD H. CARTIER £17.00

THE NATIONAL GEM COLLECTION:

SMITHSONIAN INSTITUTION

by JEFFREY E. POST £14.95

Prices exclusive of postage and packing

Gem-A Instruments

27 Greville Street (Saffron Hill entrance)

London EC1N 8TN, UK

t: +44 (0)20 7404 3334

f: +44 (0)20 7404 8843

e: shop@gem-a.info

Diffraction Enhanced Imaging: a new X-ray method for detecting internal pearl structures

Jochen Schlüter¹, Michael Lohmann², Joachim Metge³
and Bernd Reime²

1. Mineralogical Museum, University of Hamburg, Grindelallee 48,
20146 Hamburg, Germany

2. HASYLAB at DESY Hamburg, Notkestrasse 85, 22607 Hamburg, Germany

3. GKSS Forschungszentrum Geesthacht GmbH, c/o DESY, 22603 Hamburg, Germany
Correspondence author's e-mail address: Jochen.schlueter@uni-hamburg.de

Abstract: *The X-ray based Diffraction Enhanced Imaging method (DEI) has been applied to examination of pearls of different origin. DEI images – especially of large pearls – indicate internal growth features more clearly than the usual X-radiographs and show structures which could not be made visible with conventional methods. The DEI method furthermore offers a tool for the separation of larger tissue-nucleated cultured pearls from natural freshwater pearls if conventional X-ray methods fail.*

Keywords: *cultured pearl, diffraction, pearl structure, pearl testing, radiograph, X-ray*

Introduction

Still the most sophisticated and reliable way to identify the nature of pearls is an examination by using various X-ray techniques. The combination of X-radiography, X-ray diffraction and X-ray luminescence can identify pearls in almost all cases (Kennedy, 1998; Schlüter and Rättsch, 1999).

X-ray diffraction, which produces indicative Laue patterns of a pearl's interior, always reveals the shell bead in bead-nucleated cultured pearls.

A radiograph shows internal pearl structures because the inorganic components (aragonite, calcite) are less radiolucent than their organic component (conchiolin). Due to the different absorption strengths of X-rays by these components a radiograph reflects

internal growth structure in different grades of shading.

With the interpretation of such X-ray images it is usually possible to distinguish natural pearls from tissue-nucleated cultured pearls like those from Asian freshwaters or from marine sources, and of course from bead-nucleated cultured pearls as well.

Finally X-ray luminescence separates fluorescent freshwater from non-fluorescent marine pearls, regardless of their natural or cultured origin.

With the appearance of large high-quality tissue-nucleated freshwater cultured pearls on the markets a new problem arises. Tissue nucleated pearls have irregularly shaped centres composed of conchiolin, a conchiolin-

aragonite mixture or tiny cavities initially caused by the implanted epithelial cells. However, in many pearls and especially in those of larger size, the fine central growth irregularity, which proves a pearl to be tissue-nucleated, can no longer be detected by conventional X-radiography. The large outer pearl body, which has grown like a natural pearl, around the tiny irregularity in the centre of the pearl conceals the fine differences in the X-ray absorption evoked by those irregularities, so that they are no longer visible on X-ray radiographs.

Actually, if a bead-nucleus is not detectable and no structures of tissue-nucleation are visible, a differentiation between natural marine pearls (oriental pearls) and tissue-nucleated cultured freshwater pearls can be done by a test of their X-ray luminescence. But such an investigation gives no documented proof for the origin of the pearl. There is still the possibility that the pearl under examination – if X-ray luminescence is visible – is a natural freshwater pearl.

Our team now has applied the Diffraction Enhanced Imaging method (DEI) to pearl examination. Pearls of different origin have been tested with this method and compared with results from different well known X-ray methods like conventional and digital radiography or computed tomography. Our studies, carried out at Hamburger Synchrotronstrahlungslabor (HASYLAB) at Deutsches Elektronen-Synchrotron (DESY), Hamburg, Germany, and European Synchrotron Radiation Facility (ESRF), Grenoble, France, show that detection limits for internal pearl structures and the resolution of the features with the DEI method are far superior to the results obtained from X-ray methods for pearl examination used to date.

Principles of DEI

For the new imaging method under development monochromatic radiation in the X-ray range is essential, and this

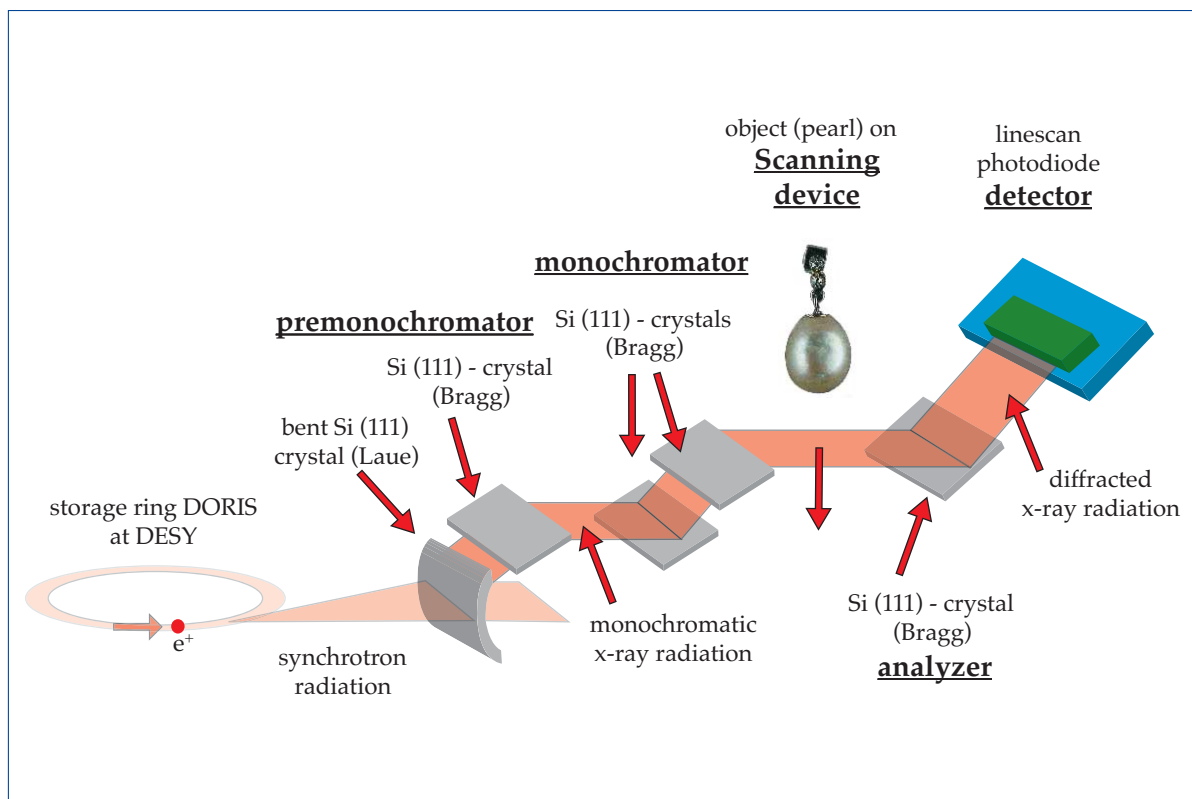


Figure 1: Schematic diagram of the experimental set-up. The incoming radiation is made monochromatic by perfect silicon crystals. This beam illuminates the pearl on the scanning device and is analysed with the analyser silicon crystals.

can be provided with sufficient intensity from synchrotron radiation. Synchrotron radiation with a spectrum from visible light wavelengths to hard X-rays is produced in particle storage rings, as for example the Doppel-Ring-Speicher (DORIS) at DESY. Synchrotron radiation is several orders of magnitude more intense than X-ray radiation from conventional X-ray tubes and has a very small divergence (opening angle). With the help of perfect silicon crystals, beam energies between 15keV and 60keV can be selected. Following Bragg's law, radiation (X-rays) with a certain energy is selected. This leads to a monochromatic X-ray beam with a bandwidth of about 10eV.

The principle of the DEI method (Chapman *et al.*, 1997) is based on the separation of scattered from non-scattered X-rays behind the imaged object. The small angle of scattering of the monochromatic X-ray beams in a sample is due to refraction at the boundaries of two materials with different refractive index. Therefore, the separation

between the direct and the refracted part of the beam allows an extreme enhancement of contrast in the images at the edges between the materials and thus enables distinction between different materials.

How results are obtained from the equipment

The DEI system at HASYLAB (Figure 1) consists of a tunable premonochromator with two silicon crystals and a second double crystal monochromator for precise selection of the energy. The 1 mm high and 5 cm wide beam illuminates the sample which is mounted on a vertically moving stage. Behind this scanning device the silicon analyzer crystal is installed, which separates the scattered and non-scattered beams. Finally, either a line detector with 25 μm pixel size or a CCD-camera with 5 μm pixel size records the images.

The angle dependence of the intensity of the X-rays within the accepted energy band

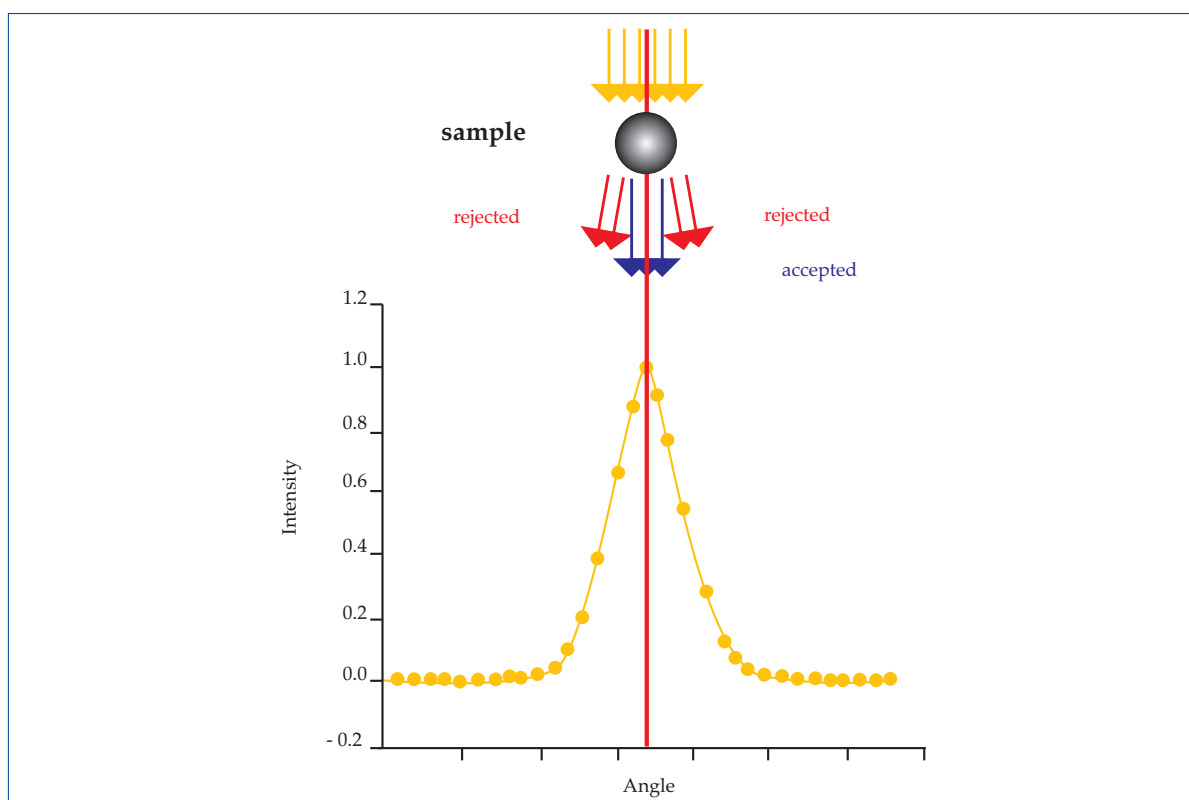


Figure 2a: The rocking curve of the analyser crystal in the monochromatic beam. The image is taken at the maximum intensity position.

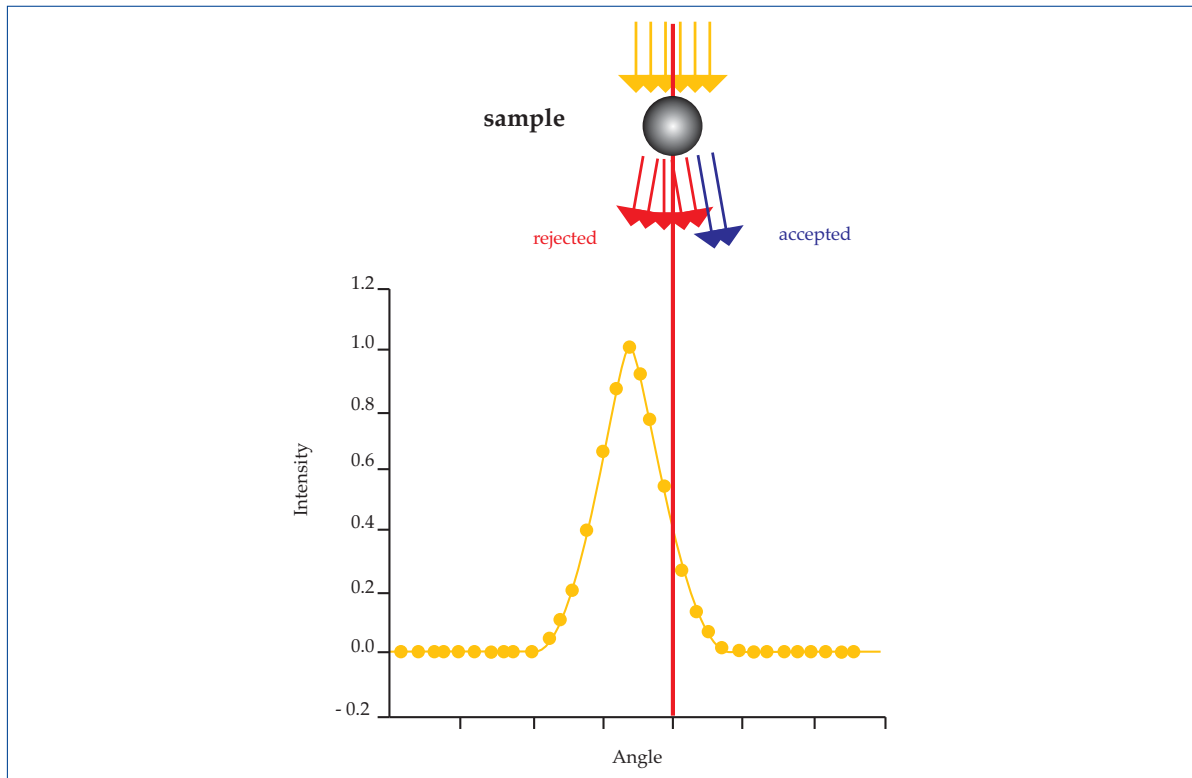


Figure 2b: Analyzer crystal at the high angle side of the rocking curve. Radiation scattered in a certain direction is enhanced or suppressed, respectively.

selected by a crystal is described by the so-called 'rocking curve' (Figure 2). The analyzer crystal is used to scan over the rocking curve of the monochromator crystal by changing its angle of incidence. If the angles of the two crystals exactly match (Figure 2a), then the X-rays which are scattered from the object are rejected. The resulting images are called 'top images'. If the angles of the two crystals are slightly detuned, the non-scattered beam is at the 'shoulder' of the monochromator's rocking curve (Figure 2b). Then the non-scattered X-rays are diminished, whereby the scattered part leads to a higher and a lower intensity, respectively, depending on the scattering direction, due to the slope of the rocking curve. In the latter set-up of the system the analyzer crystal is tuned first to the high angle side and then to the low angle side of the rocking curve (Figure 2b) and gives two shoulder images. A mathematical algorithm using both shoulder images delivers the 'refraction image' which clearly shows the boundaries of two materials with different refraction indices.

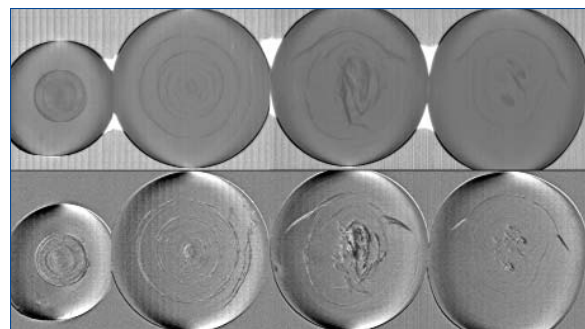


Figure 3: Comparison of two natural (left) and two tissue-nucleated freshwater pearls (right). The top row shows the 'top images' (as described in Figure 2a), whereby an unsharp-masking algorithm was applied, and the bottom row shows the 'refraction images'. The natural pearls reveal well-known concentric growth patterns whereas the two tissue-nucleated freshwater pearls show both concentric patterns which are less regular and major central growth irregularities.

Examination of different pearl types

Top and refraction images of two natural pearls produced with the DEI system clearly show concentric growth patterns as expected, but in a much more accentuated manner

than shown by conventional X-radiographs (Figure 3). In addition to concentric growth lines, circular central structures are visible in the DEI images of the natural pearls. They correspond to circular central shadows, which often can be observed in X-radiographs of natural pearls, and are due to conchiolin-rich centres.

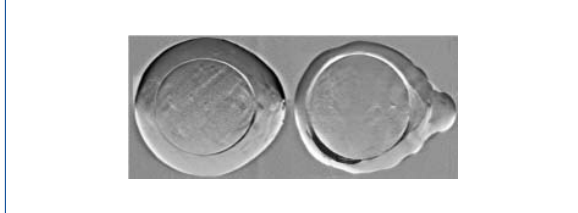


Figure 4: Oval (left) and drop-shaped (right) black, bead-nucleated cultured pearls from the Tuamotu Islands, French Polynesia: The 'refraction images' show the nuclei with outer nacreous layers. The 'refraction image' of the oval pearl in addition shows the laminated structure of the shell bead. The image of the drop-shaped pearl indicates gaps between the shell bead and the outer nacreous layer.

Bead-nucleated cultured pearls (Figure 4) clearly show the nucleus with outer nacreous layer as well as gaps between the shell bead and the nacreous layer. Rarely seen in conventional X-ray radiographs, one of the 'refraction images' in Figure 4 also indicates the laminated structure of the shell bead.

DEI images of tissue-nucleated cultured freshwater pearls reveal concentric growth lines in their outer parts around variform anomalies at or near the centre of the pearl (Figures 3 and 5), caused by organic-rich domains and/or tiny cavities. These structures correspond with the dark irregular shaped central features on X-radiographs of pearls of this type. They are indicative of tissue-nucleated growth and are the result of the initial behaviour and decay of the implanted tissue.

DEI images of tissue-nucleated marine pearls from NW-Australia, often referred to

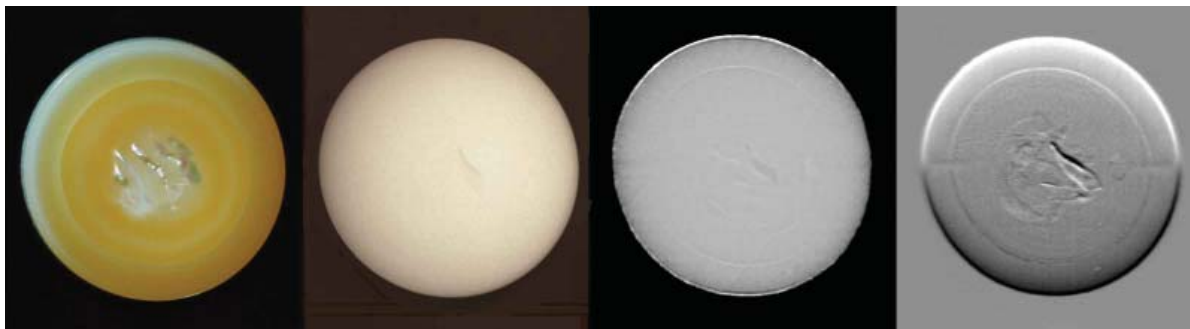


Figure 5: The images of a Chinese tissue-nucleated cultured freshwater pearl show (from left to right): the original pearl cut in half after examination to reveal its interior (Photo by K.-C. Lyncker); a conventional X-radiograph; a 'top image' using the DEI method; and a 'refraction image' using the DEI method. Compared to the conventional X-radiograph, the central growth irregularity and growth lines visible from the DEI images are clearer.

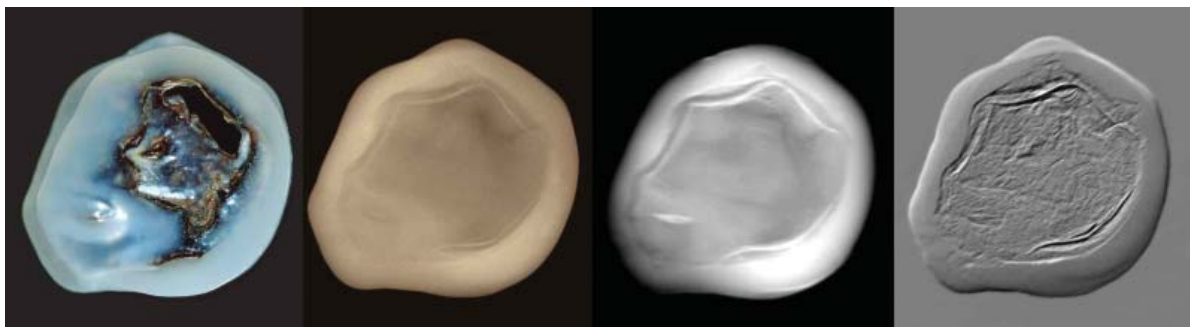


Figure 6a: This tissue-nucleated cultured marine pearl ('keshi') from Australian waters has a central cavity lined with pale brown organic material followed by a thin nacreous layer. Beginning with a fine open gap this sequence repeats itself towards the outer nacreous layer. The images show (from left to right): the original pearl sectioned after examination to reveal its interior (Photo by K.-C. Lyncker); a conventional X-radiograph; a 'top image' using the DEI method; and a 'refraction image' using the DEI method.

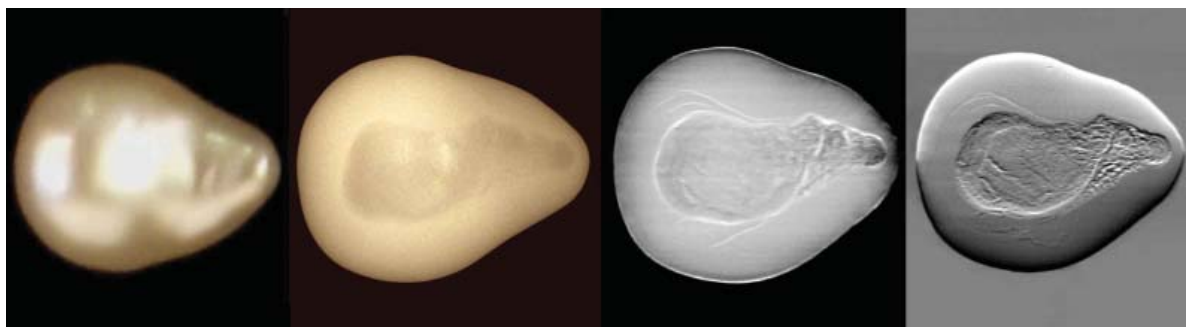


Figure 6b: These images of another tissue-nucleated cultured marine pearl from Australia show (from left to right): the original pearl (Photo by M. Müller), a conventional X-radiograph, a 'top image' and a 'refraction image' using the DEI method for comparison.

as 'South Sea keshis', presented very detailed structures (Figure 6a and b). To verify the structures visible in the DEI images, parts of one were removed to reveal its interior (Figure 6a). This pearl disclosed a large central cavity lined with pale brown organic material, followed by a thin nacreous layer. Beginning with a fine open gap this sequence repeats itself towards the outer nacreous layer. The internal structures of this 'keshi pearl' are most clearly portrayed within the DEI refraction image, demonstrating the potential of the DEI method to reveal even the finest growth structures.

Conclusions

The DEI method applied to pearls can reveal internal pearl structures formerly not visible using conventional X-ray methods. However, although the high specifications of the equipment mean that this method is too expensive for routine pearl testing, it nevertheless offers the opportunity to perfectly document internal pearl structures. Thus it is useful for scientific purposes and for large pearls whose value depends on determining their origin as tissue-nucleated pearls or as natural freshwater pearls.

Acknowledgements

We thank Dr A. Bravin, and P. Coan for the beamline support at ESRF as well as Dr R.-H. Menk and Dr L. Rigon from ELETTRA for fruitful discussion. We also thank Prof. Dr H. Vogel and Beatrice Vogel for stimulating the cooperation and for valuable

discussions. Thanks are due to K.-C. Lyncker for providing photographs and L. Schneider, Martin Wolf Company, for providing natural pearls. The DEI project is supported by the European Commission under contract number HPRI-CT-1999-50008.

References

- Chapman, D., Thomlinson, W., Johnston, R.E., Washburn, D., Pisano, E., Gmür, N., Zhong, Z., Menk, R., Arfelli, F., and Sayers, D., 1997. Diffraction enhanced X-ray imaging. *Phys. Med. Biol.*, 42, 2015-25
- Kennedy, S.J., 1998. Pearl identification. *Australian Gemmologist*, 20, 2-19
- Schlüter, J., and Rättsch, C., 1999. *Perlen und Perlmutter*. Ellert & Richter-Verlag, Hamburg, 176 pp

A microscopy-based screening system to identify natural and treated sapphires in the yellow to reddish-orange colour range

Dr Karl Schmetzer¹ and Dr Dietmar Schwarz²

1. Taubenweg 16, D-85238 Petershausen, Germany

2. Gübelin Gem Lab, Maihofstr. 102, CH-6006 Lucerne, Switzerland

Abstract: Features visible under a microscope of untreated, heat-treated and beryllium-diffusion-treated yellow, orange and reddish-orange sapphires, including padparadschas, are presented. A microscopy-based screening system for recognition and distinction of untreated, heat-treated and diffusion-treated sapphires combines structural features such as growth structures, colour zoning and inhomogeneous colour distribution patterns with the visual appearance of inclusions. Spectra and chemical compositions may be added to these microscopic characteristics and applied to an evaluation of samples of unknown origin and unknown treatment history. These properties combine to form a type of locality-specific data set, and are considered in the light of present knowledge about treatment techniques. The screening system allows the recognition of most untreated or heat-treated samples from Sri Lanka and Montana, U.S.A., and their distinction from beryllium-diffusion-treated samples from Sri Lanka, Montana, U.S.A., Ilakaka, Madagascar, and Songea, Tanzania.

Keywords: absorption spectroscopy, beryllium diffusion, colour zoning, growth structures, heat-treatment, inclusions, padparadscha, sapphire, screening system, trace-element chemistry

In a previous paper (Schmetzer and Schwarz, 2004) we summarised the knowledge of causes of colour in untreated, heat-treated and diffusion-treated orange and pinkish-orange sapphires (Figure 1a, b, c, d). The present paper deals with methods for the recognition of beryllium-diffusion-treated sapphires in the yellow, orange or reddish-orange colour range and for distinction of these sapphires from different types of untreated or heat-treated samples. The paper consists of three parts:

Part I: Introduction; Materials and methods; Alteration of inclusions

Part II: Growth structures; Colour zoning and inclusions; Chromium and iron contents; Spectra of sapphires from Sri Lanka, Montana, Ilakaka and Songea

Part III: A microscopy-based screening system; Case studies; Conclusions



PART I

Introduction

Orange sapphires 'enhanced' by beryllium diffusion treatment at elevated temperatures appeared on the market at the end of 2001 (see, e.g., McClure *et al.*, 2002). According to trace-element analyses, the new type of treated sapphires, especially samples from Songea, Tanzania, and Ilakaka, Madagascar, contained elevated beryllium concentrations, with the highest amounts of beryllium detected in the rims of the stones. It was suggested that Thai treaters first used this new heat treatment process on stones which did not respond to heat treatment with any colour improvement, e.g. purplish to purple Songea or Ilakaka material, which was not transformed to bright ruby or pink sapphire.

However, for proof that a sample has undergone beryllium diffusion, direct determination of beryllium content in the 5 to 40 ppm range in corundum is necessary using SIMS (McClure *et al.*, 2002; Wang and Green, 2002; Emmett *et al.*, 2003) or LA-ICP-MS (Peretti and Günther, 2002; Hänni, 2002; Hänni and Pettke, 2002; Fritsch *et al.*, 2003; Peretti *et al.*, 2003; Pisutha-Arnond *et al.*, 2003, 2004a). Both methods require highly sophisticated instrumentation and are extremely costly; thus, they are not useful as routine techniques for the examination of larger quantities of sapphires, or for small stones.

To overcome these problems, it was recently announced that LIBS might be useful as a somewhat cheaper routine method for quantitative beryllium determination in corundum (Hänni *et al.*, 2004; Krzemnicki *et al.*, 2004; Themelis, 2004). LIBS is a technique applied to a great number of analytical problems (see, e.g., Singh *et al.*, 1998) and has already been applied successfully for

beryllium determination (Radziemski and Cremers, 1985). Nevertheless, its cost still means that this method will be limited to laboratories.

Consequently, the distinction of treated and untreated samples (Figure 1a, b, c, d) and the definitive detection of any type of treatment by use of traditional gemmological methods, e.g. by microscopic examination, is still one of the major challenges for a gemmologist.

According to Emmett *et al.* (2003), at that time there were only two reliable criteria



Figure 1a: Untreated padparadschas from Sri Lanka, range of samples from 4.51 to 9.05 ct. Photo by M. Glas.



Figure 1b: Different types of orange or reddish-orange sapphires from Sri Lanka; untreated chromium-bearing sample (left), heat-treated chromium-bearing sample (centre) and heat-treated chromium-free sample (right); range of samples from 1.45 to 2.17 ct. Photo by M. Glas.

Abbreviations used in this article for equipment

EDXRF	Energy-dispersive X-ray fluorescence
LA-ICP-MS	Laser ablation-inductively coupled plasma-mass spectroscopy
LIBS	Laser-induced breakdown spectroscopy
SIMS	Secondary ion mass spectroscopy



Figure 1c: Beryllium-diffusion-treated chromium-free sapphires from Sri Lanka; range of samples from 0.78 to 1.66 ct. Photo by M. Glas.



Figure 1d: Beryllium-diffusion-treated sapphires from Ilakaka, Madagascar; range of samples from 1.10 to 1.47 ct. Photo by M. Glas.

for the recognition of diffusion-treated and untreated sapphires:

- | untreated sapphires are only recognisable if there is definite proof of the presence of undistorted inclusions. Samples which show inclusions in the 'natural' state, i.e. neither altered nor decomposed nor partly molten mineral inclusions, constitute such proof;
- | beryllium-diffusion-treated sapphires may show surface-conformal colour zoning with varying penetration depth into the faceted stone. This feature is common in many sapphires produced in the early months and years of beryllium treatment.

Nowadays, however, diffusion-treated sapphires from Thailand, occasionally even labelled 'deep diffusion treatment' (Figure 2a, b, c, d), are less likely to possess this feature.

One must also guard against natural material, sometimes with complex colour zoning (Figure 3a, b; see also Hänni and Pettke, 2002) which has been occasionally mistaken for a rim caused by diffusion treatment.

Some microscopic inclusion features have been used as 'highly indicative evidence' for beryllium diffusion treatment (Emmett *et al.*, 2003). However, because of the often similar appearance of altered inclusions in simply heat-treated and diffusion-treated sapphires (see Box A), a distinction between these two types of material based on microscopic observations is not easy.

According to Notari *et al.* (2003), the observation of orange or red homogeneous or inhomogeneous luminescence may also be useful in detecting beryllium-diffusion-



Figure 2a: Diffusion-treated originally pink or purplish-pink sapphire of 1.44 ct originating from Ilakaka, Madagascar; this sample was labelled 'deep diffusion treated' in Thailand. Photo by M. Glas.

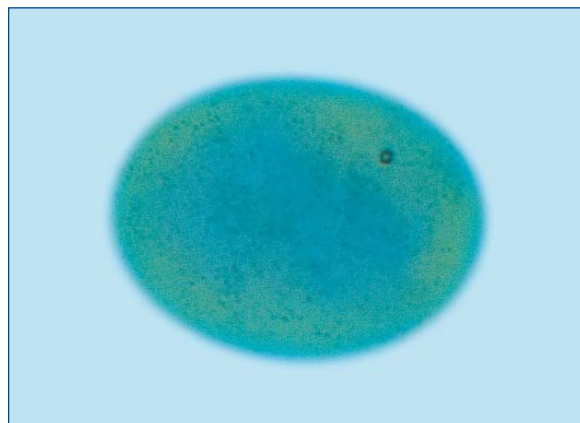


Figure 2b: Occasionally a distinct colour boundary between core and rim is still visible in immersion in beryllium-diffusion-treated sapphires as seen in the sample pictured in Figure 2a. In many stones, however, this boundary is not visible. Photo by K. Schmetzer.



Figure 2c: Diffusion-treated originally pink or purplish-pink sapphire of 1.29 ct originating from Ilakaka, Madagascar. Photo by M. Glas.

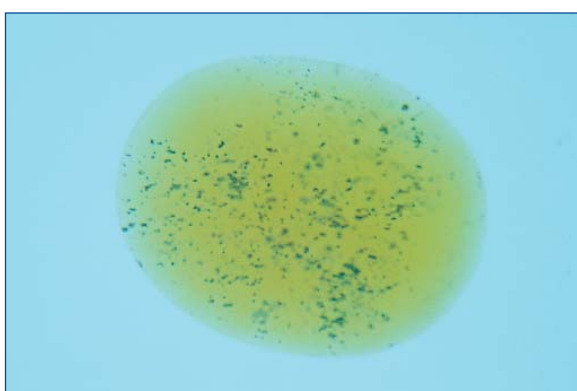
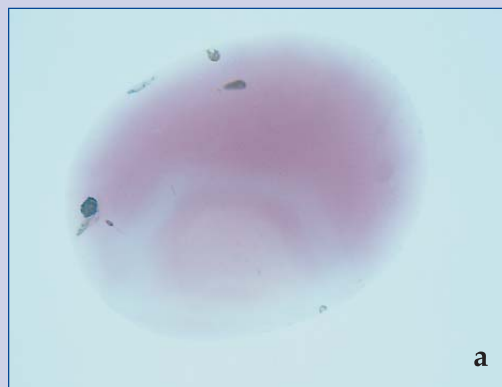


Figure 2d: In the sample pictured in Figure 2c, no distinct colour zoning between rim and core is visible; only numerous tiny inclusions are seen. In the past, the diagnostic rim/core boundary was best seen in beryllium-diffusion-treated Ilakaka sapphires, simply because these gemstones do not show any growth pattern and colour zoning in the untreated state. Photo by K. Schmetzer.

treated sapphires. However, red fluorescence caused by chromium could mask any orange fluorescence caused by beryllium, and a special red colour filter, the observation of luminescence under immersion, or luminescence spectroscopy may be needed to make a final decision.

Only limited information has been presented about colour zoning other than describing the rim/core boundary which is related to the diffusion range and/or the depth of colour change in the diffusion-treated samples. In addition, a comparison of beryllium-diffusion-treated samples according to the locality of origin of the untreated material with untreated padparadscha from Sri Lanka and simple heat-treated sapphires in the same colour range (i.e. treated without Be-diffusion) has



a



b

Figure 3: Even in immersion, the colour zoning of untreated Songea rubies and sapphires (a) may closely resemble the pattern observed for diffusion-treated material (b) from the same locality; sample (a) 0.54 ct, sample (b) 0.75 ct. Photos by K. Schmetzer.

not been addressed in detail. At present, the known heat-treated orange or reddish-orange sapphires are mainly from Sri Lanka and Montana, U.S.A. (Notari, 1996, 1997; Emmett and Douthit, 1993).

The aim of the present paper is to fill – at least partly – this gap and to assess whether a screening technique for the distinction of treated and untreated samples in the ruby – yellow sapphire colour series, is a practical possibility with traditional microscopic methods. In addition, we have tried to evaluate a combination of these with gemmological laboratory techniques such as absorption spectroscopy or trace-element analysis. The aim is to find specific properties or a combination of features which would avoid costly quantitative determination of beryllium contents, and allow at least

some sapphires, including smaller stones, to be identified as untreated, heat-treated or diffusion-treated sapphires.

The techniques applied in the present research are traditional microscopic techniques and – more or less – the methods that are used for origin determination of sapphires by laboratories, i.e. determination of microscopic properties (growth structures and colour zoning, inclusions) with and without immersion liquids, absorption spectroscopy in the visible and ultraviolet range, and – in some instances – determination of colour-causing trace-elements such as Ti, V, Cr, and Fe by EDXRF spectroscopy. In other words: the present study was performed to evaluate whether the number of samples that can be determined as untreated, heat-treated or beryllium-diffusion-treated can be increased by combining locality information with present knowledge about properties of these different categories of samples.

As with origin determination of sapphire, which depends on a sufficient number of samples with characteristic properties related to a specific natural source, it was always expected that even a combination of techniques could fail to identify the treatment status if insufficient samples possessed significant features. This situation is comparable with that of high-pressure high-temperature (HPHT) treated diamonds, some of which have properties which overlap with those of untreated type IIa natural diamonds (see, e.g., Fisher and Spits, 2000; Collins 2001). The screening technique presented here for beryllium-diffusion-treated sapphires is comparable to the screening technique for HPHT-treated diamonds as developed by De Beers (Lawson, 2002).

Materials and methods

For this study 279 sapphires were added to the research material (349 sapphires) used earlier (see Schmetzer and Schwarz, 2004). Most new samples originated from or belonged to four additional groups of samples, i.e. diffusion-treated sapphires from Sri Lanka, and untreated, heat-treated and diffusion-

treated corundums from Montana, U.S.A. In total, we examined 628 corundum samples for this research project; an overview is given in *Table I*.

All samples were highly transparent, gem-quality rubies or sapphires, ranging from about 0.10 ct to 9 ct in weight, obtained from the trade, mostly in Europe and Thailand, from private collections, or from colleagues in gemmological laboratories. Three lots of diffusion-treated samples were specially prepared from rough of known origin, from Sri Lanka and Montana. Most samples were faceted gemstones, but we also examined some rough specimens (mainly from Montana) and numerous slices polished on both sides; the latter were prepared mostly from corundum lots which were specially diffusion-treated for us (see *Table I*).

Untreated lots of Montana sapphires, mostly in the yellowish-green, bluish-green or blue colour range and a few very pale pink sapphires, were available from two major localities which have been commercially mined in the past, i.e. from the Rock Creek and Missouri river deposits. Two lots of heat-treated samples in the orange to reddish-orange colour range were submitted from private collections and from the trade. The known history of these lots excluded any treatment by diffusion.

To complete the study and to investigate any possible overlap between heat-treated and diffusion-treated material from Sri Lanka and Montana, one of the authors (DS) obtained one parcel of diffusion-treated yellow Sri Lankan material in the Thai trade. An additional lot of Sri Lankan geuda material which had become colourless after ordinary heat treatment was diffusion-treated by J. Emmett. The technique applied is described in detail by Emmett *et al.* (2003). Because some Montana sapphires can be heat-treated to orange or reddish-orange, two lots of originally yellowish-green, bluish-green or blue Montana sapphires were diffusion-treated by J. Emmett and submitted for this research project.

The colour distribution of all samples was studied by immersion in methylene iodide, simply placing the samples on a diffused-light box in a Petri dish. Although the colour

Table I: Sources, colours, treatment history and causes of colour of corundums used in this study.

Locality	Colour	Type (number of samples examined)	Absorption bands	
			Dominant	Sub-ordinate
Sri Lanka	yellow	untreated (16)	thermally unstable colour centres	Fe ³⁺
	yellow, yellowish-orange or orange	heat-treated (67)	thermally stable colour centres	Fe ³⁺
	yellow, yellowish-orange or orange	diffusion-treated (43)	thermally stable colour centres	Fe ³⁺
	yellowish-orange, orange, pinkish-orange, reddish-orange	untreated (46)	thermally unstable colour centres, Cr ³⁺	Fe ³⁺ Fe ²⁺ /Ti ⁴⁺
	orange, pinkish-orange, reddish-orange	heat-treated (18)	thermally stable colour centres, Cr ³⁺	Fe ³⁺
Montana, U.S.A.	yellowish-green, bluish-green, blue, rarely pink	untreated (100)	Fe ³⁺ Fe ²⁺ /Ti ⁴⁺	Cr ³⁺
	orange to pinkish-orange or reddish-orange, brownish-orange	heat-treated (20)	thermally stable colour centres, Cr ³⁺ , some also Fe ³⁺	Fe ³⁺
	yellow, yellowish-orange, orange	diffusion-treated (85)	thermally stable colour centres, Fe ³⁺ ,	Cr ³⁺
Ilakaka, Madagascar	pink, purplish-pink, purple, purplish-violet, violet	untreated (75)	Cr ³⁺ Fe ²⁺ /Ti ⁴⁺	Fe ³⁺
	yellowish-pink, yellowish-orange, brownish-orange, orange brown, yellowish-brown	untreated (14)	Cr ³⁺ Fe ³⁺	
	pink, slightly purplish-pink	heat-treated (10)	Cr ³⁺	Fe ³⁺ Fe ²⁺ /Ti ⁴⁺
	brownish-orange	heat-treated (1)	thermally stable colour centres, Cr ³⁺	Fe ³⁺
	yellowish-orange, orange, pinkish-orange, orangey-red, reddish-orange, brownish-orange	diffusion-treated (49)	thermally stable colour centres, Cr ³⁺ , some also Fe ³⁺	Fe ³⁺
Songea, Tanzania	colourless to red or pink, purplish-red, purple, violet ^a	untreated (22)	Cr ³⁺ Fe ²⁺ /Ti ⁴⁺	Fe ³⁺
	colourless to red or pink, purplish-red ^a	heat-treated (10)	Cr ³⁺	Fe ³⁺ Fe ²⁺ /Ti ⁴⁺
	colourless to yellowish-orange, orange, or reddish-orange ^a	diffusion-treated (52)	thermally stable colour centres, Cr ³⁺	Fe ³⁺

^a some are colour-zoned with a colourless core and an intensely coloured rim

distribution within the samples can be seen with the naked eye, examination with a loupe (10 x) or with a microscope at low magnification (10 x to 20 x) gives better results. Exact determinations of growth structures and colour zoning related to growth patterns were performed with a horizontal immersion microscope using a special sample holder with two rotation axes and specially

designed eye-pieces (Schmetzer, 1986; Kiefert and Schmetzer, 1991; see also Smith, 1996). One could also use a vertical microscope with a sample holder which allows rotation and orientation of the sapphire in an immersion cell or a Petri dish.

Inclusions were studied using different microscopes and lighting conditions both with and without immersion liquid. A few

inclusions were identified by laser Raman microspectrometry using a Renishaw Raman microprobe or by X-ray powder diffraction. From other unpublished research projects describing untreated Ilakaka or Songea material (see *Table 1*), some samples with inclusions already identified by Raman microprobe were available for comparison.

Trace-element contents of 182 samples were analysed by EDXRF spectroscopy. These analyses were performed with a Tracor Northern Spectrace 5000 system, using a program specially developed for trace element geochemistry of corundum. The samples for chemical analyses (Sri Lanka 36, Madagascar 84, Tanzania 42, U.S.A. 20) were selected

to cover the full range of colours seen in untreated, heat-treated and diffusion-treated material from all four sources, although with this technique one is unable to detect the presence of light elements such as beryllium.

Trace-element contents and distribution in two colour-zoned diffusion-treated samples were investigated using LA-ICP-MS.

Absorption spectra of all samples were recorded in the UV-visible-NIR range with both a Leitz-Unicam SP 800 UV-Vis spectrophotometer and a Perkin-Elmer Lambda 19 spectrophotometer. Polarised or non-polarised spectra were recorded according to the orientation of faceted gemstones, rough crystals or simply polished slices.

BOX A: Alteration of inclusions upon heat treatment and diffusion treatment of corundum

Because low oxygen pressure inhibits development of the orange colour centre, Be-diffusion treatment of sapphires is generally performed in oxidizing atmospheres (Emmett *et al.*, 2003). In the 1990s, special furnaces with Kanthal Super 1900 molybdenum disilicide heating elements allowed heat treatment of corundum for longer periods at temperatures up to 1820 C in an oxygen-bearing environment. Special designs allowed treatment up to this temperature under pressures between 5 and 100 atmospheres, especially to reduce the times necessary to develop the desired colour change (*Figure 4*). With Zircothal (yttrium-stabilised zirconium oxide) heating elements, heat treatment of corundum in oxidising atmospheres at temperatures up to 2000 C can be performed. Furnaces of the types mentioned above, i.e. with both types of heating elements with or without high pressure design, have been available in Thailand since before 1995 (H. Linn, pers. com., 2002, 2003). These furnaces were used for several years for 'simple' or 'normal' heat treatment of ruby and sapphire before Be-diffusion treatment started commercially, probably in 2001 (see Coldham, 2002).

Other furnaces used for commercial heat treatment of corundum at temperatures up to at least 1850 C are fired by gas (T. Häger, pers. com., 2003).

Dissolution of rutile needles or larger crystals and diffusion of titanium within the corundum lattice takes place above 1550 C. Thus, the observation of residues of rutile needles or diffusion haloes around rutile crystals only indicates heat treatment above about 1550 C. Most silicate inclusions and apatite (see Adolfsson *et al.*, 1999) decompose or melt at temperatures below 1500 C, but zircon, monazite and xenotime commonly survive. Melting temperatures of 1995 C for xenotime and between 2045 and 2072 C for natural and synthetic



Figure 4: High temperature furnace 'ruby star' that allows commercial treatment of corundum in oxidising environment at temperatures up to 1820°C and pressures up to 100 bars; courtesy of Linn High Therm GmbH, Eschenfelden, Germany.

monazite-type compounds have been determined (Hikichi and Nomura, 1987; Hikichi *et al.*, 1998) close to that of corundum. Furthermore, monazite is considered as an extremely heat-resistant material and stable with aluminium oxide under high temperatures, at least up to 1750 C (Morgan and Marshall, 1995; Morgan *et al.*, 1995; Hay and Boakye, 2001; Zhang and Guan, 2003). A similar high temperature stability with aluminium oxide is also expected for xenotime (Kuo and Kriven, 1995). Thus, inclusions of these minerals can survive heat treatment of sapphires and rubies at elevated temperatures. This indicates that even samples heated up to 1750 or 1800 C can contain monazite or xenotime inclusions which are neither melted nor otherwise decomposed by the treatment process.

Zircon crystals are also common inclusions in sapphires and may be used as indicators for high temperature treatment. As inclusions in corundum, pure zircons are stable up to about 1685 C. This temperature may decrease somewhat for impure natural zircons which are variable in chemical composition. Zircon is decomposed to tetragonal ZrO_2 and cristobalite above this temperature (Butterman and Forster, 1967). Melts in the system $Al_2O_3-ZrO_2-SiO_2$ coexisting with crystalline ZrO_2 indicate a heat treatment temperature above 1750 C (Rankin and Edwards, 2003). Consequently, the decomposition of zircon and other inclusions and the production of melt upon heat treatment (see also Emmett *et al.*, 2003) occur in the temperature range used for heat treatment of corundum before Be-diffusion treatment started commercially.

The papers published since the first recognition of Be-diffusion-treated sapphires on the market have presented details on the appearance of various types of inclusions that changed dramatically according to the high temperatures applied in the treatment (Figure 5a, b). Although there are comments by a number of authors that Be-diffusion treatment is performed at higher temperatures than 'normal' heat treatment in the range of 1600 to 1750 C (see, e.g., Emmett *et al.*, 2003) it has already been successfully performed at temperatures between 1625 and 1775 C by Themelis (2003), personal comments from others suggest that heat treatment was performed in the past at temperatures up to and even above 1800 C. The average maximum temperatures used in the beryllium diffusion process may be somewhat higher than those used for 'normal' heat treatment in the past, i.e. without adding colour-causing trace-elements to diffuse into the corundum lattice. But, because there is an almost complete overlap of temperature ranges used in both processes, no single microscopic inclusion feature described so far can be used to determine whether a sapphire is diffusion-treated or simply heat-treated.

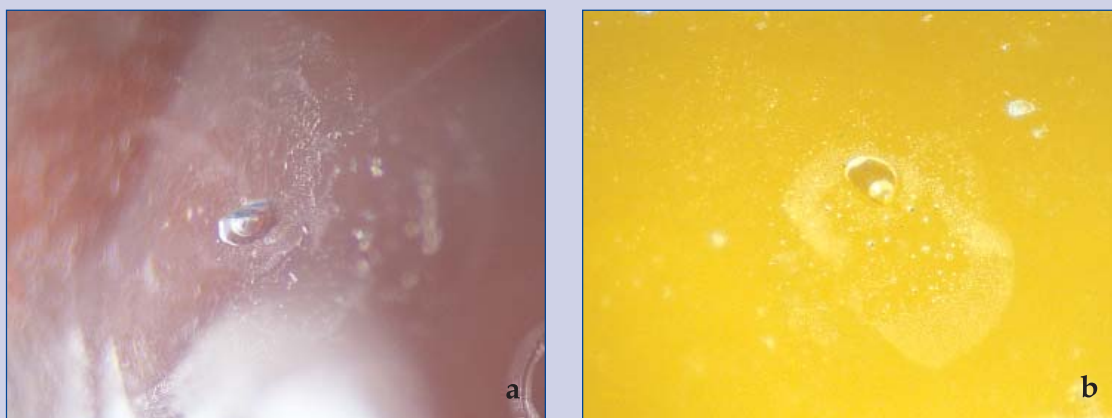


Figure 5: Because the temperature ranges of the two forms of treatment can overlap, the inclusion features observed in heat-treated and diffusion-treated sapphires (here a sort of bubble surrounded by transparent solid material) may closely resemble each other as seen in a heat-treated pinkish-orange Montana sapphire (a) and in a diffusion-treated yellowish-orange Montana sapphire (b). 50x. Photos by L. Kiefert.

PART II

Growth structures

General remarks

In the past, growth zoning has been found to be extremely helpful in establishing the locality of origin of rubies and sapphires. As will be shown below, growth structures combined with colour zoning can provide key identification features for the recognition of untreated, heat-treated and diffusion-treated sapphires.

Growth structures in the form of series of parallel growth lines may or may not be combined with colour zoning. All parts of a faceted sapphire which are related to one series of parallel growth lines are called growth sectors. Upon heat treatment, specific colours are generally developed only in some growth sectors of a crystal, e.g. in rhombohedral r sectors, or with different intensities in different growth sectors, e.g. in rhombohedral r and in dipyrmidal n sectors. Diffusion treatment may be superimposed on colour zoning and cause dramatic changes, but growth zoning, i.e. the specific growth pattern of a crystal, is not affected by heat or diffusion treatment. Thus, the common growth patterns of the sapphires are described for first untreated, then 'normally' heat-treated and finally Be-diffusion-treated samples.

Sri Lanka

Rough padparadscha crystals from Sri Lanka are normally elongated along the c -axis with barrel-shaped to dipyrmidal habit (see, e.g., Crowningshield, 1983). The hexagonal dipyrmidal crystals of this material frequently show growth striations with an orientation perpendicular to the c -axis.

The microscopic examination in immersion shows the presence of growth lines parallel to the basal pinacoid c {0001}, parallel to different second-order hexagonal dipyrmidal faces such as z {22 $\bar{4}$ 1}, w {11 $\bar{2}$ 1}, and n {22 $\bar{4}$ 3} and parallel to the positive rhombohedron r {10 $\bar{1}$ 1}. In examining faceted stones, checking three orientations of the sapphire under the microscope, should allow us to reconstruct the external morphology of the rough crystal (Figure 6).

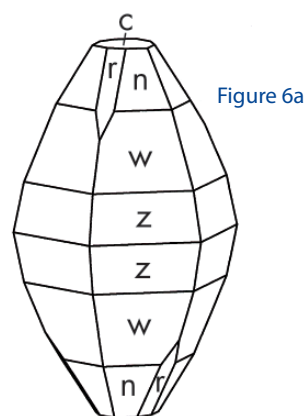


Figure 6a

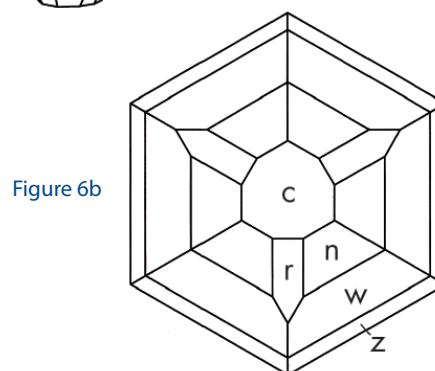


Figure 6b

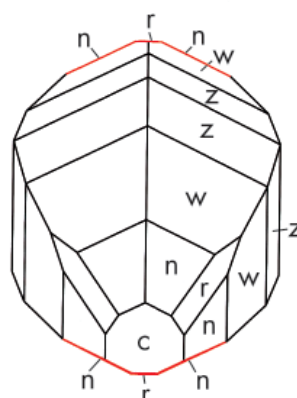


Figure 6c

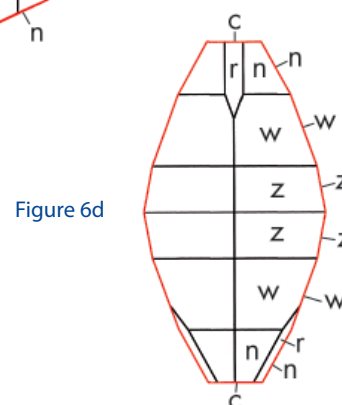


Figure 6d

Figure 6: Typical habit of padparadscha from Sri Lanka consisting of the basal pinacoid c , different hexagonal dipyrmidal z , w , and n and the positive rhombohedron r ; (a) clinographic projection, (b) view parallel to the c -axis, (c) view at an angle inclined at about 30° to the c -axis, (d) view perpendicular to the c -axis. The traces of crystal faces which are parallel to the direction of view and, thus, can be seen in the microscope are indicated in red in Figures b, c and d.

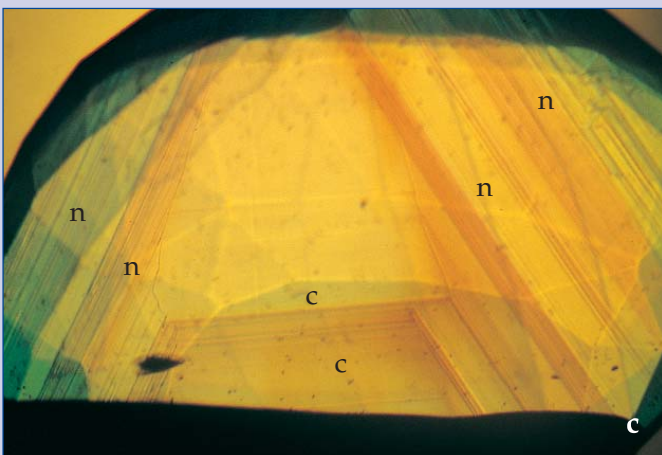
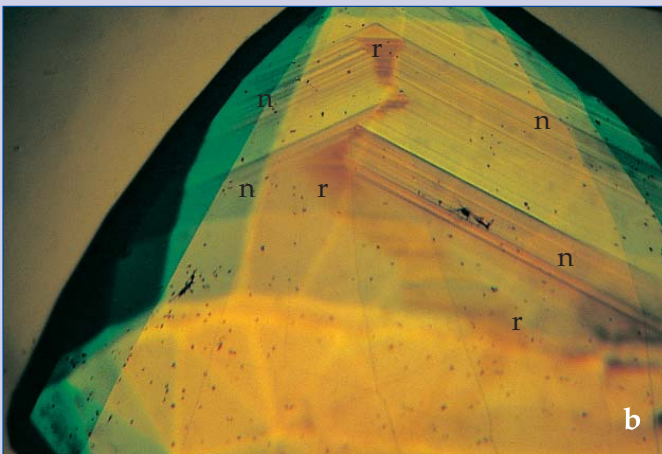
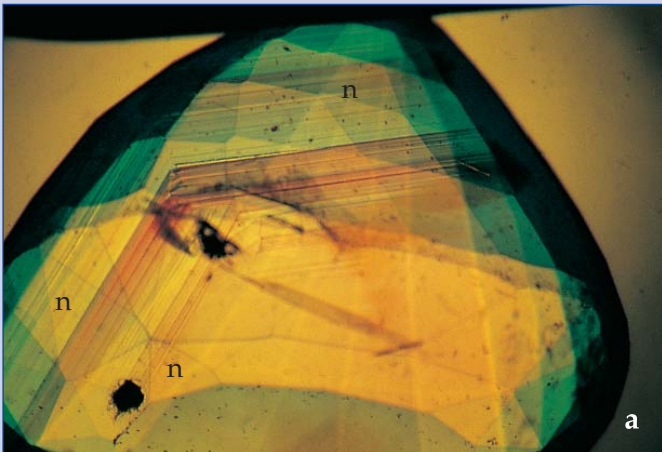


Figure 7: Growth pattern and colour zoning in a heat-treated padparadscha from Sri Lanka: (a) view inclined at about 30° to the c -axis, two hexagonal dipyramids n are visible, (b) view inclined at about 30° to the c -axis, two hexagonal dipyramids n and the rhombohedron r are visible, (c) view perpendicular to the c -axis, two hexagonal dipyramids n and the basal pinacoid c are visible. 40x. Photos by K. Schmetzer.

The first orientation is a view parallel to the c -axis. In Sri Lankan padparadschas, normally no prism crystal faces are developed or visible (see overleaf) and, thus, there are no sharp growth lines in this direction. In a view with an inclination approximately 30° to the c -axis (Figure 7a, b), normally a growth pattern consisting of two n faces or of two n faces in combination with r is present. In a view perpendicular to the c -axis, there is either a pattern consisting of the basal pinacoid c in combination with one or several hexagonal dipyramids z , w or n , where n is normally dominant (Figure 7c). After rotation of the crystal through 30° about the c -axis, a pattern consisting of basal c and rhombohedral r faces (Figure 8) should be visible. This growth pattern should completely reflect the external morphology of a rough crystal.

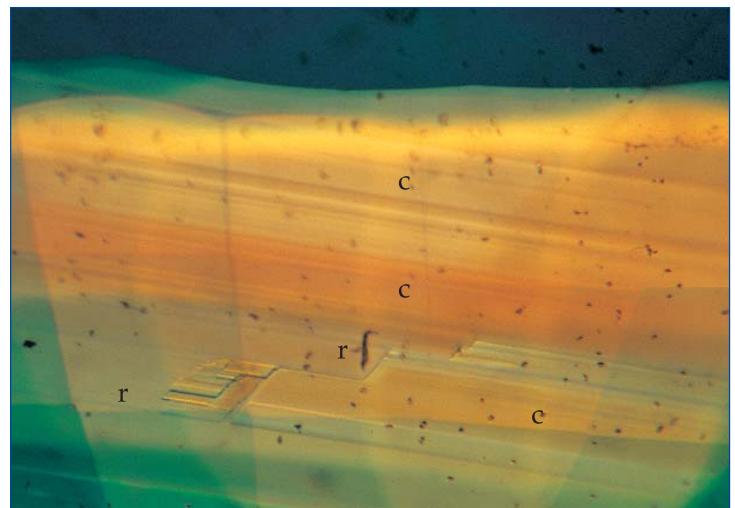


Figure 8: Growth pattern and colour zoning in a heat-treated padparadscha from Sri Lanka; view perpendicular to the c -axis, the rhombohedron r and the basal pinacoid c are visible. 50x. Photo by K. Schmetzer.

There are additional microscopic growth features in some crystals from Sri Lanka which are not completely understood at present. One feature is characterised by a fine structure which can be described as a mosaic-like pattern of oscillating growth lines on an extremely small scale (Figures 9, 10). These growth lines are parallel to different hexagonal dipyramids, mostly n , to the basal pinacoid and to the prism a $\{11\bar{2}0\}$, which is not developed macroscopically.

Because Sri Lankan sapphires are generally elongate (see Figure 6), faceted stones

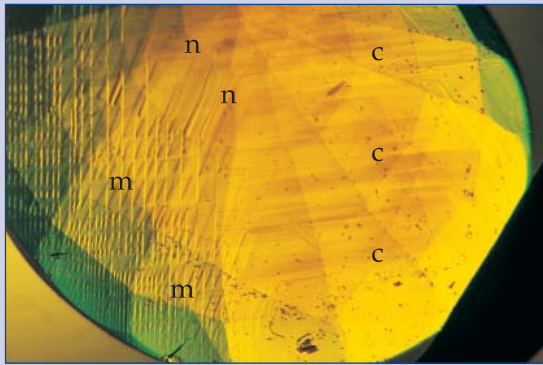


Figure 9: Growth pattern and colour zoning in a heat-treated yellowish-orange chromium-free sapphire from Sri Lanka; view perpendicular to the c-axis, the hexagonal dipyramid n and the basal pinacoid c are visible, a large area showing a mosaic-like growth pattern m is also present. 50x. Photo by K. Schmetzer.

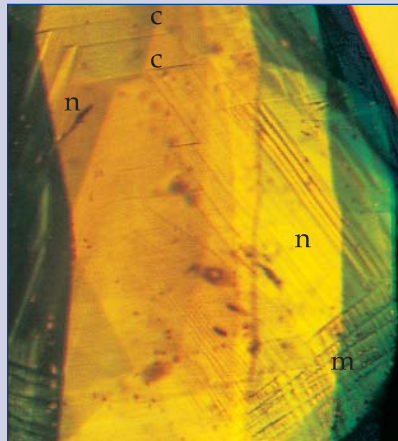


Figure 10: Growth pattern and colour zoning in an untreated padparadscha from Sri Lanka; view perpendicular to the c-axis, two hexagonal dipyramids n and the basal pinacoid c are seen, an area showing a mosaic-like growth pattern m is also present. 50x. Photo by K. Schmetzer.

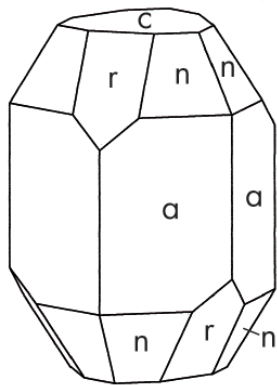


Figure 11a

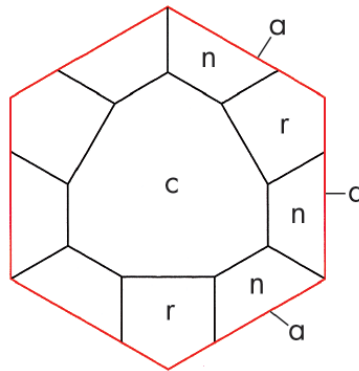


Figure 11b

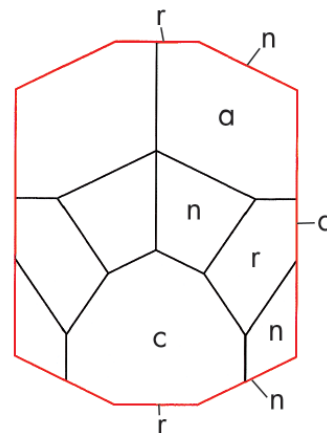


Figure 11c

Figure 11: Typical habit of sapphire from Montana consisting of the basal pinacoid c, the hexagonal prism a, the hexagonal dipyramid n and the positive rhombohedron r; (a) clinographic projection, (b) view parallel to the c-axis, (c) view at an angle inclined about 30° to the c-axis, (d) view perpendicular to the c-axis, (e) view perpendicular to the c-axis; Figures d and e are related by a rotation of 30° about the c-axis. The traces of crystal faces which are parallel to the direction of view and, thus, can be seen in the microscope are indicated in red in Figures b, c, d and e.

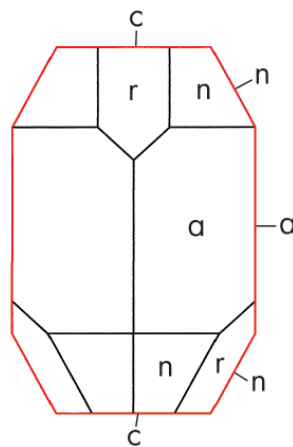


Figure 11d

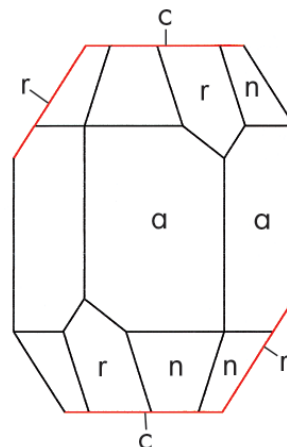


Figure 11e

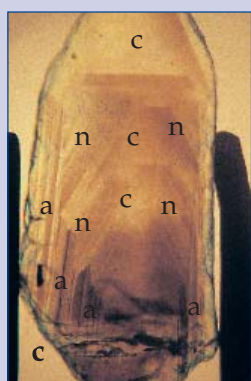
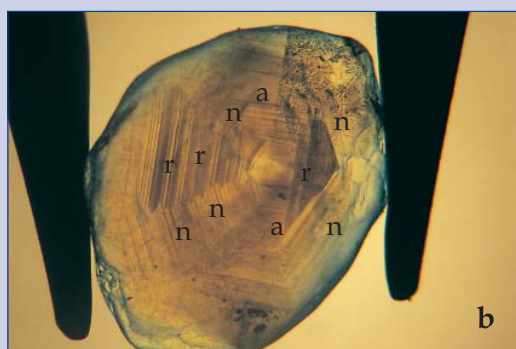
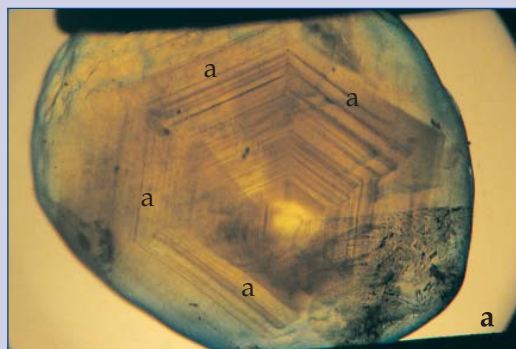


Figure 12: Growth pattern and colour zoning in an untreated greenish-blue sapphire from Montana; (a) view parallel to the c -axis, six hexagonal prism faces a are visible, (b) view inclined at about 30° to the c -axis, two hexagonal prism faces a , four hexagonal dipyramids n and two rhombohedra r are visible, (c) view perpendicular to the c -axis, the basal pinacoid c , two hexagonal prism faces a and four hexagonal dipyramids n are visible, (d) view perpendicular to the c -axis, the basal pinacoid c and the positive rhombohedron r are visible; Figures c and d are related by a rotation of 30° about the c -axis. 40x. Photos by K. Schmetzer.

rarely show a complete growth pattern, i.e. one which indicates both ends of the crystal. In general, a faceted gemstone contains only the faces related to one end of a crystal, e.g. one basal pinacoid and one series of hexagonal dipyramids.

Montana

The growth patterns in Montana sapphires mainly from the Rock Creek and the Missouri river deposits (Figure 11), are quite different from those seen in Sri Lankan material.

The dominant forms present are the basal pinacoid c $\{0001\}$, the hexagonal prism a $\{11\bar{2}0\}$, the positive rhombohedron r $\{10\bar{1}1\}$ and the hexagonal dipyramid n $\{22\bar{4}3\}$. Due to large variation in the size of the hexagonal prism compared to the basal pinacoid c , there is a large habit range from tabular to more or less equidimensional to prismatic, of which the prismatic crystals are more common.

To determine the complete external morphology of a crystal, the three typical orientations as described above for Sri Lankan crystals should be examined. In a view parallel to the c -axis, Montana sapphires show growth lines parallel to the hexagonal prism a (Figure 12a). In a view with an inclination approximately 30° to the c -axis, in samples with prismatic habit, there is a growth pattern consisting of two a prism faces in combination with two hexagonal dipyramids n and one rhombohedral r face. In samples with more equidimensional habit, both ends of a crystal may be represented. This complex growth pattern (Figure 12b) consists of two prism faces a in combination with four hexagonal dipyramids n and two rhombohedra r faces. In a view perpendicular to the c -axis, there is a pattern consisting of the basal pinacoid in combination with the prism a and the hexagonal dipyramid n (Figure 12c). After rotation of the crystal through 30° about the c -axis, a pattern consisting of basal c and rhombohedral r faces (Figure 12d) should be visible.

Another characteristic of many Montana sapphires is that growth planes are outlined by different concentrations of small particles resembling mineral dust.

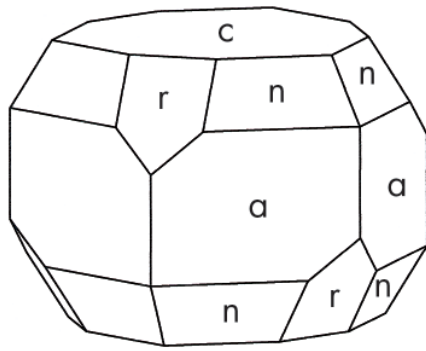


Figure 13a

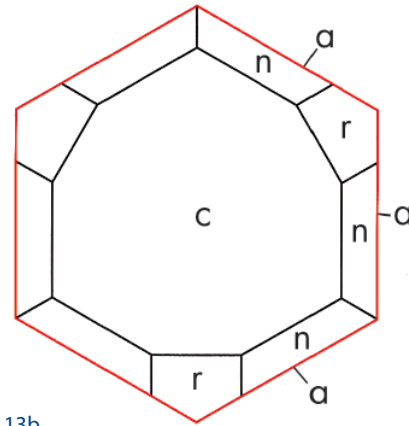


Figure 13b

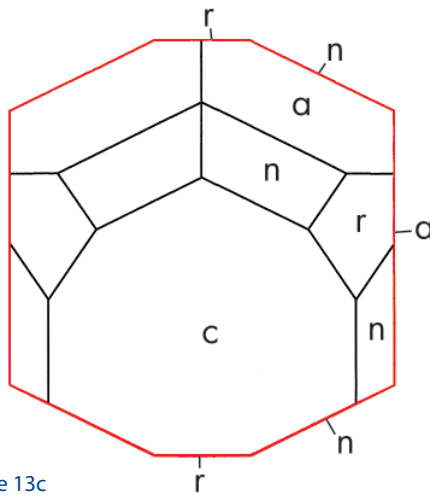


Figure 13c

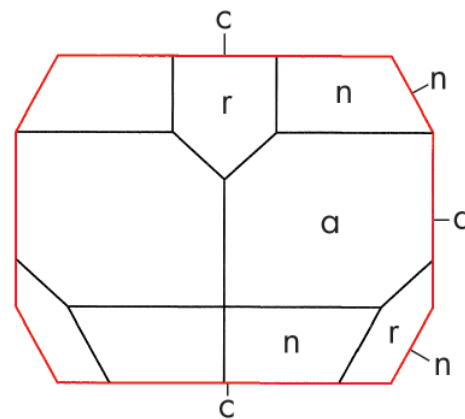


Figure 13d

Figure 13: Typical habit of ruby from Songea consisting of the basal pinacoid c , the hexagonal prism a , the hexagonal dipyramid n and the positive rhombohedron r ; (a) clinographic projection, (b) view parallel to the c -axis, (c) view at an angle inclined at about 30° to the c -axis, (d) view perpendicular to the c -axis. The traces of crystal faces which are parallel to the direction of view and, thus, can be seen in the microscope are indicated in red in Figures b, c and d.

Ilakaka

In some samples, inclusions are concentrated along specific growth planes of the basal pinacoid c and the hexagonal prism a , and under the microscope, this feature is seen as parallel lines of tiny inclusions tracing these faces. But most Ilakaka sapphires are free of visible growth planes.

Songea

The growth patterns in Songea sapphires and rubies (Figure 13) are closely similar to those seen in Montana material. Our samples would be described as having short prismatic, almost equidimensional habits. The dominant faces are the basal pinacoid c $\{0001\}$ and the hexagonal prism a $\{11\bar{2}0\}$. Also present are faces parallel to the hexagonal dipyramid n $\{22\bar{4}3\}$ and the positive rhombohedron r $\{10\bar{1}1\}$.

The patterns visible under the microscope in different orientations (Figure 14) are almost identical to those of Montana sapphires. So in a view of a short prismatic crystal perpendicular to the c -axis, the patterns of both crystal ends are generally visible. At an inclination of about 30° to c , two prism a faces with two n and one r face related to the upper half of the crystal in combination with two n and one r face related to the lower half of the crystal are visible.

It is worth mentioning that for most Montana sapphires with prismatic habit, in the view at 30° to the c -axis only one half of the growth line orientations are visible, while in Songea sapphires and rubies, the faces related to the terminations at both ends of the crystals are generally present.

Colour zoning and inclusions

General remarks

Colour zoning may be very complex, but is extremely helpful for diagnosing untreated, heat-treated or Be-diffusion-treated sapphires. Colour zoning may occur between different growth sectors of a crystal, e.g. between dipyramidal *n* and rhombohedral *r* sectors, and along parallel growth planes within the same growth sector. *Figure 15* shows colour zoning in a heat-treated padparadscha from Sri Lanka with different orientations of the sample (the same sapphire is pictured at high magnification in *Figure 7*). In general, a combination of both techniques is recommended in order to obtain the full information from a sample. Occasionally,

the use of a blue light filter is also helpful to recognise extremely weak colour variation in different growth zones, e.g. in untreated Sri Lankan material.

All types of colour zoning are a function of different trace-element distribution in different areas of a crystal. This zoning of colour-causing trace-elements is present before heat or diffusion treatment, and different reactions and changes may be caused according to the treatment applied. Colour zoning in different growth sectors or in different areas of the same growth sector may gradually increase or decrease without sharp growth boundaries.

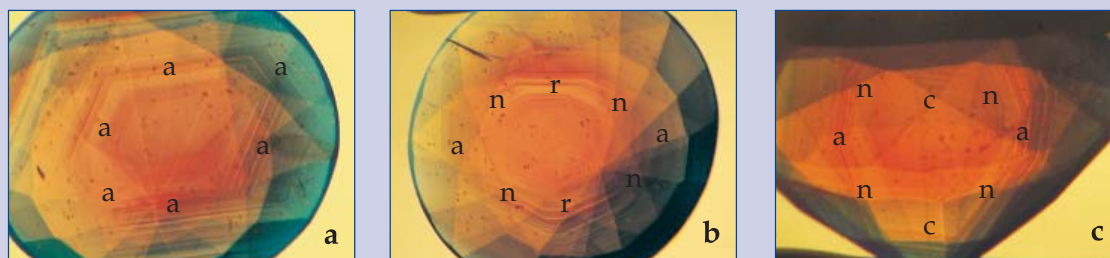


Figure 14: Growth pattern and colour zoning in a diffusion-treated reddish-orange sapphire from Songea; (a) view parallel to the *c*-axis, six hexagonal prism faces *a* are visible, (b) view inclined at about 30° to the *c*-axis, two hexagonal prism faces *a*, four hexagonal dipyrramids *n* and two rhombohedra *r* are visible, (c) view perpendicular to the *c*-axis, the basal pinacoid *c*, two hexagonal prism faces *a* and four hexagonal dipyrramids *n* are visible. 50x. Photos by K. Schmetzer.



Figure 15: Colour zoning associated with growth zoning in a heat-treated padparadscha from Sri Lanka of 3.20 ct in different orientations, but without exactly orientating the sapphire according to specific growth structures present. Size of the sample 7.1 x 7.9 mm. Photos by K. Schmetzer (see the same sapphire at high magnification in *Figure 7*).

Growth zoning, on the other hand, may have sharp boundaries and differently coloured sectors will also be sharply divided.

Some types of colour zoning in corundum are not changed by heat or diffusion treatment, e.g. that caused by chromium. Other types of colour zoning may be superimposed on an already existing colour pattern by heat or diffusion treatment.

When orange colour centres are developed by heat treatment it is generally in particular growth sectors, e.g. in rhombohedral growth sectors of Sri Lankan sapphires. By diffusion treatment, an orange rim may be developed in suitable raw material, in the right temperature and treatment conditions. In the present study, about half of the diffusion-treated samples from Ilakaka had an orange rim in contrast to its presence in only a few sapphires from Songea. This may be explained as follows: there is a general lack of colour zoning in untreated sapphires from Madagascar, and so the newly developed rim contrasts clearly with the homogeneous body colour. On the other hand, an intense rim and an almost colourless core is common in natural rubies and sapphires from Songea, and any superimposed colour developed by diffusion treatment, following, at least partly, the outline of the rim, would be less clearly apparent.

Heat-treated Ilakaka sapphires were pink or slightly purplish-pink, and heat-treated Songea sapphires were colourless to red or pink (colour-zoned) or purplish-red (see *Table 1*). In most sapphires from these localities, no orange colour centres are developed by simple heat treatment and, consequently, the colour of heat-treated samples is not in the reddish-orange to yellow colour range. Therefore, heat-treated Ilakaka and Songea sapphires are not described in detail in this paper, although one stone, a heat-treated slightly brownish-orange Ilakaka sapphire with orange colour centres, is described below in *Box B* as an example of an unusual stone.

Most heat-treated orange and yellowish-orange sapphires examined in this study, contain the decomposition products of zircon and other mineral inclusions such as apatite in Ilakaka stones or various silicates in Songea

sapphires. Some also contain two-phase inclusions of what appears to be glass with a bubble. However, much less common were completely molten inclusions with melt that escaped into discoid fractures (see *Figures K10 – K12*), features to be described later for diffusion-treated sapphires.

Consequently, the average maximum temperature for heat-treated samples seen at present in the trade may have been lower (possibly in the range of 50 to 100 C) than the temperatures applied in most Be-diffusion treatment. It should be born in mind that the heat-treated sapphires seen in the trade are sometimes kept in company stock for years and that, for this study, heat-treated yellow, yellowish-orange and orange Sri Lankan material less than two years old was not used in order to avoid mixing simply heat-treated and diffusion-treated samples.

Thus, the visual appearance of inclusions in a sapphire is not a sufficient indicator for diffusion treatment and should only be used with colour zoning, chemical and spectroscopic properties to determine whether Be-diffusion treatment has been performed.

Sri Lanka Untreated

Untreated padparadscha and padparadscha-like sapphires (*Figure 16*) in general show various types of colour zoning. In immersion liquid, at low magnification without a special orientation of the samples, colour zoning may be observed within different growth sectors or within different areas of the same growth sector



Figure 16: Untreated padparadschas from Sri Lanka, range of samples from 1.80 to 3.12 ct. Photo by M. Glas.

(Figures A1 – A3). The different colours may be a lighter and a more intense orange, yellow and orange, pink and orange, yellow, pink and orange, or even bluish-violet or purple and orange in different combinations. Using immersion and with exact orientation of the samples (Figures A4 – A7), one can conclude that the colour zoning is confined to growth planes. Mosaic-like growth structures may also be related to colour zoning (Figure 10, A8, A9).

The inclusions in untreated Sri Lankan padparadschas in this study are broadly similar to those in most Sri Lankan sapphires (Figures A10 – A12). These include zircon crystals, occasionally with tension cracks, negative crystals, tiny rutile needles, other unidentified mineral inclusions, and cavities filled with fluid and multiphase inclusions (see Koivula, 1986), some with diaspore needles (see Schmetzer and Medenbach, 1988). Multiphase inclusions may also contain graphite and rutile, gaseous and liquid CO₂ and diaspore needles (Notari, 1996; see also De Maesschalck and Oen, 1989; Francis *et al.*, 2003). These multiphase inclusions are commonly tabular negative crystals oriented parallel to the basal pinacoid of the corundum crystal. Further mineral inclusions determined by the Raman microprobe in padparadscha from Sri Lanka are apatite and mica (Notari, 1996).

Heat-treated

In chromium-free orangey-yellow or yellowish-orange heat-treated material from

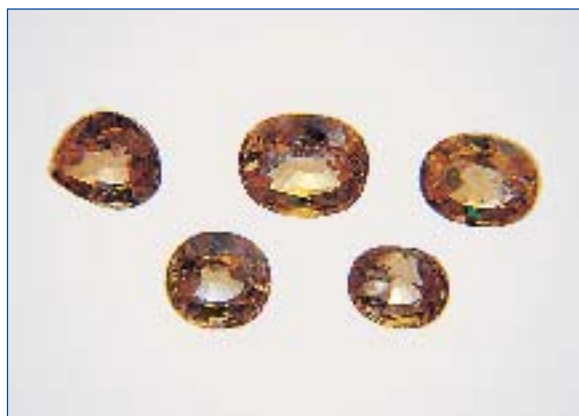


Figure 17: Heat-treated, chromium-bearing padparadschas from Sri Lanka, range of samples from 0.94 to 1.45 ct. Photo by M. Glas.

Sri Lanka (Figure 18) and in chromium-bearing reddish-orange or brownish orange samples (Figure 17), a strong colour zoning associated with growth-zoning is normally present (Figures 7 – 9, 15, B1 – B3, C1 – C3). Chromium-bearing samples may contain a distinct chromium zoning confined to specific growth sectors. Orange colour centres are normally developed to different concentrations in different growth sectors of a crystal, and are generally more abundant in *r* sectors. Thus, it is evident that the orange colour is, in general, only caused by the coloration of specific growth sectors, and complex structures may be observed when both types of colour zoning are present. In general, colour zoning in heat-treated samples, e.g. between orange brown *r* and adjacent pink *n* growth sectors, is much stronger than in untreated padparadschas. In chromium-free samples (Figures C4 – C6), colour zoning consisting of very light yellow (almost colourless) and very intense orange or brownish-orange areas is common. In chromium-bearing samples (Figures B4 – B9), the colour zoning may be pink and light orange or pink and intense orange or orange brown. This colour zoning is commonly also associated with sharp growth boundaries. Due to the heat treatment, no blue or purplish-blue sectors are present in this type of padparadscha. Mosaic-like growth structures connected with colour zoning are common in both types of heat-treated sapphire (Figures C7 – C9).

Heat-treated sapphires in the range yellow to reddish-orange (i.e. without and with



Figure 18: Heat-treated, chromium-free yellow and yellowish-orange sapphires from Sri Lanka, range of samples from 1.31 to 2.17 ct. Photo by M. Glas.

Figures A1 to A12: Colour and inclusion features of untreated chromium-bearing padparadschas from Sri Lanka

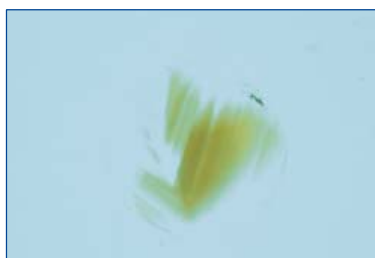


Figure A1: I, 2.9 x 3.0 mm

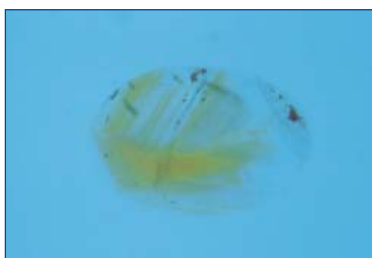


Figure A2: I, 3.1 x 4.6 mm

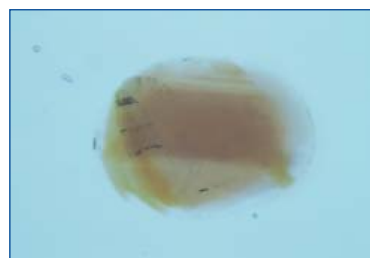


Figure A3: I, 3.7 x 4.9 mm



Figure A4: I, 6.8 x 7.9 mm

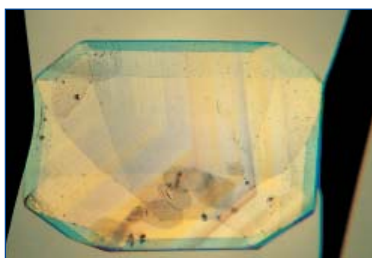


Figure A5: I, 8.0 x 11.0 mm

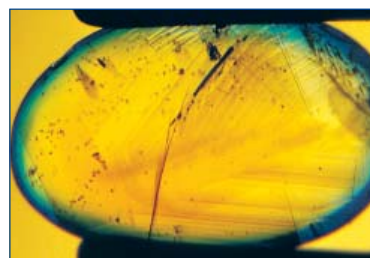


Figure A6: I, 3.1 x 4.6 mm

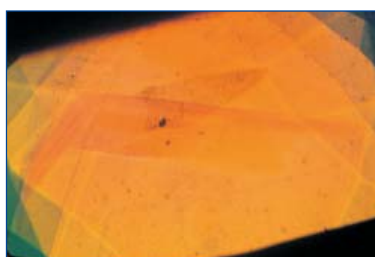


Figure A7: I, 50 x

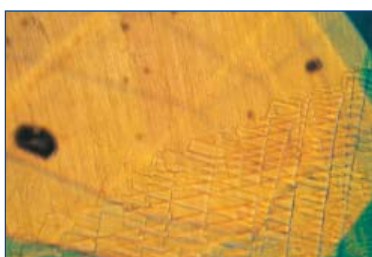


Figure A8: I, 50 x

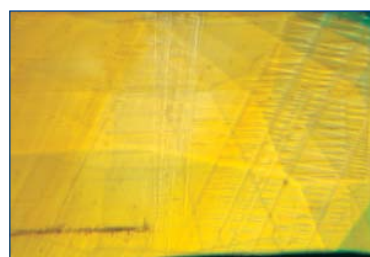


Figure A9: I, 50 x



Figure A10: I, # pol 80 x



Figure A11: 100 x

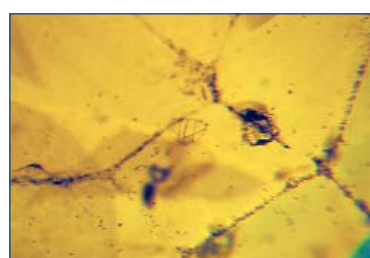


Figure A12: I, 70 x

At low magnification in un-oriented samples, colour zoning may be observed within different growth sectors or within different areas of the same growth sector (A1 – A3). With exact orientation (A4 – A9) the colour zoning can be correlated with growth planes of the sapphire crystal.

Inclusions typical of Sri Lankan sapphires are zircon crystals, occasionally with tension cracks (A10), negative crystals, tiny rutile needles, and cavities filled with fluid and multiphase inclusions (A11, A12). The multiphase inclusions are commonly in the form of tabular negative crystals with an orientation parallel to the basal pinacoid.

A1 – 3: Growth and colour zoning at low magnification. A4 – 7: Growth and colour zoning of oriented stones. A8 – 9: Mosaic-like growth structure and colour zoning. A10: Zircons with tension cracks. A11: Two-phase inclusion (diaspore and liquid). A12: Three-phase inclusion (diaspore, liquid and gas bubble). Pictures 1-10 and 12 by K Schmetzer, 11 by L. Kiefert.

nb: I = immersion, # pol. = crossed polarisers

Cr) commonly contain thermally altered inclusions, especially mineral inclusions with stress fractures (*Figures B10 – B12, C10 – C12*). In some samples, these stress fractures or stress haloes are oriented parallel to the basal pinacoid. Some samples also contain decomposed mineral inclusions similar in appearance to the various forms of altered inclusions found in Be-diffusion-treated sapphires from Ilakaka and Songea. In particular, former diaspore needles, now decomposed, are common in negative crystals in a matrix of what appears now to be glass or polycrystalline material with a bubble. Inclusions of completely molten material, with part of the melt flowing into fractures and fissures (similar to the typical inclusion features of Be-diffusion-treated sapphires) are present but not common.

Beryllium-diffusion-treated

Except for the two stones described below, the Be-diffusion-treated Sri Lankan sapphires (*Figure 19*) show no distinct colour zoning. In a light box in immersion liquid, the stones are an almost homogeneous yellow to yellowish-orange. The alternating very light (almost colourless) and very intense colour bands normally seen in heat-treated material (see *Figures C1 – C3*) are absent.



Figure 19: *Beryllium-diffusion-treated, chromium-free yellow and yellowish-orange sapphires from Sri Lanka, range of samples from 1.17 to 2.15 ct. Photo by M. Glas.*

With exact orientation of diffusion-treated samples under an immersion microscope, the characteristic growth patterns of Sri Lankan material including the mosaic-like growth structures are commonly visible (*Figures D1*

– *D3*). In 41 of 42 samples no distinct colour zoning related to growth structures was visible. In some samples the homogeneous yellow gives way to an extremely weak zoning of alternating light and slightly more intense yellow areas. This extremely weak colour zoning is quite distinct from the strongly contrasting light yellow, almost colourless areas alternating with intense yellow, or yellowish-brown or yellowish-orange areas of heat-treated samples (see *Figures C4 – C9*).

One diffusion-treated yellow Sri Lankan sapphire showed a pattern of transparent yellow alternating with translucent zones which contained a high concentration of undissolved fine particles (*Figure D4*); such particles are common in untreated Sri Lankan geuda materials.

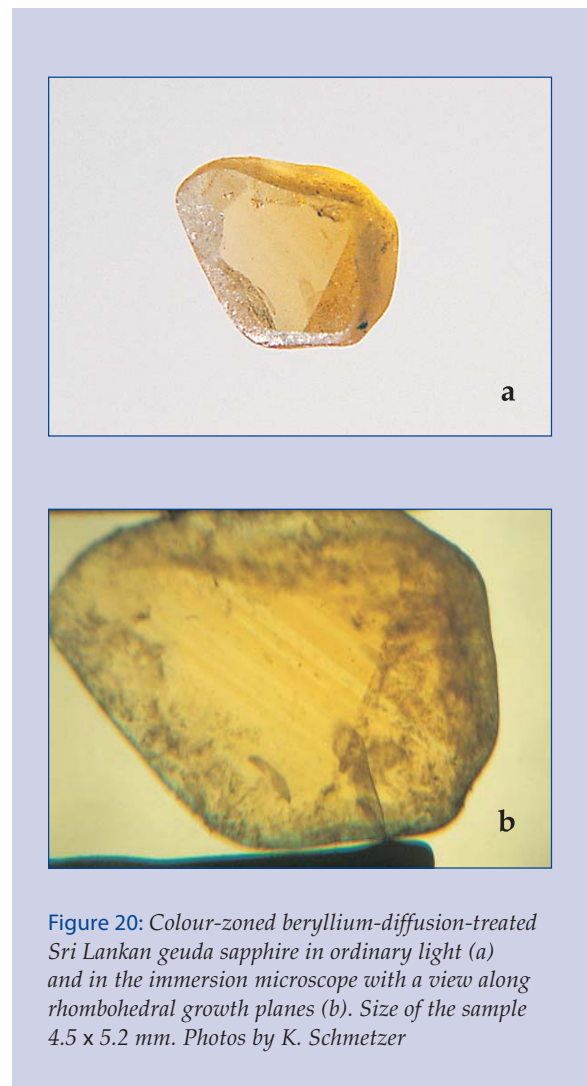


Figure 20: *Colour-zoned beryllium-diffusion-treated Sri Lankan geuda sapphire in ordinary light (a) and in the immersion microscope with a view along rhombohedral growth planes (b). Size of the sample 4.5 x 5.2 mm. Photos by K. Schmetzer*

Figures B1 to B12: Colour and inclusion features of heat-treated chromium-bearing padparadschas from Sri Lanka

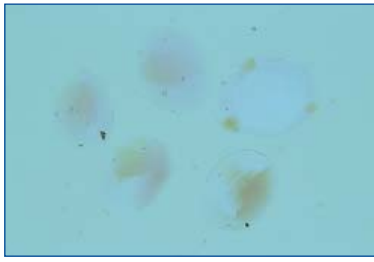


Figure B1: I, 0.83 to 2.23 ct

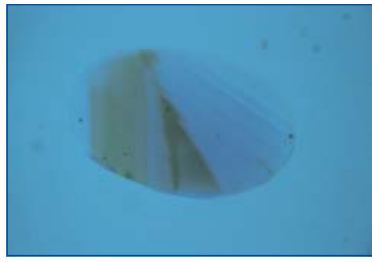


Figure B2: I, 5.1 x 6.8 mm

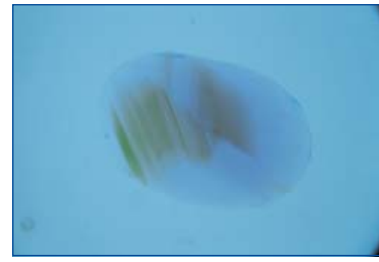


Figure B3: I, 5.1 x 6.8 mm

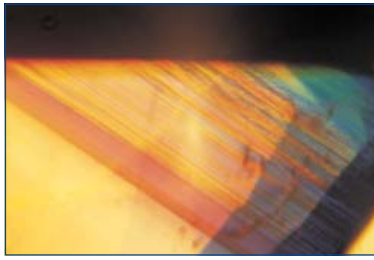


Figure B4: I, 60 x

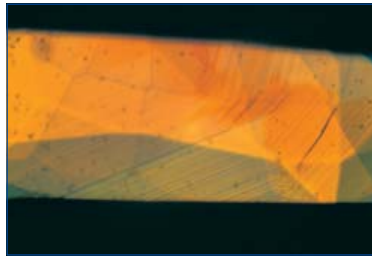


Figure B5: I, 50 x

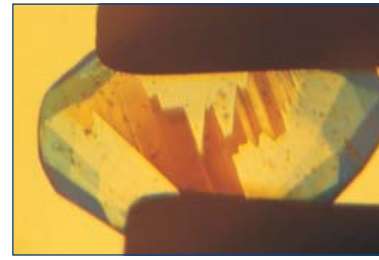


Figure B6: I, 50 x

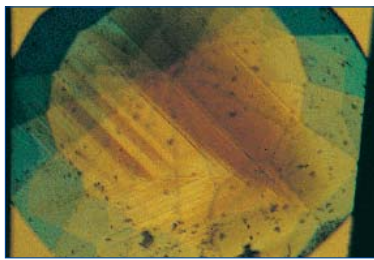


Figure B7: I, 60 x

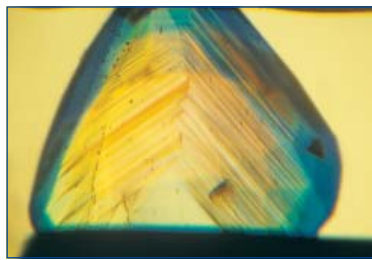


Figure B8: I, 50 x

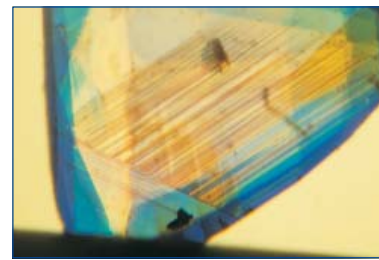


Figure B9: I, 50 x

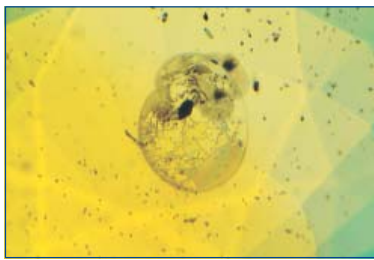


Figure B10: I, 60 x

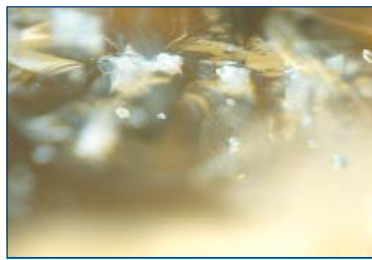


Figure B11: 50 x



Figure B12: 100 x

In heat-treated sapphires from Sri Lanka, a strong colour zoning associated with growth zoning is normally present (B1 – B3). In addition to colour zoning due to varying chromium content (B4, B5), orange colour centres can be developed to different degrees within different growth sectors of a crystal, especially in r sectors (B6 – B9).

Heat-treated padparadscha sapphires commonly contain thermally altered mineral inclusions, with stress fractures (B10) and decomposed mineral inclusions (B11, B12).

B1 – 3: Growth and colour zoning at low magnification. B4 – 9: Growth and colour zoning of oriented samples. B10 – 12: Thermally altered inclusions. Pictures 1 by M. Glas, 2 – 10 by K. Schmetzer, 11-12 by L. Kiefert.

nb: I = immersion

Two sapphires with unusual properties deserve separate description:

1 The first stone (*Figure 20a*) was diffusion-treated by J. Emmett and shows a weak colour zoning after proper orientation in the immersion microscope (*Figure 20b*). The coloration of the sapphire consists of somewhat lighter and more intense yellowish-orange zones parallel to rhombohedral growth planes. This sapphire is the only one of our samples with optical properties intermediate between heat-treated and diffusion-treated samples. Trace-element distribution in this sample was obtained using LA-ICP-MS. A scan perpendicular to the colour zoning across a polished surface of the sapphire consisting of six analysis points revealed only small variation in the iron and titanium concentrations, but distinct variation of both magnesium and chromium. Thus, the differently coloured growth zones contain variable concentrations of these two colour-related trace-elements. A more detailed interpretation is beyond the scope of the present paper.

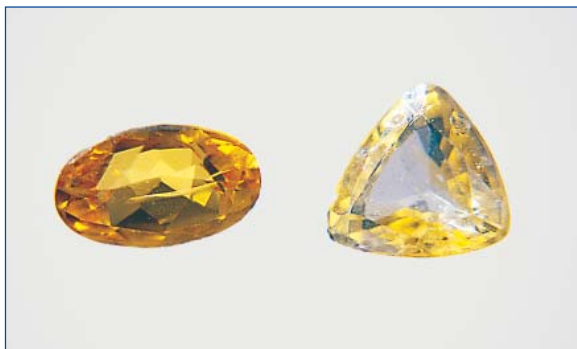


Figure 21a: Colour-zoned beryllium-diffusion-treated yellow sapphire of 0.97 ct (right) compared to an ordinary diffusion-treated Sri Lanka sample of 1.16 ct with homogeneous colour distribution (left). Photo by M. Glas.

1 The second colour-zoned yellow sapphire (*Figure 21a*) was found in a mixed lot of diffusion-treated samples originating – according to their properties – either from Songea or from Ilakaka. The exact treatment history of this lot treated in Thailand is unknown. This particular sapphire has a growth pattern associated with colour zoning and shows colour concentrations in rhombohedral *r* growth sectors (*Figure 21b, c*),

features typical of heat-treated Sri Lankan material. Trace element contents by LA-ICP-MS were obtained at two analysis points on the table of the faceted stone. These showed distinct variation of the magnesium concentration, but almost constant values for titanium, chromium, and iron. Although the most intense yellow sectors of the sample were not exposed on the table of the stone and, thus, were not analysed, we may conclude that the colour zoning of the sample is related to distinct magnesium zoning in different growth sectors.

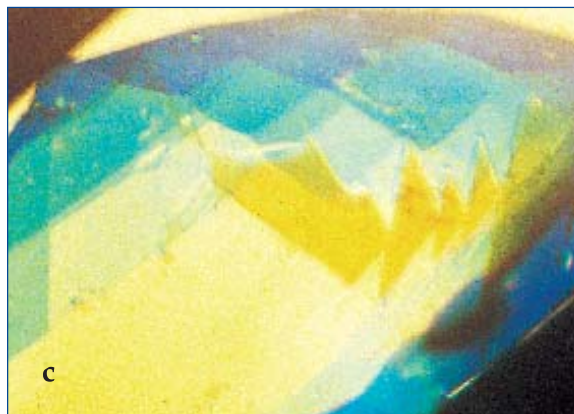
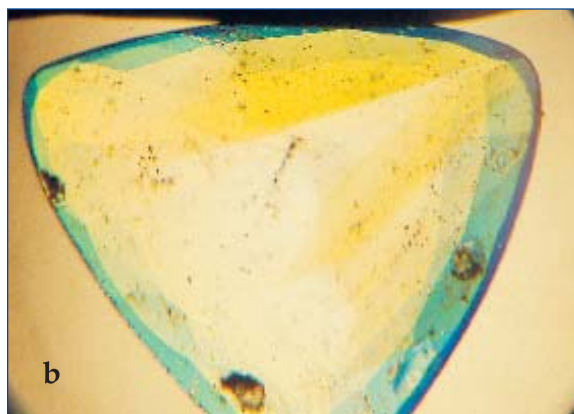


Figure 21b, c: Colour zoning in beryllium-diffusion-treated yellow sapphire (right sample in *Figure 21a*); the coloration of the sample is almost exclusively related to very intense yellow rhombohedral growth zones. (b) 40x, (c) 60x. Photos by K. Schmetzer.

The diffusion-treated yellow and yellowish-orange sapphires from Sri Lanka were, in general, extremely clean samples and showed only a few inclusions. Most of these were of decomposed minerals, some with stress fractures (*Figure D5*). Others were of two-phase inclusions consisting of glass or polycrystalline material with a bubble

Figures C1 to C12: Colour and inclusion features of heat-treated chromium-free yellow and yellowish-orange sapphires from Sri Lanka

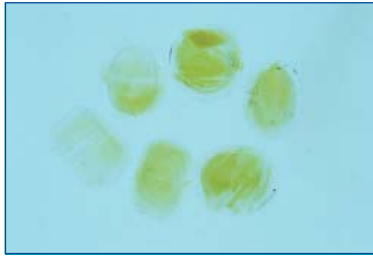


Figure C1: I, 0.74 to 0.95 ct

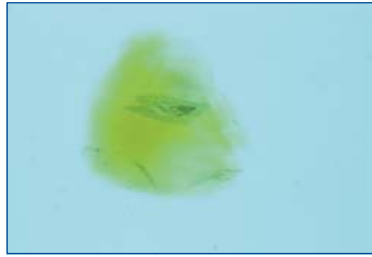


Figure C2: I, 5.5 x 6.0 mm

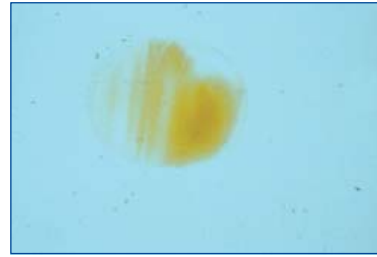


Figure C3: I, 4.9 x 6.1 mm

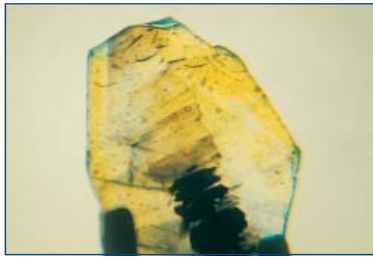


Figure C4: I, 30 x

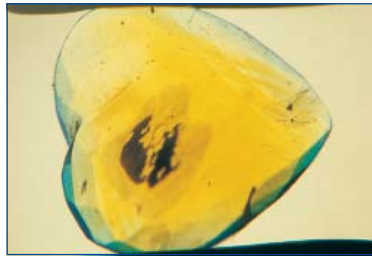


Figure C5: I, 40 x

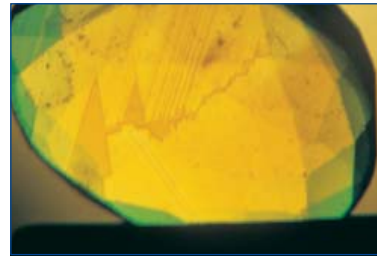


Figure C6: I, 40 x



Figure C7: I, 50 x

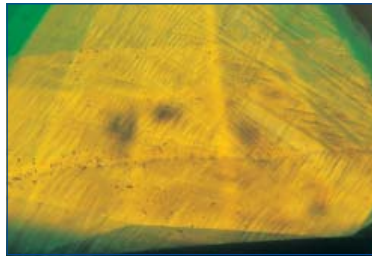


Figure C8: I, 50 x



Figure C9: I, 50 x



Figure C10: I, 50 x

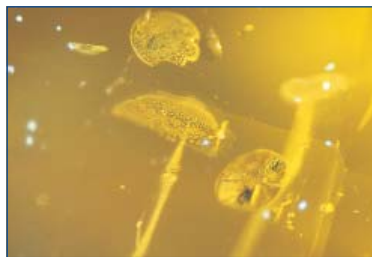


Figure C11: 50 x



Figure C12: 50 x

In heat-treated chromium-free sapphires from Sri Lanka, a strong colour zoning is associated with growth zoning (C1 – C3). Colour centres are normally developed to different degrees within different growth sectors of a crystal, especially in r sectors (C4 – C6). In general, colour zoning in heat-treated samples, e.g. between orange brown r and adjacent pink n growth sectors, is much stronger than in untreated yellow sapphires.

Many heat-treated yellow and yellowish-orange, chromium-free sapphires contain thermally altered inclusions (C10 – C12), especially mineral inclusions with stress fractures, some oriented parallel to the basal pinacoid.

C1 – 3: Growth and colour zoning at low magnification. C4 – 6: Growth and colour zoning of oriented sapphires. C7 – 9: Mosaic-like growth structure and colour zoning. C10 – 12: Thermally altered inclusions. Pictures 1 by M. Glas, 2 – 9 by K. Schmetzer, 10 – 12 by L. Kiefert.

nb: I = immersion

(Figure D6). No characteristic inclusion feature that would easily allow a distinction between simply heat-treated and diffusion-treated Sri Lankan sapphires was found.

Montana Untreated

Colour zoning in untreated yellowish-green, bluish-green or blue Montana sapphires (Figure 22) is extremely weak if present at all. Concentrations of small particles along internal growth faces is the commonest feature (Figures 12, E1).

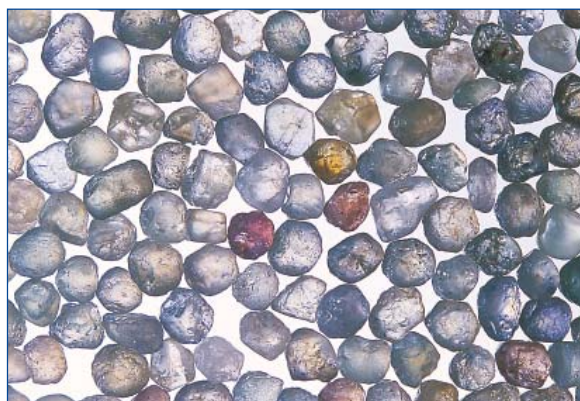


Figure 22: Untreated yellowish-green to bluish-green or blue, with a few pink sapphires from Rock Creek, Montana; samples are about 4 to 6 mm across. Photo by M. Glas.

The Rock Creek and Missouri river sapphires show only minor differences in their inclusion populations. Some samples contain isolated or intersecting twin lamellae with boehmite particles along the twin boundary. Small particles ('mineral dust') are common in various concentrations emphasising the growth patterns (Figure E1). Rutile crystals and other mineral inclusions are also present (Figures E2, E3). The most characteristic inclusion feature of the Montana sapphires that we examined were mineral inclusions surrounded by fluid discs oriented in planes parallel to the basal pinacoid.

Heat-treated

In contrast to untreated stones, heat-treated orange to reddish- or brownish-orange sapphires (Figure 23), show extreme and characteristic colour zoning. The colour of most samples consists of a more or less uniform light pink or brownish-pink on

which is superimposed a strong orange developed only in specific growth sectors (Figures F1, F2). In most samples, the strong orange zoning is related to growth zones of the basal pinacoid, and the zones are terminated by basal *c* and rhombohedral *r* faces (Figures F3 – F5). This specific colour zoning is characteristic of heat-treated orange and pinkish-, reddish- or brownish-orange Montana sapphires, and was not found in untreated or heat-treated padparadschas from Sri Lanka nor in sapphires from Ilakaka and Songea. Less common in heat-treated Montana sapphires was colour zoning parallel to the hexagonal dipyramid *n* and/or parallel to the rhombohedron *r*.



Figure 23: Heat-treated chromium-bearing Montana sapphires, range of samples from 0.41 to 0.85 ct. Photo by M. Glas.

In a few heat-treated samples, the small particles outlining the growth planes survived the treatment. The most characteristic features are altered – decomposed or molten – mineral inclusions, which commonly form glass-like, somewhat rounded bodies with small bubbles (Figures 5a, F6). In many stones, this pattern is combined with stress fractures and haloes. The original mineral inclusions with fluid rosettes parallel to the basal plane are also decomposed and reveal discoid-like stress haloes after heat treatment.

Beryllium-diffusion-treated

The diffusion-treated Montana sapphires are yellow to orange, uniformly coloured, with no colour zoning related to growth zoning (Figure 24).

Figures D1 to D6: Colour and inclusion features of beryllium-diffusion-treated chromium-free yellow and yellowish-orange sapphires from Sri Lanka



Figure D1: I, 50 x

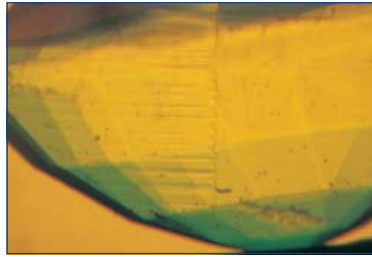


Figure D2: I, 50 x

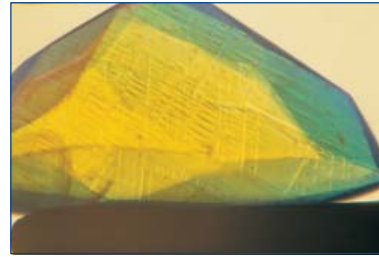


Figure D3: I, 60 x

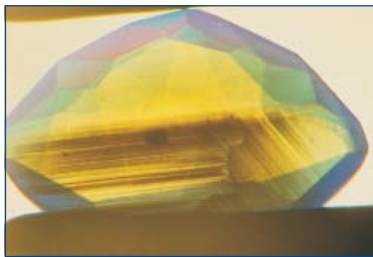


Figure D4: I, 50 x



Figure D5: 50 x

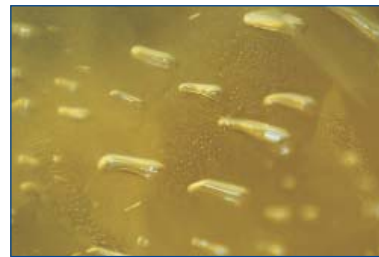


Figure D6: 100 x

Yellow diffusion-treated sapphires from Sri Lanka show no distinct colour zoning. In most orientations a sapphire will appear almost homogeneous yellow to yellowish-orange, but with an exact orientation the characteristic growth patterns of Sri Lankan sapphire, including the mosaic-like growth structures, are commonly visible (D1 – D3).

Some diffusion-treated yellow Sri Lankan sapphires contain zones of alternating transparent yellow and translucent areas (D4), the latter with undissolved fine particles. Decomposed mineral inclusions (D5), and two-phase inclusions with a bubble (D6) are present.

D1 – 2: Growth zoning in oriented samples. D3: Mosaic-like growth structure. D4: Growth zones of hexagonal dipyramids with undissolved particles. D5 – 6: Thermally altered inclusions. Pictures 1 – 4 by K. Schmetzer, 5 – 6 by L. Kiefert.

nb: I = immersion

Figures E1 to E3: Growth and inclusion features of untreated yellowish-green to bluish-green or blue, rarely pink, sapphires from Montana

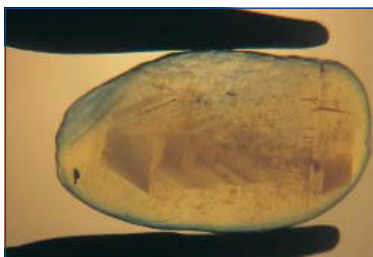


Figure E1: I, 40 x

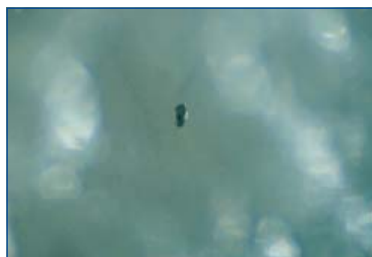


Figure E2: 100 x



Figure E3: 50 x

E1: Growth zoning of oriented sample, the c-axis runs horizontally. E2: Rutile and small unidentified particles. E3: Mineral inclusions. Pictures 1 by K. Schmetzer, 2 – 3 by L. Kiefert.

nb: I = immersion



Figure 24: Beryllium-diffusion-treated, chromium-free yellow and yellowish-orange sapphires from Rock Creek, Montana; samples are about 4 to 6 mm across. Photo by M. Glas.

The most characteristic inclusion pattern (Figures 5b, G3 – G6) consists of thermally decomposed and at least partly molten mineral inclusions, frequently in the form of two-phase inclusions with stress haloes and altered discoid-like rosettes. This is similar to the pattern for heat-treated Montana sapphires, the only difference being that rutile inclusions have distinctive diffusion haloes (Figures G1, G2); these resemble those in Songea sapphires.

Ilakaka **Untreated**

In untreated pink to violet or orange brown Ilakaka sapphires (Figure 25), colour zoning with or without a particular growth pattern has not been found. Parallel lines of inclusions concentrated along crystal faces (Figure H1) are present in some stones. (For heat-treated Ilakaka sapphires, see



Figure 25: Untreated sapphires from Ilakaka, Madagascar; range of samples from 0.56 to 1.38 ct. Photo by M. Glas.

‘General remarks’ and discussion of difficult stones below).

Many Ilakaka sapphires show twin lamellae parallel to the positive rhombohedron, the most common form of twinning in corundum. If there are several series of intersecting twin lamellae, boehmite particles (polycrystalline material) are present along the twin boundaries. In some gemmological texts, these inclusions are referred to as ‘boehmite needles’. Most Ilakaka sapphires contain numerous tiny mineral inclusions (Figures H2 – H5) such as apatite, zircon, monazite and xenotime (identified using the Raman microprobe). These tiny mineral inclusions commonly form irregular clusters. There are a few other mineral inclusions which are slightly larger (Figure H6).



Figure 26: Beryllium-diffusion-treated sapphires from Ilakaka, Madagascar; range of samples from 0.99 to 1.82 ct. Photo by M. Glas.

Beryllium-diffusion-treated

In diffusion-treated material (Figure 26), a colour boundary between the rim and the core of the faceted sapphire is commonly seen at low magnification (Figures 2, I1 – I3), but is not present in every stone. Any colour caused by the diffusion treatment is superimposed on the original homogeneous colour, and the depth of any colour change varies according to the trace-elements present and to the treatment conditions. If a sapphire has significant iron and chromium contents, the rim may be orange and the core may be pink (at lower iron concentrations), but other combinations may also be observed. Since there is a lack of visible growth patterns in

Figures F1 to F6: Colour and inclusion features of heat-treated chromium-bearing sapphires from Montana

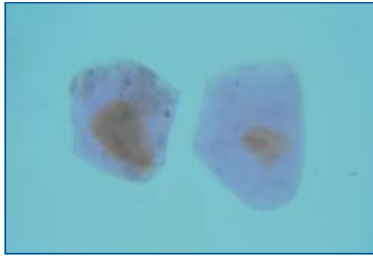


Figure F1: I, 0.77 and 1.01 ct

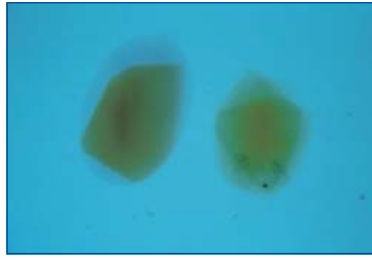


Figure F2: I, 0.41 and 0.56 ct

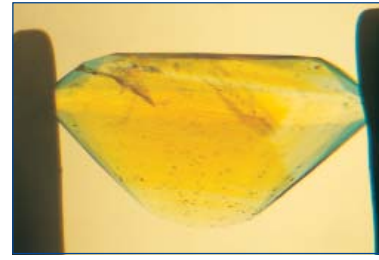


Figure F3: I, 40 x

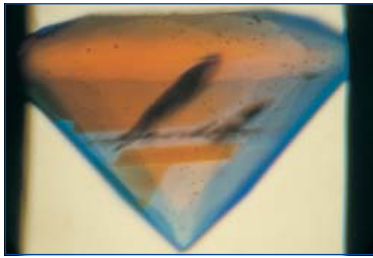


Figure F4: I, 40 x

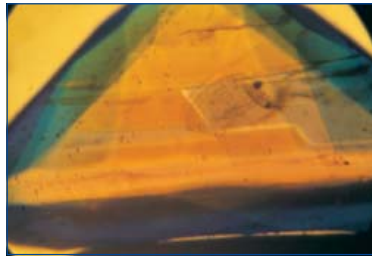


Figure F5: I, 60 x

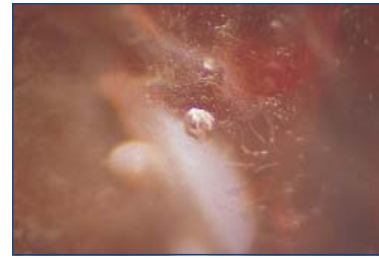


Figure F6: I, 100 x

Strong orange is developed only in specific growth sectors of the sapphire crystals (F1, F2). The areas with strong orange coloration are terminated by basal *c* and rhombohedral *r* faces (F3 – F5).

F1 – 2: Growth and colour zoning at low magnification. F3 – 5: Growth and colour zoning of oriented samples. F6: Thermally altered inclusions. Pictures 1 – 5 by K. Schmetzer, 6 by L. Kiefert.

nb: I = immersion

Figures G1 to G6: Colour and inclusion features of beryllium-diffusion-treated chromium-free yellow and yellowish-orange sapphires from Montana

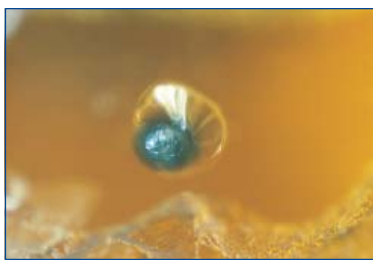


Figure G1: 50 x

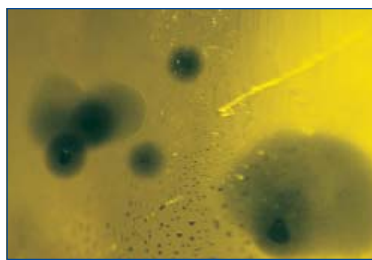


Figure G2: 50 x



Figure G3: 100 x

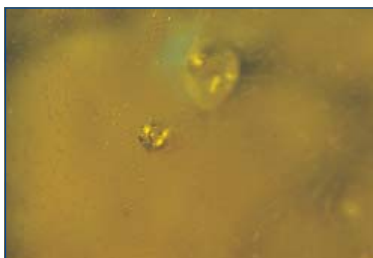


Figure G4: 100 x

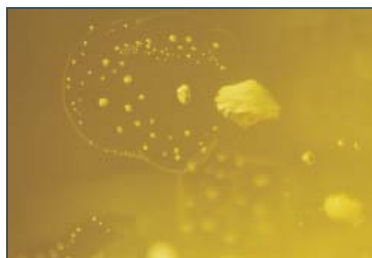


Figure G5: 100 x

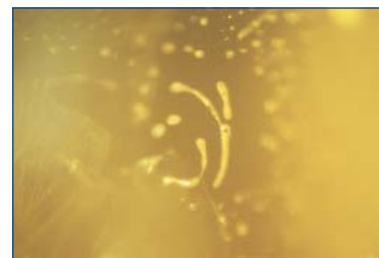


Figure G6: 100 x

G1: Thermally altered rutile crystal with tension crack and diffusion halo. G2: Rutile crystals with diffusion haloes. G3-G6: Thermally altered inclusions. Pictures 1-6 by L. Kiefert.

Figures H1 to H6: Colour and inclusion features of untreated chromium-bearing sapphires from Ilakaka.

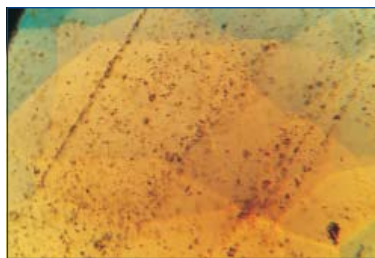


Figure H1: I, 50 x

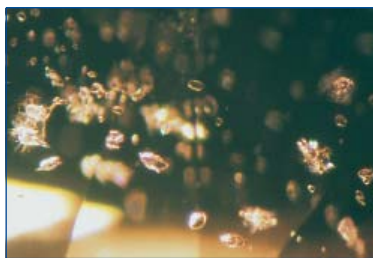


Figure H2: 70 x



Figure H3: 100 x



Figure H4: 100 x

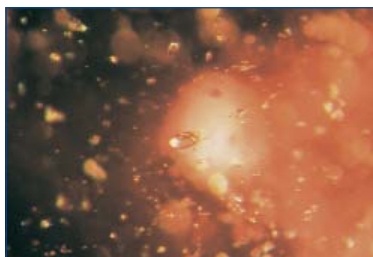


Figure H5: 100 x



Figure H6: I, 80 x

H1: Parallel lines of inclusions. H2: Zircon inclusions. H3: Zircon inclusions. H4: Zircon inclusions with monazite. H5: Zircon inclusions with xenotime. H6: Mineral inclusion and 'boehmite needles'. Pictures 1 and 6 by K. Schmetzer, 2 and 5 by E. Gübelin, 3 and 4 by L. Kiefert.

nb: I = immersion

untreated material, there is a corresponding absence of structural pattern or colour zoning in treated sapphires, even at high magnification.

On the surfaces of some samples and in some repolished stones, polycrystalline material formed during the diffusion process was present (Figures I4, I5). This material was determined by X-ray powder diffraction as corundum. In some samples fractures were filled with residual matter from the flux in which the diffusion process was performed.

Other inclusions consist of decomposed apatite and zircon crystals and/or molten and decomposed zircons (Figures I6 – I11). Stress fractures or haloes formed around the original crystals may be unoriented, or they may be parallel to the basal pinacoid. The altered mineral inclusions may be non-transparent, but transparent inclusions with a bubble are also present. If molten material were present, it migrated into stress fractures and haloes where it formed multiphase inclusions of glass with bubbles and/or other solid components.

Along twin planes, decomposed boehmite grains were transformed into polycrystalline corundum (Figure I12). New corundum was formed in an orientation different to that of the host, related to twin lamellae in some samples, but also occurring in untwinned stones.

Songea Untreated

Untreated mostly purplish- or brownish-red Songea rubies (Figure 27) typically show great variation in colour zoning. Many have a colourless core and a red or purplish-red rim (Figures 3a, J1) and this is consistent with increasing chromium concentration from the core to the rim of a crystal (see Hänni and Pettke, 2002). This change in colour is in most crystals gradual without sharp boundaries and within particular growth sectors. In a few crystals however, sharp boundaries between different growth sectors were present, and even sharp curved boundaries resembling swirl-like colour zoning in rubies from Mogok, Myanmar, were observed.

Figures I1 to I12: Colour and inclusion features of beryllium-diffusion-treated chromium-bearing sapphires from Ilakaka.

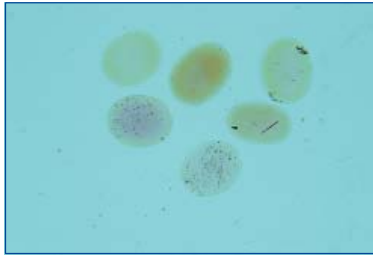


Figure I1: I, 0.34 to 0.53 ct

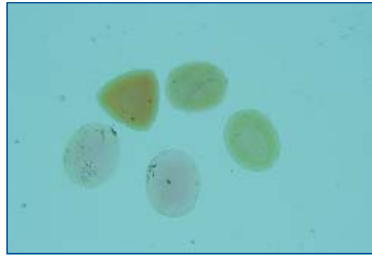


Figure I2: I, 0.38 to 0.57 ct



Figure I3: I, 0.38 ct

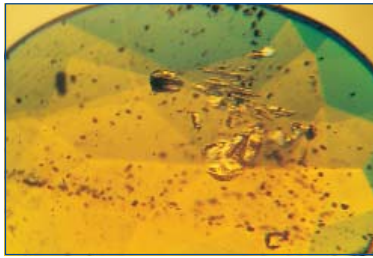


Figure I4: I, 40 x



Figure I5: I, 40 x # pol.



Figure I6: 100 x



Figure I7: 100 x

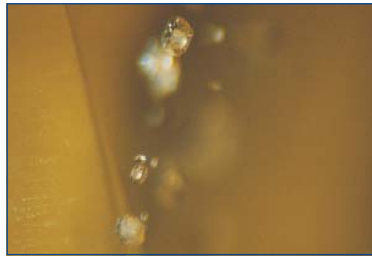


Figure I8: 100 x

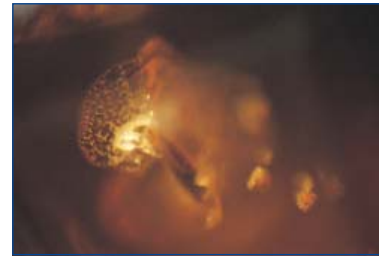


Figure I9: 100 x



Figure I10: 100 x



Figure I11: 100 x



Figure I12: 100 x

A colour boundary between the rim and the core of the faceted sapphire is commonly visible at low magnification (I1 – I3). Due to the iron and chromium contents, the rim may be orange and the core may be pink, but there can be other colour combinations. Growth patterns are absent in untreated material, and no characteristic pattern or colour zoning is visible at high magnification.

On the surface of some samples, polycrystalline corundum formed during the diffusion process remains (I4, I5). Ilakaka material commonly contains decomposed apatite and zircon crystals and/or molten and decomposed zircons (I6 – I11).

I1 – 3: Growth and colour zoning at low magnification. I4 – I5: Polycrystalline corundum on surface. I6 – I11: Thermally altered inclusions. I12: Thermally altered 'boehmite needle'. Pictures 1 – 2 by M. Glas, 3 – 5 by K. Schmetzer, 6 – 12 by L. Kiefert.

nb: I = immersion, # pol. = crossed polarisers

Figures J1 to J6: Colour and inclusion features of untreated chromium-bearing sapphires from Songea.

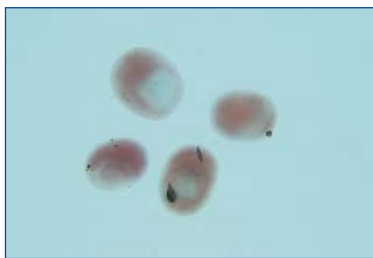


Figure J1: I, 0.52 to 0.85 ct

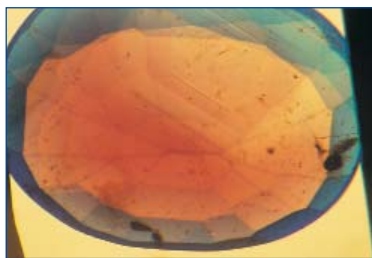


Figure J2: 40 x



Figure J3: 100 x

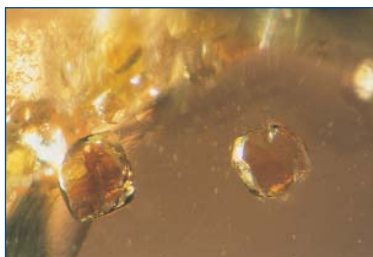


Figure J4: 65 x

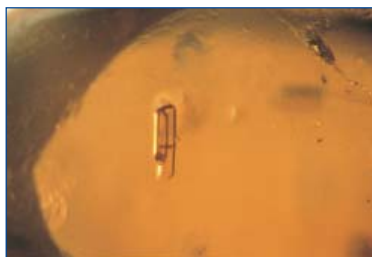


Figure J5: 65 x

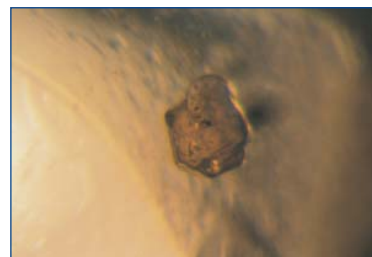


Figure J6: 100 x

Many Songea rubies contain a colourless core and a more intense red or purplish-red rim (J1).

The inclusions consist of zircon crystals, black to red rutile crystals (J3) and rutile in the form of oriented, short needles, together with apatite, phlogopite mica, olivine, garnet (J4), epidote (J5) and monazite (J6).

J1: Growth and colour zoning at low magnification. J2: Growth and colour zoning of oriented sample. J3: Rutile crystals. J4: Garnet crystals. J5: Epidote crystal. J6: Monazite crystal. Pictures 1 by M. Glas, 2 by K. Schmetzer, 3 by L. Kiefert, 4 – 6 by E. Gübelin.

nb: I = immersion

Some sapphires contained a growth pattern with basal, prism, dipyrimal and rhombohedral faces, a few without distinct colour zoning, but more with the growth pattern combined with a more or less intense variation of colour (Figure J2). Some crystals contain several light and more intense colour



Figure 27: Untreated purplish-red rubies from Songea, Tanzania; range of samples from 0.69 to 0.95 ct. Photo by M. Glas

zones from the rim to core. To make the visual impression even more complex, the different types of colour and growth zoning may be observed within one Songea sample. (For heat-treated Songea material see 'General remarks')

Many purple or red Songea corundums contain zircon crystals, rutile, both as black to red larger crystals and as oriented short needles (Figure J3), and tiny, unidentified grains. Rutile was identified using Raman spectroscopy, as were the rarer inclusions of apatite, phlogopite, monazite, garnet, epidote and olivine (see Figures J4–J6, and Schwarz, 2001). The presence of garnet, epidote and olivine indicate an unusual geological origin for the Songea corundums. Negative crystals are rare.

Beryllium-diffusion-treated

In diffusion-treated Songea rubies and sapphires (Figure 28), further complexity can result if an orange rim or an orange zone of

Figures K1 to K12: Colour and inclusion features of beryllium-diffusion-treated chromium-bearing sapphires from Songea.

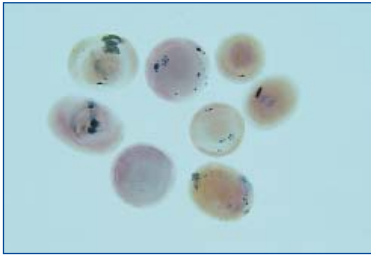


Figure K1: I, 0.32 to 0.75 ct

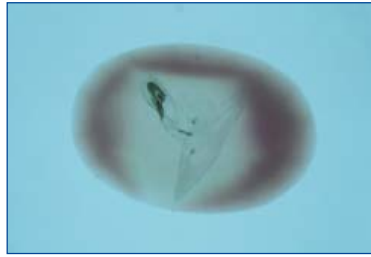


Figure K2: I, 0.50 ct



Figure K3: I, 0.62 ct



Figure K4: I, 0.27 ct

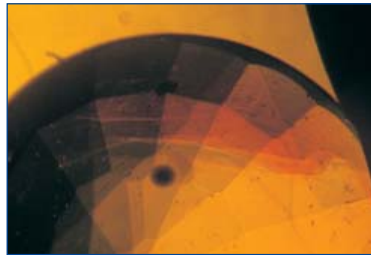


Figure K5: I, 50 x

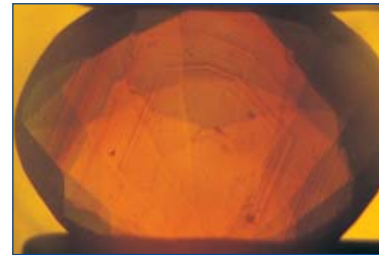


Figure K6: I, 50 x

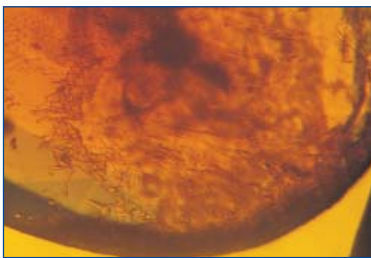


Figure K7: I, 60 x

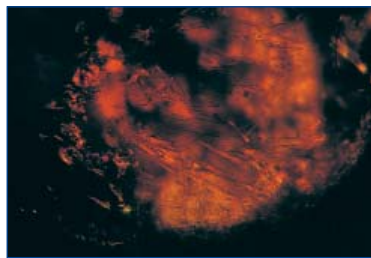


Figure K8: I, 60 x # pol.

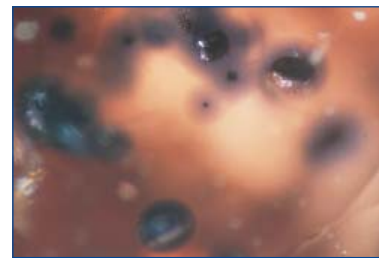


Figure K9: 50 x



Figure K10: 100 x



Figure K11: 100 x

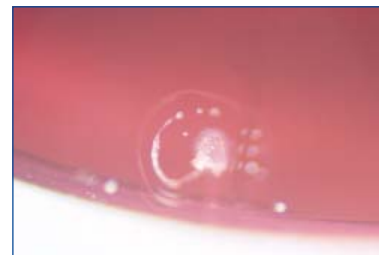


Figure K12: 100 x

Growth and colour zoning may be very complex, especially if an orange rim or an orange zone of greater depth is superimposed on chromium-related growth and colour zoning (K1 – K6).

Newly-grown polycrystalline corundum is present on the surfaces of some treated samples from Songea (K7, K8). Around the larger rutile crystals, bluish-violet diffusion haloes may be formed (K9).

K1-4: Growth and colour zoning at low magnification. K5-6: Growth and colour zoning of oriented samples. K7-8: Polycrystalline corundum on surface. K9: Rutile crystals with diffusion haloes. K10-12: Thermally altered inclusions. Pictures 1 by M. Glas, 2-8 by K. Schmetzer, 9-12 by L. Kiefert.

nb: I = immersion, # pol. = crossed polarisers

greater depth is superimposed on existing growth and colour zoning (Figures 3b, 14, K1 – K4). The most easily recognisable treated Songea stone is one with a red or purplish-red rim that became orange by diffusion treatment, still with a more or less colourless core. If the colour zoning before treatment, however, was already complex, a simple rim to core zoning may not be recognisable. This situation is not changed at higher magnification (Figures K5, K6). The overall colour impression given by a treated stone comprises the average of the coloured rim, the colourless core and the intensity of orange colour centres formed at some depth within the crystal.



Figure 28: Beryllium-diffusion-treated sapphire of 0.94 ct from Songea. Photo by M. Glas.

As described for Ilakaka material, newly-grown polycrystalline corundum is present on the surface of some treated samples from Songea (Figures K7, K8). Around the larger rutile crystals, bluish-violet diffusion haloes were formed during the diffusion treatment process (Figure K9). In stones where the diffusion halo was in contact with internal melt from mineral inclusions, bluish-violet flow structures were formed.

Treated Songea stones are also characterised by various forms of decomposed and/or molten mineral inclusions (Figures K10 – K12) and many have stress fractures and haloes with various forms of melt and spherical bubbles. The visual appearance of these inclusions is similar to that observed for altered mineral inclusions in treated Ilakaka samples but, on average, inclusions were less abundant and some Songea sapphires were clean. In some

samples partly healed fissures and fractures that were occasionally filled with foreign material, probably flux, are present.

Chromium and iron contents of the sapphires

Table II contains data published by Schmetzer and Schwarz (2004, p.160) enhanced by results from 20 new samples from Montana and 10 from Sri Lanka. A graphical representation of the analytical results is shown in Figure 29.

Since the distribution of trace-elements from all four sources was not related to whether the samples were untreated, heat-treated or diffusion-treated, these categories are not specified in Table II and Figure 29.

It is evident from Figure 29 that the Cr-Fe population fields for Sri Lanka and Madagascar samples, for Madagascar and Montana, and for Madagascar and Tanzania partly overlap. In some areas without overlap, a distinction between different localities would be indicated on the basis of these chemical contents. In other areas, the data may indicate that localities are highly improbable, e.g. there are no Songea sapphires with low iron contents or there are no Sri Lanka stones with high iron. Using other trace elements or trace element ratios, the overlaps between samples from different sources as seen in the iron-chromium variation diagram of Figure 29 could be further reduced (for 'chemical fingerprinting' of sapphires compare, e.g., Sutherland *et al.*, 1998; Schwarz and Schmetzer, 2001; Saminpanya *et al.*, 2003; Rankin *et al.*, 2003).

Spectra of sapphires from Sri Lanka, Montana, Ilakaka and Songea

Causes of colour and spectroscopic features of different types of sapphires are summarised in Table I and a visual summary linking origins, compositions and treatments is presented in Figure 30. A more detailed discussion about various types of colour centres in sapphire and the possible

Table II: Chromium and iron contents of untreated, heat-treated and diffusion-treated Sri Lankan padparadschas and yellowish-orange sapphires, and of untreated and treated rubies and sapphires from Montana, Madagascar, and Tanzania

Wt.%	Sri Lanka (36 samples)	Montana (20 samples)	Ilakaka (84 samples)	Songea (42 samples)
Cr ₂ O ₃	bdl. – 0.11	bdl. – 0.07 ^a 0.01 – 0.07 ^b	0.02 – 0.21 ^c 0.06 – 0.15 ^d	0.11 – 0.53
Fe ₂ O ₃	0.03 – 0.25	0.53 – 1.15 ^a 0.25 – 0.26 ^b	0.05 – 1.95 ^c 2.64 – 3.20 ^d	1.04 – 1.80

bdl. = below detection limit

^a 18 heat-treated and diffusion-treated samples

^b 2 heat-treated orange or pinkish-orange samples

^c 80 untreated and diffusion-treated samples in different colours

^d 4 untreated samples with orange brown or yellowish-brown colour

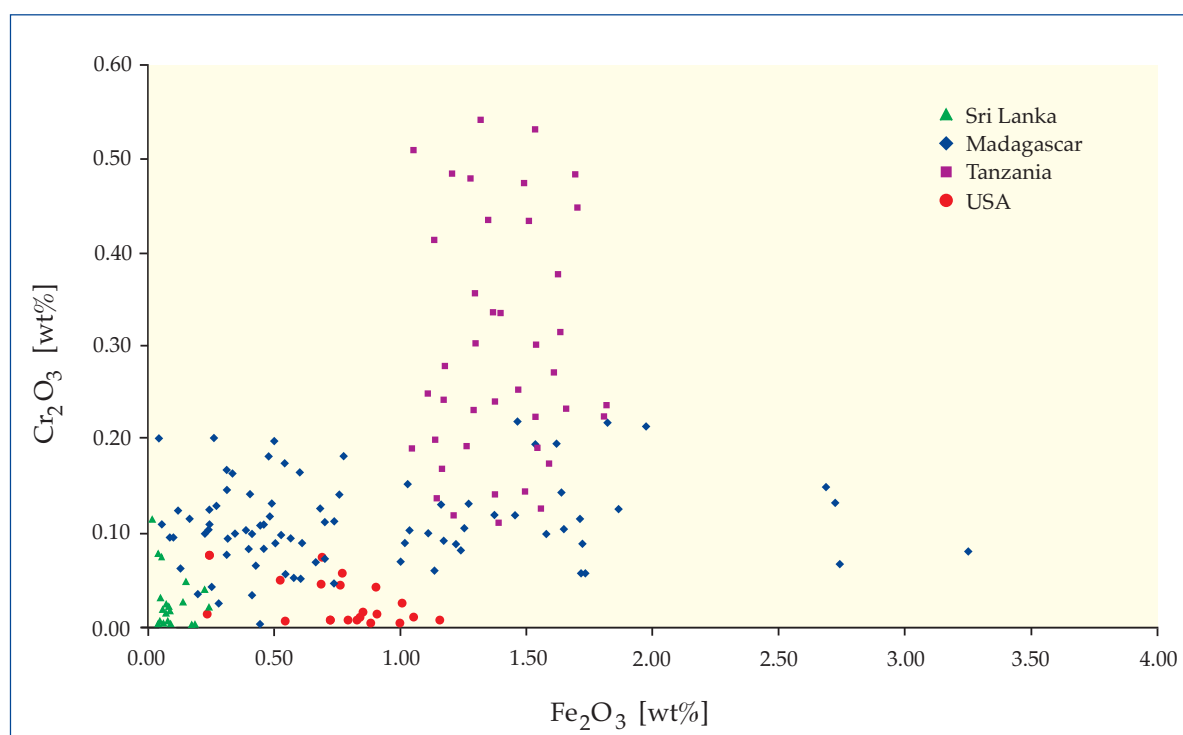


Figure 29: Graphical representation of iron and chromium contents of 182 sapphires from Sri Lanka, U.S.A., Madagascar and Tanzania by EDXRF; for further characterisation of samples see Table I. It is evident that some population fields for samples from different occurrences partly overlap.

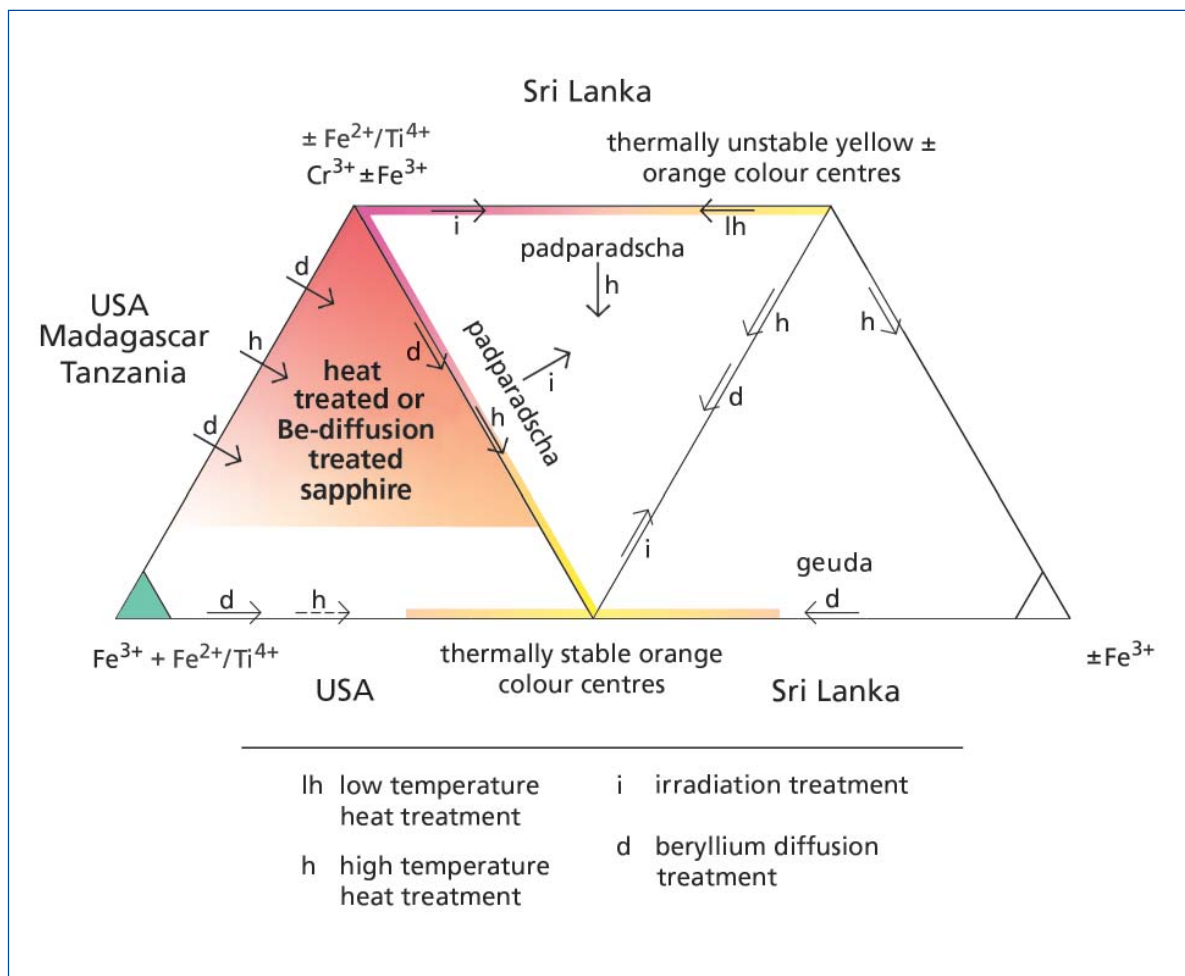


Figure 30: This schematic diagram summarises the causes of colour in untreated, heat-treated and diffusion-treated sapphires in the yellow to red colour range from Sri Lanka, U.S.A., Madagascar and Tanzania; approximate directions of the shift of colour by heat treatment, diffusion treatment and irradiation are indicated with arrows. A dashed arrow indicates the colour change of chromium-free Montana sapphires by high temperature heat treatment (not explained in detail in this paper).

Thermally unstable 'yellow' and/or 'orange' colour centres are present in untreated padparadscha and yellow sapphires from Sri Lanka, thermally stable 'orange' colour centres are developed by simple heat treatment or by diffusion treatment in sapphires from different localities. These thermally stable 'orange' colour centres add to the main causes of colour that are present before treatment, i.e. iron and chromium. The wide variety of colours in untreated and treated samples is due to large variation in chromium and/or iron contents and to the intensity of thermally unstable or thermally stable colour centres in untreated samples or after heat or diffusion treatment.

assignments of absorption bands in the visible and ultraviolet range is given by Schmetzer and Schwarz (2004) and the references cited therein.

- In general, there are five main colour-causing components of absorption spectra to consider for untreated, heat-treated and beryllium-diffusion-treated sapphires.
- The absorption bands of two of these components, namely Cr^{3+} and Fe^{3+} , are – in general – not changed in intensity by various types of treatment.
- The absorption bands assigned to $\text{Fe}^{2+}/\text{Ti}^{4+}$ pairs (related to a blue sapphire component)

in contrast, are present mainly in untreated samples, e.g. in specific growth zones of some Sri Lanka padparadschas, in untreated purple to violet sapphires from Songea and Ilakaka and in bluish-green and blue Montana sapphires. This blue sapphire component is reduced in intensity by heat treatment in an oxidizing atmosphere and was not present in our diffusion-treated samples.

- Thermally unstable yellow and/or orange colour centres are only present in untreated Sri Lanka sapphires, the absorption bands of these colour centres are removed by low

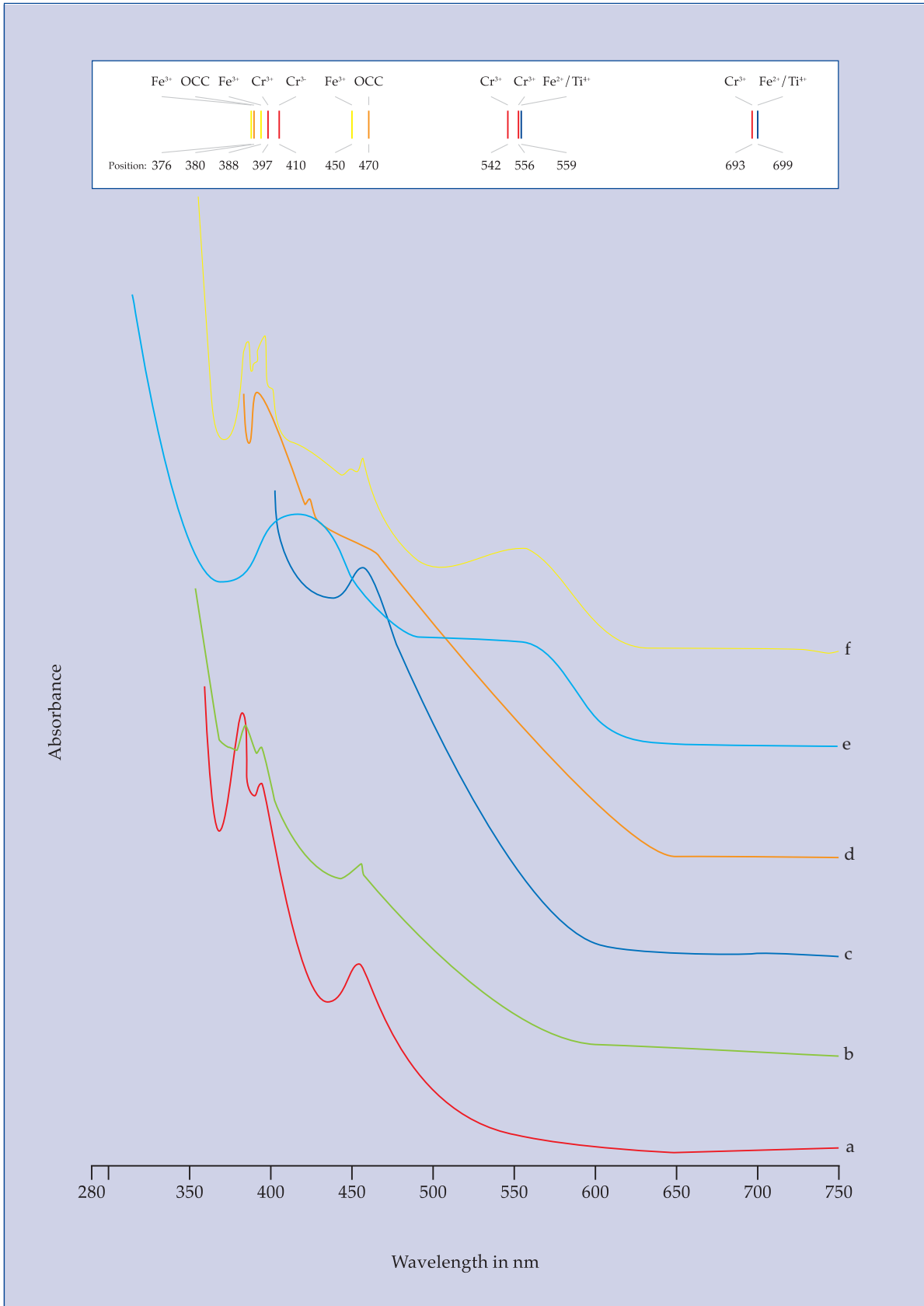


Figure 31: Absorption spectra of heat-treated and beryllium-diffusion-treated sapphires from Montana, in the yellow to brownish-orange colour range: (a) diffusion-treated yellow sapphire, (b) diffusion-treated yellowish-orange sapphire, (c) diffusion-treated orange sapphire, (d) heat-treated orange sapphire, (e) heat-treated pinkish-orange sapphire, (f) heat-treated brownish-orange sapphire. The positions and assignments of absorption maxima are indicated at the top of the Figure; spectra (b) to (e) are vertically displaced for clarity.

temperature heat treatment up to about 600 C.

- Thermally stable orange colour centres are produced by high temperature heat treatment or by high temperature diffusion treatment. Both types of treatment applied to natural sapphires with Fe and Cr produce identical absorption features.

The following discussion augments the spectroscopy described by Schmetzer and Schwarz (2004, p.162 *et seq.*).

For the group of diffusion-treated yellow, yellowish-orange or orange (chromium-free) sapphires from Sri Lanka (not covered by our previous paper), the spectra are more or less identical with those of simply heat-treated Sri Lankan sapphires of the same colour range.

For untreated, diffusion-treated and heat-treated sapphires from Montana which were also not discussed in our previous paper, the following results are summarised:

The absorption spectra of untreated Montana sapphires in the yellowish-green, bluish-green and blue colour range are characterised by strong absorption bands of Fe^{3+} , on which are superimposed $\text{Fe}^{2+}/\text{Ti}^{4+}$ absorption bands (blue) of varying intensity. With increasing intensity of the blue sapphire component, the coloration shifts from yellowish-green to bluish-green or blue. Diffusion treatment of such stones produces yellow, yellowish-orange or orange colours. Their absorption spectra are characterised by strong absorption bands of Fe^{3+} and by absorption caused by orange colour centres (*Figure 31*). With increasing intensity of these orange colour centres, the colour of the samples is shifted from yellow to orange. Absorption bands of the blue sapphire component were completely removed by the beryllium diffusion treatment.

Absorption spectra of simply heat-treated orange, pinkish-orange, reddish-orange or brownish-orange Montana sapphires (*Figure 31*) are a combination of bands due to chromium and orange colour centres. Samples with colour centres dominant are orange, while samples with more intense chromium bands are pinkish- or reddish-orange. Sapphires with additional strong iron absorption bands are brownish orange. As described by Emmett and Douthit (1993),

padparadscha-like colours are produced by oxidising heat treatment of originally pink Montana sapphires. This colour change is caused by the development of orange colour centres by heat treatment. Similar absorption spectra have been obtained from high temperature heat-treated sapphires from Sri Lanka.

The diagram (*Figure 30*) summarises the reaction to various treatments of untreated, heat-treated and beryllium-diffusion-treated sapphires from all four localities. Thermally unstable 'yellow' and/or 'orange' colour centres in Sri Lankan sapphires are removed by low temperature heat treatment. High temperature heat treatment causes the development of thermally stable 'orange' colour centres in sapphires from Sri Lanka and Montana. By beryllium diffusion treatment, similar or identical 'orange' thermally stable colour centres are developed in samples from all four countries.

PART III

A microscopy-based screening system

It is evident that without a detailed knowledge of diagnostic features of the types of treated and untreated sapphires on the international market, a gemmological examination would be incomplete and inconclusive. Furthermore, one needs that knowledge to decide whether a quantitative and costly beryllium determination is justified.

This costly option should be avoided if possible by determining gemmological properties which can indicate a locality of origin as well as any possible treatment. To assist this process and add to the microscopic properties such as inclusion features already described by different authors, we propose growth pattern, colour zoning and colour distribution pattern, observed at low and high magnifications, as key features for identification.

Figure 32 summarises the identification procedure. Any gemmologist equipped with a horizontal immersion microscope or with a more simple immersion cell which can be

added to a vertical microscope can use this flow diagram starting at steps a, b, and c. For those gemmologists unused to immersion microscopy, some training would be necessary to determine correctly the growth pattern and colour zoning of a faceted sapphire. Having done that, it would be helpful to compare this pattern with characteristic examples shown in this paper.

In order to identify untreated, heat-treated or beryllium-diffusion-treated yellow, orange, pinkish-orange or reddish-orange sapphires, one needs to know the nature of any growth patterns and colour zoning (in immersion by low and high magnification) and to identify any inclusions that might be in a 'natural' state or that might be altered. In many cases, the results of these visual observations can lead to a conclusive result.

If, however, the data are inconclusive, the gemmologist should go to steps d and e which are nowadays available as routine procedures in gemmological laboratories. The measurement of an absorption spectrum in the visible and UV and the determination of trace-element contents might be helpful, especially for the assessment of locality-

specific features and possible treatment history of a sample. The additional information from spectroscopic and chemical examination may confirm preliminary results of microscopic examination or they can, in other cases, definitely exclude some possibilities of origin or treatment.

If absorption spectroscopy and trace-element chemistry (steps d and e) cannot be done or if they – in combination with steps a, b and c – do not lead to a possible identification of the sample, a direct determination of the beryllium content is necessary (step f).

Even if the data from steps a, b, and c do not lead to a precise result, regarding the treatment history of a sapphire with unknown origin, they may help determine the category to which a sapphire belongs and which types or groups of samples can be excluded. If, for example, we consider a sapphire with inclusions altered by high temperature treatment and with a growth pattern typical of a Songea stone, Sri Lankan and Montana origins would be ruled out for the stone, but the possibilities of high temperature or

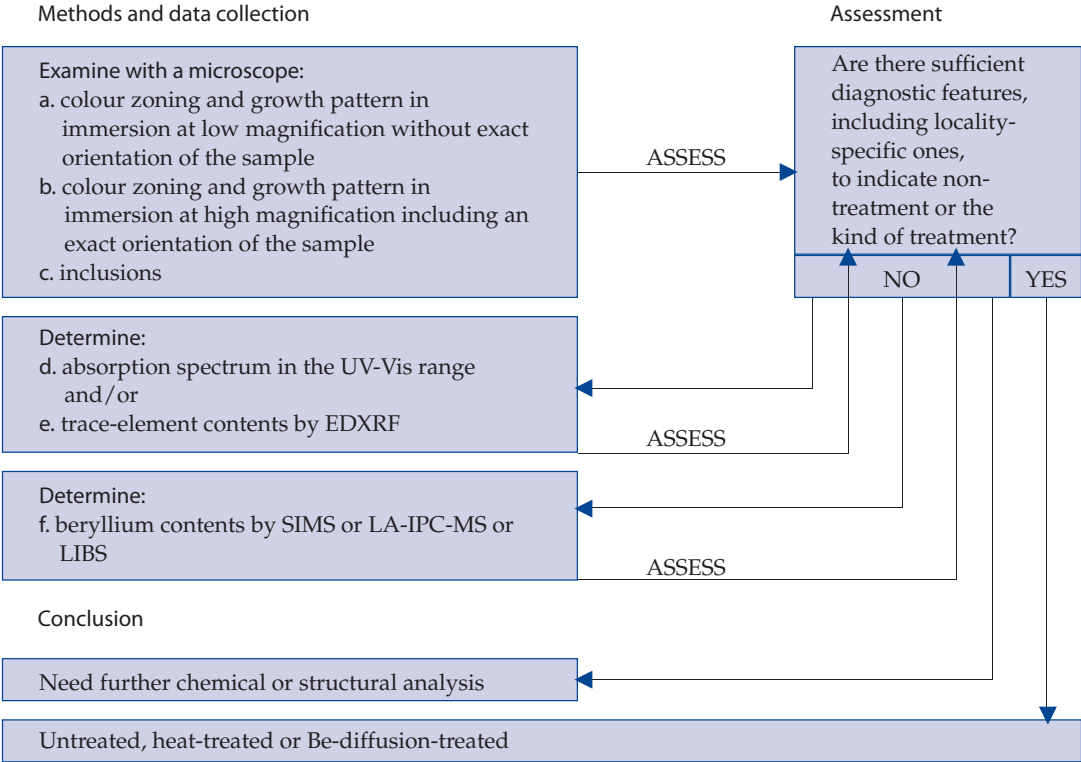


Figure 32: Summary of the suggested screening process for sapphires.

Be-diffusion treatment remain. It would then be for the client to decide if a quantitative beryllium determination is desirable.

Using the diagnostic features outlined above and other characteristic properties for each locality, it is – in general – possible to recognise a great percentage of orange to reddish-orange sapphires (padparadschas) from Sri Lanka as untreated or heat-treated, and to confirm their locality of origin. In most sapphires of this type, the colour is distributed in such way that there should be no confusion with beryllium-diffusion-treated sapphires from the localities examined. This applies also for heat-treated orange, reddish-orange or brownish-orange Montana sapphires.

Diffusion-treated sapphires, on the other hand, which do not show a characteristic strongly-coloured rim, may also be recognised

by the lack of any typical colour zoning (in the case of Ilakaka and Sri Lanka material) or by a characteristic growth pattern associated with a typical colour zoning (typical of Songea sapphires as described in the example below).

Neither untreated nor heat-treated orange or reddish-orange sapphires from Sri Lanka or Montana, nor untreated brownish-orange sapphires from Ilakaka, show a combination of the identification features mentioned below for this particular orange Songea sapphire and, consequently, this sample is identifiable as diffusion-treated sapphire because neither untreated nor heat-treated samples from any natural source show this combination of diagnostic features. A similar general assignment to the specific category of diffusion-treated sapphires is also possible

Example: Beryllium-diffusion-treated orange sapphire from Songea

A 1.42 ct orange sapphire submitted from Bangkok for examination (*Figure 33a*) gave the following results:

- a. *Immersion at low magnification*: Colour zoning light orange/intense orange is related to growth zoning (*Figure 33b*).
- b. *Immersion at high magnification*: A complex growth pattern consisting of the basal pinacoid c combined with rhombohedral r {1011} and dipyrarnidal n {2243} faces (*Figure 33c*). The c growth sectors are more strongly coloured than r and n sectors.
- c. *Inclusions*: No mineral inclusions useful in indicating if any treatment were present.
- d. *Chemistry*: Fe_2O_3 1.26 wt.%, Cr_2O_3 0.05 wt.%
- e. *Spectroscopy*: Intense iron and chromium absorption bands on which are superimposed an intense 470 nm absorption band caused by orange colour centres (*Figure 34a*).

Discussion: The growth pattern and iron content are typical for sapphires from Songea. The chromium content is smaller than that determined for our red to orange red samples, but untreated yellowish-green to greenish-blue and blue samples from Songea with lower chromium contents are known (Schwarz and Schmetzer, unpublished). These samples commonly have an almost colourless core and a more intensely coloured rim.

The colour zoning with a more intense centre related to a basal growth sector and a less intense rim related to rhombohedral and bipyramidal growth sectors is consistent with the use of this type of material for diffusion treatment. A lighter colour is produced in the rim, because part of the beryllium is needed to compensate titanium in the originally blue or greenish-blue part of the sample, which is not necessary in the originally colourless core. The spectrum shows an intense absorption band at 470 nm which is not obtained by simple heat treatment and confirms this result.

In summary, sapphires heat-treated only with no Be-diffusion, with this combination of properties, are not known, so this is a Be-diffusion-treated sapphire.

for orange Ilakaka sapphires which lack any growth and colour zoning but most of which contain typical altered inclusion clusters. It is also possible to identify diffusion-treated samples from Sri Lanka which contain altered inclusions and a typical mosaic-like growth pattern in the absence of any colour zoning. Again, untreated material from Sri Lanka should show no altered inclusions and heat-treated samples from Sri Lanka or Montana should reveal a distinct colour zoning.

As expected at the beginning of this study, there were insufficient diagnostic properties in some samples to determine their treatment history or origin. These few samples were almost free of inclusions and without any growth and colour zoning. Such samples, found in lots from any locality, and within categories of treated and untreated material, would need to be tested for beryllium for a final identification.

All heat-treated yellow sapphires from Sri Lanka showed a clear colour zoning with intense yellow or orangey-yellow and near-colourless alternating zones. Of the diffusion-treated sapphires from Sri Lanka, all but one were homogeneously coloured. This exception had weak colour zoning with light and medium yellow areas which are related to variable Cr and Mg contents. So although the microscopic screening system works for most yellow to orange Cr-free sapphires from Sri Lanka, the gemmologist should be particularly careful with weakly colour-zoned stones.

The most problematic sample examined was an intensely colour-zoned, diffusion-treated yellow sapphire, possibly of Sri Lankan origin and without an exactly known treatment history. Distinct magnesium zoning was indicated by LA-ICP-MS examination. It is obvious that samples that would have become yellow (and colour-zoned) by simple high temperature heat treatment, could also become yellow (and colour-zoned) by beryllium diffusion treatment if trace-element contents were appropriate. This may explain the colour zoning in this particular sample. Again, the gemmologist should critically review all the evidence a stone can offer.

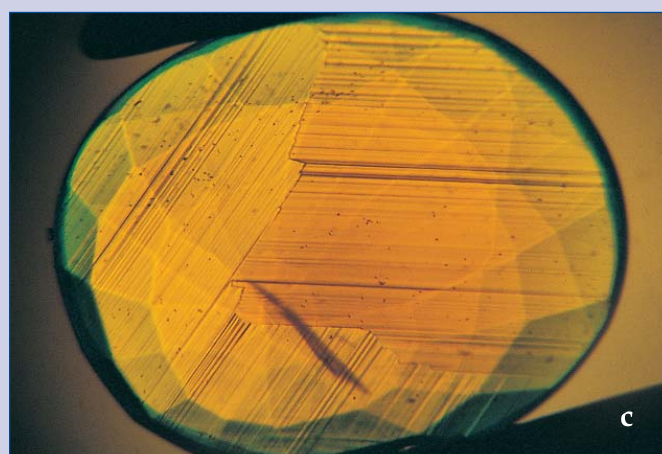
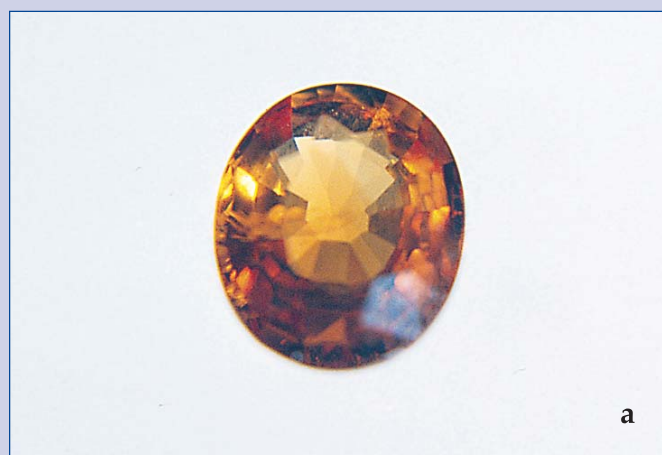


Figure 33: (a) Beryllium-diffusion-treated reddish-orange sapphire of 1.42 ct from Songea. Photo by M. Glas; (b) Colour zoning in this sapphire is visible in immersion at low magnification; differently coloured growth sectors are visible. Photo by K. Schmetzer; (c) Colour zoning in this sapphire in immersion at high magnification; differently coloured basal c (darker) and dipyramidal r (lighter) growth sectors are visible. I, 40x. Photo by K. Schmetzer.

Box B: Two case studies using the proposed system

For untreated light yellow, greenish-yellow, yellowish-green, greenish-blue or blue sapphires with multiple colour zones and using the experimental results described previously by Emmett *et al.* (2003) and Pisutha-Arnond *et al.* (2004 a, b), a blue coloration can be removed or lightened and a yellow coloration can be produced in originally blue areas of a sapphire by diffusion treatment. According to the mechanism of colour change as far as it is understood at present (see also Schmetzer and Schwarz, 2004) we can expect, after beryllium diffusion treatment, a more intense yellow or yellowish-orange coloration in the sapphire zones with lower titanium concentration compared to those with higher titanium. In colour-zoned sapphires with high iron concentrations, e.g. in sapphires of basaltic origin, these areas are frequently (in the untreated state) yellow, yellowish-green or light blue, in contrast to greenish-blue or more intense blue areas with higher titanium concentrations. Diffusion treatment of basaltic sapphires with extreme chemical zoning, can result in sapphires with very intense orange and blue zones, a feature not yet observed in untreated sapphires or in ones that had been simply heat-treated.

For the interpretation of the absorption spectra presented, the reader should compare the data given in our previous paper (Schmetzer and Schwarz, 2004); for an overview of absorption spectra of various types of untreated and heat-treated yellow to yellowish-orange sapphires the reader should also refer to Schmetzer *et al.* (1983).

Case study 1: Beryllium diffusion-treated yellow to yellowish-orange sapphires from Antsiranana, Madagascar

Beryllium diffusion-treated sapphires from Antsiranana province, northern Madagascar (and also from other basaltic sources) are now released in quantity from Bangkok on to the international market (see Atichat, 2004). Untreated and heat-treated material from this source was described in detail by Schwarz *et al.* (2000). We examined three diffusion-treated intense yellow to yellowish-orange sapphires (*Figure 35a*) with the following results:

- a. Immersion at low magnification: One sample showed a weak colour zoning and two samples showed a more intense colour zoning related to growth structures (*Figure 35b*).
- b. Immersion at high magnification: The three samples showed growth structures parallel to the basal pinacoid c (0001) and parallel to the hexagonal dipyrmaid z {2241} (*Figure 35c*), the colour zoning was confined to z growth sectors.
- c. Inclusions: The three samples did not contain any mineral inclusions useful to indicate a possible heat or diffusion treatment.
- d. Chemistry: Fe_2O_3 1.50, 1.66, and 1.90 wt.% for the three samples, Cr_2O_3 was below the detection limit in each stone.
- e. Spectroscopy: Each sample showed intense iron absorption bands, the 470 nm absorption of orange colour centres was also present (*Figure 34b*).

Discussion: From the Antsiranana province, many untreated basaltic sapphires are colour-zoned with yellow, greenish-blue and blue areas. This colour zoning is always confined to growth structures, with, e.g. the basal pinacoid c and the hexagonal dipyrmaid z as dominant growth planes. The possibility to improve samples of this nature by simple heat treatment into sapphires with the more 'marketable' homogeneous colours is limited (Schmetzer and Schwarz, unpublished research). Iron values are in the range observed for our three samples, chromium contents are also below detection limit (see Schwarz *et al.*, 2000). The growth and colour zoning

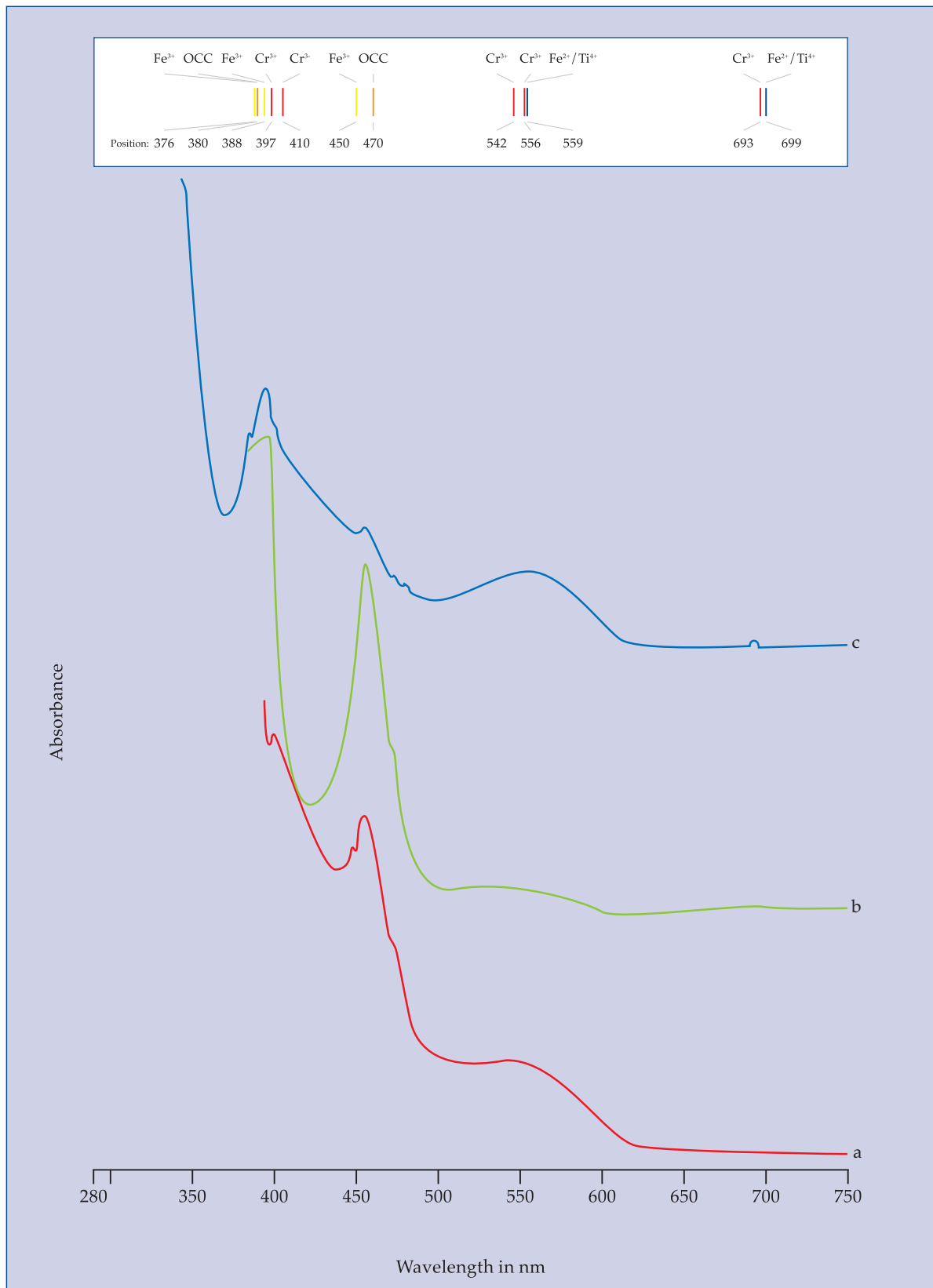


Figure 34: Absorption spectra of heat-treated and beryllium-diffusion-treated sapphires: (a) beryllium-diffusion-treated reddish-orange sapphire of 1.42 ct from Songea; the spectrum shows the absorption bands of Fe³⁺, Cr³⁺ and orange colour centres; (b) beryllium-diffusion-treated yellow sapphire from Antsiranana province, Madagascar; the spectrum shows the absorption bands of Fe³⁺ and orange colour centres; (c) heat-treated brownish-orange sapphire from Ilakaka, Madagascar; the spectrum shows the absorption bands of Cr³⁺, Fe³⁺ and orange colour centres. The positions and assignments of absorption maxima are indicated at the top of the Figure; spectra (b) and (c) are vertically displaced for clarity.

patterns of the three samples are related to those of the untreated sapphires. A more intense yellow is produced in originally yellow zones with lower titanium contents and a less intense yellow is produced in originally greenish-yellow to greenish-blue or blue areas. This is consistent with Be compensating for Ti as discussed above.

In summary: Sapphires with this combination of properties are unknown in the untreated or simply heat-treated categories.



Figure 35: (a) Beryllium-diffusion-treated yellow sapphires from Antsiranana province, Madagascar; range of samples from 2.01 to 2.86 ct. Photo by M. Glas; (b) Colour zoning in the yellow sapphire of 2.86 ct in immersion at low magnification; differently coloured growth sectors are visible. Photo by K. Schmetzer; (c) Colour zoning associated with dipyrnidal z growth planes in the yellow sapphire of 2.86 ct in immersion at higher magnification. I, 25x. Photo by K. Schmetzer.

Case study 2: Heat-treated orange sapphire from Madagascar

During this study we also received a slightly brownish-orange sample of 2.56 ct described as heat-treated Madagascar ‘padparadscha’ (Figure 36a). The owner was unable to provide a history for the stone. The following properties were determined:

- Immersion at low magnification: the orange colour of the sample is related to an irregularly shaped core of the sapphire (Figure 36b), but not to the rim.
- Immersion at high magnification: No specific sharp growth lines or colour zoning seen.
- Inclusions: Numerous tiny mineral inclusions were present, and some showed thermal decomposition and alteration (Figure 36c) but there was no sign of any melt in fractures and fissures.
- Chemistry: Trace-elements not determined.
- Spectroscopy: Absorption bands of chromium and iron (Figure 34c) with superimposed bands from orange colour centres.

Discussion: The inclusion features are consistent with those in heat- or diffusion-treated sapphires from Ilakaka, and the alteration indicates temperatures of treatment in the range of about 1700 to 1750 C. Although this absorption spectrum is common in diffusion-treated Ilakaka sapphires, it alone is not sufficient to indicate diffusion treatment. The presence of colour zoning related to an irregularly shaped core indicates that orange colour centres were developed upon treatment only in the core of the sapphire, but not in the rim. Beryllium diffusion treatment would have created colour in the rim, and so this pale rim allows – in combination with the other properties mentioned – characterisation of the sample as heat-treated brownish-orange Ilakaka sapphire.

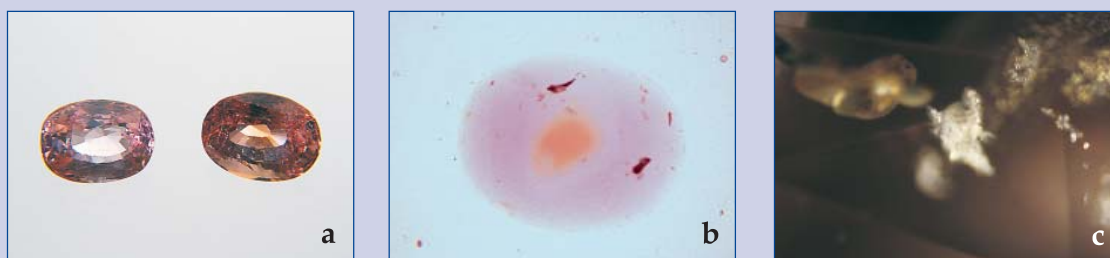


Figure 36: (a) Heat-treated padparadscha from Sri Lanka of 2.23 ct (left) and heat-treated slightly brownish-orange sapphire from Ilakaka, Madagascar of 2.56 ct (right). Photo by M. Glas; (b) colour zoning in brownish-orange sapphire of 2.56 ct; the core of the sample shows a higher colour concentration compared to the much lighter rim, the orange coloration of the sapphire is related to the core. The sapphire measures 7.0 x 9.0 mm. Photo by K. Schmetzer; (c) brownish-orange sapphire of 2.56 ct with decomposed inclusions, most probably zircons. 50x. Photo by L. Kiefert.

Conclusions

The microscopy-based screening system presented here is mainly based on a combination of structural microscopic properties such as growth pattern, colour zoning and distribution, and inclusion features. The addition of chemical and spectroscopic properties as characteristic, origin-related features may be helpful in indicating possible beryllium diffusion treatment. Nevertheless, it should be recognised that although the system is based on a comprehensive sample of sapphires on the market, there could still be some from other, unsampled localities which are commercially treated.

That said, the combination of characteristics used to date enables the recognition of most untreated and heat-treated Sri Lanka padparadschas, heat-treated Montana sapphires and beryllium-diffusion-treated materials. For a small percentage of diffusion-treated orange sapphires, a lack of characteristic inclusions should prompt further analysis.

The key for successful screening of lots of samples of unknown origin and unknown treatment history will always be to compare their features with those of treated and untreated samples from a specific

locality. Without this specific combination of characteristic features related to locality, i.e. considering sapphires only in three groups, namely 'untreated', 'heat-treated' and 'diffusion-treated' as in the past, much information is overlooked. If one can use locality-related information, the percentage of samples which can be recognised in a normally equipped gemmological laboratory as untreated, heat-treated or diffusion-treated would rise significantly; this in turn would reduce the need for Be analysis.

Printing of the article generously sponsored by the Dr Eduard Gübelin Association for research and identification of precious stones in Lucerne, Switzerland

Acknowledgements

The authors are grateful to the following for providing research material: Dr J.L. Emmett, Brush Prairie, Washington, U.S.A.; Ernst Färber company, Munich, Germany; Fine Gems International, Helena, Montana, U.S.A.; Rolf Goerlitz company, Idar-Oberstein, Germany; Dr E.J. Gübelin, Lucerne, Switzerland; Dr H.A. Hänni, SSEF,

Basel, Switzerland; T. Hainschwang, Ruggell, Liechtenstein; J.I. Koivula, GIA, Carlsbad, U.S.A.; Rudolf Schupp company, Pforzheim, Germany; Martin Steinbach company, Köln, Germany; T. Themelis, Bangkok, Thailand; Dr Pornsawat Wathanakul, Kasetsart University, Bangkok, Thailand; Paul Wild company, Idar-Oberstein, Germany; Wild & Petsch company, Idar-Oberstein, Germany. Dr J.L. Emmett, Brush Prairie, Washington, U.S.A., performed beryllium diffusion treatment of three lots of samples originating from Montana, U.S.A. and Sri Lanka. Dr E.J. Gübelin, Lucerne, Switzerland, Dr L. Kiefert, SSEF, Basel, Switzerland, and M. Glas of Starnberg, Germany, were helpful with photography of faceted gemstones and inclusions (see figure captions). Mr. C. Dunaigre of the Gübelin GemLab, Lucerne, Switzerland, performed some mineral examinations with the Raman microprobe. Dr T. Pettke, ETH, Zürich, Switzerland, and Dr M. S. Krzemnicki, SSEF, Basel, Switzerland, provided trace element analyses by laser ablation-inductively coupled plasma-mass spectroscopy (LA-ICP-MS) of two specific samples. Problems of Be-diffusion of sapphires were discussed with Dr H.A. Hänni, SSEF, Basel, Switzerland, and Dr T. Häger of Mainz University, Germany, which is also acknowledged. We also thank those individuals or companies who wish to remain anonymous.

All photos by M. Glas, Starnberg, Germany, E.J. Gübelin, Lucerne, Switzerland, L. Kiefert, SSEF, Basel, Switzerland (now at AGTA-GTC, New York, U.S.A.), and K. Schmetzer, Petershausen, Germany

References

- Adolfsson, E., Nygren, M., and Hermansson, L., 1999. Decomposition mechanisms in aluminium oxide-apatite systems. *Journal of the American Ceramic Society*, 82(10), 2909-12
- Atichat, W., Sriprasert, B., Wathanakul, P., Pisutha-Arnond, V., Tay, T.S., Puttarat, T., and Leelawatanasuk, T., 2004. Characteristics of 'beryllium' heat-treated yellow sapphires. *29th International Gemmological Conference, 2004, Abstracts*, 207-14
- Butterman, W.C., and Forster, W.R., 1967. Zircon stability and the ZrO_2 - SiO_2 phase diagram. *American Mineralogist*, 52(5/6), 880-5
- Coldham, T., 2002. Orange sapphires or just lemons? *Australian Gemmologist*, 21(7), 288-93
- Collins, A.T., 2001. The colour of diamond and how it may be changed. *Journal of Gemmology*, 27(6), 341-59
- Crowningshield, R., 1983. Padparadscha: What's in a name? *Gems & Gemology*, 19(1), 30-6
- De Maesschalck, A.A., and Oen, I.S., 1989. Fluid and mineral inclusions in corundum from gem gravels in Sri Lanka. *Mineralogical Magazine*, 53(5), 539-45
- Emmett, J.L., and Douthit, T.R., 1993. Heat treating the sapphires of Rock Creek, Montana. *Gems & Gemology*, 29(4), 250-72
- Emmett, J.L., Scarratt, K., McClure, S.F., Moses, T., Douthit, T.R., Hughes, R., Novak, S., Shigley, J.E., Wang, W., Bordelon, O., and Kane, R.E., 2003. Beryllium diffusion of ruby and sapphire. *Gems & Gemology*, 39(2), 84-135
- Fisher, D., and Spits, R.A., 2000. Spectroscopic evidence of GE POL HPHT-treated natural type IIa diamonds. *Gems & Gemology*, 36(1), 35-42
- Francis, M.D.P.L., Matsueda, H., Torimoto, J., Dharmaratne, P.G.R., and Giuliani, G., 2003. Recent study of fluid inclusions in corundum of Sri Lanka. *Gemmologie. Zeitschrift der Deutschen Gemmologischen Gesellschaft*, 52(4), 163-76
- Fritsch, E., Chalain, J.-P., Hänni, H., Devouard, B., Chazot, G., Giuliani, G., Schwarz, D., Rollion-Bard, C., Garnier, V., Barda, S., Ohnenstetter, D., Notari, F., and Maitrallet, P., 2003. Le nouveau traitement produisant des couleurs orange à jaune dans les saphirs. *Revue de Gemmologie A.F.G.*, 147, 11-23
- Hänni, H.A., 2002. Orange treated sapphire – towards finding a name for a new product. *Journal of the Gemmological Association of Hong Kong*, 23, 23-9
- Hänni, H.A., Krzemnicki, M.S., Kiefert, L., and Chalain, J.P., 2004. Ein neues Instrument für die analytische Gemmologie: LIBS. *Gemmologie. Zeitschrift der Deutschen Gemmologischen Gesellschaft*, 53(2/3), 79-86
- Hänni, H.A., and Pettke, T., 2002. Eine neue Diffusionsbehandlung liefert orangefarbene und gelbe Saphire. *Gemmologie. Zeitschrift der Deutschen Gemmologischen Gesellschaft*, 51(4), 137-52
- Hay, R.S., and Boakye, E.E., 2001. Monazite coatings on fibers: I, Effect of temperature and alumina doping on coated-fiber tensile strength. *Journal of the American Ceramic Society*, 84(12), 2783-92
- Hikichi, Y., and Nomura, T., 1987. Melting temperatures of monazite and xenotime. *Journal of the American Ceramic Society*, 70(10), C-252-3
- Hikichi, Y., Ota, T., Daimon, K., Hattori, T., and Mizuno, M., 1998. Thermal, mechanical, and chemical properties of sintered xenotime-type RPO_4 ($R = Y, Er, Yb, \text{ or } Lu$). *Journal of the American Ceramic Society*, 81(8), 2216-18
- Kiefert, L., and Schmetzer, K., 1991. The microscopic determination of structural properties for the characterization of optical uniaxial natural and synthetic gemstones. Part 1: General considerations and description of the methods. *Journal of Gemmology*, 22(6), 344-54
- Koivula, J.I., 1986. Carbon dioxide fluid inclusions as proof of natural-colored corundum. *Gems & Gemology*, 22(3), 152-5
- Krzemnicki, M.S., Hänni, H.A., and Walters, R.A., 2004. A new method for detecting Be diffusion-

- treated sapphires: Laser-induced breakdown spectroscopy (LIBS). *Gems & Gemology*, 40(4), 314-22
- Kuo, D.-H., and Kriven, W.M., 1995. Characterization of yttrium phosphate and an yttrium phosphate/yttrium aluminate laminate. *Journal of the American Ceramic Society*, 78(11), 3121-4
- Lawson, S., 2002. *Instrument for examining a gemstone*. International patent application, publication number WO 02/06797 A1, Jan. 24, 2002
- McClure, S., Moses, T., Wang, W., Hall, M., and Koivula, J.I., 2002. A new corundum treatment from Thailand. *Gems & Gemology*, 38(1), 86-90
- Morgan, P.E.D., and Marshall, D.B., 1995. Ceramic composites of monazite and alumina. *Journal of the American Ceramic Society*, 78(6), 1553-63
- Morgan, P.E.D., Marshall, D.B., and Housley, R.M., 1995. High-temperature stability of monazite-alumina composites. *Materials Science and Engineering A*, 195, 215-22
- Notari, F., 1996. *Le saphir Padparadscha*. Diplôme d'Université de Gemmologie de Nantes, 95 pp
- Notari, F., 1997. Le saphir Padparadscha. *Revue de Gemmologie A.F.G.*, 132, 24-7
- Notari, F., Fritsch, E., and Grobon, C., 2003. Comment l'observation de la luminescence (fluorescence) peut aider à l'identification des corindons jaunes, rose orangé et orange, traités par diffusion de béryllium. *Revue de Gemmologie A.F.G.*, 148, 40-3
- Peretti, A., and Günther, D., 2002. The color enhancement (E) of fancy sapphires with a new heat-treatment technique (Part A): Inducing color zoning by internal (I) migration (M) and formation of color centers. *Contributions to Gemology*, 1, 1-48
- Peretti, A., Günther, D., and Graber, A.-L., 2003. The beryllium treatment of fancy sapphires with a new heat-treatment technique (part B). *Contributions to Gemology*, 2, 21-33
- Pisutha-Arnond, V., Häger, T., Wathanakul, P., and Atichat, W., 2004a. Yellow and brown coloration in beryllium-treated sapphires. *Journal of Gemmology*, 29(2), 77-103
- Pisutha-Arnond, V., Häger, T., Wathanakul, P., and Atichat, W., 2004b. Chemical characteristic of 'classical' versus 'beryllium' heat-treated ruby and sapphire. *29th International Gemmological Conference, 2004, Abstracts*, 92-4
- Pisutha-Arnond, V., Wathanakul, P., Atichat, W., Haeger, T., Win, T., Leelawatanasuk, T., and Somboon, C., 2003. Beryllium-treated Vietnamese and Mong Hsu rubies. In: Hofmeister W., Quang V.X., Doa N.Q., Nghi T. (Eds.) *Proceedings of the 2nd International Workshop on Geo- and Material-Science on Gem-Minerals of Vietnam, Hanoi, October 1-8, 2003*, 171-5
- Radziemski, L.J., and Cremers, D.A., 1985. *Apparatus and method for quantitative determination of materials contained in fluids*. United States Patent 4,561,777, Dec. 31, 1985
- Rankin, A.H., and Edwards, W., 2003. Some effects of extreme heat treatment on zircon inclusions in corundum. *Journal of Gemmology*, 28(5), 257-64
- Rankin, A.H., Greenwood, J., and Hargreaves, D., 2003. Chemical fingerprinting of some East African gem rubies by laser ablation ICP-MS. *Journal of Gemmology*, 28(8), 473-82
- Saminpanya, S., Manning, D.A.C., Droop, G.T.R., Henderson, C.M.B., 2003. Trace elements in Thai gem corundums. *Journal of Gemmology*, 28(7), 399-415
- Schmetzer, K., 1986. An improved sample holder and its use in the distinction of natural and synthetic ruby as well as natural and synthetic amethyst. *Journal of Gemmology*, 20(1), 20-33
- Schmetzer, K., Bosshart, G., and Hänni, H.A., 1983. Naturally-coloured and treated yellow and orange-brown sapphires. *Journal of Gemmology*, 18(7), 607-22
- Schmetzer, K., and Medenbach, O., 1988. Examination of three-phase inclusions in colorless, yellow, and blue sapphires from Sri Lanka. *Gems & Gemology*, 24(2), 107-11
- Schmetzer, K., and Schwarz, D., 2004. The causes of colour in untreated, heat-treated and diffusion-treated orange and pinkish-orange sapphires – a review. *Journal of Gemmology*, 29(3), 149-82
- Schwarz, D., 2001. Sapphires and rubies from the Ruvuma (Tunduru and Songea), Lindi (Liwale) and Mtwara (Mbekenyeru) districts in Southern Tanzania. *XXVIII International Gemmological Conference, Spain 2001, Abstracts*, 82
- Schwarz, D., and Schmetzer, K., 2001. Rubies from the Vatmandry area, eastern Madagascar. *Journal of Gemmology*, 27(7), 409-16
- Schwarz, D., Kanis, J., and Schmetzer, K., 2000. Sapphires from Antsiranana province, northern Madagascar. *Gems & Gemology*, 36(3), 216-33
- Singh, J.P., Yueh, F.-Y., Cook, R.L., and Zhang, H., 1998. *Analytical method using laser-induced breakdown spectroscopy*. United States Patent 5,751,416, May 12, 1998
- Smith, C.P., 1996. Introduction to analyzing internal growth structures: Identification of the negative d plane in natural ruby. *Gems & Gemology*, 32(3), 170-84
- Sutherland, F.L., Schwarz, D., Jobbins, E.A., Coenraads, R.R., Webb, G., 1998. Distinctive gem corundum suites from discrete basalt fields: a comparative study of Barrington, Australia, and West Pailin, Cambodia, gemfields. *Journal of Gemmology*, 26(2), 65-85
- Themelis, T., 2003. *Beryllium-Treated Rubies & Sapphires*. Themelis, Bangkok, 48 pp
- Themelis, T., 2004. LIBS: a spark of inspiration in gemmological analytical instrumentation. *Australian Gemmologist*, 22(4), 138-45
- Wang, W., and Green, B., 2002. An update on Be-diffused corundum. *Gems & Gemology*, 38(4), 363-5
- Zhang, Y., and Guan, H., 2003. Hydrothermal synthesis and characterization of hexagonal and monoclinic CePO₄ single-crystal nanowires. *Journal of Crystal Growth*, 256, 156-61

Growth of hexagonal bipyramidal ruby crystals by the evaporation of molybdenum trioxide flux

Katsuya Teshima, Hitoshi Kondo¹ and Shuji Oishi

*Department of Environmental Science and Technology,
Faculty of Engineering, Shinshu University, Wakasato, Nagano 380-8553, Japan.
E-mail: teshima@gipwc.shinshu-u.ac.jp*

*1. Present address: Plastic Laminated Package Division, Shinko Electric Industries Co., Ltd.,
Wakaho, Nagano 380-0103, Japan*

Abstract: *Ruby crystals with hexagonal bipyramidal shape have been grown by the evaporation of MoO₃ flux isothermally. Red transparent crystals up to 1.8 mm in length and 1.7 mm in width were obtained, their sizes depending on the solute concentration and the holding temperature. Their form was a double six-sided pyramid bounded by twelve well-developed {112̄3} faces of isosceles triangle shape. The habit of ruby crystals grown by this isothermal method of MoO₃ flux evaporation is quite different from the habits of ruby crystals grown by slow-cooling or temperature-gradient.*

Keywords: *flux growth, hexagonal bipyramid, molybdenum trioxide, synthetic ruby*

Introduction

Ruby (Al₂O₃:Cr) is one of the most attractive of red gemstones and belongs to the rhombohedral system.¹ Chemically, ruby is mainly composed of aluminium oxide (Al₂O₃), and the crystalline form found in nature is called corundum. Alumina is a general name for all forms of aluminium oxide, while corundum refers only to the crystalline material. Pure corundum is colourless and in gem deposits, may be called 'white sapphire'. On the other hand, ruby is aluminium oxide doped with chromium, and the chromium is responsible for the characteristic red colour. Therefore, although ruby can be thought of as 'red sapphire', its name was used long before the similarities of its characteristics with those of sapphire

were realised and made public. Many crystal growth techniques, including Verneuil, Czochralski, hydrothermal, vapour phase and flux²⁻¹¹ have been utilized successfully to synthesize ruby single crystals. Among these techniques, the flux growth is very convenient and can produce ruby crystals at temperatures well below the melting point of the solute. Furthermore, the most important advantage is that the grown crystals have an idiomorphic or euhedral habit.

Flux growth procedures can be categorized into slow-cooling, flux-evaporation and temperature-gradient by the difference in the driving force of crystallization. Many researches have been reported on the slow-cooling growth of ruby crystals using

systems of lead compounds, PbF_2 ^{4,8} $\text{PbO-B}_2\text{O}_3$ ^{6,9} and PbO-PbF_2 ^{5,7}, as solvents. However, lead compounds are not safe to store and handle because of their toxicity. In addition, it is very difficult to separate grown crystals from these fluxes. Most ruby crystals grown from these fluxes are thin hexagonal plates with well-developed {0001} faces.⁴⁻⁹ In flux growth using the temperature-gradient method, Na_3AlF_6 and $\text{Na}_3\text{AlF}_6\text{-Li}_3\text{AlF}_6$ were employed as solvents.^{10,11} The grown crystals displayed faces in the forms {0001}, {2243} and {1011}. However, except for Oishi *et al.*², no study has been reported on the MoO_3 flux-evaporation of ruby crystals.

In carrying out flux growth of ruby crystals, there is an obvious necessity for less dangerous flux materials. In the case of flux-evaporation, molybdate system fluxes are much less dangerous than lead compounds and are, therefore, good candidates as alternatives. Recent work in growth of gem crystals using systems of molybdate fluxes¹²⁻¹⁵ has led to a recent conclusion that hexagonal bipyramidal ruby crystals can be synthesized from molybdenum trioxide flux. In this paper, we report on the growth of hexagonal ruby crystals from a MoO_3 flux at a growth temperature much less than the melting point of ruby. Additionally, the morphology and size of the resulting crystals are discussed in terms of growth conditions, such as solute concentration and growth temperature.

2. Experimental method

Ruby crystals were grown by flux-evaporation (an isothermal technique) from mixtures of reagent grade Al_2O_3 and Cr_2O_3 using MoO_3 as flux. The typical growth conditions are shown in Table I. The solute (0.430-2.200 g) and flux (27.881-29.572 g) powders were weighed out, mixed together and put into platinum crucibles (36 mm diameter x 40 mm height) with loosely sealed lids. The crucibles were heated at a rate of about 45 C per hour to 1000, 1050, 1100 or 1200 C and held at this temperature for 5 h. Subsequently, the crucibles were taken out from the furnace and rapidly cooled at

room temperature. The crystal products were separated from the remaining flux in warm water. The morphology of grown crystals was observed by optical microscope (Keyence, VH-Z450+VH-7000C) and a confocal laser scanning microscope (Leica, TCSNT). The structure and chemical composition of the grown crystals were studied by X-ray diffraction (XRD, Rigaku, RINT-1500) and electron probe microanalysis (EPMA, JEOL, JXA-8900R). The length (L , parallel to the c -axis) and width (W , perpendicular to the c -axis) of the ruby crystals were measured and their average length (L_{av}) and width (W_{av}) were calculated for each growth run.

Table I: Growth conditions of the ruby crystals

Run No.	Solute			Flux	Holding temperature / C
	Content (mol%)	Al_2O_3 /g	Cr_2O_3 /g	MoO_3 /g	
1	2	0.428	0.002	29.572	1100
2	4	0.860	0.004	29.140	1100
3	5	1.078	0.005	28.922	1100
4	6	1.298	0.007	28.702	1100
5	7	1.519	0.008	28.481	1100
6	8	1.741	0.009	28.259	1100
7	10	2.189	0.011	27.811	1100
8	7	1.519	0.008	28.481	1000
9	7	1.519	0.008	28.481	1050
10	7	1.519	0.008	28.481	1200

3. Results and discussion

3.1 Growth of ruby crystals

Bipyramidal ruby crystals, up to 1.8 mm L x 1.7 mm W in size, were isothermally grown from the MoO_3 flux (Table I; runs 1-5, 9 and 10). Figure 1 shows the typical grown crystals of ruby. The crystals were red and transparent. After 5 hours holding at 1100 and 1200 C the flux evaporation ratios of all runs were higher than 98 mass%.

In order to examine the effect of solute content on crystal averages (L_{av} and W_{av}), the growth experiments (runs 1-7) were attempted with a constant holding temperature of 1100 C and various solute contents. The L_{av} and W_{av} are plotted against solute content in Figure 2. Relatively large crystals of $L_{av} = 1.2$ mm and $W_{av} = 1.0$ mm



Figure 1: Ruby crystals grown from MoO_3 flux.

were grown from flux with 7 mol% of solute (run 5). The number of crystals was 798 and the yield was 91.5 mass %. The average mass of the crystals was 1.8×10^{-3} g. The crystal size decreased drastically with decreasing solute content. When the solute amount was 2 mol%, 1564 small crystals (0.384 g) of $L_{\text{av}} = 0.6$ mm and $W_{\text{av}} = 0.5$ mm were grown. The average mass of the crystals was 2.46×10^{-4} g. On the other hand, a countless number of crystallites was produced in runs 6 and 7, which contain higher than 8 mol% of solute.

The relationship between the holding temperature and the loss of flux or the

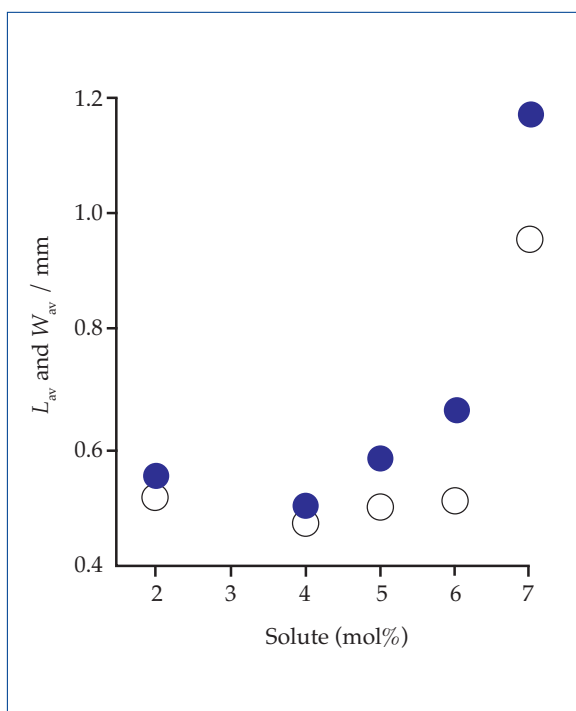


Figure 2: Variation of average length (L_{av} , closed circles) and width (W_{av} , open circles) values of ruby crystals grown with solute concentration (runs 1-5).

averages of the grown crystals are studied. The solute amount was fixed at 7 mol% (runs 8-10). At 1000 C the evaporation loss was about 40 mass%, thereafter linearly increasing with holding temperature and reaching about 99.5 mass% at higher than 1100 C. The crystal sizes were dependent on evaporation loss with a limit in crystal size ($L_{\text{av}} \sim 1.1 - 1.2$ mm) being reached when the mass loss exceeded 99%. In run 8 at 1000 C, the grown crystals were not large and bipyramidal, but very small crystallites because of a much smaller evaporation loss (about 40 mass%). However, it is possible that bipyramidal crystals could be grown by increasing the holding time at this same temperature. From these results, the optimum holding temperature for growth of large crystals was determined to be higher than 1100 C.

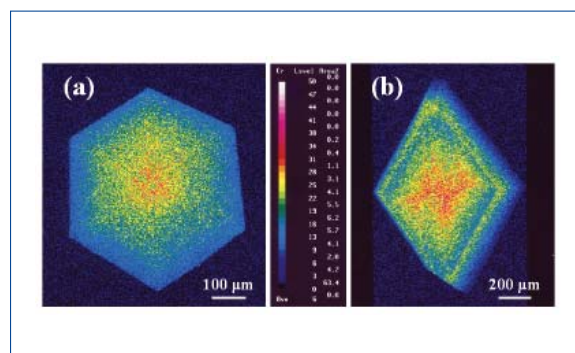


Figure 3: Electron probe microanalysis data showing the distribution of chromium in the faces cut (a) perpendicular and (b) parallel to the c -axis.

3.2 Evaluation of ruby crystals

The grown crystals exhibit the red colour typical of ruby and measure up to 1.2 mm (L_{av}) \times 1.0 mm (W_{av}). The XRD pattern of pulverized crystallites was identical to that of $\alpha\text{-Al}_2\text{O}_3$.¹ The variations in the concentration of the major constituents in the grown crystals were investigated by means of EPMA. Aluminium and oxygen are distributed almost homogeneously in the crystals. The EPMA data showing the distribution of chromium in the grown crystals are shown in Figure 3. Figures 3a and 3b indicate the chromium distributed in sections cut perpendicular and parallel to the c -axis, respectively. The chromium was

preferentially incorporated in the centre of the crystals (Figure 3a), while a small growth zone of increased chromium is visible in the outer parts of the crystal in longitudinal section (Figure 3b). In addition, the chromium was equally distributed in all directions so the characteristic red colour appeared isotropic. Molybdenum from the flux and platinum from the crucible were not detected.

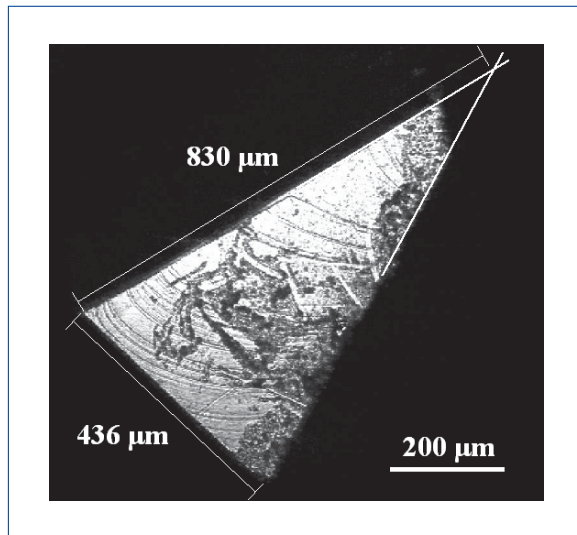


Figure 4: Confocal laser scanning micrograph showing $\{11\bar{2}3\}$ face of the hexagonal bipyramidal ruby crystal.

In order to determine the Miller indices of the crystal faces, the obtained crystals were investigated by XRD without pulverizing them. In the XRD result, only one diffraction line was detected at $2\theta=43.35^\circ$, and assigned to the $\{11\bar{2}3\}$ plane. Furthermore, the Miller indices of the triangular faces were also calculated from their shape. The confocal laser scanning micrograph (CLSM) image of the triangle face is shown in Figure 4. We defined the parameter R to be the side ratio of the triangle face, i.e. $R = (\text{length of a longer side}) / (\text{length of a shorter side})$. The R value obtained from the CLSM image is approximately 1.90. This value is very close to the theoretical value, 1.87, of $\{11\bar{2}3\}$ faces, based on lattice constants $a=4.759$ and $c=12.991$ Å in a hexagonal setting.¹ If the bipyramidal crystals were bounded by $\{22\bar{4}3\}$ faces, the theoretical R value would be 3.31 which is very different from the observed 1.90. In addition, the measured interfacial angles, that is $(11\bar{2}3) \wedge (11\bar{2}3)$ and

$(11\bar{2}3) \wedge (2\bar{1}1\bar{3})$ are, respectively, about 57 ± 1 and 52 ± 1 , which are essentially the same as the theoretical values of 57.57 and 51.98.

As mentioned above, most ruby crystals synthesized from a system of lead compound fluxes are of thin hexagonal platelike habit with well-developed $\{0001\}$ faces.⁴⁻⁹ In contrast, the ruby crystals grown from the MoO_3 flux have a characteristic and unusual habit. Figure 5 shows a typical grown ruby crystal and a schematic drawing of the crystal form consisting of $\{11\bar{2}3\}$ faces. As clearly seen in the optical image, the ruby crystal grown from MoO_3 flux is a hexagonal bipyramid which consists of twelve well-developed $\{11\bar{2}3\}$ faces. The faces are isosceles triangles and their surfaces appear to be comparatively smooth (Figure 5). $\{11\bar{2}3\}$ faces seem not to develop in platy ruby crystals grown by the slow-cooling or temperature-gradient methods. However, in MoO_3 flux, the $\{11\bar{2}3\}$ faces of ruby may adsorb molybdate ions more easily than other faces such as $\{0001\}$, $\{10\bar{1}1\}$ and $\{22\bar{4}3\}$, and so the growth of the $\{11\bar{2}3\}$ faces becomes dominant. However, it is not known why molybdate ions selectively adsorb on the $\{11\bar{2}3\}$ faces.

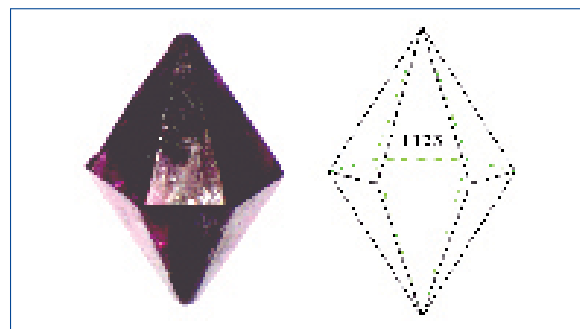


Figure 5: Typical ruby crystal and a schematic drawing of a crystal bounded by the $\{11\bar{2}3\}$ faces.

4. Conclusions

Hexagonal bipyramidal ruby crystals, exhibiting the typical red colour, have been successfully grown by a flux-evaporation technique. To fabricate this unusual form of ruby with MoO_3 as a flux is of primary importance. The grown crystals are bounded by well-developed $\{11\bar{2}3\}$ faces and can be up to 1.8 mm x 1.7 mm in size. The crystal sizes are dependent on the evaporation losses

of the flux which are related to the holding temperature and the solute amount. Since this flux growth process can be conducted at a low temperature far below the melting temperature of Al_2O_3 , the technique will be favourable for the fabrication of not only bulk ruby crystals but also other corundum crystals, such as white, blue, yellow, pink and green sapphire. Furthermore, various surfaces such as Al_2O_3 materials (plate, ball, tube, etc.) and crystal substrates (sapphire, ruby, etc.) can be coated with a corundum crystal layer using epitaxial growth from a MoO_3 flux.

References

- JCPDS card 46-1212
- Oishi, S., Teshima, K., and Kondo, H., 2004. Flux growth of hexagonal bipyramidal ruby crystals. *J. Am. Chem. Soc.*, 126, 4768-9
- Elwell, D., 1979. *Man-made gemstones*. Ellis Horwood Ltd., Chichester
- White, E.A.D., 1961. A new technique for the production of synthetic corundum. *Nature*, 191, 901
- Linares, R.C., 1962. Growth of refractory oxide single crystals. *J. Appl. Phys.*, 33, 1747-9
- Nelson, D.F., and Remeika, J.P., 1964. Laser action in a flux-grown ruby. *J. Appl. Phys.*, 35, 522-9
- Stephens, D.L., and Alford, W.J., 1964. Dislocation structures in single-crystal Al_2O_3 . *J. Am. Ceram. Soc.*, 47, 81-6
- Adams, I., Nielsen, J.W., and Story, M.S., 1966. Growth of broad linewidth ruby crystals. *J. Appl. Phys.*, 37, 832-6
- Oishi, S., Kondo, H., Kobayashi, T., Watanabe, S., Wakabayashi, S., and Sumiyoshi, Y., 1997. Flux growth of ruby crystals. *Nippon Kagaku Kaishi*, 107-11
- Watanabe, K., and Sumiyoshi, Y., 1976. Relationship between habit and etch figures of corundum crystals grown from molten cryolite flux. *J. Cryst. Growth*, 32, 316-26
- Watanabe, K., and Sumiyoshi, Y., 1977. Growth of corundum single crystals from Na_3AlF_6 - $x\text{Li}_3\text{AlF}_6$ system fluxes. *J. Cryst. Growth*, 41, 1-4
- Oishi, S., and Hirao, M., 1991. Growth of emerald crystals from $\text{PbO V}_2\text{O}_5$ flux. *J. Mater. Sci.*, 26, 6401-7
- Oishi, S., and Mochizuki, K., 1993. Growth of emerald crystals by the evaporation of molybdenum trioxide flux. *Br. Ceram. Trans.*, 92, 214-6
- Oishi, S., and Mochizuki, K., 1995. Growth of emerald crystals by the evaporation of $\text{Li}_2\text{O-MoO}_3$ flux. *J. Mater. Chem.*, 5, 1257-60
- Oishi, S., and Yamamoto, H., 1996. Growth of emerald crystals by evaporation of $\text{K}_2\text{O-MoO}_3$ flux. *J. Mater. Chem.*, 6, 1687-91

Sapphire diffusion treatment and the behaviour of iron and titanium

Yang Ruzeng, Yang Yuan and Xu Hongyi

School of Ocean and Earth Science, State Key Laboratory of Marine Geology, Tongji University, Shanghai 200092, China

Abstract: Using the parameters of thickness of diffusion layer and the conditions under which diffusion was carried out in a sample of blue sapphire from Thailand, the diffusion coefficients of iron (D_{Fe}) and titanium (D_{Ti}), the colouring ions, have been calculated. The results indicate that the diffusion coefficient of Ti^{4+} is $6.57 \times 10^{-9} \text{ cm}^2\text{s}^{-1}$ and that of Fe^{2+} is $1.62 \times 10^{-9} \text{ cm}^2\text{s}^{-1}$. The factors affecting D_{Ti} and D_{Fe} are discussed.

Keywords: diffusion coefficient, diffusion treatment, Fick's law of diffusion, sapphire

1. Introduction

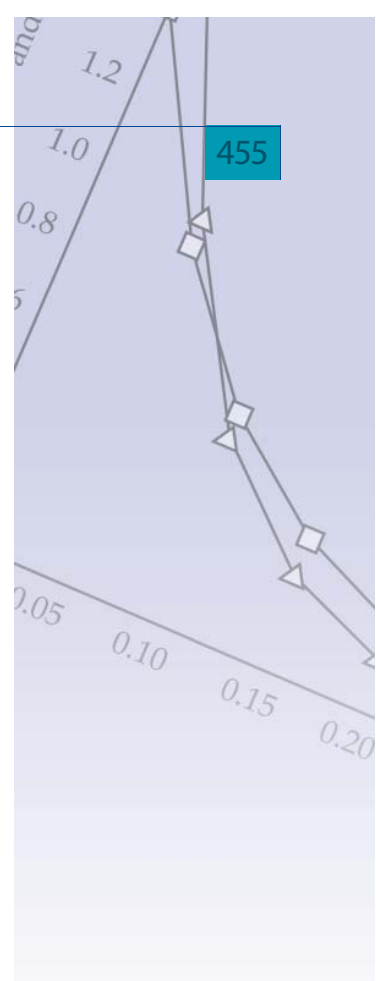
The theoretical foundation of a sapphire's colour treatment lies in the diffusion process of a colouring element or elements into the gemstone. At a high temperature, colouring ions infiltrate into the surface layer of a gemstone through its crystal defects, enhancing its colour appearance. The technique of treating near-colourless sapphire to a deep blue only affected the global gemstone market towards the end of the 1980s.^{1,2} After more than ten years' experimenting and perfecting, the craft has been greatly developed. But mainly for financial reasons, systematic study has not been comprehensive and most treatments are empirical, proceeding by trial and error. Consequently, developed theory is inadequate for communication. So it is hard to forecast the dependability and the precise effect that this colour-altering craft will have on any one batch of gemstones.³ It is both theoretically and practically relevant to discuss the

technique and mechanism of sapphire diffusion treatment, because the microscopic mechanism controls the macroscopic effect. Further, researching the diffusion coefficient of colouring ions, and guiding the experiment and production by theory, can improve the dependability of this craft and reduce the waste of gemstone resources.

2. Preparation of sapphires for diffusion treatment

First, near-colourless sapphires are washed in acid and classified, and those with blemishes or cracks making them unfit for diffusion treatment are rejected. Then, the rest are cut into semi-manufactured stones; these stones are not polished at this point.

The samples are then put into an alumina crucible with the chemical reagent containing Fe^{2+} and Ti^{4+} and slowly heated to 1800~1900 C in an oil fired furnace. After 72



hours at this temperature they are allowed to cool down along with the furnace.

The sapphire diffusion treatment experiment was carried out in the laboratory of the Thailand Jewelry and Gem Company. There are numerous pits on the surfaces of the samples treated in this way and their colour is deep blue. For determining the thickness of the diffusion layer and the concentration distribution of the colouring ions (Fe^{2+} , Ti^{4+}), a 0.8 mm-thick slice was cut from the centre following the direction of the long axis (see Figure 1). From numerous measurements, the diffusion layer is of similar thickness all the way round the stone apart from the girdle, where it is thicker, ranging from 0.34-0.38 mm.

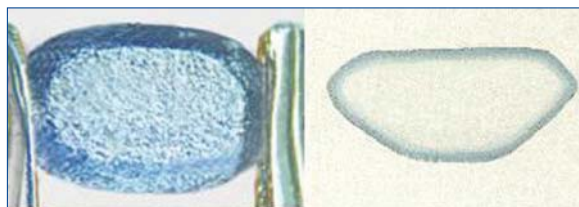


Figure 1: Sapphire with a blue layer, 0.34 - 0.38 mm thick, around the surface caused by diffusion of iron and titanium.

3. Fick's law of diffusion

In 1855, Adolf Fick published a paper entitled 'Über Diffusion' in which he described the molecular diffusion process and derived his law. The law has direct relevance in understanding the diffusion treatment of sapphire. Fick's first law of diffusion states that the mass of a solute crossing a unit area per unit time in a given direction is proportional to the gradient of solute concentration in that direction.

$$J = -D \frac{d\rho}{dx} \quad (1)$$

Where:

J = the flux of the diffusing species, $\text{gcm}^{-2}\text{s}^{-1}$

D = diffusivity or diffusion coefficient = the proportionality constant, cm^2s^{-1}

ρ = the mass concentration of diffusing solute, gcm^{-3}

x = distance; $\frac{d\rho}{dx}$ is the concentration gradient.

The negative sign means that the flow (flux) is in the direction opposite to that in which ρ increases.

Fick's first law of diffusion is only applicable for steady-state diffusion (the diffusion flux doesn't change with time). But the process of sapphire diffusion treatment is a process of non-steady-state diffusion, where the diffusion flux and the concentrations vary with time (t). Non-steady-state diffusion is governed by Fick's second law.

$$\frac{\partial \rho}{\partial t} = D \frac{\partial^2 \rho}{\partial x^2} \quad (2)$$

The solution of the diffusion equations is given in the Appendix.

4. The meaning of the diffusion coefficients of Fe^{2+} (D_{Fe}) and Ti^{4+} (D_{Ti}) in sapphire diffusion treatment

4.1. D_{Fe} and D_{Ti}

The research results concerning the cause of the blue colour in sapphire are well established, and are attributed to charge transfer between Fe^{2+} and Ti^{4+} . Therefore, the treatment to alter the colour of sapphire to blue is always related to the diffusion of Fe^{2+} , Ti^{4+} . To understand this diffusion, it is first necessary to know the diffusion coefficients of Fe^{2+} and Ti^{4+} in sapphire (D_{Fe} , D_{Ti}). The important factors affecting diffusion coefficient are types of crystal defect, form of diffusion, characters of ions, mass concentration and diffusion temperature. Consequently, from the ion diffusion coefficient, the possibility of ion diffusion, the velocity of diffusion and the thickness of the diffusion layer under some particular time condition can be deduced. To determine and analyze the diffusion coefficients of Fe^{2+} , Ti^{4+} in blue sapphire, the concentration distributions of Fe^{2+} , Ti^{4+} in the diffusion layer were analysed and determined by electron probe microanalysis (EPMA) using

Table I: Sapphire compositions in the diffusion layer

Analysis number	1	2	3	4	5	6	7	8	9	10	11
Distance x from surface of sapphire in mm	0	0.05	0.10	0.15	0.20	0.25	0.30	0.35	0.40	0.45	0.50
Wt. %											
Al ₂ O ₃	96.04	96.78	97.83	98.57	98.52	98.76	98.54	98.63	98.76	98.82	98.76
MgO	0.23	0.45	0.35	0.26	0.33	0.35	0.43	0.37	0.31	0.30	0.33
Na ₂ O	0.06	0.02	0.03	0.01	0.03	0.05	0.07	0.03	0.02	0.04	0.05
K ₂ O	0.06	0.03	0.03	0.04	0.05	0.03	0.03	0.03	0.01	0.02	0.03
FeO	1.65	0.97	0.50	0.26	0.15	0.10	0.06	0.03	0.01	0.01	0.01
TiO ₂	1.39	0.88	0.54	0.34	0.22	0.15	0.10	0.06	0.02	0.02	0.01
Cr ₂ O ₃	0.02	0.03	0.02	0.03	0.05	0.04	0.04	0.03	0.04	0.04	0.05
V ₂ O ₅	0.01	0.01	0	0	0.01	0	0.01	0	0.01	0.01	0.01
SiO ₂	0.31	0.26	0.22	0.24	0.32	0.32	0.30	0.28	0.29	0.30	0.32
Total	99.77	99.43	99.52	99.75	99.68	99.80	99.58	99.46	99.47	99.56	99.57

NB: Total iron reported as FeO

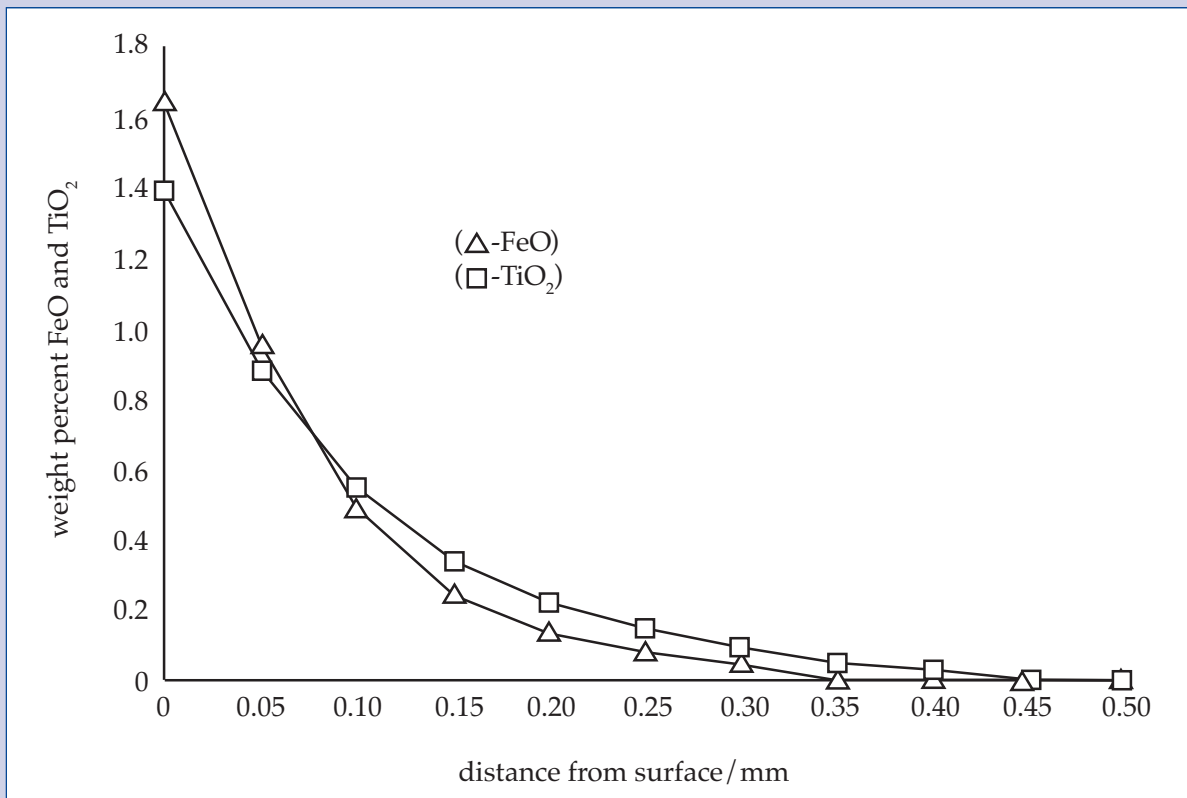


Figure 2: Graph showing variation of weight percent FeO and TiO₂ due to diffusion with distances from sapphire surface.

a JEOL JXA840A. The results are shown in Table I and Figure 2.

Putting the original concentrations of Fe²⁺ and Ti⁴⁺ in the reagent (ρ_1), the original concentrations of Fe²⁺ and Ti⁴⁺ in the blue sapphire (ρ_2), the maximum diffusion distance (x) and the concentrations of Fe²⁺ and Ti⁴⁺ at the point (ρ_{Fe} , ρ_{Ti}) at different times into

equation (4) (see Appendix), we can calculate the diffusion coefficients of Fe²⁺ and Ti⁴⁺ (D_{Fe} , D_{Ti}). Some values are shown in Table II.

The data in Table II indicate that D_{Fe} and D_{Ti} decrease slowly with diffusion treatment time but are basically, under a fixed temperature, relatively steady. The diffusion constants D_{Ti} $6.57 \cdot 10^{-9} \text{ cm}^2\text{s}^{-1}$ and D_{Fe} $1.62 \cdot 10^{-9} \text{ cm}^2\text{s}^{-1}$ indicate

that Ti diffuses about 4 times faster than Fe.

4.2. The factors affecting the diffusion coefficients of Fe²⁺ and Ti⁴⁺

4.2.1. Diffusion treatment temperature

The temperature at which blue sapphire undergoes diffusion treatment plays an important role in the effects on the diffusion coefficients of colouring ions. From $D = D_0 e^{-Q/RT}$ we can deduce that the diffusion coefficient increases exponentially with the rise of temperature. Thus, the quantity of the ions meeting the transition energy condition and the vacancies increase acutely when the temperature rises. So the diffusion treatment of blue sapphire is always carried out under a high temperature. The higher the temperature, the larger the diffusion coefficient, and the thicker is the diffusion layer. But too high a temperature would cause eroded pits on the surface of the sapphire, or even make the crystal melt.

4.2.2. Crystal defects in a gemstone

Various defects often exist in crystals of blue sapphire. These crystal defects have a large effect on the diffusion coefficient. The more crystal defects there are, the larger the quantity of vacancies in the crystal. This is favourable to a higher diffusion coefficient of a displacement ion. The main process in sapphire diffusion treatment is the displacement of Fe²⁺, Ti⁴⁺ and Al³⁺. Typically, diffusion in sapphire belongs to displacement ion diffusion, and the diffusion coefficient is closely related to the number of vacancies. If there is an edge dislocation in a crystal, Fe²⁺ and Ti⁴⁺ can diffuse quickly into the crystal's surface along what is in effect a pipeline to replace Al³⁺. Its activation energy of diffusion in this situation is only about half of that in the crystal lattice. At crystal surfaces and grain boundaries the atomic patterns are relatively irregular. Compared with the atoms inside a crystal, they are at a higher energy state and the extra activation energy needed to make them diffuse is relatively small. As a result, the diffusion of atoms at a crystal surface or grain boundary is faster. These conclusions are consistent with the results of

diffusion treatment — the diffusion layer near the girdle of blue sapphire is thicker than for example on the table facet, and also D_{Fe} and D_{Ti} appear to decrease as t increases (Table II).

Table II: Diffusion coefficients of Fe and Ti measured after different treatment times.

Diffusion treatment time: hours	$D_{\text{Fe}} \times 10^{-9} \text{ cm}^2\text{s}^{-1}$	$D_{\text{Ti}} \times 10^{-9} \text{ cm}^2\text{s}^{-1}$
36	1.82	7.05
48	1.73	6.55
72	1.31	6.10
Average	1.62	6.57

4.2.3. Ion radius and coordination number

An ion's diffusion activation energy is affected by factors such as its size, its affinity with other elements, its charge and coordination number. If the sizes of ions are similar, any distortion in a crystal lattice caused by diffusion is relatively small, so the activation energy needed for diffusion is also small, while the diffusion coefficient is relatively large. For example, when the coordination number is 6, the radii of Fe²⁺, Fe³⁺ and Ti⁴⁺ are respectively 0.77, 0.65 and 0.61 Å. While the radius of Ti⁴⁺ is close to that of Al³⁺, the radii of Fe²⁺ and Fe³⁺ are larger than the radius of Al³⁺ by 45.3% and 22.6% respectively. Consequently, the displacement diffusion of iron ions would cause relatively large distortion in the crystal lattice of blue sapphire. Thus the capacity of Fe to diffuse in sapphire is weaker than that of Ti⁴⁺ (see Table II).

4.3. The meaning of ion diffusion coefficients in sapphire diffusion treatment

The diffusion coefficient of colouring ions plays an important leading role in the process of sapphire diffusion treatment. Because of the differences in the character of Fe²⁺ and Ti⁴⁺ ions (ion radius, coordination number, affinity with other elements, charge and valence state), their diffusion coefficients in blue sapphire are quite different. Diffusion treatment of sapphire may be either colour-intensifying or colour-lightening. For example, treaters in Thailand have turned

near-colourless sapphires into attractive blue sapphire by diffusion treatment. At one time, because of the high concentration of iron in the blue sapphire of Shandong, its colour was too 'heavy', i.e. dark blue or even blue-black. For improving the quality of Shandong blue sapphire, the concentration of iron ions needed to be reduced, and colour-lightening diffusion treatment was carried out.

In the process of colour-intensifying diffusion treatment of blue sapphire, it is important to control the difference of Fe^{2+} and Ti^{4+} ions concentration in the diffusion reagent and to adjust the ratio of the colouring ions concentration in blue sapphire. In colour-lightening diffusion treatment, we should take account of the loss of Ti^{4+} due to its relatively large diffusion coefficient, compensating with a supply of Ti^{4+} if necessary to achieve the correct ratio of Fe^{2+} and Ti^{4+} for blue sapphire. Much Shandong blue sapphire yields an unattractive grey in the process of colour-lightening diffusion treatment, and the reason is loss of Ti^{4+} .

5. Conclusions

1. Fick's law is important in understanding the process of sapphire diffusion treatment. The diffusion coefficient of a colouring ion can reflect the diffusion ability of ions and diffusion velocity in general. We can also obtain the thickness of the diffusion layer at different temperatures and times using the diffusion coefficient.
2. The diffusion coefficients of the iron and titanium ions are quite different and $D_{\text{Ti}} > D_{\text{Fe}}$ by a factor of about four.
3. There are many factors affecting the diffusion coefficient. When the coordination number is 6, the radius of Ti^{4+} and that of Al^{3+} are relatively close. This is one of the main reasons why the diffusion coefficient of Ti^{4+} is relatively large.
4. Using the diffusion coefficients of colouring ions, we can monitor the technique of sapphire diffusion treatment effectively, advance the dependability of sapphire diffusion treatment and reduce the waste of gemstone resources.

Appendix. Solution of the diffusion equation

By specifying the boundary conditions in the process of sapphire diffusion treatment and considering the error function, we can solve the diffusion equation. Referring to the situation of the colour-altering technique, we combined the reagent containing the colouring ions (A) with the sapphire to establish the diffusion couple (Figure 3).

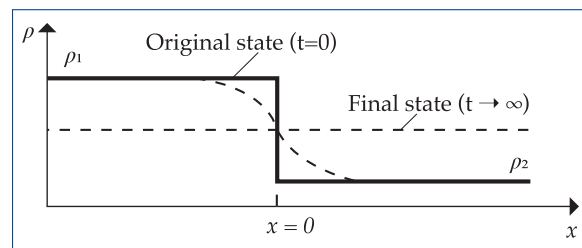


Figure 3: Model of the solute concentration distribution.

The solute (colouring ions) concentration in A is ρ_1 , while that in B is ρ_2 , and $\rho_1 > \rho_2$. When the diffusion couple is heated to a stable temperature, the solute will diffuse under the concentration gradient. The dashed line in Figure 2 shows the distribution function of solute (ρ) concentration in the direction of x at different times (t) in the diffusion couple. The sapphire diffusion layer is very thin, so as a result, the diffusion components A and B can be assumed to be very large in comparison. So we can also assume that the end-member compositions of the diffusion couple remain unaffected by diffusion. Then the boundary conditions can be derived as follows:

$$\text{For } t = 0, \rho = \rho_2, \text{ at } x > 0;$$

$$\text{For } t = 0, \rho = \rho_1, \text{ at } x < 0;$$

$$\text{For } x \rightarrow \infty, \rho = \rho_2$$

$$\text{For } x \rightarrow -\infty, \rho = \rho_1$$

Through integration, we can then use the Grube-Jedele solution of Fick's second law of diffusion.

$$\rho = \frac{\rho_1 + \rho_2}{2} + \frac{(\rho_1 - \rho_2)}{\sqrt{\pi}} \int_0^\beta e^{-\beta^2} d\beta \quad (3)$$

Where, $\frac{2}{\sqrt{\pi}} \int_0^\beta e^{-\beta^2} d\beta$ is the defined error

function $\operatorname{erf}(\beta)$. This yields equation (4)

$$\rho = \frac{\rho^1 + \rho^2}{2} + \frac{(\rho_2 - \rho_1)}{2} \operatorname{erf}\left[\frac{x}{2\sqrt{Dt}}\right] \quad (4)$$

However, because $\rho_1 \gg \rho_2$, equation 4 can be written as:

$$\rho = \frac{1}{2}\rho_1 \left[1 - \operatorname{erf}\left(\frac{x}{2\sqrt{Dt}}\right)\right]$$

and the appearance of this equation can be improved using the complementary error function to yield:

$$\rho = \frac{1}{2}\rho_1 \operatorname{erfc}\left(\frac{x}{2\sqrt{Dt}}\right)$$

Equation (4) shows the solute concentration distribution in the direction of x at different times in the diffusion couple. The diffusion coefficient D is a function of temperature defined as:

$$D = D_0 e^{-Q/RT}$$

Where:

D_0 = frequency factor,

Q = activation energy of diffusion, $Jmol^{-1}$,

R = gas constant, $Jmol^{-1} \cdot K^{-1}$,

T = absolute temperature, K .

Therefore, equation (4) states the function relationship of temperature, time, thickness of diffusion layer and solute concentration in the process of sapphire diffusion treatment. Through it we can analyze and guide the colour-altering technique theoretically to understand and anticipate the effect of sapphire diffusion treatment.

References

- Kane, R.E., Kammerling, R.C., Koivula, J.I., Shigley, J.E., and Fritsch, E., 1990. The identification of blue sapphires. *Gems & Gemology*, 26(2), 115-33
- Nassau, K., 1984. The early history of gemstone treatment, *Gems & Gemology*, 20(1), 22-33
- Peng, M.S., 1995. *Gemstone enhancement and its modern testing technology*. Beijing: Science publishing house
- Qi, Z.F. 1998. *Solid state metals diffusion and phase transformation*. Beijing: Machine industry publishing house

Two remarkable taaffeite crystals from Sri Lanka

Dr Karl Schmetzer¹, Dr Lore Kiefert²,
Dr Heinz-Jürgen Bernhardt³ and Murray Burford⁴

1. Taubenweg 16, D-85238 Petershausen, Germany

2. SSEF Swiss Gemmological Institute, Falknerstr. 9, CH-4001 Basel, Switzerland
(now at AGTA-GTC, New York, U.S.A.)

3. Central Microprobe Facility, Ruhr-University, D-44780 Bochum, Germany

4. 136 Beechwood Avenue, Victoria, British Columbia V8S 3W5, Canada.

Abstract: Two slightly waterworn taaffeite crystals from Sri Lanka are described. A greyish violet crystal of 2.35 ct with bipyramidal habit exhibits two opposing basal pedions, three different hexagonal pyramids and one hexagonal prism as crystal forms. The morphology of a 0.73 ct chromium-bearing crystal with pyramidal habit is characterized by one pedion and one hexagonal pyramid. Gemmological, chemical and spectroscopic properties of the samples are in the range known for iron- and for iron- and chromium-bearing taaffeites from Sri Lanka.

Introduction

Since the discovery of the first taaffeite as a cut gemstone in 1945, faceted taaffeites of gem quality have come predominantly from Sri Lanka, with only a few rare stones reported to come from Myanmar and Tanzania. The first 11.23 ct rough waterworn taaffeite crystal from Sri Lanka was described briefly by Saul and Poirot (1984), who mentioned two opposing basal pedions, pyramidal and prismatic faces.

In a more detailed study of five taaffeite crystals from Sri Lanka including the 11.23 ct sample of the John Saul collection, Kampf (1991) determined the crystal faces of the more or less waterworn crystals by means of a contact goniometer. Only one less waterworn crystal permitted reflected light goniometry. According to Kampf (1991), all crystals were described as pale to deep greyish purple and exhibit at least one basal pedion (0001) and two hexagonal pyramids {11 $\bar{2}$ 4} and {11 $\bar{2}$ 2}. Additional hexagonal pyramids {11 $\bar{2}$ 4} and {11 $\bar{2}$ 2} and one

hexagonal prism {10 $\bar{1}$ 0} were present in some crystals. Only the John Saul sample was truly bipyramidal with two opposing (0001) and (000 $\bar{1}$) pedions. The morphology is consistent with the crystal class of taaffeite (C_{6v} – 6mm).

Chromium-bearing taaffeites are purple, purplish red or red and considered as extremely rare gemstones. The first stone discovered led to some confusion about naming the different minerals of the taaffeite group (see Schmetzer 1983 a, b), and a detailed mineralogical and gemmological description of seven faceted and one rough chromium-bearing samples was published by Schmetzer *et al.* (2000). The rough stone examined in that study was a crystal fragment which showed the pedion (0001) in combination with two pyramids ($\bar{1}$ 123) and $\bar{1}$ (123). The eight taaffeites revealed chromium contents from 0.10 to 0.33 wt.% Cr₂O₃ and iron contents in the range of 1.37 to 2.59 wt.% FeO.

The two rough taaffeite crystals of 2.35





Figure 1a, b: This crystal of 2.35 ct and measuring 6.8 x 7.2 x 5.8 mm, is taaffeite with a bipyramidal habit and two opposing basal pedions; it is slightly waterworn. Photos: M. Burford.



Figure 2: This crystal of 0.73 ct and measuring 4.0 x 5.3 x 4.4 mm is a chromium-bearing taaffeite with pyramidal habit. It is slightly waterworn, and in this picture is resting on a polished window with the crystallographic c-axis near vertical or north-south. Photo: M. Burford.

and 0.73 ct to be described in this paper were purchased in 2004 and 2002 by one of the authors (MB) in Sri Lanka. The 2.35 ct greyish violet sample (Figure 1a, b) is only slightly waterworn and allowed the determination of the complete morphology of another taaffeite crystal. The 0.73 ct red crystal (Figure 2) is the second red (chromium-bearing) taaffeite crystal known to the authors.

Materials and methods

The 2.35 ct taaffeite crystal was bought by one of the authors in Ratnapura and was said to come from this area. The 0.73 ct sample was sold by a Sri Lankan gem merchant with the information that the taaffeite was unearthed in a gem pit in the Kuruwita area, Ratnapura district.

The morphology of both samples was determined using an immersion microscope and a combination of techniques for the identification of crystal faces by measurement of specific angles which was described in detail by Kiefert and Schmetzer (1991). For the two taaffeites described in this paper, the accuracy of the measurement of different angles for the determination of crystal faces is estimated to be $\pm 2^\circ$. This accuracy was sufficient for an unequivocal determination of the morphology of the two stones. Standard microscopic techniques were used to examine internal features under different lighting conditions, both with and without immersion liquids.

The samples were identified and confirmed as taaffeites by Raman microspectrometry using a Renishaw 1000 system. Polarized UV-Vis (300–800 nm) absorption spectra were recorded for both samples using a Cary 500 Scan spectrophotometer.

The 2.35 ct violet crystal was preserved as recovered from a gem pit in Sri Lanka, and contrary to common practice in this country, no polished window had been fashioned to determine refractive indices. It was decided not to polish a window on this unique crystal, so although we could determine specific gravity, neither refractive indices by standard gemmological techniques nor quantitative chemical analysis by electron

microprobe could be carried out.

The 0.73 ct red crystal was obtained from the gem trade in Sri Lanka already with a polished window (to measure refractive indices). Standard gemmological methods were used to determine refractive indices (RI), optic character and specific gravity (SG). In addition, we analysed its solid inclusions by laser Raman microspectrometry using the Renishaw 1000 system mentioned above. To further characterize the sample, a Cameca Camebax SX 50 electron microprobe was used to obtain 8 point analyses from a traverse across the polished window of

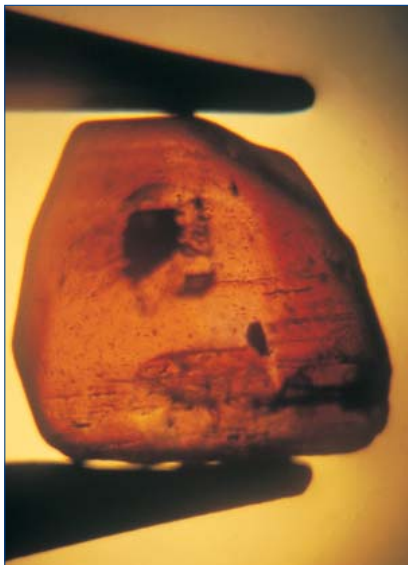


Figure 3: In this orientation, the taaffeite crystal shows two opposing basal pedions as well as three different hexagonal pyramids, the angles between different crystal faces can be determined using the microscope. Immersion, height of the crystal 5.8 mm. Photo: K. Schmetzer.

the gemstone.

Results

1. Greyish violet taaffeite crystal of 2.35 ct Morphology

The taaffeite is a completely preserved crystal (Figure 1) which exhibits opposing basal pedions, (0001) and $(000\bar{1})$ of different size. Three hexagonal pyramids $\{11\bar{2}3\}$, $\{11\bar{2}2\}$ and $\{11\bar{2}\bar{2}\}$ were determined (Figure 3), with $\{11\bar{2}2\}$ being dominant and the remaining two pyramids $\{11\bar{2}3\}$ and $\{11\bar{2}\bar{2}\}$ being somewhat smaller. The hexagonal pyramid $\{11\bar{2}4\}$, which was frequently mentioned by Kampf (1991), is

not present in our sample. Subordinate $\{10\bar{1}0\}$ prism faces are also present. An idealized clinographic drawing of the taaffeite crystal is pictured in Figure 4a, which is consistent with the visual appearance of the sample in the same orientation (Figure 4b).

Gemmological properties and identification

The specific gravity of the crystal was determined as 3.63. Pleochroism was not observed; the sample is inert to both long- and short-wave UV radiation. The Raman spectrum of the specimen is more or less identical with literature data of taaffeites (Kiefert and Schmetzer, 1998;

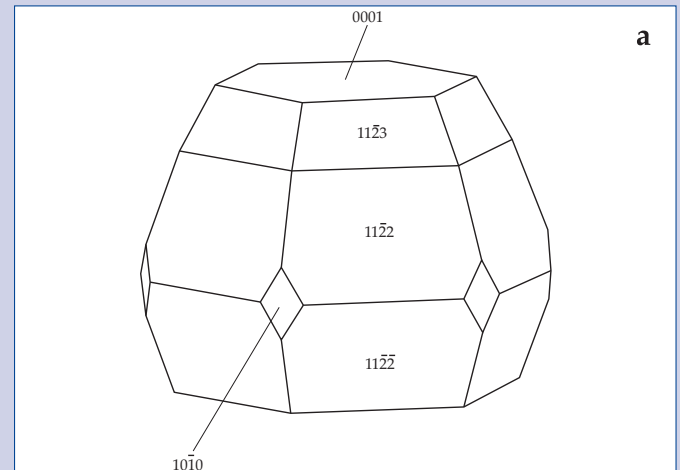


Figure 4: (a) Idealized drawing of the 2.35 ct greyish purple taaffeite crystal (clinographic projection); the sample exhibits two basal pedions (0001) and $(000\bar{1})$ [below, not visible] as well as three different hexagonal pyramids $\{11\bar{2}3\}$, $\{11\bar{2}2\}$, $\{11\bar{2}\bar{2}\}$ and one hexagonal prism $\{10\bar{1}0\}$ as crystal forms; (b) photo with the sample in the same orientation. Photo: K. Schmetzer.

Schmetzer *et al.*, 2005).

Features observed with the microscope

Under the gemmological microscope, a few mineral inclusions similar in appearance to apatites determined in other taaffeite samples were observed. The taaffeite crystal also contained several large healed fractures with liquid and two-phase (solid and liquid) inclusions similar to some already described (see Schmetzer *et al.*, 2000).

Spectroscopic properties

Absorption spectra in the UV – Vis range are identical with those of violet to greyish violet iron-bearing taaffeites from Sri Lanka as described by Schmetzer (1983b) and Schmetzer *et al.* (2000). This spectrum pattern is very similar to that of iron-bearing spinel, where the absorption maxima are predominantly assigned to ferrous iron, Fe²⁺.

II. Red taaffeite crystal of 0.73 ct Morphology

The crystal (*Figure 2*) is terminated by a pedion (0001) and the hexagonal pyramid {1122}. No other hexagonal pyramids are present. At the opposite end to the pyramids and parallel to its basal face the (originally broken?) sample is terminated by a polished

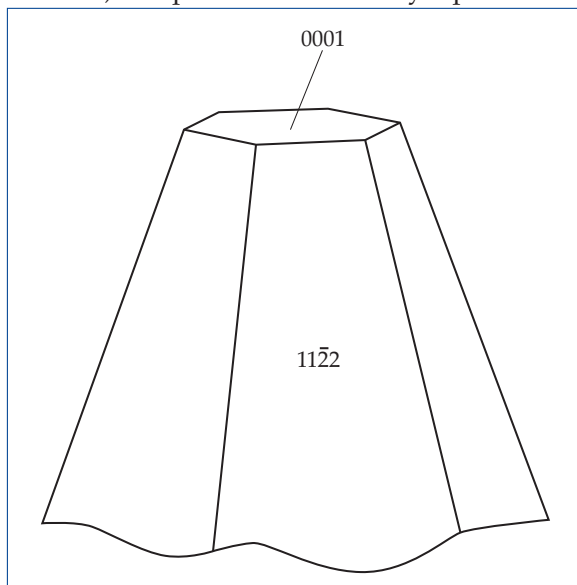


Figure 5: Idealized drawing of the 0.73 ct chromium-bearing taaffeite crystal (clinographic projection); the sample exhibits one basal pedion (0001) and one hexagonal pyramid {1122} as crystal forms.

face (*Figure 5*).

Gemmological properties and identification

The colour of the transparent taaffeite is red with a slight purplish tint; pleochroism is light pinkish red parallel to the *c*-axis and somewhat more intense purplish red perpendicular to the *c*-axis. The stone is uniaxial negative and showed clear RI readings with n_o 1.723, n_e 1.719. The SG was determined as 3.63. The sample was inert to both long- and short-wave UV radiation. The Raman spectrum of the specimen is consistent with published data for taaffeites (Kiefert and Schmetzer, 1998; Schmetzer *et al.*, 2005).

Features observed with the microscope

Using the gemmological microscope, with different lighting conditions, with and without immersion, numerous mineral inclusions were observed, and these were identified as apatites and zircons by laser Raman microspectrometry. The crystal also contains a small healed fracture with two-phase (solid and liquid) inclusions.

Chemical composition

The results of electron microprobe analysis are presented in *Table I*. No distinct chemical zoning was observed in a traverse across the polished window of the sample. In addition to the major components of taaffeite, Al₂O₃ and MgO, the crystal contains major percentages of iron as well as minor amounts of zinc and chromium. Smaller traces of other transition metals, e.g. manganese, are also present. Cation proportions calculated for 16 oxygens per formula unit (*Table I*) are in good agreement with the theoretical formula of taaffeite, which requires 8 trivalent cations (Al, Cr, V) and 3 bivalent cations (Mg, Fe, Zn, Mn) per formula unit.

Spectroscopic properties

Absorption spectra in the UV – Vis range are identical with those of chromium-bearing taaffeites from Sri Lanka as described in detail by Schmetzer *et al.* (2000). The dominant chromium absorption band is found in the 550 nm range. The

Table I: Gemmological properties and chemical composition of a red taaffeite crystal from Sri Lanka

Gemmological properties

Weight (ct)	0.73	RI	n_o n_e	1.723 1.719
Size diameter (mm) height (mm)	4.0 x 5.3 4.4	Birefringence		-0.004
Colour	Red with a slight purplish tint	Pleochroism	$\parallel c$ $\perp c$	Light pinkish red Intense purplish red
Specific gravity	3.63	Inclusions ^a		Apatites, zircons

Chemical composition

Microprobe analysis ^b (wt. %)		Cation proportions based on 16 oxygens (assuming Be = 1.000)	
Al ₂ O ₃	71.67	Al	8.009
V ₂ O ₃	0.01	V	0.001
Cr ₂ O ₃	0.11	Cr	0.008
TiO ₂	0.01	Ti	0.001
		Sum	8.019
MgO	19.51	Mg	2.757
FeO ^c	2.46	Fe	0.199
ZnO	0.22	Zn	0.015
MnO	0.05	Mn	0.004
		Sum	2.975
BeO ^d	4.39	Be	1.000
Sum	98.47		

- a. Determined by Raman microspectrometry.
b. Average of 8 point analyses using a Cameca electron microprobe.
c. Total iron as FeO.
d. Since beryllium is not detectable by microprobe analysis the BeO figure has been calculated for 1 BeO per formula unit; for the theoretical composition of taaffeite (BeMg₃Al₈O₁₆) an amount of 4.52 wt.% BeO is required.

different intensity of this band parallel and perpendicular to the *c*-axis is also responsible for the pleochroism of the taaffeite crystal.

Discussion and conclusions

Both specimens described are rare examples of only slightly waterworn taaffeite crystals. The 2.35 ct greyish violet crystal is complete with two opposing pedion faces. In addition, three hexagonal pyramids and a hexagonal prism are present as macroscopically recognizable crystal forms. The 0.73 ct red crystal is only the second chromium-bearing rough taaffeite known to the authors. In both crystals, the hexagonal prism {1122} is the dominant crystal form present. The hexagonal prism {1124} which was mentioned as the dominant crystal form

of taaffeite crystals from Sri Lanka by Kampf (1991) is not present in these two crystals.

These morphological results confirm the crystal class of taaffeite as $C_{6v} - 6$ mm.

Gemmological, spectroscopic and chemical properties of both taaffeites are within the ranges already determined for gem quality taaffeites from Sri Lanka and described by Schmetzer (1983 a, b) and Schmetzer *et al.* (2000).

References

- Kampf, A.R., 1991. Taaffeite crystals. *Mineralogical Record*, 22(5), 343-7
Kiefert, L., and Schmetzer, K., 1991. The microscopic determination of structural properties for the characterization of optical uniaxial natural and synthetic gemstones. Part 1: General considerations and description of the methods. *Journal of*

- Gemmology*, 22(6), 344-54
- Kiefert, L., and Schmetzer, K., 1998. Distinction of taaffeite and musgravite. *Journal of Gemmology*, 26(3), 165-7
- Saul, J., and Poirot, J.-P., 1984. Le premier crystal de taaffeite gemme? *Revue de Gemmologie a.f.g.*, No. 78, 28
- Schmetzer, K., 1983a. Taaffeite or taprobanite – a problem of mineralogical nomenclature. *Journal of Gemmology*, 18(7), 623-34
- Schmetzer, K., 1983b. Crystal chemistry of natural Be-Mg-Al-oxides: taaffeite, taprobanite, musgravite. *Neues Jahrbuch für Mineralogie Abhandlungen*, 146(1), 15-28
- Schmetzer, K., Kiefert, L., and Bernhardt, H.-J., 2000. Purple to purplish red chromium-bearing taaffeites. *Gems & Gemmology*, 36(1), 50-9
- Schmetzer, K., Kiefert, L., Bernhardt, H.-J., and Burford, M., 2005. Gem-quality musgravite from Sri Lanka. *Journal of Gemmology*, 29(5/6), 281-9

Nephrite jade from Scortaseo, Switzerland

Dr Douglas Nichol¹ and Herbert Giess²

1. 39 Buckingham Road, Wrexham, Wales.
2. Geerigstr. 60, 8049 Zürich, Switzerland.

Abstract: *At Scortaseo in the eastern Swiss Alps, two lenses of nephrite jade occur within the central core of a talc orebody associated with metamorphosed dolomitic limestone of Triassic age. Although mining operations were initiated for exploitation of talc, several thousand tonnes of nephrite were also extracted as a by-product. Predominant colours of the nephrite jade are of uneven pale green and grey-green hue. Grain size ranges from fine- to medium-grained and subordinate constituents include calcite and talc. In addition to massive nephrite jade, a major part of the deposit includes a distinctive variety of mixed nephrite-calcite rock termed 'Swiss jade'. It consists of pea-like spherules of nephrite set in a matrix of calcite. The nephrite jade is classified as para-nephrite in type and formed together with talc by intense hydrothermal alteration of dolomitic marble along shear zones. The quantity of nephrite jade available remains uncertain but appears substantial. Recent production involves recovery of material previously discarded during talc mining operations. The nephrite jade is fashioned into costume jewellery at a local workshop nearby at Poschiavo.*

Keywords: *bead, carving, nephrite, serpentinite, spherule, Swiss jade, talc*

Introduction

The nephrite jade deposit at Scortaseo is generally acknowledged as the largest and most significant in Europe. It has been worked for over fifty years for the manufacture of costume jewellery, hardstone carvings and ornamental pieces.

Scortaseo is located 30 km southeast of St Moritz and 4 km south-southwest of Poschiavo in southeast Switzerland (Figure 1). From just south of the village of Poschiavo, access to the site is southwestwards along the Selva road, thence by track towards Alpe Vartegna and the Canciano Pass. Here, the eastern Swiss Alps form steep terrain with spectacular and rugged mountains.

The writers carried out a field visit to Scortaseo as part of a wider study of nephrite jade in Europe. This paper provides a brief

review and a description of the geological setting of the deposit of nephrite jade at Scortaseo.

Historical background

Mining operations at Scortaseo commenced around 1950 for talc, which was produced to supply nearby Italian paper factories. The discovery of the nephrite jade is attributed to Mr J. Olinto, a local resident, who collected attractive pieces of rock from the discarded spoil materials from the talc mine. He termed one unusual specimen 'Forellenstein' (trout stone) because of the unusual spotted pattern evident on broken surfaces. This was subsequently identified as nephrite jade at the federal technical university (ETH) in Zürich.

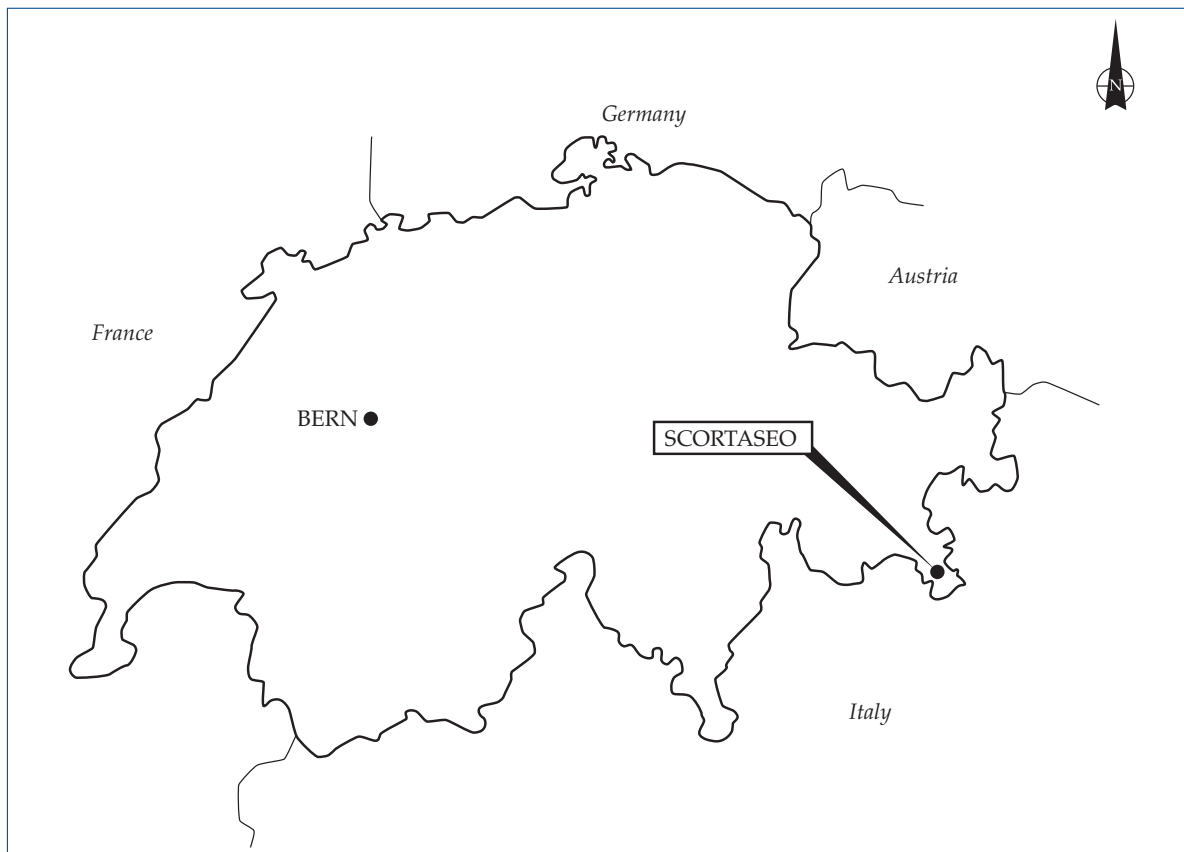


Figure 1: Location of Scortaseo in southeastern Switzerland.

Shortly after discovery, a substantial quantity of nephrite jade was produced. According to Jaffé (1986), annual production reached 1500 tonnes of nephrite-bearing rock, some of which was shipped to lapidary workshops in Idar-Oberstein, the German centre for hardstone processing. During the early 1960s, Schweizer Heimatwerk, an organisation promoting Swiss handicrafts, encouraged processing of the nephrite as a cottage industry in the local region (Gross, 1963). They achieved considerable success, marketing a wide range of items including necklaces, cabochons, cufflinks, small cups and dishes. However, by 1993 talc mining operations were discontinued because of the danger of rockfalls and so output of nephrite jade became limited to the residual stockpiles.

More recently, operations at the site have restarted for the production of construction aggregate by reusing the waste rock from the old spoil heaps. The crushed stone (which includes nephrite jade) is used locally for road-making material.

Geological setting

The regional geology of the Scortaseo district appears complex due to extensive tectonic disruptions associated with a stack of Alpine nappes (Penninic and Austroalpine nappe systems). The solid geology is outlined in simplified form in *Figure 2*.

In the neighbourhood of Scortaseo, the principal rock type consists of metamorphosed dolomitic limestone of Triassic age. It overlies basement rocks (mainly augen gneiss) of the upper-penninic Margna nappe with a tectonic boundary separating the two rock types. These bedrocks occupy a complex shear zone between the Malenco serpentinite and ophiolite complex to the west and Austroalpine strata to the east. The structural inlier of dolomitic limestone is thought to be a large block caught up in the shear zone.

The nephrite jade occurs as lenses within the central core of two talc orebodies. The lensoid masses measure around 100 m long by 2-5 m wide and at least 30 m

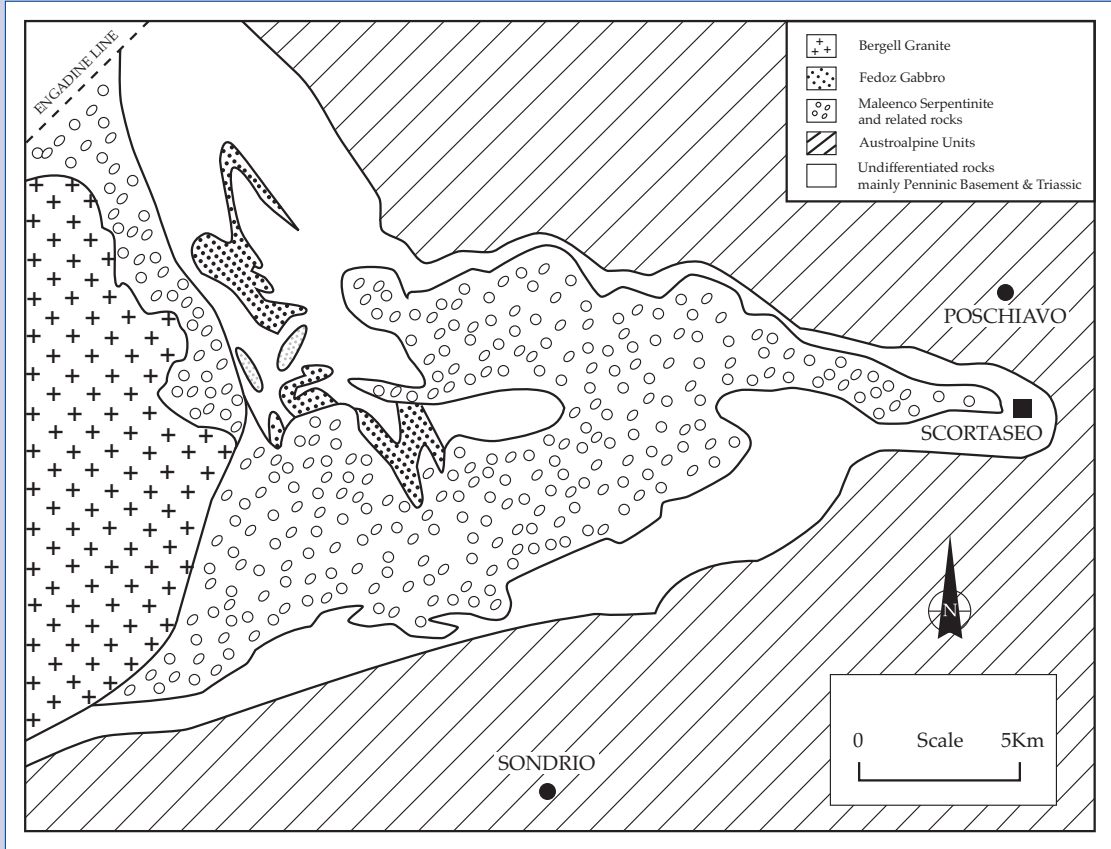


Figure 2: Simplified geological map of the Scortaseo district.

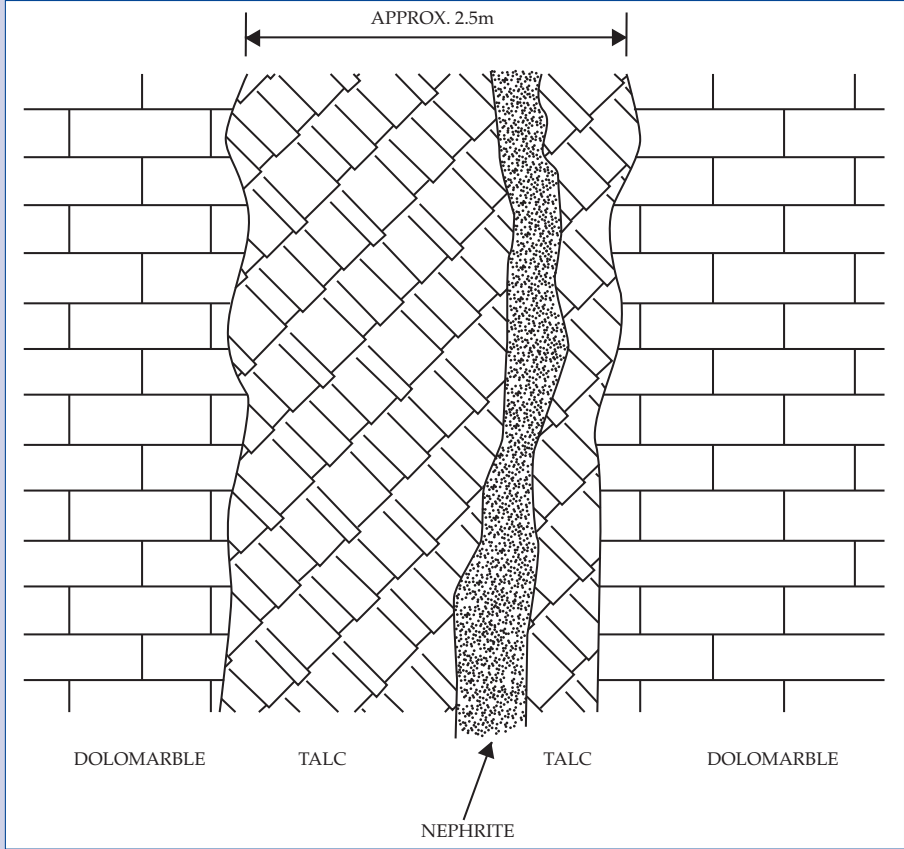


Figure 3: Schematic section illustrating rock relations at Scortaseo.

deep. One orebody is enclosed in dolomitic marbles (Figure 3) and the other follows the tectonic boundary between dolomitic marble and muscovite-chlorite gneiss.



Figure 4: Workings area, Scortaseo. View westwards towards main quarry faces.



Figure 5: Workings area, Scortaseo. View northeastwards over platform of spoil material.

The Scortaseo workings

Dietrich and De Quervain (1968) and Giess (1994) have described the mining site at Scortaseo in detail. The area of workings extends over about 2.5 ha on a steep hillside (Figures 4 and 5). Initially, opencast

quarrying methods were used to extract the talc and nephrite orebodies and later, adits were driven into the hillside and mining proceeded using underground methods. Today, the extraction area comprises a series of benches and several working platforms formed using waste rock. The openings to the underground workings are inaccessible.

The principal rocks exposed in the quarry are bedded units of dolomitic marble. The dolomitic marble is fine-grained and ranges from grey and white to pale brown in colour. Minor interbeds of calcite-marble and quartzite are also present, the whole having been affected by mild metamorphism.

Nephrite jade

Massive nephrite jade (Figure 6) consists of microcrystalline tremolite-actinolite with a finely felted texture which is intimately associated with minor but variable quantities of calcite and talc.

Using the Munsell notation (Rock-Colour Chart Committee, 1980), the nephrite jade ranges from very pale green (10G 8/2) through greyish yellow green (5GY 7/2) and greyish green (10GY 5/2) to light greenish grey (5G 8/1) and light grey (N7) but is predominantly greyish yellow green (5GY 7/2). Generally, the colours appear somewhat patchy and uneven but clearer coloured areas are quite translucent.

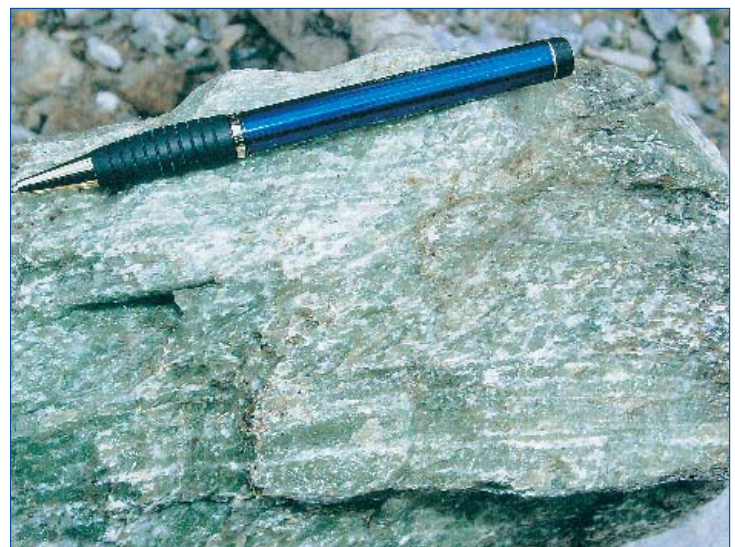


Figure 6: A typical specimen of massive nephrite jade from Scortaseo. Approx. 200 mm across.

Swiss jade

A major part of the deposit comprises a distinctive variety of nephrite rock, termed 'Swiss jade', that consists of a nephrite-talc-calcite assemblage with pea-sized spherules and globules of pure nephrite surrounded by talc margins and a calcite cement (*Figure 7*). As far as can be determined, this particular variety of nephrite rock appears unique to Scortaseo. It occurs in close association with massive nephrite jade within the central core of both talc orebodies.



Figure 7: A typical specimen of 'Swiss jade' from Scortaseo showing spherules and globules of nephrite set in a matrix of calcite. Approx. 200 mm by 100 mm

The unusual aggregations of nephrite constitute 70-90 % of the rock. They vary from spherical to lens-shaped grains and range in size from 1 to 10 mm in diameter. Certain bands contain only large spherules, others contain only small ones and a few have a mixture of large and small. Cross-cutting veinlets of nephrite are also present.

Typically, the spherules of nephrite are greyish yellow green (5GY 7/2) in colour

and the calcite matrix varies between light greenish grey (5GY 8/1) and white (N9). Small amounts of talc form a thin rim or coating around some nephrite spherules.

The formation of the spherules of nephrite appears enigmatic and the origin of the texture is difficult to explain. Conceivably, it may be a relict sedimentary texture inherited from pelletal grains in the original carbonate strata. However, a more likely explanation involves the immiscibility relations between nephrite and calcite and vigorous fluid circulation during metasomatism. The cross-cutting veins of nephrite indicate its formation in at least two generations, so some is most likely to be metasomatic.

Nephrite classification and origin

According to Dietrich and de Quervain (1968), the nephrite jade and associated talc lodes at Scortaseo formed through the metasomatism of dolomitic marbles by the introduction of silicic acid solutions. Based on the field relationships between the nephrite bodies and the metasedimentary dolomarlite, the deposits are classed as para-nephrite in type (Nichol, 2000).

It is also noteworthy that the geological features evident at Scortaseo, as well as the close association of the nephrite with a talc orebody, appear remarkably similar to the geological environment reported by Nichol and Giess (2005) for the Mastabia nephrite jade deposit in northern Italy. Indeed, the colour and general appearance of Scortaseo nephrite also appear similar to Mastabia nephrite.

Production practice

The number of small producers of finished items is difficult to ascertain but one significant workshop with a gallery and a shop exists in the village of Poschiavo. It fashions various types of jewellery and specialises in necklaces (*Figures 8 and 9*).



Figure 8: Necklaces fashioned in nephrite jade from Scortaseo.



Figure 9: Beads fashioned in nephrite jade from Scortaseo.

Conclusions

At Scortaseo in Switzerland, nephrite jade formed in hydrothermally altered zones of intense deformation associated with metamorphosed dolomitic limestone and calc-silicate rocks. The nephrite jade occurs as lenses within the central core of two talc orebodies. In addition to pure, massive nephrite a distinctive variety of mixed nephrite-calcite rock termed 'Swiss jade' constitutes a major part of the deposit.

It consists of pea-like spherules and globules of nephrite set in a matrix of calcite.

The rock is categorised as a para-nephrite jade. Colour is predominantly greyish yellow green (5GY 7/2) and texture ranges from fine- to medium-grained microfibrous.

The nephrite jade was originally extracted as waste materials generated during talc mining operations. Substantial quantities of nephrite probably exist in the vicinity of the old workings and in the associated spoil heaps.

Lapidaries and artisans have fashioned the nephrite jade into a wide variety of ornamental hardstone carvings and jewellery pieces.

References

- Dietrich, V., and de Quervain, F., 1968. Die Nephrit-Talklagerstätte Scortaseo. *Beiträge zur geologie der Schweiz, Geotechnische Serie, Lieferung 46*, 78 pp
- Giess, H., 1994. Jade in Switzerland. *The Bulletin of the Friends of Jade*, 8, 1-30
- Gross, G., 1963. Jade, der neue Schmuckstein des Schweizer Heimatwerkes. *Heimatwerk Blätter für Volkskunst und Handwerk, Zürich*, 28, 129-48
- Jaffé, F.C., 1986. Switzerland. In: Dunning, F.W., and Evans, A.M. (eds), *Mineral deposits of Europe, Volume 3: Central Europe*. Institution of Mining and Metallurgy, London, 41-54
- Nichol, D., 2000. Two contrasting nephrite jade types. *Journal of Gemmology*, 27(4), 193-200
- Nichol, D., and Giess, H., 2005. Nephrite jade from Mastabia in Valmalenco, Italy. *Journal of Gemmology*, 29(5/6), 305-11
- Rock-Colour Chart Committee, 1980. *Rock-Colour Chart*. Geological Society of America, New York

Crossed filters revisited

Dr D.B. Hoover FGA¹ and Bear Williams CG²

1. 1274 E. Crystal Wood Ln., Springfield, MO., U.S.A.
2. P.O. Box 104504, Jefferson City, MO., U.S.A.

Abstract: *The crossed filters technique, introduced to gemmologists by Basil Anderson, has not found extensive use due, in part, to the cumbersome excitation filter he used. The commercialisation of new solid state sources, and ready availability of a variety of coloured glasses now makes possible simple and inexpensive means for practice of this fluorescence method.*

Keywords: *crossed filters, chrome-bearing gems, fluorescence, gem testing*

“These instruments and appliances to be of any practical value must be simple and substantial, as cheap as possible, and such that determinations made with their aid can be as well performed by the working jeweller as by a trained mineralogist.”

Max Bauer (1904, p.561), writing about instruments for identification of gems.

Introduction

The crossed filters technique in gemmology, was first introduced in 1953 by Basil Anderson in a paper in the *Gemmologist* and later included in the sixth edition of his text *Gem Testing* (Anderson, 1959). The technique is well known to British gemmologists, but appears to be underutilised. In part, this reflects the bulky filter that Anderson used with his light source, a glass Florence flask filled with about 1 litre of copper sulphate solution. More recent mention of the technique in reference works offers little more help, repeating Anderson's filter choices or simply calling for a blue and a red filter (Harding, 1994; Hughes, 1997) giving no specifics. Hughes (1997) does state: “There is no better technique of observing fluorescence in ruby---”, with which the authors agree. This paper looks at the history of the method, and offers practical and low cost means for implementing the technique which the gemmologist can easily accomplish.

As implemented in the past, the crossed filters technique principally provided a

means of testing for chromium present within several gem materials. It is based on fluorescence due to the chromium ion (Cr^{3+}) present in gems such as ruby, emerald, spinel and alexandrite. The fluorescence is excited not only by ultraviolet light, but also by wavelengths in the visible region. Hoover and Theisen (1993) published excitation-emission spectra for a number of chromium-bearing gems with excitation in the range of 270 to 600 nm. Their results show that the predominant chrome excitation occurs in a blue band and a green-yellow band; the blue centred near 440 nm, and the broader green band centred at or below 600 nm. A central minimum is around 480 nm. Details vary among the various gem species and individual gems. As might be expected the excitation bands correspond approximately to the absorption bands seen in the spectroscope. Ruby shows a much broader excitation band than emerald for example. Their data also show a band in the UV from about 260 to 360 nm which is not very effective at exciting fluorescence.



Iron quenching increases the wavelength at which fluorescence starts at the UV-violet excitation end. The effect of iron on emission spectra is mostly in an overall reduction in the strength of emission. For emeralds examined, a change of 2 orders of magnitude is seen, and for ruby about 1 order. These data are important in selection of a light source and excitation filter for detection of chromium in gems. The data suggest the optimum source should be broad and extend at least to the orange.

To determine the optimum viewing (emission) filter, the fluorescence spectra of chrome-bearing gems need examination. Most gemmologists are familiar with the 693-694 nm doublet in ruby, and the 'organ pipe' lines of red spinel, principally at 675, and 686 nm. Data from Hoover and Theisen (1993) show that very little emission due to chromium occurs at wavelengths shorter than 650 nm, but that much occurs well into the near-infrared, between 700 and 800 nm. In fact many of these gems have their emission peaks, and most of their emission, in the near infrared. Chrome tourmaline, chrome diopside, chrome grossular, and emerald are examples. Thus, the ideal viewing filter would have a very sharp cutoff near 650 nm, passing the longer wavelengths.

The problem for the practising gemmologist is whether he/she can find practical, inexpensive, light sources and colour filters to implement the technique. This paper presents several possibilities, but the basic requirements given above permit anyone to improve or to modify the details as new sources and filters become available.

A short history

Although the crossed filters technique for use in gemmology is due to Anderson, it was first used many years ago by Sir G.G. Stokes (1819 1903) for determination of very weak fluorescing materials. A dense cobalt glass combined with a thin signal green glass was used as an excitation filter, or a solution of ammoniacal copper sulphate. A yellow glass, or solution of potassium dichromate (yellow) was used for the viewing filter (Wood, 1934).

Anderson (1959) mentions Stokes's work, and the possibility of filters similar to those that Stokes used for gemmological work. However, he substituted a simple copper sulphate solution for the blue filter, and, because only red fluorescence is involved with chrome gems, a red gelatine filter was used for viewing. This red gelatine filter was commonly used in photo processing at that time. With good filters the effect is quite pronounced.

Anderson describes it as "like glowing coals against a dead-black background—a sight so beautiful that it still delights the author after years of repetition." (Anderson, 1959, p.168). He notes that it was first used as a lecture demonstration, but goes on to say that he found it so sensitive and useful in gem testing that it was constantly in use in the London laboratory. Anderson (1959), and Harding (1994) provide explanations of the use of fluorescence in gem testing, and for which gems crossed filters are most useful.

Another fluorescent effect described by Wood (1934) is important in practice of the crossed filters technique, but not normally mentioned. Fluorescence is principally a surface phenomenon, because the excitation light incident on the surface is absorbed to give the fluorescence. Wood presents an elegant experiment showing that the observed intensity of fluorescence is found to be many times brighter if viewed in a direction perpendicular to the surface, than if viewed through the material. The intensity difference can be greater than thirty times. The implication for the gemmologist would be in general to face the table of a gem towards the blue/UV source so as to present the greatest surface area of the stone to excitation light. Then he/she should view the fluorescence looking towards the girdle, as indicated in *Figure 1*. This also minimises the small amount of direct light that might get through the crossed filters, from transmission through the stone or by reflection from facets. With practice or common use, one will come to recognise the difference between the fluorescence, and light due to

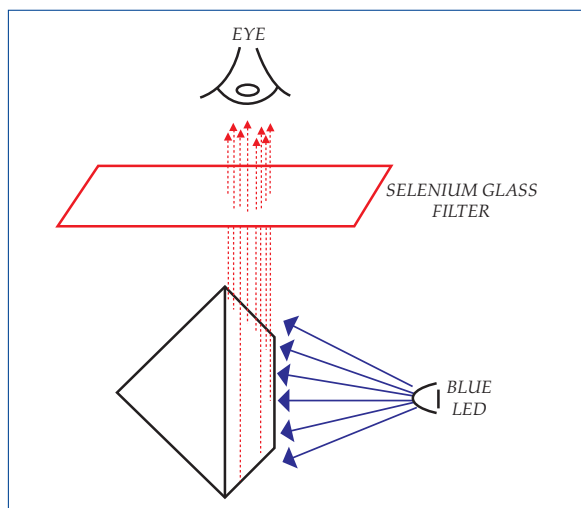


Figure 1: Schematic diagram showing optimum illumination and viewing orientation for examination of a weakly fluorescing gem.

simple reflection from facets. For strongly fluorescing gems there will be little need for orientation. It should also be noted that fluorescence from some solids is polarised. This can be seen in ruby by observing the change in the fluorescing image while rotating a polaroid plate during observation of the gem.

Modern sources and filter materials

Technology has given today's gemmologist a much wider range of light sources and advanced filter materials than Anderson had in his day, opening the possibility that simpler and perhaps less expensive components might be used for implementing a crossed-filters inspection unit. The authors are continuing to look at a number of possibilities with the prime motivation to keep costs low. For this reason, modern interference filters which can be tailored to almost any pass/block range have not been examined in detail, because they would make for rather expensive equipment. The focus was on keeping cost low enough for any gemmologist to be able to get materials and set up a simple viewing unit.

With the popularity of hobby stained glass work, a wide variety of coloured glass is now available everywhere. This was

an obvious source for filter material. Two common glasses available to the hobbyist are blue cobalt and red selenium glasses (*Figure 2(a)*), whose spectra are given in Gem-A's introductory course, since they are used in glass simulants. The selenium glass with only a pass band in the red cutting at 630 nm makes a good viewing filter if an appropriate source-excitation filter combination can be found. *Figure 2(b)* shows the transmission spectra of selenium, cobalt and a green glass used by the authors. All spectra shown were obtained with an Oceans Optics S-2000 spectrometer and software running on a personal computer. Light from the cobalt glass has some red components that would pass the selenium glass, so a means of limiting this is needed. A green glass, similar to Stokes's signal green, was found at a local stained glass shop, and this was found to cut some of the red that passed the cobalt glass (*Figure 2*). This also passed more light in the green where greater fluorescence should occur. Other green to violet glasses were also tested.

The coloured glasses were all 2.5 mm thick, and had no patterning so that one could read print through a sheet. A single pane of selenium glass for viewing, and one and two thicknesses of the cobalt and green glasses were tested for minimum transmission using an incandescent source. The bulb filament could be seen in all cases, but other light was not evident. In use, the double pane cobalt filter appeared to give the best viewing when testing with a synthetic ruby. This appears to give adequate results for a simple crossed-filters apparatus, and is quite simple and inexpensive.

Also tested was a fluorescent light source using cool white bulbs which produced little light at wavelengths longer than 650 nm. This source, with two panes of the cobalt or green filters, produced better results than with an incandescent source. The cobalt glass is better than the green, producing an essentially black background against which the ruby appears as Anderson described it, "a glowing coal". Thus, the crossed filters technique can easily be implemented by any

gemmologist for a few dollars. Comparison illumination spectra for an incandescent, a cool white fluorescent source, and a white Light Emitting Diode (LED) source, all with the cobalt glass filter are shown in *Figure 3*. The disadvantage of an incandescent source used with a cobalt glass filter is seen by the relatively large amount of red light present in such an excitation source.

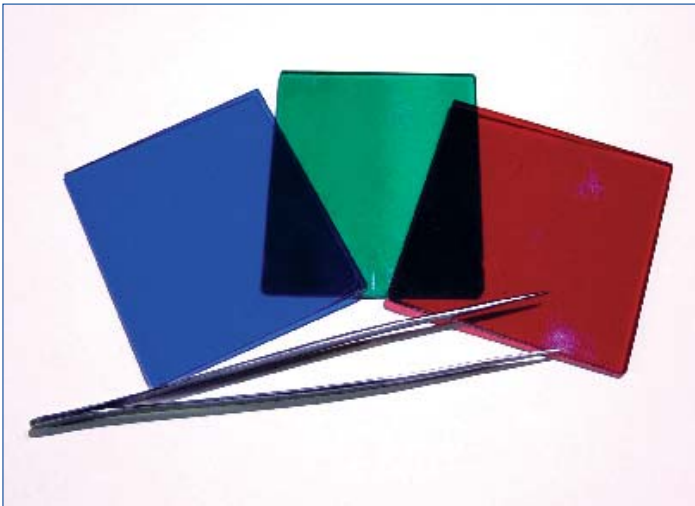


Figure 2a: Photograph of the glass filters used in this investigation with gem tweezers for scale.

The applicability of solid-state sources was also investigated. Recently available are LED sources in various colours including a bright blue and green, sold as miniature flashlights (torches), in addition to white LED torches. The blue produces little emission in the red, and from *Figure 3* is very near to the excitation provided by a white LED and cobalt glass excitation filter. All these LED sources are quite intense, and inexpensive. We also tested a three-element LED white source, using one pane of cobalt glass for an excitation filter (*Figure 3*), and found this excellent as well. The high brightness of the LED sources gives increased fluorescence from a gem. While a 'white' LED source may be used effectively with a cobalt glass filter the authors strongly recommend that the blue LED discussed below be used due to the simplicity of not needing a separate excitation filter.

Various blue LED units and one green unit have also been tried by the authors and appear very similar in effectiveness. Tests were made with these sources, and with no source filter on synthetic ruby. The results

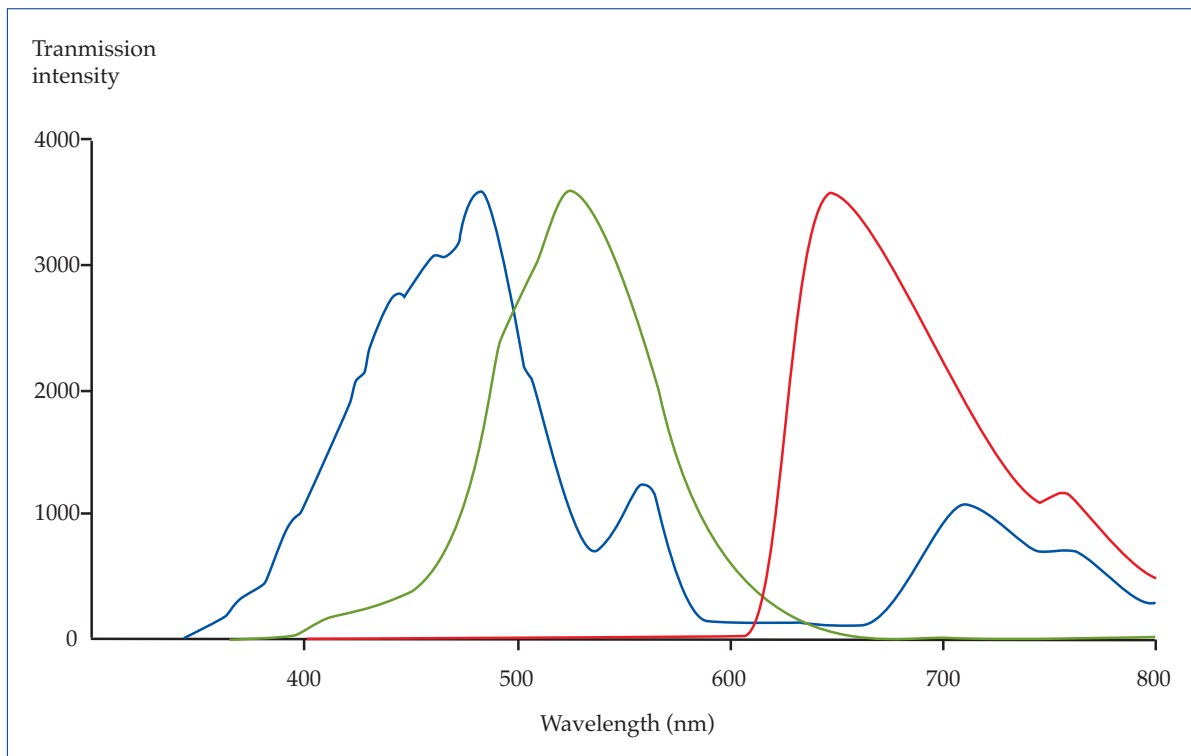


Figure 2b: Transmission spectra of green (green curve), cobalt (blue curve) and selenium (red curve) glasses taken with an incandescent source.

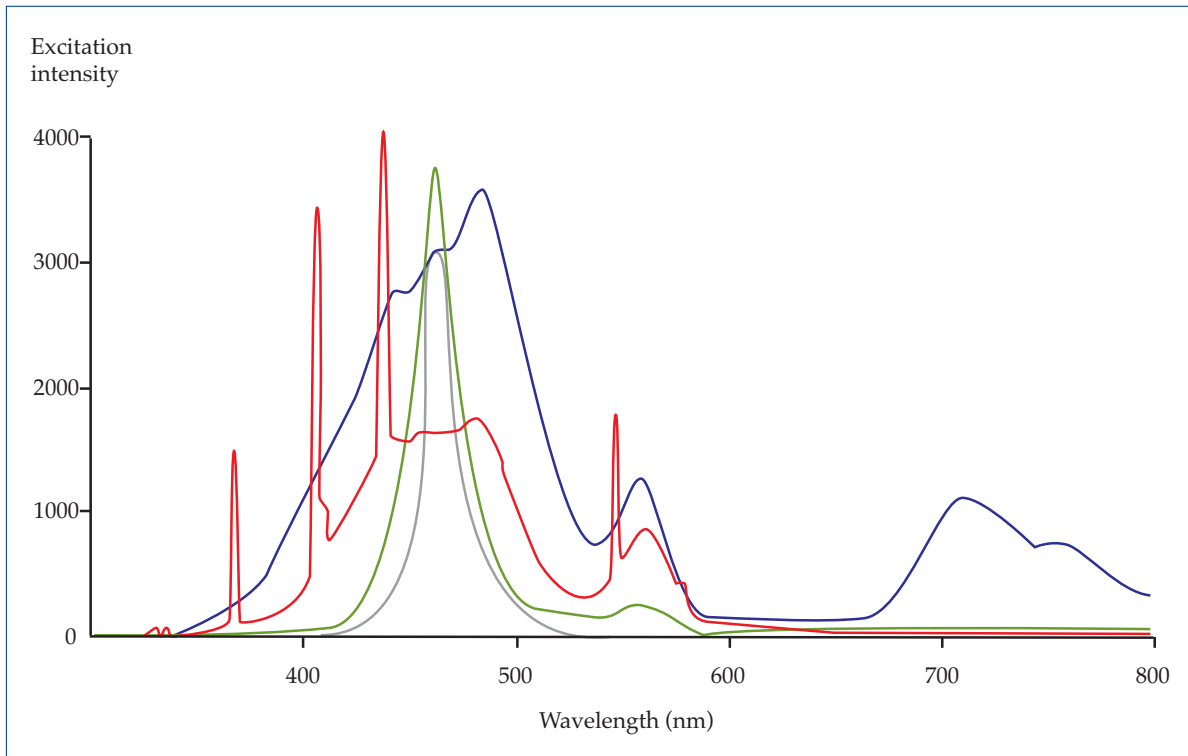


Figure 3: Excitation spectra for a cobalt glass filter with incandescent (blue curve), fluorescent (red curve) and white LED (green curve) sources, and a blue LED (black curve) source.

were truly amazing when the source was within a centimetre of the stone, which appeared almost alive (Figure 4). For ruby and red spinel the green source gave stronger fluorescence, as would be expected from the results of Hoover and Theisen (1993). However, there was too much transmission in the red for it to be considered as effective for weakly fluorescing gems. The authors will continue to investigate green sources, but for this paper will concentrate on the blue LED source. Readers are encouraged to experiment further.

For simplicity of use, effectiveness and cost (under \$10) the blue LED source and single pane of selenium glass are recommended as the most practical, and best, way to implement the crossed filters technique. The equipment will fit in a shirt pocket or purse, and one is ready to test anywhere, especially when buying in the field, where it would be easy to test a parcel of stones quite rapidly.

Note should be made of the potential for extending the utility of the technique to those chrome-bearing gems fluorescing

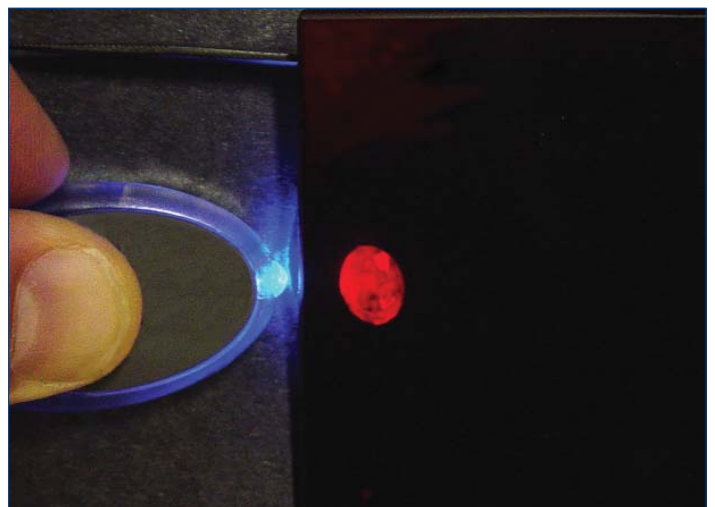


Figure 4: Photograph of a synthetic ruby fluorescing using the crossed filters technique. Excitation with a blue LED source, and viewed with a selenium glass viewing filter. The selenium filter only covers the ruby.

at wavelengths in the near infrared range, longer than 700 nm (emerald, jadeite, kyanite, chrome tourmaline, chrome diopside, chrome grossular, and probably others) by the use of infrared sensors, such as night vision devices, or cameras. Viewing should extend to 800 nm for best results. Harding (1994) notes

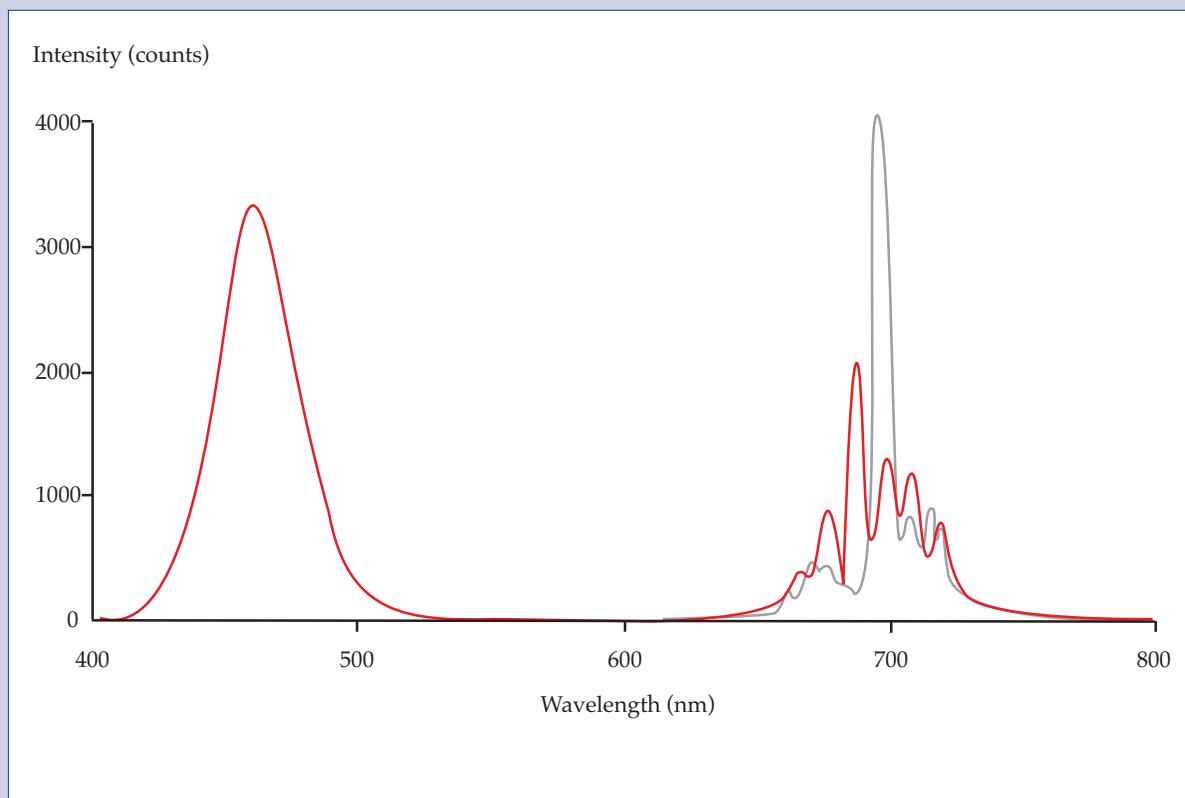


Figure 5: Emission spectra of ruby (blue curve) and red spinel (red curve) from Myanmar using a blue LED for excitation. In the case of the spinel (red curve) the excitation curve of the blue LED has been superposed on the spinel emission, and shows as the prominent band between 400 and 500 nm.

that Mitchell used a photographic infrared filter in place of the conventional red viewing filter, but evidently his eye was the sensor. His vision range would have been limited to a very narrow band near 700 nm, but Mitchell does note that synthetic emeralds were much more brilliant than natural stones with this combination. The fluorescent emission spectra of ruby and red spinel from Myanmar are shown in *Figure 5*, and for Sri Lankan sinhalite, mottled Myanmar jadeite jade, and Colombian emerald in *Figure 6*. The latter especially show that much emission occurs at wavelengths longer than 700 nm, and is a convincing illustration of the potential for examination of this region.

Comments on practical application

Gems that fluoresce strongly can be viewed in a normally lit room by limiting the amount of extraneous light entering the test region. For some gems the fluorescence

is evident even without a selenium glass viewing filter. However, for best results crossed-filters testing should be done in a darkened room, eyes dark-adapted, and with the gems to be tested placed on dead black paper. This is essential for very weakly fluorescing gems such as sinhalite which, the authors discovered, may be separated from peridot in this simple manner. An added advantage of using visible light for excitation is that common glass lenses may be used to focus the blue or green light to a small intense spot if needed.

The authors have not done extensive testing either on large quantities of gems, or on gems from numerous sources. The applications for crossed filters given by Anderson (1959) and Harding (1994) are in general confirmed by our testing. However, the reader should remember that the excitation wavelengths we used are somewhat different than those produced by an incandescent source and a copper sulphate filter, so emissions may differ as

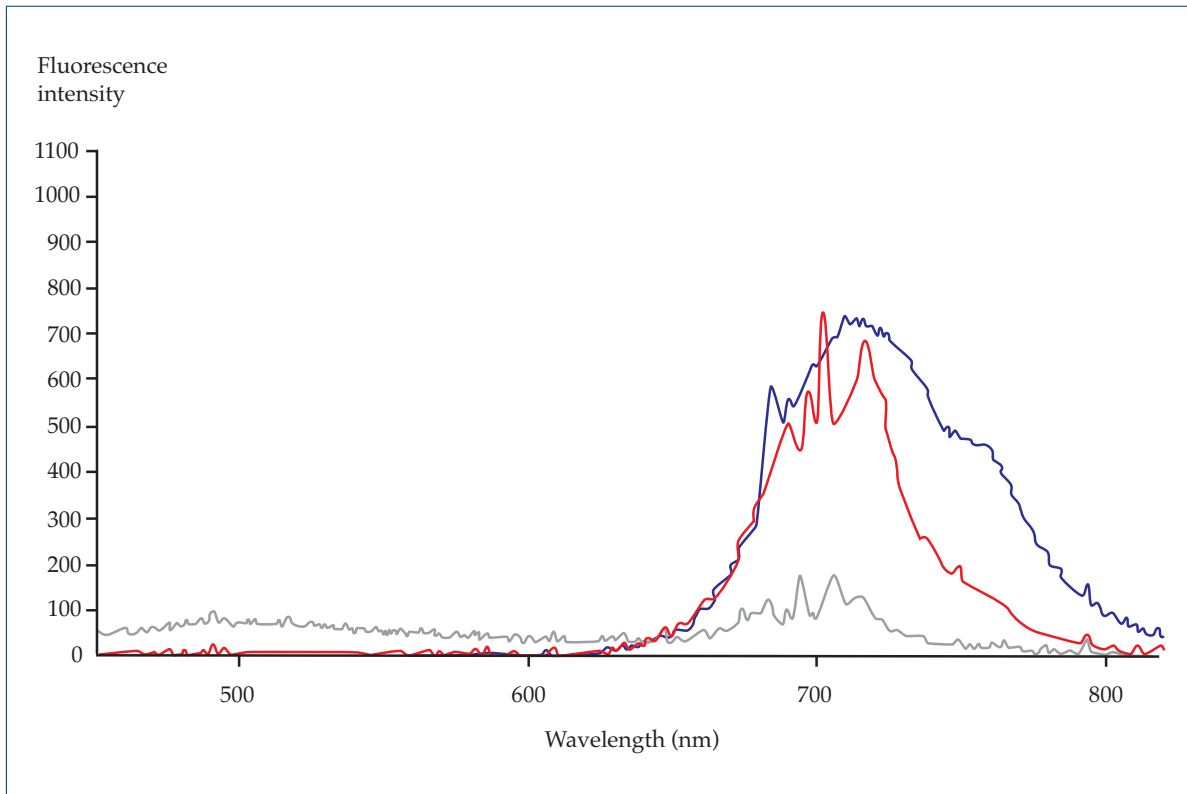


Figure 6: Emission spectra of Colombian emerald (blue curve), Myanmar jadeite jade (red curve) and Sri Lankan sinhalite (black curve) using a blue LED for excitation.

well. This corresponds to the differences Harding (1994) cautions about between different ultraviolet sources and illustrates in his figure 36.10. Harding also comments that comparison of luminescent response between two or three different illuminants can greatly increase the value of fluorescence in diagnostic testing. Having a simple means for crossed-filter testing adds another dimension to discrimination by traditional ultraviolet excitation methods. The authors have noted that in general the longer the wavelength of excitation light used the stronger the emission. Results reported below are from preliminary testing using a blue torch. Much additional testing is needed before the full capability of this variation on crossed-filters is known.

Results using a blue source

Looking at chromium-bearing gems, it is clear that there is a large variation in the strength of fluorescence of natural stones of one type, even from one source. In the following we

will summarise what we have observed from limited observations.

All rubies observed fluoresce, the strongest being synthetic stones and natural rubies from Myanmar. Thai stones give a weak to moderate response, as expected from their iron contents. The strong emission at 694 nm is visible as the dominant emission in *Figure 5*.

Sapphires for the most part don't respond, although some light-coloured stones, light blue, pink, yellow or colourless, of varied provenance give a moderate to good response.

Red, and some lilac to purple spinels show good to poor responses. Myanmar stones fluoresce strongly. *Figure 5* shows that the 'organ pipe' lines of red spinel extend well beyond 700 nm.

Chrysoberyl is inert except for alexandrite although this varies according to source. From Minas Gerais, Brazil and India, alexandrites respond well to a blue light, in contrast to no response for the deep coloured cabochon material from Carnaiba, Bahia, Brazil.

Natural emeralds from different sources also show different responses, ranging from a strong response from Colombian stones to no response from Carnaiba, Brazil stones; this is generally similar to Anderson's observations. The good response of Colombian stones may reflect the generally low iron content in comparison with emeralds from other localities (Schwarz, 1987). However, concentration of chromium also determines the intensity of fluorescence and Colombian stones show higher average chrome contents than stones from deposits other than Brazil. This question needs further examination. Because almost all of emerald's fluorescence is in the infrared (*Figure 6*), we suspect that part of the variability in reported visual response is due to differences in human vision, and to differences in excitation spectra.

Jadeite jade from Myanmar was quite variable, ranging from a good response to no response. Mottled green/white cabochons may show red fluorescence with little correlation to visual colour patterning. *Figure 6* shows that the two principal emission peaks are on the high-wavelength side of 700 nm.

Examination of topaz showed that chrome-bearing varieties do fluoresce red, and give a much stronger response to the blue light than they do to LWUV. Brown, colourless, and blue varieties from volcanic or pegmatitic sources were found not to fluoresce. Many samples from the Ouro Preto district, Brazil, do react, with the strongest response from those having pinkish tones in white light, while light coloured to pure yellow stones show very weak to no response. The rare pink topaz from Brumado, Brazil, gives a strong response, as does the amber to pink topaz from Ghundao Hill, Pakistan. This probably reflects low iron contents coupled with significant chrome contents. Surprisingly, the pale yellow Schneckenstein topaz of Germany gave a moderate response from two samples tested. This substantiated the reports of crimson and pale violet topaz from the deposit reported many years ago by Feuchtwanger and Streeter, as mentioned by Hoover (1992).

Demantoid, and tsavorite garnets both gave no visible response – understandable because their emissions are weak and too far into the near infrared to be seen.

Because the blue torch/selenium glass combination was so effective for many common chrome-bearing gems, it was tested on a large variety of other stones. The results show that some other UV-fluorescing gems also fluoresce by crossed-filters examination.

Some surprises were found when comparing responses to LWUV and the blue LED crossed-filter technique. Diamonds give different responses to LWUV and to blue excitation. Diamonds that fluoresce blue-white under LWUV show varying strengths of orange to red fluorescence under blue light without a viewing filter, and red with the filter of course. Diamonds fluorescing yellow to whitish-yellow under LWUV, show a varying strength orange without the viewing filter, and red with the filter. In some stones the fluorescence is stronger under blue excitation than under LWUV. In the above tests with diamonds, it was found that a yellow viewing filter such as Stokes used, is a better detector of any response and colour differences due to the better match between the emitted light spectrum and the pass band of the yellow filter.

Other stones tested that fluoresced include: anorthite, Alaska, very weak; light coloured apatites, weak, but blue and green ones gave no response; calcite, some fluorescent varieties good; brown fluorite, Clay Center Ohio, strong, others no; colour-change garnet, Madagascar, fair; kyanite, Nepal, and Brazil, weak; scheelite, weak; sinhalite, Sri Lanka, very weak; sphalerite, weak; spodumene, weak to moderate, with no apparent relation to colour; tugtupite, good.

Of the organic gems, amber, ivory, and red coral all gave fair to good responses. The real surprise was the sinhalite which is considered to be non-fluorescing (Henn, 1994). Although the response is extremely weak, tests on three samples have shown that it can be differentiated from peridot if care is taken with the crossed-filters technique. *Figure 6* shows the emission spectrum of one

of the examined sinhalites, suggesting that chromium is present.

Summary

The red selenium glass and blue LED are simple and easy to use. The authors believe that the sources and filters described in this paper provide an important advance in application of the crossed-filters technology because it can be easily implemented by the average gemmologist at very little cost. However, with technology advancing at a rapid pace it would not be surprising if even better sources and/or filters become available in the near future. The information given in this paper should be sufficient for any gemmologist to easily determine which future technical advancements he/she might be able to adapt to the method.

The authors expect that this simple procedure will aid gemmologists in separation and discrimination between a number of gems. However, development and effectiveness of the technique will depend on testing sufficient quantities of stones, looking for differences to assist in distinguishing between synthetics and natural stones, and in distinguishing provenance. We feel that it should supplement conventional UV fluorescence testing. Also, with potential to exploit in the deep red region, it is possible that infrared-sensitive (digital) cameras could extend the limited range of the human eye.

Acknowledgements

The authors thank G. Pearson, Melbourne, Australia, for many stimulating discussions on spectral responses of gemstones, from which the impetus to pursue this study was derived, and the Stone Group Labs for the use of their spectrophotometers.

References

- Anderson, B.W., 1959. *Gem Testing*, 6th edn. Emerson, New York, 324pp
- Bauer, M., 1904. *Precious stones*. trans. L.J. Spencer. Charles Griffin & Company Ltd., London. Reprinted 1968 by Dover Publications Inc., New York

- Harding, R.R., 1994. Luminescence. In: *Gems*, by R. Webster, edited by P.G. Read. Butterworth-Heinemann, Oxford, 837-53
- Henn, U., 1994. Lesser-known ornamental and gem materials. In: *Gems* R. Webster, edited by P.G. Read. Butterworth-Heinemann, Oxford, 309-88
- Hoover, D.B., 1992. *Topaz*. Butterworth-Heinemann, Oxford, 207pp
- Hoover, D.B., and Theisen, A.F., 1993. Fluorescence excitation-emission spectra of chromium-bearing gems: an explanation for the effectiveness of the crossed filter method: *Australian Gemmologist*, 18(6), 182-7
- Hughes, R.W., 1997. *Ruby and Sapphire*. RWH Publ., Boulder, 511pp
- Schwarz, D., 1987. *Esmaraldas, Inclusões em Gemas*. Univ. Fed. Ouro Preto., 439pp (in Portuguese)
- Wood, R.W., 1934. *Physical Optics*. Dover reprint (1967), New York, 846pp

Letters to the Editor

Asterism and chatoyancy

Further to the recent paper on asterism and chatoyancy¹, as far as I have been able to ascertain, the credit for being the first to draw attention (in 1981) to the position of the image in asterism must go to A. Wüthrich and M. Weibel². They quote, as I did, the standard optics formula for the position of the real image formed when light passes through a plano-convex lens backed by a mirror. They consider, however, that the fundamental process in asterism is the scattering of light by thin cylinders, rather than reflection.

A.R. Moon and M.R. Phillips^{3,4} point out that, in sapphire, the inclusions are flat strips, not cylinders, and further that the scattering model does not account for the observed fact that sharper stars result when the inclusions are long, rather than short. They say that a mechanism which does fit these observations is Fraunhofer diffraction. Babinet's Principle is cited to allow the opaque strips to be considered as if they were slits of the same dimensions. The authors agree with Wüthrich and Weibel about the position of the image.

So, although my paper turns out not to be the first to draw attention to the position of the image in chatoyancy and asterism, I hope it will have served a useful purpose in repeating this information, which seems not to have had the attention it deserves.

Harold Killingback FGA
Oakham, Leicestershire

1. H. Killingback, 2005. *Journal of Gemmology*, 29(5/6), 312-5
2. A. Wüthrich and M. Weibel, 1981. *Phys. Chem. Minerals*, 7, 53-4
3. A.R. Moon and M.R. Phillips, 1984. *Schweiz. Mineral. Petrogr. Mitt.*, 64, 1
4. A.R. Moon and M.R. Phillips, 1985. *The Australian Gemmologist*, 15(11), 395-9

Use of the polarising filter on the refractometer

I was sorry to find that B.D. Sturman, author of the article 'The use of the polarising filter on the refractometer' (*Journal of Gemmology*, 2005, 29, 5/6) has not acknowledged two published works on this subject^{1,2}. Contrary to the claim in the abstract, the stated method suitable for gemmologists unfamiliar with the indicatrix to use a polarising filter with the refractometer is, I feel, not strictly a 'new comprehensive method'. What Sturman is offering is an original table and his own approach to a known method.

However, in this table there is a minor error in that if instructions in pattern number I were followed, a person could fail to correctly diagnose a constant RI of 1.597 as a rhodochrosite with optic axis perpendicular to the facet because for this pattern a polarizing filter is not used. For those who find his diagrammatic representations easier to consider than the other approaches referred to above, I recommend a correction in 'pattern number I' with this polarising filter reference changed from 'not used' to read instead 'rotated, no blink confirms isotropism; for blink use pattern II or IV, presuming one shadow over the limit'.

Richard Cartier
Toronto, Ontario, Canada

1. Hodgkinson, A., 1992. Simple advanced refractometer technique: determining optic sign. *Canadian Gemmologist*, XIII(4), 114-17
2. Cartier, R.H., 2004. *Seeing the light, understanding optics without the mathematics*. Published by the author. ISBN 0-9735316-1-4, pp 234-44

Response from B.D. Sturman

In the article I took special care to use terms such as ‘new approach’ and ‘graphical presentation’ when referring to the set of instructions in the Table, and I describe in detail what is new and what was taken from the selected published works. The term ‘new comprehensive method’ in the abstract was chosen by the editor; I am sorry I missed it during the proof-reading.

I do not believe that the instructions in the Table should be changed so that the polarising filter *must be used every time* a single shadow edge is observed. This would be the required procedure in order to avoid problems with rhodochrosite identification. (The gemstone must be cut in a very special orientation - the gem table is *exactly* perpendicular to the optic axis). Read, 1999¹ (see the reference in the article) provides examples of other gemstones on page 89 (smithsonite and painite) that may cause similar problems. This problem will be dealt with in a separate note that will be given in an article (in preparation) with a description of other possible problems, for example, biaxial gemstones with small 2V – producing patterns similar to uniaxial gemstones.

Determination of the optic sign in biaxial gemstones (when β is determined) is not as useful as determination of 2V (for example in identification of sinhalite or peridot). It does not require additional time if the optic angle diagram is kept next to the refractometer.

There are several reasons why references mentioned in Cartier’s letter were not listed in my article. The Hodgkinson article² was not mentioned because my article was not intended as an overview of the methods presented in the literature; its main thrust was to describe a new approach and a new graphical presentation. I have great respect for Alan Hodgkinson and his work, but his article in the *Canadian Gemmologist* was not needed for the description of the new approach.

On the other hand, Cartier’s book³ was not mentioned for very different reasons. The *Canadian Gemmologist*, Autumn 2005, contains a review of the book which is very

negative. The reviewer listed many confusing or incorrect statements in the book and readers should be aware of these.

However, I decided not to quote the book for another reason. In his two articles on doubling^{4,5} and one article on the optic axes⁶ in *The Journal of Gemmology*, Cartier gives many confusing and incorrect statements. The best example is Cartier’s description of birefringence as a “property of the medium” and double refraction as “the action of light as it enters the medium”. It does not have any practical use and can only result in confusion. Every optical property is determined by observing the interactions of light and a gemstone – all optical properties are properties of the medium. This is a fact that has been accepted for hundreds of years and stays the same no matter how much we discuss “the use of the plural, the singular and contractions maintain the same conceptions throughout to avoid optics theory confusion,” or that “Refraction, double refraction, birefringence and refringence should have continuity of concept between the singular and the plural.” (The quotes are from Cartier’s articles). I do not want to use a book as a reference if I find it confusing and I do not believe that readers would be well served by referring them to it.

Darko Sturman

Curator Emeritus, Royal Ontario Museum

1. Read, P.G., 1999, *Gemmology* (2nd edn). Butterworth-Heinemann, London
2. Hodgkinson, A., 1992. Simple advanced refractometer technique: determining optic sign. *Canadian Gemmologist*, XIII(4), 114-17
3. Cartier, R.H., 2004. *Seeing the light, understanding optics without the mathematics*. Published by the author. ISBN 0 9735316-1-4
4. Cartier, R.H., 2002. Birefringence vs. double refraction divergence. *Journal of Gemmology*, 28(4), 223-6
5. Cartier, R.H., 2003. A note on the directions of maximum double refraction divergence (DD) in uniaxial and biaxial stones. *Journal of Gemmology*, 28(8), 489-93
6. Cartier, R.H., 2004. A new definition of optic axis for gemmology and four kinds of optic axis. *Journal of Gemmology*, 29(4), 228-34

Abstracts

Diamond

Colombian diamonds.

T. CHAVEZ-GIL AND F.H. ROMERA-ORDOÑEZ. *Gemmologie. Z. Dt. Gemmol. Ges.*, 53(2/3), 2004, 67-78, 10 photographs, 2 maps, 2 graphs, bibl.

The alluvial diamonds were found in gravel deposits in the south-eastern part of Colombia in the Alba Rosa stream in the Eastern Cordilleras, near the border with Venezuela and Brazil. The origin of the deposits is assumed to be in the Roraima series of Precambrian rocks, which in Venezuela, Brazil and Guyana are in parts diamond bearing. All examined material showed certain etch and corrosion markings which was taken to be proof of transportation in some corrosive medium, i.e. kimberlite or lamproite magma. In the gravel concentrate various heavy minerals were present, such as pyrope, almandine, ilmenite and some traces of olivine. The occurrence of these diamonds is rare. 100 diamonds were studied, mostly between 1 and 3 mm in diameter, but some up to 5 mm have been found. E.S.

Coated pink diamond -- a cautionary tale.

D.J.F. EVANS, D. FISHER AND C.J. KELLY. *Gems & Gemology*, 41(1), 2005, 36-41.

The examination of a cut 0.85 ct purple-pink diamond, reputed to have been HPHT treated, determined that this diamond, probably pale yellow originally, had been coated to change its colour. A microscopic examination revealed evidence of a coating only on the pavilion faces. This coating may have been calcium fluoride with a gold impurity added either to generate the absorption responsible for the pink colour or to assist as a nucleating agent for the calcium fluoride film. R.A.H.

Diamond mining project

Panna: an overview.

A.K. GUPTA AND R.K. GARG. *Indian gemmologist*, 13(1/2), 2005, 13-8.

The Panna diamond area is situated in the north of Madhya Pradesh at the junction of the Bundelkhand and the Vindhyan regions. Details are given of the occurrence with notes on its history from its discovery in 1827 through its various upgrades up to the present. Mining is entirely mechanised; 28% of the crystals recovered are of gem quality, 38% are off-coloured and 34% dark brown or industrial quality. M.O'D.

Gem news international.

B.M. LAURS (Ed.) (blaur@gia.edu). *Gems & Gemology*, 40(4), 2004, 334-57.

Items noted included a 1.33 ct orange-yellow natural diamond with an estimated 30-50 ppm of Ni. R.A.H.

The diamond pipeline –

A literature review.

H.H. LIM. *Australian Gemmologist*, 22(6), 2005, 244-52, 4 Illus., 1 table.

The traditional diamond pipeline which traces the passage of rough diamonds from the mine to the market has been modified by the changes that have taken place in the diamond industry since De Beers was privatised and its business strategy was revised. The review includes brief descriptions of the history of diamond trading, prospecting, mining and recovery, the Central Selling Organisation (its role and its renaming as the new DTC), sorting and valuing, the Sights, cutting and polishing, diamond clubs and bourses, jewellery manufacturers and the retail market. P.G.R.

Global occurrences of primary host rocks of diamonds.

T. MARATHE. *Indian Gemmologist*, 13(1/2), 2005, 50-3.

The geology of some of the world's major diamond deposits is discussed with particular reference to Indian sites. M.O'D.

Lab notes.

T.M. MOSES, I. REINITZ, S. F. McCLURE and M.L. JOHNSON (Eds). *Gems & Gemology*, 40(4), 2004, 323-33.

Notes are given on a yellow-luminescent 2.03 ct 'hopper' diamond and a 0.12 ct Fancy Intense purplish pink natural diamond showing apparent magnetism (due to iron-bearing residue in surface cavities) R.A.H.

Lab notes.

T.M. MOSES AND S.F. McCLURE (Eds). *Gems & Gemology*, 41(1), 2005, 42-50.

Notes are given on HPHT-treated type IIa yellow diamond and on an inhomogeneous yellow type Ia Cape diamond. R.A.H.

Evolution of the Indian diamond industry.

J. PANJIKAR AND K.T. RAMCHANDRAN. *Indian Gemmologist*, 13(1/2), 2005, 27-38.

The beginning of diamond production in India is believed to go back 3500 years. Geographical and geological details are given for the northern, southern and eastern groups of mines. Two maps pinpoint the main areas. M.O'D.

Kalimantan diamond.

TAY THYE SUN, P. WATHANAKUL, W. ATICHAT, LING HENG MOH, LEE KIEN KEM AND R. HERMENTO. *Australian Gemmologist*, 22(5), 2005, 186-95, 9 illus., 1 map, 1 table.

Diamond occurs in commercial quantities in the Indonesian state of Kalimantan which is part of the island of Borneo. These diamonds are found mainly in West, Central and Southeast Kalimantan. They are of fine quality and are recovered in a range of fancy colours such as blue, pink and canary-yellow. The authors visited the diamond mines in the Banjarmasin-Martapura area of Southeast Kalimantan in March 2002 to study mining and trading activities. They purchased 14 diamond specimens for further study, and this paper contains a description of the morphology, surface and spectroscopic features of these diamonds. P.G.R.

Treated-color pink-to-red diamonds from Lucent Diamonds Inc.

W. WANG, C.P. SMITH, M.S. HALL, C.M. BREEDING AND T.M. MOSES. *Gems & Gemology*, 41(1), 2005, 6-19.

Naturally-coloured diamonds in the pink-to-red range are among the most exotic and expensive gemstones. Lucent Diamonds of Denver has developed a new treatment process for natural type 1a diamonds that produces colours ranging from pink-purple through red to orangy brown, using a multi-step process that involves HPHT annealing, irradiation and low-pressure annealing at relatively lower temperatures. The stones that achieve a predominant pink-to-red or purple colour are marketed as 'Imperial Red Diamonds'. The gemmological properties and characteristic spectra for 41 of these diamonds are described. They can be readily identified by distinctive colour zoning, internal graphitisation and surface etching, and reactions to long- and short-wave UV radiation. The colour is caused by the absorption of the (N-V)-centre, with further influence from other centres; the IR absorption spectra are presented. R.A.H.

Gems and Minerals

A miscellany of organics – part 3.

G. BROWN. *Australian Gemmologist*, 22(6), 2005, 264-8, 15 Illus.

This is a further compilation of laboratory reports that cover a range of identification problems associated with organic gem materials. Included are Berber beads, dyed paua shell, 'rattler' pearl beads, and lacquerware. P.G.R.

Gemstone treatments – are they stable?

G. CHOUDHARY AND C. GOLECHA. *Indian Gemmologist*, 13(1/2), 2005, 54-7.

Common gemstone treatments are listed with examples and notes on stability. M.O'D.

The diamondiferous peridot (olivine) – garnet deposit of Shavryn Tsaram, Central Mongolia, with special reference to its placer deposits.

H.G. DILL, S. KHISHIGSUREN, YO. MAJIGSUREN, J. BULGAMAA, O. HONGOR AND W. HOFMEISTER. *Gemmologie*.

Z. Dt. Gemmol. Ges., 53(2/3), 2004, 87-104, 14 photographs, 1 graph, 2 tables, 4 diagrams, bibl.

The deposit is located in the Khangai mountains of central Mongolia. Extensive hotspot volcanism occurred in the Mongolian plateau during the Tertiary and Quaternary periods, resulting in mainly alkaline basanites and olivine basalts, the host rock of the gemstones. Mainly garnets, olivine and sanidine were mined in opencast mines from the placer deposits during the mid-seventies and manufactured in Ulaanbaatar. Diamonds were found as a rare constituent. Gems and some heavy minerals may lead the geologists to the source rock of the gemstones. Reworking the gemstones in a secondary deposit may help refine gemstone quality. E.S.

Les gisements de rubis du Pakistan et du Viêt-nam.

V. GARNIER, G. GIULIANI, D. OHNENSTETTER, ALLAH BAKHSH KAUSER AND HOANG QUANG VINH. *Revue de gemmologie AFC*, 151, 2005, 6-12.

The relationship of marble-hosted ruby deposits in both Pakistan and Vietnam to major tectonic structures is discussed with particular reference to the colliding Indian and Eurasian plates. The deposits were formed in the Cenozoic during the Himalayan orogenesis. The occurrence of ruby is restricted to impure marble horizons enriched in detrital minerals. M.O'D.

Les isotopes de l'oxygène: un traceur de l'origine géologique des rubis et saphirs.

G. GIULIANI, A. FALLICK, V. GARNIER, C. FRANCE-LONORD, D. OHNENSTETTER AND D. SCHWARZ. *Revue de gemmologie AFC*, 152, 2005, 9-11.

Study of the two principal isotopes of oxygen, ^{18}O and ^{16}O can provide evidence of the origin of some rubies and sapphires. M.O'D.

Rubellite and other gemstones from Momeik township, Northern Shan State, Myanmar.

U.T. HLAING AND A.K. WIN. *Australian Gemmologist*, 22(5), 2005, 215-8, 6 illus., 2 maps.

Colourful tourmalines, including pink rubellite, are found in the vicinity of Molo village in the

Momeik township of Shan State. The tourmaline crystals are associated with pegmatites that intrude peridotite, and occur either as single euhedral crystals or as mushroom-shaped aggregates and botryoidal masses. The paper describes the properties of the gems and their associated minerals which include quartz, orthoclase feldspar, beryl, petalite and hambergite. P.G.R.

The creation of a magnificent suite of peridot jewelry: from the Himalayas to Fifth Avenue.

R.E. KANE (finegemsint@msn.com). *Gems & Gemology*, 40(4), 2004, 288-302.

The ultimate value of a gemstone suite lies not only in the cost and quality of the materials themselves, but also in the selection of the rough, the quality of the faceting and the intricacy of the setting in a well-designed and well-manufactured suite of jewellery. This article describes in detail the whole process from the mine in the Sapat Valley region of Pakistan to the manufacture of the necklace, bracelet, ring and earrings. Eight kg (40 000 ct) of peridot rough eventually yielded a precisely matched suite of 54 gems ranging from 3.57 to 18.30 ct for a total weight of 350.40 ct. R.A.H.

Gem news international.

B.M. LAURS (Ed.) (blaur@gia.edu). *Gems & Gemology*, 40(4), 2004, 334-57.

Items noted include 0.68 and 1.59 ct faceted yellow-orange clinohumites from the Pamir Mountains, Tadjikistan, jeremejevite from Madagascar, deep blue sapphires from southern Baffin Island, and a rare transparent 7.16 ct orange-red triplite from Pakistan. R.A.H.

Gem news international.

B.M. LAURS (Ed.) (blaur@gia.edu). *Gems & Gemology*, 41(1), 2005, 52-73.

Cut specimens of aquamarine from Nigeria have a saturated blue colour (ϵ 1.582, ω 1.589, SG 2.76); a new deposit in western Xinjiang Province, China, is yielding rough and cut emeralds. The Santa Barbara mine near Parelhas, Rio Grande Norte State, Brazil, is producing iolite from pods in narrow quartz veins. Mention is also made of a cut 1.11 ct pink pezzottaite reportedly from Afghanistan (ϵ 1.598, ω 1.605, SG.2.97;

EPMA shows Cs 10.18 and 12.56 wt %). A 5.0 mm inclusion of pezzottaite in quartz from the Sakavalana pegmatite in Madagascar is also described. A 10.53 ct gem-quality diamond is reported from a core sample of kimberlite from the Fort à la Corne diamond project in central Saskatchewan. R.A.H.

Les corindons à changement de couleur.

L. MASSI. *Revue de gemmologie AFC*, 152, 2005, 16-19.

Many corundum specimens display a change of colour when examined under different types of light source. Details of the relevant absorption spectra are given. M.O'D.

Gemmologie Aktuell.

C.C. MILISENDA. *Gemmologie. Z. Dt. Gemmol. Ges.*, 53(2/3), 2004, 63-6, 6 photographs.

A colourless chrysoberyl weighing 0.68 ct was found amongst sapphires from Mogok, Myanmar (Burma). It was easily identified as a natural chrysoberyl. In some opal mosaic triplets which were examined, the opal fragments were embedded in black glass and proved to be synthetic. The term is misleading because 'mosaic opal' can also describe natural precious opal showing a colour play with a mosaic type pattern. Some mounted and unmounted faceted stones were identified as dyed natural corundum, the stones are translucent grey with yellow, blue, green and also red tints and had been filled with artificial blue or red dye. A necklace made of 15 mm round turquoise blue beads from Asia was examined and found to be a dyed carbonate. The surface had a grainy appearance and the colour was more intense in veins and fissures. E.S.

Lab notes.

T.M. MOSES, I. REINITZ, S.F. McCLURE AND M.L. JOHNSON (Eds). *Gems & Gemology*, 40(4), 2004, 323-33.

Notes are given on a 4.45 ct transparent orange-brown iolite, a 22.77 ct greyish purple pearl from a natural saltwater mussel, and strands of drop-shaped 'golden' South Sea cultured pearls shown to have been colour-treated. R.A.H.

Lab notes.

T.M. MOSES AND S.F. McCLURE (Eds). *Gems & Gemology*, 41(1), 2005, 42-50.

A 'night glowing pearl' pearl was found to be a sphere of a talc-serpentine rock with a phosphorescent coating. Cut specimens represented as 'pink fire quartz' from Minas Gerais, Brazil, were found to contain inclusions of covellite showing bright pink iridescence. R.A.H.

Gemstones of Chattisgarh – an overview.

S. PANDEY. *Indian Gemmologist*, 13(1/2), 2005, 85-6.

Diamond, alexandrite, ruby, sapphire, kornerupine, beryl, garnet and rock crystal are described from the Chattisgarh area of Raipur, India. M.O'D.

Gem deposits of Rajasthan.

S. PAREEK. *Indian Gemmologist*, 13(1/2), 2005, 79-84.

Emerald, almandine garnet, dark green epidote, yellow chrysoberyl, variously-coloured tourmaline, amethyst, aquamarine, topaz, green apatite, variously-coloured fluorite, kyanite and andalusite, all with some gem potential are reported and described from Rajasthan. M.O'D.

A review of gemstone belts of eastern and southern India and guidelines for the search of gemstone deposits.

S.K. SARKAR AND A.I. GURU. *Indian Gemmologist*, 13(1/2), 2005, 41-9.

The majority of gemstones found in India originate from the states of Andhra Pradesh and Orissa in the east and Tamil Nadu in the south. Geological conditions are described; main centres are listed and there is a useful short bibliography. M.O'D.

Flux filled corundums and their identification.

A. SHARMA. *Indian Gemmologist*, 13(1/2), 2005, 39-40.

Hints on the identification of lead glass-filled rubies. M.O'D.

La moule perlière d'Europe: margaritifera (M.) margaritifera (L.1758).

E. STRACK. *Revue de gemmologie AFC*, 151, 2005, 17-23.

Survey of the occurrence of European freshwater mussel-hosted pearls with examples of their use. M.O'D.

Opale aus Java.

H. SUJATMIKO, H.C. EINFALT AND U. HENN. *Gemmologie. Z. Dt. Gemmol. Ges.*, 53(2/3), 105-12, 14 illus., bibl.

Opal has been mined since the 1970s in the western part of Java from a strongly altered pumice layer in a late Tertiary volcano-clastic sequence. There are about one hundred miners working in small underground mines during the dry season from May to September under contract with lease holders. The opal varies from common opal to hyaline, fire opal, white and black precious opal with dominantly red, orange and green colours. Rough and pre-shaped opal pieces are sold, mainly by the lease holders, mostly to traders from Jakarta, Bandung, Yogyakarta and Bali; only a small amount is sold on the international market. E.S.

Opals from Java.

H. SUJATMIKO, H.C. EINFALT AND U. HENN. *Australian Gemmologist*, 22(6), 2005, 14 Illus., 1 map.

An English version of the article published in *Gemmologie. Z. Dt. Gemmol., Ges.* (see above). P.G.R.

Trapiche of Myanmar.

K.K. WIN. *Australian Gemmologist*, 22(6), 2005, 269-70, 2 Illus.

Myanmar is the locality of a range of trapiche gemstones that display a distinctive spoke-like star. The author illustrates a selection of these unusual stones, and suggests that these originate due to specific colouring elements, to the presence of other mineral inclusions, and to intergrowth of the same material. P.G.R.

Pearl resources of China.

ZHANG HUI AND ZHANG BEILI. *Australian Gemmologist*, 22(5), 2005, 196-209, 40 illus., 5 tables.

China has a long history of both natural pearl harvesting and pearl cultivation, the latter being invented and developed by the Chinese people early in the 13th century. However, pearl cultivation was not a large scale industry until the middle of the 20th century. Seawater pearl cultivation takes place in the Guangdong, Guangxi and Hainan provinces, and fresh-water cultivation localities are in Zhejiang and Jiangsu provinces. The Zhuji pearl market in Zhejiang and the Weitang pearl market in Jiangsu also play key

roles in the global marketing of Chinese freshwater pearls. The paper describes and illustrates the varieties of seawater and fresh-water Chinese cultured pearls and includes the National Standards used for grading and appraising of the pearls. P.G.R.

Instruments and Techniques

Professional Gem Light 3.

R. BEATTIE AND T. LINTON. *Australian Gemmologist*, 22(5), 2005, 210-4, 4 illus.

The Professional Gem Light 3 is an advanced laboratory hand lens lighting system. The compact lighting unit is mounted on a flexible arm and uses daylight-type (5500 degrees K) light sources to provide the three essential lighting systems for gemstone analysis; high intensity dark-field illumination, diffused and direct bright-field illumination, and very high intensity incident illumination. The authors describe the various features of the unit when used to examine gemstones and jewellery in conjunction with a hand lens, a combination which exploits the ease of use of the 10 lens as opposed to the more restricted use of a microscope. P.G.R.

Ein neues Instrument für die analytische Gemmologie: LIBS.

H.A. HÄNNI, M.S. KRZEMNICKI, L. KIEFERT, AND J.P. CHALAIN, *Gemmologie. Z. Dt. Gemmol. Ges.*, 53(2/3), 2004, 79-86, 3 photographs, 1 diagram, a graph, bibl.

The identification of Be-diffused corundum showed that it is essential for a gem laboratory to be able to analyse even low traces of chemicals in gemstones. The Be detection was made possible by micro mass spectrometry a costly process possibly outside the means of most gem laboratories. The new method is based on laser induced optical emission spectroscopy. Laser induced breakdown spectroscopy (LIBS) can be successfully used to identify Be-diffused corundum. A focused pulse of a Nd:YAG laser transforms some micrograms of the sample into plasma. The light emission is diffracted and recorded by a multi-channel analyzer. The line spectrum can be used for qualitative and

quantitative analysis. Almost all chemical elements are detectable and it allows chemical fingerprinting of the gem material. The new method is slightly destructive as a tiny spot remains after the laser shot. E.S.

A new method for detecting Be diffusion-treated sapphires: laser-induced breakdown spectroscopy (LIBS).

M.S. KRZEMNICKI, H.A. HÄNNI AND R.A. WALTERS. *Gems & Gemology*, 40(4), 2004, 314-22.

The first application of laser-induced breakdown spectroscopy (LIBS) to gemmology is described. Until now, the detection of Be-diffused sapphire and ruby has been based on LA-ICP-MS or SIMS techniques, neither of which is readily available to most laboratories. In the study reported here, LIBS is used to detect Be in corundum at very low concentrations (down to ~2 ppm). This technique is a reliable tool for identifying Be diffusion-treated sapphires, and is affordable for most commercial gemmological laboratories. As with other laser-based techniques, LIBS may cause slight damage to a gemstone, but this can be minimised by choosing appropriate instrument parameters. R.A.H.

Une nouvelle méthode pour la détection des corindons traités par diffusion du béryllium: Laser-Induced Breakdown Spectroscopy (LIBS).

M.S. KRZEMNICKI, H.A. HÄNNI, R.A. WALTERS AND J.-P. CHALAIN. *Revue de gemmologie AFC*, 152, 2005, 13-5.

The technique of Laser-Induced Breakdown Spectroscopy (LIBS) has been used for the detection of beryllium-diffused corundum. M.O'D.

Krüss refractometer – ER 6010.

T. LINTON, R. BEATTIE AND K. HUGHES (GAA Instrument Evaluation Committee). *Australian Gemmologist*, 22(6), 2005, 260-2, 2 Illus.

The Krüss ER 6010 German-made refractometer contains a glass hemisphere 'table' which gives it the ability to measure refractive indices at wavelengths used for the determination of dispersion. The

instrument has a scale calibrated in RI units of 0.01 covering the range of 1.30 – 1.83. Calibration of this scale can be adjusted over the limits of ± 0.002 . The refractometer is supplied with a twin high-intensity yellow LED light source (with a bandwidth of 50nm) which plugs into the refractometer's rear port and is powered from a 240-volt plug pack. A compact student version of the instrument, model ER 6040, is also available. An evaluation of the refractometer's performance is included in the report. P.G.R.

Identification des corindons chauffés avec addition de verre au plomb.

V. PARDIEU. *Revue de gemmologie AFC*, 152, 2005, 20-2.

Methods of detection of lead glass-filled corundum specimens are given. M.O'D.

Use and misuse of optical mineralogy constants in gemmology.

D.B. STURMAN. *Australian Gemmologist*, 22(6), 2005, 234-43, 5 Illus., 3 graphs.

The author provides examples where the direct transfer of optical data from mineralogy to gemmology can cause misunderstanding. One example of such a transfer results in the calculated dispersion coefficient being an unreliable indicator of the actual amount of visible 'fire' produced by a faceted gemstone (although the coefficient may still be a useful identification constant for that gemstone). In a second example, the rules for the determination of birefringence cannot be applied to the 'doubling' of images as these are different optical properties. Factors contributing to doubling are described and diagrams are provided for a fast and reliable estimate of the doubling effect in gemstones. P.G.R.

Synthetics and Simulants

CVD diamonds; the biggest achievement in the diamond synthesizing.

A. JAIN. *Indian gemmologist*, 13(1/2), 2005, 22-6.

Brief details of diamonds grown by chemical vapour deposition are

given with notes on identification.

M.O'D.

Tanzanite v/s forsterite.

P.R. JHAVERI. *Indian Gemmologist*, 13(1/2), 2005, 68-70.

The usefulness of a synthetic forsterite as a tanzanite stimulant is discussed with notes on identification. The trade name Tanzanion has been suggested.

M.O'D.

An updated chart on the characteristics of HPHT-

grown synthetic diamonds.

J.E. SHIGLEY, C.M. BREEDING AND A. H.-T. SHEN. *Gems & Gemology*, 40(4), 2004, 303-13.

A new chart is presented, supplementing an earlier one published in 1995, which summarises the features of both as-grown ('non-modified') and treated ('modified') synthetic diamonds currently in the gem market (i.e. those grown by the high-pressure/high-temperature technique). It includes photographs

of visual features, information about visible-range absorption spectra and illustrations of growth-structure patterns as revealed by ultraviolet fluorescence imaging. The chart is designed to help gemmologists to recognise the greater variety of laboratory-created diamonds that might be encountered today. R.A.H.

For further information on many of the topics referred to, consult *Mineralogical Abstracts*.

Abstractors

R.A. Howie R.A.H. M. O'Donoghue M.O'D. P.G. Read P.G.R. E. Stern E.S.

Book Reviews

Diamonds. The world's most dazzling exhibition, 8 July 2005 – 26 February 2006

Natural History Museum, 2005. Natural History Museum, London. pp 60, illus. in colour. Softcover. ISBN 0 565 09201 4. £7.00.

This short but very attractive catalogue is published to accompany an exhibition of diamonds held at the Natural History Museum, London. It is worthy of the exhibition which includes many famous diamonds, with some items of jewellery and some of the early attempts at diamond synthesis as well as current synthetic diamonds. The catalogue illustrates many of the exhibits and includes in the text a summary of the properties and history of diamond. Recent growth techniques are also described. This is a useful short study of diamond and would make a good introduction for study at any level.

M.O'D.

Edle Steine vom Dach der Welt.

Various authors, 2003. Christian Weise Verlag, Munich, Germany. pp 96, illus. in colour. Softcover.

ISBN 3 921 65662 1 [ISSN 0945 8492] extraLapis no 14. €28.40

As beautifully illustrated and as well written as the other numbers in this excellent series [now appearing in English], the present number describes the gem materials of Afghanistan and Pakistan (the title can be translated as Gemstones from the roof of the world). As always the different sections follow one another without a break and an extensive bibliography concludes the survey. As the reviewer is familiar with some at least of the gem mines of Pakistan it was interesting to read that pargasite of appropriate colour is being called 'Hunza emerald' and that the list of Pakistan gem species has grown to include fine green transparent zoisite and fine orange scheelite.

M.O'D.

Bernstein-Fenster in die Urzeit.

M.J. KOBBERT, 2005. Planet Poster Editions Göttingen. pp 224, Illustrated in colour, Hardcover. ISBN 3 933922 25 X. €19.80

Well-presented and attractively illustrated study of insect inclusions in amber with fairly short captions

and brief introductions to the families represented. There is a short bibliography of works from 1951 and some advice on specimen investigation using the microscope. The price is very reasonable and the quality of reproduction good. This will be a useful addition to the still scarce literature on amber.

M.O'D.

The National Gem Collection, Smithsonian Institution.

J.E. POST with photographs by Chip Clark, 2005. Harry N. Abrams, Inc., New York. pp 144, landscape format, paperback, illus. in colour. ISBN 0-8109-2758-6. £14.95.

Paperback edition of the original hardback edition published in 1997 and reviewed in the *Journal*, 26(5), 338-9. The selection from the more than 10 000 gems and jewellery pieces in the Smithsonian Institution's collection is a constant reminder of the qualities to which collectors and those in the gem trade aspire. The text opens up the topic for anyone with an interest in gems and at this price, is a good starting point for study.

R.R.H.

Gemmology (3rd edn).

P.G. READ, 2005. Elsevier Butterworth-Heinemann, Oxford. pp 307, paperback. ISBN 0 7506 6449 5. £24.99.

This is the 3rd edition of a book providing a comprehensive introduction to the theory and practice of gemmology.

It begins with a straightforward summary of chemistry and geology, and an explanation of the physical properties of gemstones. Gemmological instruments and their uses are covered interestingly and in depth, before an account of synthetic and treated gemstones, and the methods used by gemmologists to recognise them. Styles and methods of gem cutting are described and illustrated, and a chapter on gem identification includes recommendations for a testing procedure which should be helpful to readers who are unfamiliar with the art.

Appendices describe natural and artificial materials, covering a wider range than the Gemmology Diploma syllabus. Lists and tables of gemstone properties, units of measurements and chemical elements provide useful reference sources. Advice given on examination techniques will be useful to gemmology students.

It is unfortunate that the usefulness of photographs is limited by the quality of reproduction. Some anomalies might be eliminated, e.g., is a spectroscopy prism diagram, a ray of light passing from light into air appears to 'bend' towards the normal. Not all dyed green jadeite looks pink through the Chelsea Filter.

Notwithstanding these criticisms, the book contains a wealth of information which make it a useful reference work. It should be especially useful to Gem-A Gemmology Foundation Certificate and Diploma students. Additionally it is moderately priced, compact and relatively lightweight; an unusual and desirable combination of features for a textbook. P.D.

Dictionary of gems and gemology.

M. MANUTCHEHR-DANAI, 2005. Second revised and extended edition. Springer, Berlin. pp 879, Hardcover. ISBN 3 540 23970 7. £154.

This is a baffling book as the nature of the projected readership

is unclear. It is of no use at all to professional gemmologists or practitioners of any other science as there are too many mistakes, whimsicalities, hundreds of names which have never been generally used, pointless translations of phrases into a number of languages and uncertain grasp of the wide area into which the compiler has expanded 'gemmology'.

This is a pity as the book is very well produced with good page layout, typeface and diagrams. It lies open very easily and were it not for the inaccuracies would almost be worth the very high price. Examples of some unfortunately-worded entries (easy to find) include 'green tourmaline-a green variety of tourmaline; hessonite garnet-another term for cinnamon stone; nitrogen oxide-NO₃, impurity in emerald lost one electron probably [sic] by irradiation to form color centers as seen in Maxixe-type beryl'.

As with many entries the reader can see what the compiler is attempting to say and with knowledge sufficient to spot the traps the reader can enjoy leafing through the book; unfortunately this does not benefit the beginner or visitor from the geological or mineralogical disciplines.

The (unpaginated) preliminary matter includes the compiler's thanks to a team of advisers: gemmologists will decide the value of such advice. I remember the first edition which was as equally plagued by similar or the same faults as this one - this is a great opportunity missed. M.O'D.

Faszination Turmalin.

P. RUSTEMEYER, 2003. Spektrum Akademischer Verlag, Heidelberg, Germany. pp 309, illus. in colour. Hardcover. ISBN 3 8274 1424 5. € 99.95

The book is certainly designed to catch the eye and tourmaline serves this purpose admirably. This is the second book on tourmaline to have come from Germany in the past few years and though it is not on the same physical scale as Benesch (1990-one of the largest books on a single gemstone) the general conception is similar. Photographs in colour appear on the recto of every page and are faced either with text, diagrams or additional photographs. The reader is left in no doubt that tourmaline can often be sectioned to give beautiful

and intriguing patterns.

Readers should be advised that this is not a study of fashioned stones but only of crystals, their symmetry and some of their inclusions as displayed by tourmaline. In this context this is a beautiful book. There is a useful bibliography and an index. M.O'D.

Tourmaline: a gemstone spectrum.

Lapis International LLC, East Hampton, Conn., USA. pp 106, illus. in colour. Softcover ISBN 0 971 5371 2 7. extraLapis English no.3. Price on application.

Published independently from but in collaboration with the journal Lapis the extraLapis series translated into English has at the time of writing covered emeralds (issue 2) and calcite (4). The texts are literal translations of the German versions [reviewed in *The Journal passim*] and the illustrations are equally excellent. M.O'D.

Mineralfundorte und ihre Minerale in Deutschland.

A. WITTERN, 2005. E. Schweizerbart'sche Verlagsbuchhandlung, Stuttgart. pp vii 288, Softcover. ISBN 3 510 65213 4. €22.80

The welcome second edition of a good friend to German mineral hunters, this book is a guide for intending visitors to sites of interest in Germany. The text shows clearly shows where the sites are and how to reach them. There is an extensive bibliography but no colour photographs apart from the azurite/malachite on the cover. The price is very reasonable and the addition of colour pictures (which are easily accessed from other sources) would have inflated it. M.O'D.

Laboratory created diamonds.

S. WOODRING AND B. DELJANIN. 2005. EGL USA [New York]. pp. 39, illus. in colour. Softcover. £12.50

Short but informative guide to the growth, production and identification of HPHT and CVD-grown diamonds, with numerous photographs and diagrams incorporated within the text. This is an ideal short guide to an area in which developments are outpacing information sources and is to be welcomed. M.O'D.

Proceedings of the Gemmological Association and Gem Testing Laboratory of Great Britain and Notices

Photo Competition

The 2005 Photo Competition on the theme 'Rare Treasures' attracted a large number of entries of very high quality, illustrating rare gems, rare inclusions, rare jewels and rare phenomena.

First Prize

The first prize was awarded to Luella Dykhuis FGA DGA, Tucson, Arizona, U.S.A. *'Lepidocrocite inclusions in Quartz'*.



Second and Third Prize

The second and third prizes were both awarded to Zeng Chunguang FGA of Singapore, for his entries *'Hematite inclusions in Sunstone'* (second prize) and *'Trapiche emeralds'* (third prize).



We are pleased to announce that the prizes were sponsored by Harley UK, and the Association is most grateful to them for their generosity. The winning entries will be exhibited at the Gem-A Conference to be held on 30 October.

Gem-A Awards

Gem-A Examinations were held worldwide in June 2005. In the Examinations in Gemmology 195 candidates sat for the Diploma Examination of whom 101 qualified, including three with Distinction and 14 with Merit. In the Foundation Gemmology Examination, 236 candidates sat of whom 174 qualified. In the Gem Diamond Examination 102 candidates sat of whom 60 qualified, including seven with Distinction and nine with Merit.

The Anderson Bank Prize for the best non-trade candidate of the year in the Diploma in Gemmology Examination was awarded to Chaman Golecha of Chennai, India.

The Christie's Prize for Gemmology for the best candidate of the year in the Diploma Examination who derives his or her main income from activities essentially connected with the jewellery trade has been awarded to Sheila Barron Smithie of Boston, Massachusetts, U.S.A.

The Anderson Medal for the candidate who submitted the best set of answers in the Foundation Certificate examination which, in the opinion of the Examiners, are of sufficiently high standard, and the Hirsh Foundation Award for the best candidate of the year in the Foundation Certificate Examination have been awarded to Nicola K. Sherriff of Verdun, Quebec, Canada.

The Deeks Diamond Prize for the best candidate of the year in the Gem Diamond Diploma examination has been awarded to Torbjorn Lindwall of Lannavaara, Sweden.

The Tully and Bruton Medals were not awarded.

EXAMINATIONS IN GEMMOLOGY

Gemmology Diploma

Qualified with Distinction

Dong Qingqing, Wuhan, Hubei, P.R. China

Golecha, Chaman, Chennai, India

Mao Yuanjiong, Guilin, Guangxi,
P.R. China

Qualified with Merit

Bayoumi-Stefanovic, Nevin, London

Cai HuiHua, Shanghai, P.R. China

Chawla, Jaspreet Kaur, London

Fellows, Andrew Simon, Aldridge,
West Midlands

Lee Tin Wan, New Territories, Hong Kong

Li Dan, Wuhan, Hubei, P.R. China

Li Na, Guilin, Guangxi, P.R. China

Lv Feng, Shanghai, P.R. China

Miyazaki, Satoshi, Toyonaka City,
Osaka, Japan

Rajaobelina, Tsialiva, Antananarivo,
Madagascar

Rajnikant Manisha, Antananarivo,
Madagascar

Raelison, Ivan Ludovic, Antananarivo,
Madagascar

Torres, Eric, Antananarivo, Madagascar

Zhang Yonghua, Guilin, Guangxi,
P.R. China

Qualified

Ahren, Anna Ekstrom, Tyreso, Sweden

Anderson, Judith S., Manchester,
New Hampshire, U.S.A.

Andrianarimanana, Maminirina,
Antananarivo, Madagascar

Andrianoelison, Hery Miadana,
Antananarivo, Madagascar

Bardehle, Petra, Munich, Germany

Bergman, Marit, Johanneshov, Sweden

Brohi, Nosheen, Wanstead, London

Chan Pak Lin, Tsuen Wan, Hong Kong

Chan Fung Ping, Kowloon, Hong Kong

Chen Jie, Wuhan, Hubei, P.R. China

Cheng Qi, Shanghai, P.R. China

Cheung Ching Chung, Hong Kong

Chong Joon Yau, Singapore

Davis, Shelley, Toronto, Ontario, Canada

Dinapandresena, Hardi, Antananarivo,
Madagascar

Eeckhout, Tiphaine, Thomery, France

Fossurier, Anne, Montreal,

Quebec, Canada

Gem-A Awards

- Geng Yan, Shanghai, P.R. China
 Gillman, Scott, Sudbury,
 Massachusetts, U.S.A.
 Glass, Krista-Leigh Fay, Stratford,
 Ontario, Canada
 Godfrey, Kay, Halstead, Essex
 Gu Jun, Singapore
 Hok Yee Po, Kowloon, Hong Kong
 Hong Xiao Bin, Shanghai, P.R. China
 Ip, Renée, Thornhill, Toronto,
 Ontario, Canada
 Janssen, Marjo, Voorschoten,
 The Netherlands
 Kandalepa, Theophano, Athens, Greece
 Kiamos, George K., Maroussi,
 Athens, Greece
 Kim, Yoonjin, Bucheon City, South Korea
 Kim, Su Hyun, Jincheon-Dong,
 Dalseo-Gu, Korea
 Konstantopoulos, Konstantinos,
 Athens, Greece
 Kwan-Kai-Lion, Antananarivo, Madagascar
 Lawton, Sarah, Enderby, Leicestershire
 Lee Lai Ha, New Territories, Hong Kong
 Leondaraki, Marialena, Athens, Greece
 Leung Chi Fai, Hong Kong
 Li, Kehan, Enfield, Middlesex
 Li On Kei, Sai Kung, Hong Kong
 Li Po Man, North Point, Hong Kong
 Liang Mai, Haidian District, Beijing,
 P.R. China
 Lin Jie, Guilin, Guangxi, P.R. China
 Lina S.W. Cheng, New Territories,
 Hong Kong
 Lo Chun Kin, James, Tin Shui Wai,
 Hong Kong
 Lu Shan, Tokyo, Japan
 Lu Yi, Guilin, Guangxi, P.R. China
 Ma Qin, Shanghai, P.R. China
 McKercher, Jennifer A., Toronto,
 Ontario, Canada
 Natsuka, Masaki, Toyonaka City,
 Osaka, Japan
 Ng Yee Kar, Carolina, Chai Wan,
 Hong Kong
 O'Dwyer, Michael, Wicklow Town,
 Co. Wicklow, Ireland
 Omotedani, Hiroki, Matsudo City,
 Chiba, Japan
 Paterson, Vanessa Ann, Arnold,
 Nottinghamshire
 Pearson, Heather, Belper, Derbyshire
 Pelletier, Lise, Montreal, Quebec, Canada
 Peng Conghui, Guilin, Guangxi,
 P.R. China
 Philogene, Stephanie, Montreal,
 Quebec, Canada
 Rakotoarison Ony, Dominique,
 Antananarivo, Madagascar
 Rakotoson, Eric, Antananarivo, Madagascar
 Rasoanaivo, Sylvie Annick, Antananarivo,
 Madagascar
 Razafimahefa, Hery Tiana Albert,
 Antananarivo, Madagascar
 Sakonuma, Tomoko, Osaka City,
 Osaka, Japan
 Sanders, Jacqueline, Yardley Gobion,
 Northamptonshire
 Sardjono, Grace W., New Territories,
 Hong Kong
 Satis, Amrita, Antananarivo, Madagascar
 Saull, Elanor Nico, Stourbridge,
 West Midlands
 Segi, Naoko, Nagoya City, Aichi Pref., Japan
 Sun Dan, Wuhan, Hubei, P.R. China
 Susawee, Namrawee, Bangkok, Thailand
 Tammilehto, Eero, Helsinki, Finland
 Taylor, Daniel, Leeds, West Yorkshire
 Teng, Terry, West Hampstead, London
 Thawornmongkolkij, Monruedee,
 Patumwan, Bangkok, Thailand
 Wada, Natsuko, Takarazuka City,
 Hyogo Pref., Japan
 Wang Sen, Wuhan, Hubei, P.R. China
 Wong Yi Tat, Eddy, Kowloon, Hong Kong
 Wong Ching Man, Ruby, New Territories,
 Hong Kong
 Wong Oi Chun, New Territories,
 Hong Kong
 Xiao Mai, Wuhan, Hubei, P.R. China
 Yang Xinlei, Wuhan, Hubei, P.R. China

Gem-A Awards

Yin Yu, Guilin, Guangxi, P.R. China
 Yu Dongsheng, Wuhan, Hubei, P.R. China
 Yuki Chiu Wai Yu, Sheung Shui,
 Hong Kong
 Zee Gar Bo, Michelle, Kowloon,
 Hong Kong
 Zhang Guangrui, Wuhan, Hubei, P.R. China

Gemmology Foundation Certificate Qualified

Abduriyim, Ahmadjan, Tokyo, Japan
 Almroth, Kerstin Maria, Umea, Sweden
 Alyawer, Najwa, Wimbledon, London
 Anderson, James Ian, Hythe, Hampshire
 Andrianarimanana, Maminirina,
 Antananarivo, Madagascar
 Andrianoelison, Hery Miadana,
 Antananarivo, Madagascar
 Au Chui Yee, Homantin, Hong Kong
 Au Yeung Shun Wai, Aberdeen, Hong Kong
 Bailey, J. Laurel, Citrus Heights,
 California, U.S.A
 Bakken, Linda L., Trysil, Norway
 Bedhavar, V. Subash Chandra,
 Tamilnadu, India
 Bell, Lucy Kate, Kimberley,
 Nottinghamshire
 Bello, Mohammed I., London
 Benestam, Cissela, Bromma, Sweden
 Bowers, Sally F., Fulham, London
 Buchanan-Jardine, Katie, London
 Bugge, Remy, Fredrikstad, Norway
 Cao Yue, Shanghai, P.R. China
 Caplin, Marco, Lachine, Quebec, Canada
 Cen Qicong, Guilin, Guangxi, P.R. China
 Chan Kwai Chu, Kowloon, Hong Kong
 Chan Lai Fong, New Territories,
 Hong Kong
 Chang Bo Youn, Daejon, Korea
 Chen Xinxing, Guilin, Guangxi, P.R. China
 Cheng Pei-Ling, Taipei, Taiwan, R.O. China
 Cheng Yiu Pong, Chai Wan, Hong Kong
 Che-Sheung, Joanna, Kowloon, Hong Kong
 Chester, Mark, St Helens, Merseyside
 Cheung Man Yi, Kowloon, Hong Kong

Cheung Ka Yan, Michiele, Ap Lei Chau,
 Hong Kong
 Chin Yin Man, Kylie, Yangon, Myanmar
 Chitou, Aurelie Gisele Boasse,
 Antananarivo, Madagascar
 Chow Wai Lam, New Territories,
 Hong Kong
 Chui Yee Man, New Territories, Hong Kong
 Chung Yee Man, Stella, Kowloon,
 Hong Kong
 Chung Yiu-Keung, Kowloon, Hong Kong
 Clark, Jan, Charlton, London
 Cutler, Leticia, Smethwick, West Midlands
 Danjo, Keiji, Kofu City, Yamanashi Pref.,
 Japan
 Deeley, Philippa H., Etchingham,
 East Sussex
 Denney, Brian Shane, Jacksonville,
 Illinois, U.S.A
 Dinapandresena, Hardi, Antananarivo,
 Madagascar
 El-Kassir, Mariam, Acton, London
 Ellison, Armelle Inez, Bisley, Surrey
 Emond, Jacinthe, Laval, Quebec, Canada
 Farrukh, Nayir Khan, Bordesley Green,
 West Midlands
 French, Catherine B., Loomis,
 California, U.S.A.
 Fu Kim Man, New Territories, Hong Kong
 Galbraith, Stuart Mark, Lansdown,
 Gloucestershire
 Geormae, Emmanuel, Athens, Greece
 Glover, Claire, Sunningdale, Berkshire
 Goncalves Coelho, Ana Cristina,
 Antananarivo, Madagascar
 Ha Lai, Kowloon, Hong Kong
 Hall, Ian, Hatton, Warwickshire
 Harrington, Olga, London
 Harris, Nigel, Blindcrake, Cumbria
 Hartley, Pauline, Woodkirk, West Yorkshire
 Hastings, Carrie, Chico, California, U.S.A.
 Razafimahefa, Hery Tiana Albert,
 Antananarivo, Madagascar
 Heywood, Natalie Louise, Enfield,
 Middlesex
 Hu Yuan, Guilin, Guangxi, P.R. China

Gem-A Awards

- Huang Mingcai, Guilin, Guangxi, P.R. China
- Hui Yuen Wah, Kowloon, Hong Kong
- Humphrey, Brian, Fulham, London
- Ito, Yukiyo, Shinagawa, Tokyo, Japan
- Jeong Hye Jeong, Gwangju, Korea
- Johnston, Nanette, Granite Bay, California, U.S.A.
- Jones, Gary Ronald, Dudley, West Midlands
- Ju Tian, Guilin, Guangxi, P.R. China
- Kettle, Georgina Elizabeth, Solihull, West Midlands
- Khan, Qaisra Maaria, London
- Khine Shwe Wah, Yangon, Myanmar
- Kidachi, Masanobu, Sagamihara City, Kanagawa Pref., Japan
- Komvokis, Vasilis, Budapest, Hungary
- Koustoumpardi, Theo, Athens, Greece
- Kwan-Kai-Lion, Antananarivo, Madagascar
- Kwok Mei Yee, Sindy, Aberdeen, Hong Kong
- Lai Hung Tak, Kowloon, Hong Kong
- Lam Mei Hei, Cally, New Territories, Hong Kong
- Lam Siu Kuen, Kowloon, Hong Kong
- Lam Lai Wah, Tsuen Wan, Hong Kong
- Lam Suk Fan, Silvia, Taikoo Shing, Hong Kong
- Lau Ngai Sheung, Kowloon, Hong Kong
- Lau May Kwan, Kowloon, Hong Kong
- Lau Pui Sze, Kowloon, Hong Kong
- Lau Pui Ting, Kowloon, Hong Kong
- Lau Yuen Yee, Simmy, Kowloon, Hong Kong
- Lee Jeong Min, Daegu, Korea
- Lee Chi Kin, Kenneth, North Point, Hong Kong
- Lei Jin, Shanghai, P.R. China
- Lesetedi Kelebogile, Billsley, West Midlands
- Leung Shiu Lok, Taipo, Hong Kong
- Leung Nga Yee, Hong Kong
- Li Suet Lin, Happy Valley, Hong Kong
- Lin Lang-Dong, Taipei, Taiwan, R.O. China
- Liu Pui Man, Jasmine, Kowloon, Hong Kong
- Liu Xi, Guilin, Guangxi, P.R. China
- Liu Yao-Wen, Taipei, Taiwan, R.O. China
- Liu You-Ching, Taipei, Taiwan, R.O. China
- Liu Yu Chen, Taipei, Taiwan, R.O. China
- Liu Zuodong, Guilin, Guangxi, P.R. China
- Lo Nga Lai, Vicky, Kowloon, Hong Kong
- Lou Haowei, Orpington, Kent
- Lounina, Ekaterina, Birmingham, West Midlands
- Ma Jun, Guilin, Guangxi, P.R. China
- Ma Siu Ling, Sally, Kowloon, Hong Kong
- Mak Hoi Chuen, Jeff, Kowloon, Hong Kong
- Mak Bing Lan, New Territories, Hong Kong
- Maniraho, Mireille, Gatineau, Quebec, Canada
- Maske, Sandra Jay, Citrus Heights, California, U.S.A.
- McVeigh, Thomas G., Victoria, British Columbia, Canada
- McWhirter, Hannah Maeve, Bury St Edmunds, Suffolk
- Meyer, Constance Marie, Montreal, Quebec, Canada
- Meyrick, Daisy, London
- Murray, Helen Claire, Four Oaks, West Midlands
- Murtough, Isabel, Derby, Derbyshire
- Myat Zaw, Yangon, Myanmar
- Naing Sein, Yangon, Myanmar
- Newall, Myron, Citrus Heights, California, U.S.A.
- Ng, Emma, London
- Ng Sum Yi, Kowloon, Hong Kong
- Ngai Mei Ching, Bonny, Kowloon, Hong Kong
- Ngala, Kalambayi Dadou, Forest Gate, London
- Okuyama, Muneyuki, Kofu City, Yamanashi, Japan
- Pang Kin Hung, Kowloon, Hong Kong
- Panidis, Ioli, Elefsina, Greece
- Pau Khan Lian, Yangon, Myanmar
- Philogene, Stephanie, Montreal, Quebec, Canada
- Price, David, Colchester, Essex

Gem-A Awards

Qin Ting, Guilin, Guangxi, P.R. China
 Rajaobelina, Tsialiva, Antananarivo,
 Madagascar
 Rajnikant, Manisha, Antananarivo,
 Madagascar
 Rakotoarison, Ony Dominique,
 Antananarivo, Madagascar
 Raneke, Anna Maria, Stockholm, Sweden
 Ranjatoelina, Domoina, Antanimora Tana,
 Madagascar
 Raelison, Ivan Ludovic, Antananarivo,
 Madagascar
 Rasoanaivo, Sylvie Annick, Antananarivo,
 Madagascar
 Salava, Franky, Antananarivo, Madagascar
 Satis, Amrita, Antananarivo, Madagascar
 Shah, Chandni, Mumbai, India
 Sherriff, Nicola, Verdun, Quebec, Canada
 Sim Ooi Kok, Kingston-upon-Thames,
 Surrey
 Slovak, Kate, Leicester, Leicestershire
 Son Hwa Jung, Gangwon-Do, Korea
 Su Yi-Hsuan, Taipei, Taiwan, R.O. China
 Szymanska, Zofia, London
 Thi Thi Han, Yangon. Myanmar
 Torres, Eric, Antananarivo, Madagascar
 Tran, Mark Hung, Elk Grove,
 California, U.S.A.
 Tsai Chung-Yao, Taipei. Taiwan, R.O. China
 Tsui Wing Sze, New Territories, Hong Kong
 van Bruggen, Hemriette, Lunteren,
 The Netherlands
 Wahlstrom, Bengt Christer, Halmstad,
 Sweden
 Watson, John Richard, Berkhamsted,
 Hertfordshire
 Watts, Clare, Beckenham, Kent
 Westlake, Ingrid, London
 White, Susan, Bushey, Hertfordshire
 Wong Po Yi, New Territories, Hong Kong
 Wong Yu Lap, Hong Kong
 Wong Yuen Kwan, Annie, North Point,
 Hong Kong
 Wong Man Yee, Ada, Kowloon. Hong Kong
 Wong Mars, New Territories, Hong Kong
 Wong Ka Yee, Kowloon, Hong Kong
 Wong Lai Mi, Tseung Kwan, Hong Kong
 Wong Man Tung, Kowloon, Hong Kong
 Woo Mei Woon, Shirley, New Territories,
 Hong Kong
 Wu Wing Yi, Kowloon, Hong Kong
 Xu Hui, Shanghai, P.R. China
 Yau Siu-Yin, Kowloon, Hong Kong
 Yeung Tsz Ming, New Territories,
 Hong Kong
 Yip Tak Wing, Shatin, Hong Kong
 Yiu Ka Wah, Kowloon, Hong Kong
 Zeng Linghan, Guilin, Guangxi, P.R. China
 Zhuang Lingyan, Guilin, Guangxi,
 P.R. China

GEM DIAMOND DIPLOMA EXAMINATION

Qualified with Distinction

Clarkson, Mia, Salisbury, Wiltshire
 Fong Yan, William, Kowloon, Hong Kong
 Lounina, Ekaterina, Birmingham,
 West Midlands
 Lovelock, Justina Elizabeth, London
 McCrabbe, Julie Alice, Hackney, London
 Pereira Anisha, Edgbaston, West Midlands
 Van der Molen, Wouter Nicolaas, Zwolle,
 The Netherlands

Qualified with Merit

Andrews, Kitiya, Kings Norton,
 West Midlands

Glasgow, Sarah Alexandra, London
 Glover, Claire, Sunningdale, Berkshire
 Humphreys, Emma Louise, Preston
 Brockhurst, Shropshire
 Lee Ka Wai, Shatin, Hong Kong
 Qian Ying, Helen, Yuen Long, Hong Kong
 Scragg, Claire Patricia, Great Missenden,
 Buckinghamshire
 Wong Wai Lok, Kowloon, Hong Kong
 Yuen Kim Kam, New Territories,
 Hong Kong

Qualified

Bains, Neelam, Great Barr, Birmingham

Gem-A Awards

Baker, David, Bath, Avon	Ota, Shinya, Yamanashiken, Japan
Besic, Senka, Frederiksberg, Denmark	Palmares, Richard P., Sale, Cheshire
Bryan, Holly Eve, Dalkey, Co. Dublin, Ireland	Papadopoulos, Ioannis, Neapoli, Thessaloniki, Greece
Carnegie, Susan, Giffnock, Glasgow, Scotland	Peers, Sofia L.R., Leamington Spa, Warwickshire
Chan Mei, Kowloon, Hong Kong	Powar, Krishna, Smethwick, West Midlands
Davis, Samantha Angela, Bearwood, West Midlands	Seto Yee Man, Yvonne, New Territories, Hong Kong
Galbraith, Stuart Mark, Lansdown, Gloucestershire	Shah, Chandni, Mumbai, India
Gordon, Richard, London	Shen Bin, Wuhan, Hubei, P.R. China
Head, Jemima, Wilsden, West Yorkshire	Slovak, Kate, Leicestershire, Leicestershire
Kathris, Ioannis, Holargos, Greece	Tam Sze Yan, New Territories, Hong Kong
Klimek, Karina Sophia, Truro, Cornwall	Tam Chun Yu, Kowloon, Hong Kong
Konstantinidou, Maria, Petroypoli, Athens, Greece	Tsang Yuen King, New Territories, Hong Kong
Kwok Yuk Kuen, Kowloon, Hong Kong	Warner, Simon, Amersham, Buckinghamshire
Lam Shun Kwong, New Territories, Hong Kong	Welton-Cook, Elsa, West Kensington, London
Lampson, Ming, London	Wong Yui Kwan, Kowloon, Hong Kong
Lancaster, David, Hemel Hempstead, Hertfordshire	Yamout, Sabah Ibrahim, Leeds, West Yorkshire
Lee Fung Mei, Kowloon, Hong Kong	Yeung Tsz Ming, New Territories, Hong Kong
Lee Oi Yan, Christine, New Territories, Hong Kong	Yeung Yan Chu, Rosanna, Kowloon, Hong Kong
Leondaraki, Marialena, Syntagma, Athens, Greece	Yip Ching Yi, Corinna, Tai Koo Shing, Hong Kong
Leung Oi Yee, Louisa, Hong Kong	Yu Xidan, Wuhan, Hubei, P.R. China
Li Xiaolu, Wuhan, Hubei, P.R. China	
Man Lili, Wuhan, Hubei, P.R. China	
Man Ying, Wuhan, Hubei, P.R. China	

Charity status

The Council of the Association is pleased to announce that the Association became a Registered Charity on 19 May 2005, registered charity no. 1109555. Charity status will greatly help the Association to expand and develop the services offered to members. One advantage is that it will be possible to claim back tax on eligible UK donations and subscriptions. Using Gift Aid means that for every pound received, the Association can claim an extra 28 pence from the Inland Revenue, so £10 could be turned into £12.80 just as long as donations

are made through Gift Aid. UK members will be requested to complete and return Gift Aid declaration forms, to be circulated with the 2006 subscription notices, to enable them to participate in the scheme.

Members' Meetings

Gem Discovery Club

Specialist Evenings

Once a month Club members have the opportunity to examine items from the collections of gem and mineral specialists.

Gifts and Donations

The Association is most grateful to the following for their gifts for research and teaching purposes:

Maria Alferova, Geology Department, Moscow State University, for a selection of green grossular garnet crystals.

Leonardo Carrazone, SETT Stones, São José do Rio Preto-SP, Brazil, for a prasiolite crystal.

Tom Cushman, Sun Valley, Idaho, U.S.A., for a collection of crystals and cut stones including pieces of copal resin with insect inclusions, corundum, feldspar cabochons including two sunstones, grossular garnet, quartz cabochons one with dark star-shaped inclusions and four with blue flecked inclusions, and three faceted pezzottaites.

James P.M. Day FGA, Tunbridge Wells, Kent, for a donation to the appeal for funds (Pearl Donation).

De Beers, Johannesburg, South Africa, for three large samples of kimberlite, each with a polished face, from the Monastery, Uintjiesberg and Voorspoed mines in South Africa.

Harold Killingback FGA, Oakham, Leicestershire, for the rose quartz sphere (105 mm diameter) that was featured in his article 'Stereoscopic effect in asterism and chatoyancy' published in *The Journal of Gemmology*, 2005, 29(5/6), 312.

Marcia Lanyon FGA, London for parcels of faceted sapphires of various cuts and sizes.

Michele Marci, Rome, Italy, for quartz cabochons from Brazil, one with covellite and the other with gilarite inclusions.

Francesco Mazzero, GemOA sarl, Paris, France, for two Ethiopian opals.

Jason Williams FGA DGA, G.F. Williams & Co. Ltd., London, for a selection of iolite cabochons, carved amethyst leaves, synthetic Verneuil stones and paste.

Rogério Zucoloto Luz, Minas Gerais, Brazil, for specimens of mica and quartz with vivianite crystals.

Bequest

The Association has received notification that it is to benefit from the estate of the late Revd S.B. Nikon Cooper FGA DGA. Although final figures are yet to be announced, the bequest is to be in excess of £45,000.

Nikon, who died on 11 October 2004, was a Gem-A correspondence course tutor for a record 35 years, retiring from the position in 2002. He was one of a team of three tutors with Keith Mitchell and Vera Hinton when he was appointed in 1967.

The Council is most grateful to the Revd Cooper for his lifelong support of the Association and for his generous bequest.

The May guest was Cecilia Pople who gave a short slide show of some of the interesting items from her personal jewel box, some of which she brought along for Club members to examine. In June Branko Deljanin, Director of Canadian Operations at the European Gemmological Laboratories (EGL) in Toronto and a Gem-A Tutor, gave a presentation on synthetic and treated diamonds including the latest KM micro-laser treatments. This was followed by a hands-on session when Club members could

examine a variety of treated stones. David Davis brought along a selection of fine and rare specimens from his own collection for examination in July, severely testing the gemmological knowledge of Club members! Natural and imitation organic gemstones was the subject for the August meeting with Maggie Campbell Pedersen. Many of the items she provided for examination were examples of fakes currently circulating on the market. In October Harold Killingback's theme was asterism and chatoyancy, and

among the samples he brought along was the star rose quartz sphere as featured in his article 'Stereoscopic effect in asterism and chatoyancy' (*The Journal of Gemmology*, 2005, 29, 5/6).

London

A presentation was given on 15 April at the Gem-A London headquarters by Maria Alferova of the Moscow State University entitled 'Chrome-bearing green garnets'. Maria, who was visiting London en route for Scotland where she was speaking at the Scottish Branch Conference, has carried out extensive fieldwork in Russia and is currently specializing in chromium-bearing gem garnets. A report of her talk was published in *Gems & Jewellery*, June 2005.

Midlands Branch

Branch meetings held at the Earth Sciences Building, University of Birmingham, Edgbaston, included a demonstration of identification of gem materials using the microscope by Gwyn Green on 29 April and a cultured pearl evaluation workshop with Michael Houghton of Phoenix Far East Pearls Ltd on 30 September. The Branch's popular Summer Supper Party was held on 18 June.

North East Branch

On 13 April John Harris brought along a selection of specimens with prominent absorption spectra for a hands-on session on the observation, calibration and recording of gemstone spectra. 'The Chinese Pearl Revolution' was the title of John Carter's presentation on 15 June. A renowned authority on pearls, John spoke about the impact the Chinese production is having on the established trade. On 14 September Gem-A President Alan Jobbins gave a colourful pictorial presentation describing a wide range of the animal and vegetable materials which have been used for adornment over the centuries. All meetings were held at the offices of Evans of Leeds Ltd, Millshaw.

North West Branch

Regular Branch meetings were held at the new venue, the YHA Liverpool International,

25 Tabley Street, Liverpool 1. Eric Emms spoke on diamond treatments on 20 April, followed by a presentation by Wendy Simkiss on 18 May on the mineralization of fossils. On 15 June David Callaghan gave a review on twentieth-century styles, fashions and eminent designers in his talk entitled '1960 and all that'. 'Some you win, some you lose' was the title of auctioneer Stephen Whittaker's talk on 21 September. Stephen, of Fellows & Sons, Birmingham, gave Branch members the opportunity to handle auction pieces and – with his expert guidance – to value them accurately.

Scottish Branch

The Tenth Annual Scottish Branch Conference was held in Perth from 29 April to 2 May. The keynote speaker was Shane McClure, Director of the GIA West Coast Laboratory, who gave two presentations reporting on recent research and interesting and unusual stones seen at the Laboratory. A full report of the Conference was published in *Gems & Jewellery*, June 2005.

South East Branch

On 17 April a 'Jem Jumble' – a jumble sale event of gem miscellany – was held at the Gem-A headquarters in Greville Street. An illustrated lecture on amber and fakes was given by organics expert Maggie Campbell Pedersen on 26 June.

South West Branch

An afternoon of talks and hands-on sessions entitled 'Between a Rock and a Hard Place' was held at the Bath Royal Literary and Scientific Institution in Bath. Henry Meadows spoke on Blue John, followed by Richard Slater and Liz Latham on agates and other hard stones. 'Do you know if the stone you're looking at is a diamond?' was the question asked by Doug Garrod on 31 July during his afternoon presentation on synthetic, simulated and treated diamonds.

Membership

Between 1 April and 30 September 2005 the Council approved the election to

membership of the following:

Fellowship and Diamond Membership (FGA DGA)

Abrahams, Roy Henry, Ruislip, Middlesex, 1985/1987
 Cheung Yiu Hung, Kowloon, Hong Kong, 2005
 Lin Shu-Zhen, Taipei, Taiwan, R.O. China, 2005
 Wackan, Susan Kirsten, London, 1985/1986
 Williams, Benja-min Jacob, Blockley, Gloucestershire, 2003/2004

Fellowship (FGA)

Abel, Arlan, Minneapolis, Minnesota, U.S.A., 1991
 Agrawal, Puru, New Delhi, India, 2004
 Alcock, Kate, Hereford, Hereford and Worcester, 2005
 Alliston, Erika A., London, 2005
 Badrov, Irena, London, 2005
 Chiu Shu-Fen, Tapei Hsien, Taiwan, R.O. China, 2005
 Fleming, John James, Kelso, Scotland, 2005
 Fu Ming, Guilin, Guangxi, P.R. China, 2004
 Gala, Vasant Rahul, London, 2005
 Hellenbrand, Yosef, Thornhill, Ontario, Canada, 2005
 Ho Hay Mo, John, Yangon, Myanmar, 2005
 Liao Baoli, Guilin, Guangxi, P.R. China, 2004
 Ma Yaw Lan Hsiung, Ruth, Hong Kong, 2005
 O'Donnell, Craig Anthony, Smethwick, West Midlands, 2004
 Perera, Ajith, Mount Lavinia, Sri Lanka, 1979
 Petkovic, Katarina, Sabac, Serbia and Montenegro, 2002
 Phisuthikul, Piyamaporn, Bangkok, Thailand, 2005
 Smithie, Sheila Barron, Boston, Massachusetts, U.S.A., 2005
 Sue-A-Quan, Dona Marie, Cambridge, Ontario, Canada, 2005
 Taylor, Richard E., Carlsbad, California, U.S.A., 2005
 van Gorkom, Annemarie, Utrecht, The Netherlands, 2004
 Wold, William, Joure, The Netherlands, 2004
 Woodring, Sharrie, New Jersey, U.S.A., 2001

Diamond Membership (DGA)

Chan Ka Man, Wah Fu Estate, Hong Kong, 2005
 Chan Siu Ping, Kowloon, Hong Kong, 2005
 Chuang Chang-Chen, Taipei, Taiwan, R.O. China, 2005
 Davenport, Tristan Nicholas Barritt, Hereford, Hereford and Worcester, 2000
 Ho Sze Man, Helen, New Territories, Hong Kong, 2005
 Hui Ngai Yin, North Point, Hong Kong, 2005
 Konstantopoulos, Konstantinos, Athens, Greece, 2004
 Leung Kam Ping, Sai Kung, Hong Kong, 2005
 Mahmood, Zahid, Birmingham, West Midlands, 2005
 Szemencsuk, Galina, Ilford, Essex, 2004
 Wan Ching Man, New Territories, Hong Kong, 2005
 Wong Tung Wing, Shaukeiwan, Hong Kong, 2005
 Wong Yuen Leung, Kowloon, Hong Kong, 2005

Associate Membership

André, Cindy Marie, Tewkesbury, Gloucestershire
 Bai, Jonghyuck, Busan, South Korea
 Baudendistel, Joerg, Obertshausen, Germany
 Boeder, Amy, Newmarket, Suffolk
 Cox, Douglas W., Paris, Texas, U.S.A.
 Cuthbert, Sarah Krauss, Edinburgh, Scotland
 Davies, Genevieve, London
 Elliott, Duncan, Houston, Texas, U.S.A.
 Fletcher, Robin, Reading, Berkshire
 Freeman, Derek, Hove, East Sussex
 Freeman, Sarah, London
 Gallop, Jacob Lynn, Paris, Texas, U.S.A.
 Georgiou, Stephen, London
 Ileso, Kayode Samuel, Hayes, London
 Kalaya K. Min, Yangon, Myanmar
 Khin Zar Thwe, Yangon, Myanmar
 Kliever, Kathryn, Allen, Texas, U.S.A.
 Mambwe, Thomas Winter, Hawkinge, Kent
 Mansell, Melanie Anne, Laira, Plymouth, Devon
 Marshall, Patricia, Solihull, West Midlands
 Ndionyemma, Mark, London
 Richard, Lauren, Paris, Texas, U.S.A.
 Riggs, Laurie Ann, Paris, Texas, U.S.A.

Ross, Christopher Nicholas, Norwich, Norfolk
 Sedera, Mohottige Suraj Nalin, Ratmalana,
 Sri Lanka
 Sotunde, Marie-Therese, London
 Thomson, Colin, Fife, Scotland
 Troutt, Bonnie, Sumner, Texas, U.S.A
 Wise, Ruth, Barnes, London
 Wolf, Jennifer, Hugo, Oklahoma, U.S.A
 Woods, Maria, Carshalton, Surrey

Laboratory Membership

Gemmarum, Cardiff

Transfers

Fellowship to Fellowship and Diamond Membership (FGA DGA)

Deprez, Guillaume, London, 2003/2005

Kuo Chi-Cheng, Taipei, Taiwan, R.O. China,
 2003/2005

Lindwall, Torbjorn, Lannavaara, Sweden,
 1996/2005

Towers, Jill, St Heliers, Auckland,
 New Zealand, 2002/2005

Wenham, Diana L., North Harrow, Middlesex,
 2003/2005

Wong Tai-Wai, Kowloon, Hong Kong,
 2002/2005

Associate Membership to Fellowship and Diamond Membership (FGA DGA)

Berden, Angela C.M., Balham, London, 2005

Subscriptions 2006

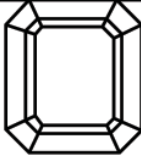
It has been agreed that the membership subscription rates will remain unchanged for 2006, as set out below. Existing Fellows, Diamond Members and Associate Members will be entitled to a £5.00 discount for subscriptions paid before 31 January 2006.

	Fellows, Diamond Members and Associate Members	Laboratory Members
UK	£72.50	£250.00 + VAT
Europe	£80.00	£250.00
Rest of the World	£85.00	£250.00

Errata

In *The Journal of Gemmology*, 2005, 29 (5/6), p.318, in Table I, for 'long wave 265 nm' read 'long wave 365 nm'

Pearls Coral Amber Bead Necklaces Carvings Cameos Mineral Specimens

The World  of Gemstones

Ruppenthal (U.K.) Limited

Gemstones of every kind, cultured pearls, coral, amber,
bead necklaces, hardstone carvings, objets d'art and
18ct gold gemstone jewellery.


We offer a first-class lapidary service.

By appointment only
1a Wickham Court Road, West Wickham, Kent BR4 9LN
Tel: 020-8777 4443, Fax: 020-8777 2321, Mobile: 07831 843287
e-mail: roger@ruppenthal.co.uk, Website: www.ruppenthal.co.uk

Modern 18ct Gem-set Jewellery

Opal Precious Topaz Ruby Star Ruby Sapphire Star Sapphire Tourmaline

Gemsstones Aquamarine Alexandrite Amethyst Emerald Jade Lapis Lazuli



MODERN MICRO-ANALYTICAL TECHNIQUES FOR GEMMOLOGISTS

**A 3-day course on Laser Raman
Spectroscopy and Imaging**

Kingston University, Surrey
15 to 16 January 2005

In collaboration with
The Gemmological Association of Great Britain

Gain a basic understanding of Raman
Spectroscopy and its application to gem testing.
Be introduced to other non-destructive methods
of micro-analysis and micro-imaging.

Course fee: £375

Participants should have a relevant qualification
(e.g. BSc or FGA) and an interest in gemmology
or applied mineralogy (max. 20 participants)

Details and booking form from:
Dr S Byrnie,
School of Earth Sciences & Geography,
Kingston University, Surrey KT1 2EE
144 (0)20 8547 6860 – s.byrnie@kings.ac.uk

© 2005 Gem-A

Gem-A MailTalk

**The email-based forum
for communication
between members**

- Share comments and ideas with other members
- Ask or answer questions
- Receive regular news from Gem-A

Have you registered yet?

For instructions on how to register go to
www.gem-a.info/information/mailTalk.htm
or contact Tara at tara@gem-a.info

ISLAND OF GEMS

10th annual exhibition

THISTLE LANCASTER GATE

75/89 Lancaster Gate, London W2 3NN

18 to 21 November 2005

A rare chance to learn about the gems of Sri Lanka

Ideal exhibition for students of gemmology and professionals in gems and jewellery fields. Over 60,000 gemstones on display in the gemstone and education units. Free advice will be given on gems and jewellery.

The entrance fee of **£6.00** (adults) includes:

- **FREE** souvenir brochure
- **FREE** sample gemstone
(0.50 ct sapphire or four mixed stones)
- **FREE** light refreshments

For further details contact the exhibition organiser:
D.H. ARIYARATNA FGA DGA FGS
P.O. Box 1837, London N17 9BW
Tel./Fax: 020 8807 8252 Email: sri@lankagems.co.uk
Website: www.lankagems.co.uk

MEGA-LOUPE

Dark Field Illumination
at your fingertips

Features optimal lighting and a 3-position lens for fast and efficient inclusion detection on loose or mounted stones



2 MODELS

Both with the same high quality fully corrected 10X triplet lens

LUMI-LOUPE 15mm lens \$90
MEGA-LOUPE 21mm lens \$115

ADD: \$20 for shipping outside the continental USA
\$8 for shipping inside the continental USA

www.nebulamfg.com
email: info@nebulamfg.com

P.O. Box 3356, Redwood City, CA 94064, U.S.A.
Tel 650-369-5966 Fax 650-363-5911

GIA®

Gemological
Research
Conference

2006
August 26-27

CALL FOR ABSTRACTS:
March 1, 2006

To explore the most recent technical developments in gemology, the Gemological Institute of America will host a GEMOLOGICAL RESEARCH CONFERENCE in conjunction with the 4TH INTERNATIONAL GEMOLOGICAL SYMPOSIUM in San Diego, California.

Invited lectures, submitted oral presentations, and a poster session will explore a diverse range of contemporary topics including the geology of gem deposits, new gem occurrences, characterization techniques, diamond and corundum treatments, synthetics, and general gemology. Also scheduled is a one-day pre-conference field trip to the world-famous Pala pegmatite district in San Diego County.

Abstracts should be submitted by **March 1, 2006**, to gemconference@gia.edu (for oral presentations) or ddirlam@gia.edu (for poster presentations). Abstracts will be evaluated for appropriateness and technical merit. To register for the GIA Gemological Research Conference, visit www.symposium.gia.edu.

For further information, contact the organizing committee at gemconference@gia.edu or visit www.gia.edu/gemsandgemology

*Pearls
Gemstones*

Lapidary Equipment

GENOT L

Since 1953

*CH. De Wavre, 850
B-1040 Bxl – Belgium*

Tel : 32-2-647.38.16

Fax : 32-2-648.20.26

E-mail : gama@skynet.be

www.gemline.org
www.geofana.net

**Museums,
Educational Establishments,
Collectors & Students**

I have what is probably the largest range of genuinely rare stones in the UK, from Actinolite to Zincite. Also rare and modern synthetics, and inexpensive crystals and stones for students.

Computerised lists available with even more detail. Please send 12 1st class stamps refundable on first order (overseas free).

Nola French
t/a A.J. French FGA
7 Orchard Lane, Evercreech,
Somerset BA4 6PA

Telephone: 01749 830673

Email: french@frencht.freemove.co.uk

**ROCK
n' gem
SHOWS**

*Exhibitors displaying & selling a huge range of
minerals, fossils, crystals & jewellery*

2005 SHOWS

CHELtenham RACECOURSE

Prestbury Park, Cheltenham, Glos

19 - 20 NOVEMBER

BRIGHTON RACECOURSE

Freshfield Road, Brighton

3 - 4 DECEMBER

Admission Prices 2005:
Adults £2.80, Seniors £2.00
Children (8-16 yrs) £1.25 at all shows.



2006 SHOWS

**For a full list of our 2006 shows,
directions of to venues including a
map & a full list of each show please
visit our website
www.rockngem.co.uk**

All shows open 10am - 5pm (Trade & Public)
Kempton Park only: Sat 10am - 8pm, Sun 10am - 5pm

For further information please contact:
HD Falra Ltd 01628 621697
Email: info@rockngem.co.uk www.rockngem.co.uk

Forthcoming Events

2 November	Gem Discovery Club Specialist Evening: JOHN I KOIVULA
3 November	North East Branch: The Naughty Nineties. BRIAN DUNN
7 November	Scottish Branch: Cairngorm gemstones. BASIL DUNLOP
16 November	North West Branch: AGM and social evening
25 November	Midlands Branch: A history of buttons. JENNY SWINDELLS
6 December	Gem Discovery Club Specialist Evening: DAVID HARGREAVES
10 December	Midlands Branch: Annual Branch dinner
27 January	Midlands Branch: AGM, Bring and Buy, and Team Quiz
24 February	Midlands Branch: Horological Jewelling. JOHN MOORHOUSE
19 March	Midlands Branch: Loupe and lamp – a one-day event
31 March	Midlands Branch: Chasing rainbows by observing gemstone spectra. JOHN HARRIS
28 April to 1 May	Scottish Branch Conference, Perth

(when using e-mail, please give Gem-A as the subject):

London: Mary Burland on 020 7404 3334;
e-mail mary.burland@gem-a.info

Midlands Branch: Gwyn Green on 0121 445 5359;
e-mail gwyn.green@usa.net

North East Branch: Mark Houghton on 01904 639761;
email sara_e_north@hotmail.com

North West Branch: Deanna Brady 0151 648 4266

Scottish Branch: Catriona McInnes on 0131 667 2199;
e-mail scotgem@blueyonder.co.uk

South East Branch: Colin Winter on 01372 360290; e-mail info@ga-seb.org

South West Branch: Richard Slater on 01635 553572; e-mail rslater@dnfa.com

Contact details

Gem-A Website

For up-to-the-minute information on Gem-A events visit our website on www.gem-a.info

Guide to the preparation of typescripts for publication in The Journal of Gemmology

The Editor is glad to consider original articles shedding new light on subjects of gemmological interest for publication in The Journal. Articles are not normally accepted which have already been published elsewhere in English, and an article is accepted only on the understanding that (1) full information as to any previous publication (whether in English or another language) has been given, (2) it is not under consideration for publication elsewhere and (3) it will not be published elsewhere without the consent of the Editor.

Typescripts Two copies of all papers should be submitted on A4 paper (or USA equivalent) to the Editor. Typescripts should be doubled spaced with margins of at least 25mm. They should be set out in the manner of recent issues of The Journal and in conformity with the information set out below. Papers may be of any length, but long papers of more than 10 000 words (unless capable of division into parts or of exceptional importance) are unlikely to be acceptable, whereas a short paper of 400-500 words may achieve early publication.

The abstract, references, notes, captions and tables should be typed double spaced on separate sheets.

Title page The title should be as brief as is consistent with clear indication of the content of the paper. It should be followed by the names (with initials) of the authors and by their addresses.

Abstract A short abstract of 50-100 words is required.

Key Words Up to six key words indicating the subject matter of the article should be supplied.

Headings In all headings only the first letter and proper names are capitalized.

A This is a first level heading

B This is a second level heading

First and second level headings are ranged left on a separate line.

Third level headings are in italics and are indented within the first line of the text.

Illustrations High resolution digital files, for both colour and black-and-white images, at 300 dpi TIFF or JPEG, and at an optimum size, can be submitted on CD or via email. Vector files (EPS) should, if possible, include fonts. Match proofs are

essential when submitting digital files as they represent the colour balance approved by the author(s).

Transparencies, photographs and high quality printouts can also be submitted. It is recommended that authors retain copies of all illustrations because of the risk of loss or damage either during the printing process or in transit.

Diagrams must be of a professional quality and prepared in dense black ink on a good quality surface. Original illustrations will not be returned unless specifically requested.

All illustrations (maps, diagrams and pictures) are numbered consecutively with Arabic numerals and labelled Figure 1, Figure 2, etc. All illustrations are referred to as 'Figures'.

Tables Must be typed double spaced, using few horizontal rules and no vertical rules. They are numbered consecutively with Roman numerals (Table IV, etc.). Titles should be concise, but as independently informative as possible. The approximate position of the Table in the text should be marked in the margin of the typescript.

Notes and References Authors may choose one of two systems:

(1) The Harvard system in which the authors' names (no initials) and dates (and specific pages, only in the case of quotations) are given in the main body of the text, (e.g. Collins, 2001,341). References are listed alphabetically at the end of the paper under the heading References.

(2) The system in which superscript numbers are inserted in the text (e.g. ... to which Collins refers.³) and referred to in numerical order at the end of the paper under the heading Notes. Informational notes must be restricted to the minimum; usually the material can be incorporated in the text. If absolutely necessary both systems may be used.

References in both systems should be set out as follows, with double spacing for all lines.

Papers Collins, A.T., 2001. The colour of diamond and how it may be changed. *J.Gemm.*, 27(6), 341-59

Books Balfour, I., 2000. Famous diamonds. 4th edn. Christie's, London. p.200

Abbreviations for titles of periodicals are those sanctioned by the World List of scientific periodicals 4th edn. The place of publication should always be given when books are referred to.



Contents

A venture into the interior of natural diamond: genetic information and implications for the gem industry G.P. Bulanova, A.V. Varshavsky and V.A. Kotegov	377	Sapphire diffusion treatment and the behaviour of iron and titanium Yang Ruzeng, Yang Yuan and Xu Hongyi	455
As-grown, green synthetic diamonds C.M. Breeding, J.E. Shigley and A.H. Shen	387	Two remarkable taaffeite crystals from Sri Lanka K. Schmetzer, L. Kiefert, H-J. Bernhardt and M. Burford	461
Iridescent colours of the abalone shell (<i>Haliotis glabra</i>) T.L. Tan, D. Wong and P. Lee	395	Nephrite jade from Scortaseo, Switzerland D. Nichol and H. Giess	467
Diffraction Enhanced Imaging: a new X-ray method for detecting internal pearl structures J. Schlüter, M. Lohmann, J. Metge and B.Reime	401	Crossed filters revisited D. B. Hoover and B. Williams	473
A microscopy-based screening system to identify natural and treated sapphires in the yellow to reddish-orange colour range K. Schmetzer and D. Schwarz	407	Letters to the Editor	482
Growth of hexagonal bipyramidal ruby crystals by the evaporation of molybdenum trioxide flux K. Teshima, H. Kondo and S. Oishi	450	Abstracts	484
		Book Reviews	488
		Proceedings of the Gemmological Association and Gem Testing Laboratory of Great Britain and Notices	490

Cover Picture: Lepidocrocite inclusions in quartz.
Photography by Luella Dykhuis FGA DGA, Tucson, Arizona, U.S.A.

First Prize in the 2005 Photographic Competition (see p.490).

The Gemmological Association and Gem Testing Laboratory of Great Britain
Registered Office: Palladium House, 1-4 Argyll Street, London W1F 7LD